Disordered elastic systems:
Fluctuations and AC-dynamics

Inaugural-Dissertation

zur

Erlangung des Doktorgrades

der Mathematisch-Naturwissenschaftlichen Fakultät

der Universität zu Köln

vorgelegt von

Andreas Glatz

aus Köln

2004

Berichterstatter: Prof. Dr. T. Nattermann

                           Prof. Dr. J. Krug

Tag der mündlichen Prüfung: 03. November 2004

Abstract.— Disordered elastic systems are studied in the quantum, classical, and dynamic regime in the present thesis. The thesis consists of two main parts:

In the first part we study the low temperature phase diagram of one-dimensional weakly disordered quantum systems like charge or spin density waves and Luttinger liquids by a *full finite temperature* renormalization group (RG) calculation. In the classical region, for vanishing quantum fluctuations those results are supplemented by an *exact* solution of the model in the case of strong disorder, described by the ground state and the correlation function. Furthermore, by a mapping of the problem onto a *Burgers equation with noise*, in the case of weak disorder, we can derive an expression for the correlation length. At *zero* temperature we reproduce the (quantum) phase transition between a pinned (localized) and an unpinned (delocalized) phase for weak and strong quantum fluctuations, respectively, as found previously by Fukuyama [Fuk84] or Giamarchi and Schulz [GS88].

At *finite* temperatures the localization transition is suppressed: the random potential is wiped out by thermal fluctuations on length scales larger than the thermal de Broglie wave length of the phason excitations. The existence of a zero temperature transition is reflected in a rich cross-over phase diagram determined by the correlation functions. In particular we find four different scaling regions: a *classical disordered*, a *quantum disordered*, a *quantum critical*, and a *thermal* region. The results can be transferred directly to the discussion of the influence of disorder in superfluids. Finally we extend the RG calculation to the treatment of a commensurate lattice potential, and for the case of density waves we discuss the influence of quantum phase-slips, which might lead to a new scenario for the unpinning (delocalization) transition at zero temperature.

Additionally, we analyze the current noise in a classical one-dimensional charge density wave system in the weak pinning regime by solving the overdamped equation of motion numerically. At low temperatures and just above the zero temperature depinning threshold, the power spectrum of the current noise reveals the existence of $1/f$ or *flicker noise*. Our results are in agreement with experimental measurements in quasi-one-dimensional charge density wave systems.

In part two, we examine the viscous motion of an interface driven by a *periodically oscillating external field* in a random medium. The velocity exhibits a smeared depinning transition showing a pronounced hysteresis, which is absent in the adiabatic case. Its width is determined by a new length scale, introduced by the frequency of the external drive and – in the low frequency regime – by the critical exponents of the zero frequency depinning transition. Scaling arguments and an approximate renormalization group treatment predict a power law behavior of the velocity as a function of frequency and field amplitude at the dc depinning threshold, which is confirmed numerically. Thermal fluctuations lead to an additional

smearing of the transition. If the amplitude of the external driving force is smaller than the depinning field, the motion of the interface by avalanches has to be taken into account in order to describe the velocity hysteresis.

To check the validity of our model with respect to experimental results, we calculate the complex susceptibilities using an adiabatic and non-adiabatic approach numerically for finite systems and compare it to measurements of the superferromagnetic granular multilayer system $[\mathrm{Co}_{80}\mathrm{Fe}_{20}(1.4\mathrm{nm})/\mathrm{Al}_2\mathrm{O}_3(3\mathrm{nm})]_{10}$ and find that the model of an ac driven interface in a disordered environment can describe the main features of the experimental results.

Additionally, the influence of a strong surface potential on the critical depinning of an elastic system, driven in a random medium is considered. If the surface potential prevents depinning completely, the curvature of the displacement profile at zero temperature exhibits a pronounced rhombic hysteresis curve with width of two times the (bulk) depinning field. The hysteresis disappears at non-zero temperatures if the driving force is changed adiabatically. If the surface depinns by the applied force or thermal creep, the curvature is reduced with increasing velocity. The results apply, e.g., to driven magnetic domain walls, flux-line lattices, and charge-density waves.

As addendum we examine low dimensional interacting, but clean Bose systems at low temperatures. The interaction leads to scattering events of the over-condensate particles for which we calculate the scattering times using *Fermi's* golden rule. With that we derive the thermal conductivity and the related *weak localization corrections*. This is done for short and long-range interactions. Since d-dimensional Bose systems can be mapped to $(d+1)$-dimensional vortex-line systems, the results for long-range interactions may lead to a stiffening of the vortex lattice.

Contents

A Introduction

1 Disordered elastic systems

In contrast to ideal (infinite) model systems, which are often used in condensed matter physics, the consideration of inhomogeneities leads (in most cases) to drastic changes and to new fascinating properties of the systems – not only from the theoretical point of view. For example, charge density waves without randomly distributed inhomogeneities would be ideal ("Fröhlich") superconductors, whereas type-II superconductors would show finite resistivity. In general the presence of random impurities creates an energy landscape with many metastable states and the determination of a global ground state becomes highly non-trivial.

A huge variety of physical systems with random inhomogeneities can be described by *elastic theories* in a disordered environment. However, one can distinguish two main classes of models: *elastic manifold models* and so-called *periodic media*. In the first class one can include domain walls of magnetically or structurally ordered systems with impurities [You99] or isolated flux- and dislocation lines. The second class of systems is periodic, examples are density waves [Grü94b, Grü88, Grü94a], Wigner crystals in random environment, flux-line lattices [BFG$^+$94, NS00], and so forth. Theses systems are subject of detailed investigations since the early 1970s. An additional way to characterize those systems, is to use a dimensional criterium: All these systems can be considered as D-dimensional objects embedded in a d-dimensional physical system, e.g., for a single flux line D would be one or $D = d - 1$ for domain walls, and for (most) periodic media $D = d$.

So far we have mentioned only random inhomogeneities, but one should note that there are also non-random ones, e.g., introduced by surfaces or periodic potentials. However, in this section we focus on the random situation, but come back to this point later on.

Therefore, we will briefly describe the main equilibrium properties of elastic objects in random media and illustrate it by some specific examples. An overview of the possible situations, controlled by the parameters for thermal (T) and quantum fluctuations (K) as well as for an external driving force (h), is shown in Fig. A.1. In the plane spanned by the K and the T-axis we have the equilibrium phases of the system. For $h \neq 0$ we are in the non-equilibrium situation (which is discussed in section 3): Without quantum fluctuations there

is a depinning transition at $h = h_c$ for $T = 0$ or the system shows classical creep motion at finite temperatures, even below h_c. At zero temperature also quantum fluctuations lead to creep motion.
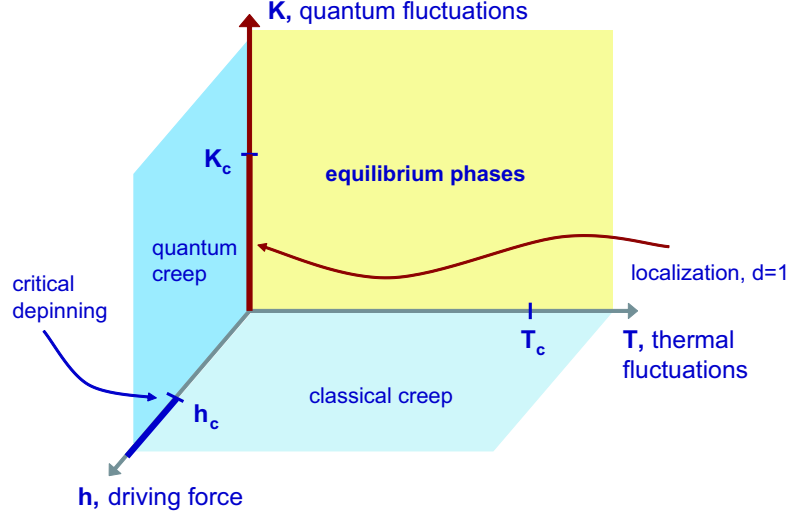
Figure A.1: Different regions in the parameter space of thermal T and quantum fluctuations K and external driving force h. At $h = 0$ we have the equilibrium phases. With external driving force we find for $K = 0$ and $T = 0$ the depinning transition at h_c, whereas for quantum or thermal fluctuations creep motion occurs even below h_c.

Let us write down a general Hamiltonian for a D-dimensional elastic object in a $d = (D+1)$ dimensional system, i.e., for a manifold, described by a displacement operator $\hat{z}(\mathbf{x}, t)$ with in general $N = d - D$ components (here $N = 1$) with quenched disorder potential V_R:

$$\hat{\mathcal{H}} = \frac{1}{2} \int d^D x \left\{ a\hat{P}^2 + c(\boldsymbol{\nabla}_{\mathbf{x}} \hat{z}(\mathbf{x}, t))^2 + V_R(\mathbf{x}, \hat{z}) - h\hat{z} \right\} , \qquad \text{(A1.1)}$$

where $\hat{P}$ is the conjugated momentum operator to $\hat{z}$, h the external driving force, and $\mathbf{x}$ the internal coordinates of the manifold. The elastic constant c is in general a temperature dependent tensor which can be non-local. In the thesis we consider only the case of a local (temperature dependent) function. Note, that this model describes only oriented elastic manifolds with single valued z, i.e., the manifold has no *overhangs*. A sketch of a manifold with $D = 1$ in a random environment is shown in Fig. A.2.

To be a bit more specific, we consider the two most important examples in the context of the present work:

(i) *domain walls in magnets*: domain walls can be described by the manifold Hamiltonian (A1.1), i.e., $D = d - 1$. The interface separates, e.g., two ferromagnetically ordered

Figure A.2: Sketch of a one-dimensional interface in a random medium. The small arrows at the impurities visualize the direction of the local pinning forces. The thick arrows show the restoring elastic forces. The interface has an internal coordinate $\mathbf{x}$ and is described by its displacement $z(\mathbf{x})$ from an initial plane.
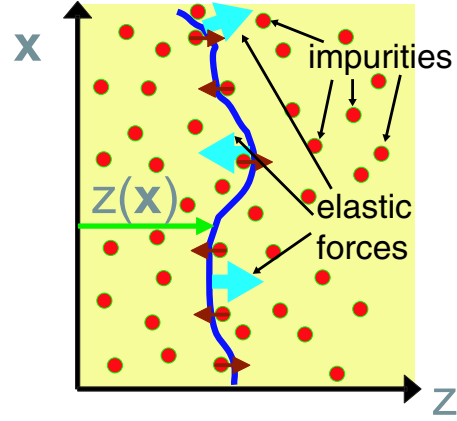
domains with different directions of the magnetization. The random forces can emerge, e.g., from fluctuations of the exchange coupling between the spins (*random-bond disorder*, cf. appendix E2.3) which couple to the domain wall or from frozen magnetic impurities (*random-field disorder*). The external driving force is directly proportional to the applied magnetic field.

(ii) *charge density waves*: In the case of charge density waves the displacement function z has to be replaced by a phase field φ and the system dimension is the same as for the elastic object; $D = d$. The impurity potential is periodic in φ and can be described by a random phase at each impurity position, which is correlated in φ-direction. The external driving force is given by the electric field applied to the system.

From the general expression, given in (A1.1), one can already obtain some basic features, if one goes over to an averaged free energy for an elastic object of linear size L, which is in appropriate units approximately given by $(h = 0)$

$$
\begin{aligned}
F \;\sim\;& L^{D-2}z^2 - VL^{D/2} - T - \left(\frac{K}{z}\right)^2 L^{-D} \\
=\;& L^{D-2}\left[z^2 - VL^{\frac{4-D}{2}} - TL^{2-D} - \left(\frac{KL^{1-D}}{z}\right)^2\right],
\end{aligned}
$$

where K is a parameter controlling the quantum fluctuations, V the averaged disorder potential, and T the temperature (z is the averaged displacement of the object). Note, that we have used the standard commutation relation for $\hat{z}$ and $\hat{P}$ to derive the last term on the right-hand side. Following Imry and Ma [IkM75] one can see from the last line, that there are some important values for D at which the physics of the system changes: For $D \leqslant 4$ the disorder term V becomes more important on larger length scales, i.e., disorder is relevant

in most realistic systems; For $D \leqslant 2$ thermal fluctuation are important and for $D \leqslant 1$ also quantum fluctuations have to be taken into account. An important length scale which can be derived directly from this expression by equating the first term, resulting from the elastic part, and the second, disorder term, is the length scale L_P on which the disorder balances the curvature forces, i.e., for $D < 4$ disorder will win on larger scales than L_P. In the context of flux-line lattices L_P is called *Larkin*, for random magnets *Imry-Ma*, and for charge-density waves *Fukuyama-Lee* length.

Therefore, perturbative methods break down on length scales larger than L_P and one has to apply renormalization group techniques to obtain the statistical properties of these systems: In three dimensional systems, the low temperature phase of these objects is determined by a zero temperature disorder fixed point resulting in quasi-long-range order and glassy dynamics (for recent reviews and further references, see e.g. [BFG$^+$94, NS00, BN04]). In two dimensions one has to distinguish between periodic media and manifolds. For the first class, this fixed point is extended to a fixed line which terminates at the glass transition temperature [CO82, VF84]. For random manifolds disorder is always relevant. In both cases the T-axis is a line of fixed points.

Since the first part of the thesis focuses on one-dimensional systems, we provide a more detailed overview of the one-dimensional case in the following section.

2 The one-dimensional case: charge density waves and Luttinger Liquids

The physics in one dimension is quite different from that in higher dimensions if interactions between particles are taken into account. In a recent book by Giamarchi the one-dimensional world is investigated in great detail [Gia03]. Therefore we will only briefly address the one-dimensional physics related to the systems under consideration in this thesis: charge or spin density waves (CDWs/SDWs) and the Tomonaga-Luttinger liquid (as usual in literature, we also drop the first name and call it only Luttinger liquid henceforth). In the quantum regime, both systems can be described by the same elastic model, essentially (there are important difference, though). For an extensive review of density waves, we refer to the book by Grüner [Grü94b].

Since we are especially interested in the low temperature behavior of CDWs, also quantum fluctuations have to be taken into account. Disorder and quantum fluctuations in one-dimensional CDWs (or Luttinger liquids) at zero temperature have been considered previously (see, e.g., [Fuk84, GS87, GS88, Sch93]) and an unpinning (delocalization) transition

as a function of the strength of quantum fluctuations was found. In Fig. A.1 this transition is found on the K-axis at K_c. Finite temperature effects were partially incorporated by truncating the renormalization group (RG) flow at the de Broglie wave length of the phason excitations [GS88]. However, for a complete study of the thermal to quantum crossover, quantum and thermal fluctuations have to be considered on an equal footing [CHN88, CHN89], which is the main aim of chapter B.

Experimentally, quasi–1D behavior can be seen in real materials, e.g., in whiskers [BDP$^+$93], hairlike single crystal fibers like NbSe$_3$, with a transverse extension smaller than the correlation length or in chain like crystals with weak interchain coupling. In the latter case there is a large crossover length scale up to which 1D behavior can be observed [Grü94b, Grü88, BM99].

The results, which we obtain in the language of CDWs or SDWs, have a large number of further applications in disordered quantum systems: they relate, e.g., to the (Anderson) localization transition of Luttinger liquids [Fuk84, GS88], superfluids [BD84, FG88, RD96, ZGvOZ97], tunnel junction chains [Kor89], and Josephson coupled chains of these systems, if the coupling is treated in mean-field theory [Fuk84].

Apart from the random inhomogeneities, also the influence of periodic potentials has a powerful effect on the low temperature behavior of these system, namely the appearance of a lock-in or Mott transition at zero temperature. The case of a commensurate lattice potential in charge density waves is discussed in chapter B. If the quantum fluctuations are weak, the CDW phase can *lock in* one of the minima of the periodic potential, leading to a localization of the system which is lifted by increasing quantum fluctuations.

Furthermore topological defects can play an important role. We examine a mechanism for so-called *phase-slips* in density waves, which create jumps in the phase field by multiples of 2π. This is motivated by the fact, that the phase is related to the phase of the order parameter of density waves, which remains unchanged under this phase-slippage process. At zero temperature the consideration of that effect leads also to another phase transition between a phase where this effect is negligible, if the quantum fluctuations are weak, and a phase for strong quantum fluctuations, where phase-slips become important.

At this point, some important remarks are in order. The Luttinger liquid (LL) model is used to describe interaction fermions in one dimension. In contrast to higher dimensions, excitations are collective (since one cannot move a single electron without affecting the others in 1D) and cannot be described by excitations of (nearly free) fermionic quasi-particles, i.e., Fermi liquid theory breaks down in one-dimension. The LL model is derived by bosonizing the linearized fermionic Hamiltonition [Voi94, Gia03]. Therefore, there is an important difference between the CDW phase and the bosonic field in the LL model, and the above mentioned

phase-slips in CDWs cannot be interpreted in the same way in the LL language. Another important assumption in our treatment of density waves is, that charge and spin can be treated separately, i.e., without coupling of spin and charge degrees of freedom.

3 Driven elastic systems

Now we go over to the non-equilibrium situation, i.e., $h > 0$ (cf. Fig. A.1) and restrict ourselves to the classical region ($K = 0$). The driven viscous motion and collective pinning phenomena of interfaces in a medium with random pinning forces is one of the paradigms of condensed matter physics (for reviews see, e.g., [Fis98, Kar98, SDM01, BN04]). If the system is driven adiabatically - which means the system is always in a steady state even if the driving force is changed - with a constant force, the mean velocity of the elastic object shows a depinning transition at zero temperature [NSTL92, NF93, NF92a, Fis83, LNST97, EK94, CDW01, DWC02] or creep motion at finite temperatures [IV87, Nat87, NSV90a, LFC$^+$98]. If the driving force is much larger then the depinning force h_c, disorder becomes irrelevant and the system *flows* as in the case without disorder, i.e., the velocity is proportional to the external force. The regions of different velocity behaviors in this dc-case are shown in Fig. A.3).
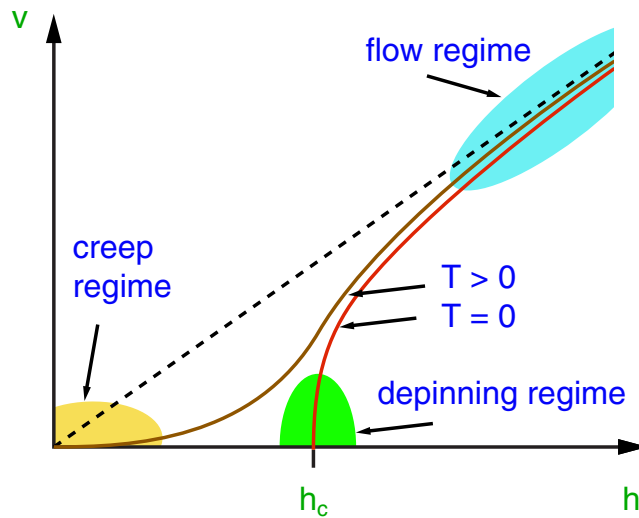

Figure A.3: Velocity of an adiabatically dc-driven interface at zero and finite temperatures as function of a dc driving force h. One can identify different regimes: (i) at $T = 0$ the depinning regime near the depinning force h_c, (ii) at finite temperature the creep regime at low driving forces, and (iii) the the flow regime for high driving forces. (Graphic taken from Ref. [BN04])

In the end of chapter B, we consider the case of a dc driven one-dimensional charge-density wave and study the fluctuations (noise) of the velocity, which is proportional to the current in the system. The noise in any system is characterized in terms of the shape of its spectral power density $S(f)$, which can be measured directly in experiments. If $S(f) \sim f^{-\gamma}$ and $\gamma \approx 1$, then such a noise is referred to as $1/f$ or *flicker noise*. Its existence has attracted the attention of researchers from various branches of the natural sciences for many years. As for physical systems, $1/f$ noise has been observed as fluctuations in the currents of diodes, vacuum tubes, and transistors, the resistance of carbon microphones, metallic thin films, and semiconductors [Vos79, Hoo76], the magnetization in spin glasses [RKM$^+$86] and in many other systems. However, motivated by experimental evidence of flicker noise in driven charge density waves, we analyze the spectrum of the related elastic model and can reproduce the experimental findings.

Other examples where the consideration of an external force is important, are domain wall motion of a magnetically or structurally ordered systems with impurities [You99] or when an interface between two immiscible fluids is pushed through a porous medium [REDG89]. Closely related problems are the motion of a vortex line in an impure superconductor [BFG$^+$94, NS00], or of a dislocation line in a solid [IV87]. More recently, the motion of interfaces in magnets, subject to an external ac force, changing *adiabatically* in time, has been studied [LNP99, NPV01a].

Up to now we have only considered the adiabatic case. The second main part, chapter C, of this thesis is, however, devoted to the non-adiabatic ac motion of driven interfaces or domain walls. An overview of the behavior of these systems in case of oscillating driving forces is shown in Fig. A.4.

With finite frequency of the external driving force the (adiabatic) depinning transition is smeared and disappears completely above a *pinning* frequency ω_P. A main feature of the non-adiabatic driving is the appearance of a velocity hysteresis, which is studied in chapter C.

In order to make a connection to experiments on driven domain walls in magnetic systems, we examine the complex ac susceptibilities obtained from the interface model. Since experimental systems are finite, we also take this effect into account, leading to a saturation of the magnetization. Using a numerical approach, the experimental results can be explained with the model.

In the last part of chapter C we study also non-random inhomogeneities - additionally to the disorder -, namely the influence of surface potentials on the dynamics of disordered elastic systems. Surface barriers are known to be relevant in many cases mentioned above, e.g.,
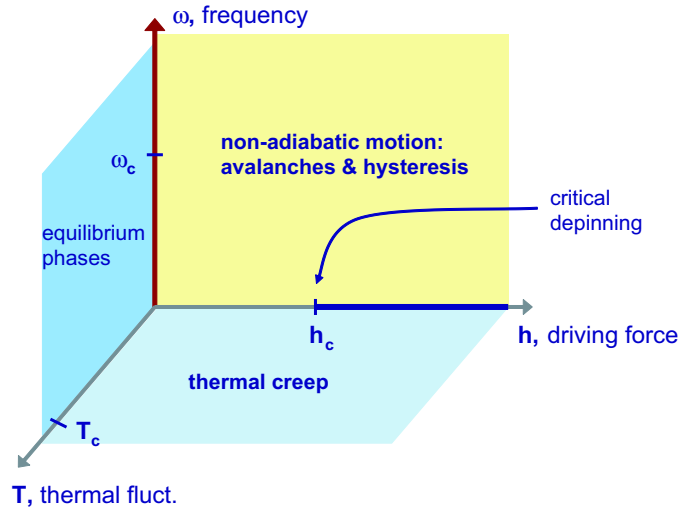
Figure A.4: Different regions in the parameter space of temperature T, external driving force amplitude h and frequency ω. Additional to the non-equilibrium regions shown in Fig. A.1, the frequency of the external driving force is another parameter, smearing the depinning transition, which disappears completely above a threshold frequency ω_c. Additional non-adiabatic phenomena like avalanches are important.

in superconductors they prevent the penetration of new flux lines into the probe [FZR$^+$98]. In CDWs normal electrons have to be converted into those condensed in the CDW at the contacts by a phase–slip mechanism which is essentially a nucleation process [BKR$^+$00, RMAE92]. The motion of domain walls may be hindered by a variation of the width of the sample such that position of minimal width are preferred etc. Experimental [MT86b] and numerical [MT86a] studies of CDWs with contact effects revealed hysteretic behavior of the polarization, which is related to the curvature of the parabolic displacement profile. We study the behavior of this curvature and focus on the hysteretic behavior, which is in agreement with the experiments.

B Influence of thermal and quantum fluctuations in one-dimensional disordered systems

1 Introduction

In this chapter we study mainly the equilibrium properties of one-dimensional disordered systems in the quantum regime at low temperature. Only in the last part we go over to the dynamics. We will use mostly the terminology of charge density waves, which is essential for the last three sections of this chapter.

The chapter is organized as follows: In section 2 we give a detailed introduction to our model and the notation used in this chapter. We also briefly discuss the influence of Coulomb interaction on the properties of the system. In section 3 the influence of disorder is studied in detail. Using an anisotropic momentum shell renormalization group calculation, in which the full Matsubara sum over frequencies is performed, we obtain flow equations for the effective strength of the disorder, thermal and quantum fluctuations (i.e., the interaction strength in the case of Luttinger liquids). These are discussed first in the case of zero temperature and are in agreement with previously obtained results [Fuk84, GS88]. At finite temperatures the disorder is always renormalized to zero. In the classical limit two more methods are applied: (i) at low temperatures and strong disorder the ground state of the model is calculated exactly. (ii) For weak disorder and strong thermal fluctuations a second RG calculation is applied which is based on the mapping onto a Burgers equation with noise. The main result of this chapter is the calculation of the low temperature quantum crossover diagram for one-dimensional CDWs. Using all these findings, the complete phase diagram, including the crossover regions, of the system is studied in section 4 with help of the density-density correlation function. In the following section 5 we discuss briefly the application of the results to superfluids by using the mapping to CDWs.

The influence of a commensurate lattice potential on a free density wave is considered in section 6. The full finite temperature renormalization group flow equation for this sine-

Gordon type model are derived and resulting phase diagram is discussed. Furthermore a qualitative picture of the combined effect of disorder and a commensurate lattice potential at zero temperature is presented in section 7, including the phase diagram.

In section 8 we present a possible mechanism for quantum phase-slips. The model which describes these processes can be written, like in the commensurate lattice potential case, as a sine-Gordon type model, with the important difference, that it is written in terms of a dual phase with respect to the density wave phase. The motivation to consider phase-slip is, that the phase field which describes the systems can be considered as the phase of the density wave order parameter. At zero temperature the consideration of those leads also to a new scenario for the unpinning (delocalization) transition, which is considered in section 9.

In the final section 10 of this chapter, we go over to the study of transport properties of CDWs in the classical creep regime. Especially we focus on the analysis of the current noise, which we compare to experimental results. The noise is studied in a classical one-dimensional charge density wave system in the weak pinning regime by solving the overdamped equation of motion numerically. At low temperatures and just above the zero temperature depinning threshold, the power spectrum of the current noise $S(f)$ is found to scale with frequency f as $S(f) \sim f^{-\gamma}$, where $\gamma \approx 1$, suggesting the existence of *flicker noise*. Our result is in agreement with experimental findings for quasi-one-dimensional charge density wave systems.

In the appendix to this chapter (E1) we present the calculation of the renormalization group flow equations and the derivation of the correlation function in the strong and weak pinning limit in some detail. Also a list of all symbols used in this chapter with corresponding references in the thesis is summarized at the end of this appendix.

2 Model

2.1 Charge and spin density

In this section we derive the effective Hamiltonian which will be the starting point for our further treatment. The strategy of the calculation is therefore separated into two steps. In the first step the system is treated in a mean-field-(MF) type approximation applied to a microscopic Hamiltonian. This leaves us with a slowly varying complex order parameter field for which we derive an effective Hamiltonian. The second step involves the consideration of the fluctuations of this order parameter.

Now we briefly summarize the result of the mean-field calculation. For a detailed review we refer to the book [Grü94b]: Well below the mean-field condensation temperature T_c^{MF} of the CDW, the underlying lattice will be periodically distorted with a period λ which is related to

the Fermi wave vector k_F by $\lambda = \pi/k_F$. This distortion of the lattice leads to the formation of a gap in the dispersion relation at $k = \pm k_F$ which is (in one dimension) proportional to the amplitude of the lattice modulation. For small displacements (which are typically smaller than 1% of the interatomic spacing [Tho96]), the increase of the elastic energy is smaller than the gain of electronic energy due to the formation of the gap and hence an instability is favored. The period of the CDW depends on the band filling factor (via $k_F = \pi/\lambda$) and is in general at arbitrary band filling incommensurate with the undistorted lattice (with lattice constant a). Different situations are shown in Fig. B.1.
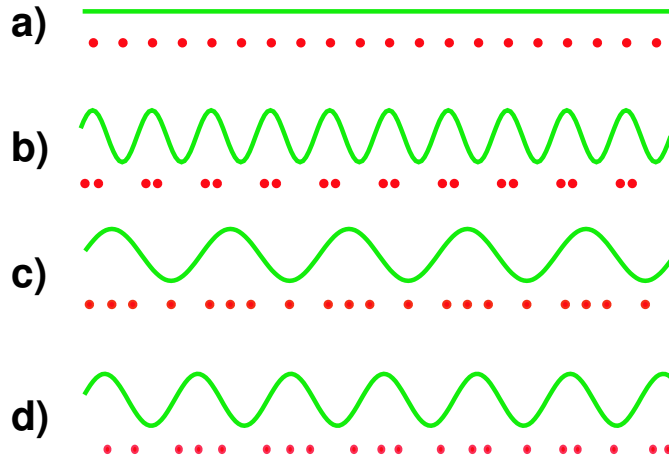
Figure B.1: Sketch of the electron density (solid line) and the atom positions (filled circles) for: a) a one-dimensional metal, b) CDW at half filling, c) quarter filling and d) incommensurate, near third filling.

In (quasi-)one–dimensional systems [Grü94a] also SDWs can be found, but in contrast to CDWs they arise due to electron–electron and not to electron–phonon interaction. A SDW can be considered to consist of two CDWs, one for spin–up and another for spin–down electrons (see, e.g., Fig. 5 in [Grü94a]). Therefore the spatial modulation of SDWs is characterized by a wave vector $Q = 2k_F$, as for CDWs.

The charge or spin density $\rho(x,t)$ can be written in the form [Grü94a, EG86, WE97]

$$\rho(x,t) = (1 + Q^{-1}\partial_x\varphi(x,t))[\rho_0 + \rho_1 \cos(p\varphi(x,t) + pQx)] \qquad \text{(B2.1)}$$

where $\rho_0 = Qf(T)/\pi$ and $\rho_1 = 2|\Delta|/(\pi g v_F)$. g is the dimensionless electron-phonon coupling constant and v_F the Fermi velocity. ρ_1 is proportional to $|\Delta|$, the CDW gap or the amplitude of the complex (mean field) order parameter

$$\Delta(x,t) = |\Delta(x,t)|e^{i\varphi(x,t)}. \qquad \text{(B2.2)}$$

f is the condensate density ($Y = 1 - f$ is the so-called *Yoshida function*) related to $|\Delta|$ by [EG86, WE97]

$$f(T) = \frac{\pi T}{\hbar} \sum_{\omega_n} \frac{(|\Delta|/\hbar)^2}{(\omega_n^2 + (|\Delta|/\hbar)^2)^{3/2}}, \quad \omega_n = 2\pi n T/\hbar. \qquad \text{(B2.3)}$$

From this expression one finds that $f(T)$ approaches 1 for $T \to 0$ (by integration) and $f(T) \simeq 2(1 - T/T_c^{MF}) \sim |\Delta|^2$ for $T \to T_c^{MF}$. T_c^{MF} denotes the mean-field transition temperature. For quasi one–dimensional systems ρ_1 has an additional factor ζ^{-2} (the inverse area perpendicular to the chain).

Note, that (B2.1) is correct for arbitrary band filling and, to be more precisely, is the particle density of the charge or spin carrying particles. Since $4k_F$ modulations of SDWs or CDWs are also possible [TS01], we introduce the factor p in the argument of the modulating cosine function, i.e., for CDWs and SDWs p is usually 1, but can also be 2 or greater.

In (B2.1) we omitted higher harmonics proportional to $\cos\left(np(\varphi(x,t) + Qx)\right)$ with $n \in \{2, 3, \ldots\}$, since these more strongly oscillating terms give close to the zero temperature transition only small contributions in the renormalization process, compared to the leading $n = 1$ contribution. They will therefore be neglected throughout this chapter. Note, that p is the integer describing the ground 'oscillation'. The particle current density j follows from (B2.2) as $j = -\rho_0 \dot{\varphi}/Q$.

2.2 Hamiltonian

In the following we use a minimal model for the low energy, long wave length excitations of the condensed charge density wave. Since fluctuations in the amplitude $|\Delta|$ are suppressed, because they are massive, we take only fluctuations of the phase φ (cf. eq. B2.2) into account. Clearly, such an approach breaks down sufficiently close to the mean-field transition temperature T_c^{MF}. Neglecting fluctuations in $|\Delta|$, the Hamiltonian for our model is given by

$$\hat{\mathcal{H}} = \hat{\mathcal{H}}_0 + \hat{\mathcal{H}}_u + \hat{\mathcal{H}}_w + \hat{\mathcal{H}}_\varpi \qquad \text{(B2.4)}$$

with

$$\hat{\mathcal{H}}_0 \equiv \int_0^L dx \frac{c}{2} \left[\left(\frac{v}{c} \right)^2 \hat{P}^2 + (\partial_x \hat{\varphi})^2 \right] , \tag{B2.4a}$$

$$\hat{\mathcal{H}}_u \equiv \int_0^L dx\, U(x) \rho(x) , \quad U(x) = \sum_{i=1}^{N_{imp}} U_i \delta(x - x_i) , \tag{B2.4b}$$

$$\hat{\mathcal{H}}_w \equiv - \int_0^L dx\, W \cos \left(q \hat{\varphi}(x) \right) , \tag{B2.4c}$$

$$\hat{\mathcal{H}}_\varpi \equiv \widetilde{W} \int_0^L dx\, \cos \left(\frac{\tilde{q} \pi}{\hbar} \int^x dy \hat{P}(y) \right) . \tag{B2.4d}$$

$\hat{\mathcal{H}}_0$ describes the phason excitations of the CDW, where $c = \frac{\hbar v_F}{2\pi} f(T)$ denotes the elastic constant. $v = v_F / \sqrt{1 + (2|\Delta|/\hbar \omega_{pQ})^2 / (gf)}$ is the effective velocity of the phason excitations with ω_{pQ} the phonon frequency. For CDWs $(2|\Delta|/\hbar \omega_{pQ})^2 / (gf) \gg 1$ is typically fulfilled and hence quantum fluctuations are weak.

$\hat{P}$ is the momentum operator, corresponding to the phase $\hat{\varphi}$, with the standard commutation relation $[\hat{P}(x), \hat{\varphi}(x')] = \frac{\hbar}{i} \delta(x - x')$

$\hat{\mathcal{H}}_u$ results from the effects of impurities with random potential strength U_i and positions x_i. The potential strength is characterized by $\overline{U_i} = 0$ and $\overline{U_i U_j} \equiv U_{imp}^2 \delta_{i,j}$, and includes a forward and a backward scattering term proportional to ρ_0 and ρ_1, respectively. The disorder average of the impurity potential $U(x)$ follows then to be given by $\overline{U(x)} = 0$ and

$$\overline{U(x)U(y)} = \frac{U_{imp}^2}{l_{imp}} \delta(x - y) . \tag{B2.5}$$

We will further assume, that the mean impurity distance $l_{imp} = L/N_{imp}$ is large compared with the wave length of the CDW and, in most parts of the chapter, that the disorder is weak, i.e.,

$$1 \ll l_{imp} Q \ll cQ/(U_{imp}\rho_1). \tag{B2.6}$$

In this case the Fukuyama–Lee length [FL78]

$$L_{FL} = \left(\frac{c \sqrt{l_{imp}}}{U_{imp} \rho_1 p^2} \right)^{2/3} \tag{B2.7}$$

is large compared to the mean impurity distance l_{imp}.

The third term in (B2.4), $\mathcal{H}_w$, includes the influence of a harmonic lattice potential. This term will be discussed section 6 in greater detail.

And the last term (B2.4d) describes the influence of quantum phase-slips by $\varphi = \pm \tilde{q}\pi$. A detailed consideration of this term can be found in section 8.

Our model (B2.4) includes the five dimensionless parameters

$$t = T/\pi\Lambda c \,, \tag{B2.8a}$$

$$K = \hbar v/\pi c \,, \tag{B2.8b}$$

$$u^2 = \frac{(U_{imp}\rho_1)^2}{\Lambda^3\pi c^2 l_{imp}} \,, \tag{B2.8c}$$

$$w = W/\pi c\Lambda^2 \,, \tag{B2.8d}$$

$$\varpi = \widetilde{W}/\pi c\Lambda^2 \,, \tag{B2.8e}$$

which measure the strength of the thermal (t), quantum (K) and disorder fluctuations (u), the periodic potential (w) and the probability of phase-slips (ϖ), respectively. $\Lambda = \pi/a$ is a momentum cut-off. Note, that for non interacting electrons, i.e., $v = v_F$, K takes the value 2 (and not 1 as in the usual Luttinger liquid notation). The classical region of the model is given by $K \ll t$ which can be rewritten as the condition, that the thermal de Broglie wave length

$$\lambda_T = \hbar\beta v = K/(t\Lambda) \tag{B2.9}$$

of the phason excitations is small compared to a.

At $T = 0$, K-values of the order 10^{-2} to 10^{-1} and 1, have been discussed for CDWs and SDWs, respectively [Grü94b, Mak95]. It has to be noted however, that the the expressions relating c and v to the microscopic (mean-field-like) theory lead to the conclusion that K and t diverge by approaching T_c^{MF}, whereas the ratio K/t remains finite.

2.3 Coulomb Interaction

We could also add a *Coulomb interaction* term to our model (B2.4) which can be written as

$$\hat{\mathcal{H}}_c = \frac{1}{2}\int dx \int dx' \hat{\rho}(x)V_c(x-x')\hat{\rho}(x') \,, \tag{B2.10}$$

where V_c is the Coulomb potential. In all dimensions the unscreened potential has the form e^2/r, in the sense that we are dealing with quasi-one-dimensional systems embedded in a 3D space. If we assume, that the quasi one-dimensional system has the finite width ζ, V_c

can be written as [MG95, Sch93]

$$V_c^0(x) = \frac{e^2}{\sqrt{x^2 + \zeta^2}} = \frac{1}{L} \sum_k e^{\imath kx} V_c^0(k) \text{ with} \tag{B2.11}$$

$$V_c^0(k) = 2e^2 K_0(|\zeta k|), \tag{B2.12}$$

where K_0 is a modified Bessel function of second kind with $K_0(x) \approx -\ln(x)$ for $x \ll 1$.

In general the Coulomb potential is screened and can be written as [AA85]

$$V_c(k, \omega) = \frac{V_c^0(k)}{1 + V_c^0(k)\Pi(k, \omega)}, \tag{B2.13}$$

with the momentum and frequency dependent polarization operator, defined by $\Pi(k, \omega) = \langle \rho(0,0)\rho(k,\omega) \rangle$.

If we only consider the static case $\omega = 0$ we can distinguish two limiting cases: First, if the typical range λ_{eff} of the screened Coulomb potential V_c is much smaller than the mean electron distance, the potential can be assumed to be a delta distribution and $\mathcal{H}_c$ can be approximated by

$$\hat{\mathcal{H}}_c \approx \frac{\hbar\chi}{2} \int dx \left(\frac{f(T)}{\pi} \partial_x \varphi(x) \right)^2 + \dots, \tag{B2.14}$$

with $\chi = \frac{1}{\hbar} \int dx V_c(x)$. The cos-terms ($\dots$) from the density can be neglected due to strong fluctuations. Therefore the Coulomb interaction gives only an additional contribution to the elastic constant of the initial model: $c = \frac{\hbar v_F}{2\pi} f + \frac{\hbar\chi}{\pi^2}$. For $\chi > 0$ the Coulomb interaction is repulsive, which leads to an increase of c and therefore a decrease of the dimensionless parameter K, i.e., the quantum fluctuations will be reduced by replusive Coulomb interaction. In the case $\chi < 0$ (attraction), K will be increased. Keeping this consideration in mind, we will not further include $\hat{\mathcal{H}}_c$ in the model explicitly.

In the other case – with weak screening – $V_c(k) \approx V_c^0(k)$ shows the dispersion given in (B2.12) and in general, the details of the k-dependence are not only up to the transverse extension ζ of the quasi one-dimensional system under consideration but also to the screening length [BD84, FG88, ZGvOZ97, MG95].

However, the logarithmic k-dependence will only weakly affect our RG-analysis, but may suppress phase transitions, as discussed later in section 3.2.

Coulomb interaction is also important if one considers multi-channel systems [LF78, Gia03] or the effect of the non–condensated normal electrons.

3 Renormalization group treatment of disorder

3.1 Flow equations

In order to determine the phase diagram we adopt a standard Wilson-type renormalization group calculation, which starts from a path integral formulation of the partition function corresponding to the Hamiltonian (B2.4). We begin with the renormalization of the disorder term and set $w = 0$ and $\varpi = 0$ in the following. The system is transformed into a translational invariant problem using the replica method, in which the disorder averaged free energy is calculated, using

$$\overline{\mathcal{F}} = -T\overline{\ln \mathrm{Tr} e^{-\mathcal{S}/\hbar}} \equiv -T \lim_{n \to 0} \frac{1}{n} \left(\overline{\mathrm{Tr} e^{-\mathcal{S}^{(n)}/\hbar}} - 1 \right) , \tag{B3.1}$$

which defines the replicated action $\mathcal{S}^{(n)}$. $\mathcal{S}^{(n)}$ is given by

$$\mathcal{S}^{(n)} = \sum_{\alpha,\nu} \int_\tau \left\{ \mathcal{L}_{0,\alpha} \delta_{\alpha\nu} + \frac{1}{2\hbar} \int_{\tau'} \overline{\mathcal{H}_u[\varphi_\alpha(\tau)] \mathcal{H}_u[\varphi_\nu(\tau')]} \right\} , \tag{B3.2}$$

where $\mathcal{L}_0$ is the Lagrangian corresponding to $\hat{\mathcal{H}}_0$, $\int_\tau \equiv \int_0^{\hbar\beta} d\tau$ and α, ν are replica indices. Using (B2.5) and consequently neglecting higher harmonics ($2pQ$-modes) one finds

$$\overline{\mathcal{H}_u[\varphi_\alpha(\tau)] \mathcal{H}_u[\varphi_\nu(\tau')]} = \frac{U_{imp}^2 \rho_1^2}{2l_{imp}} \int_0^L dx \left\{ \cos p\Big(\varphi_\alpha(x,\tau) - \varphi_\nu(x,\tau') \Big) + \right.$$

$$\left. + \frac{2\rho_0^2}{Q^2 \rho_1^2} \partial_x \varphi_\alpha(x,\tau) \partial_x \varphi_\nu(x,\tau') \right\} . \tag{B3.3}$$

Together with (B3.2) one obtains the following form

$$\frac{\mathcal{S}^{(n)}}{\hbar} = \frac{1}{2\pi K} \sum_{\alpha,\nu} \int_0^{L\Lambda} dx \int_0^{K/t} d\tau \left\{ \left[(\partial_x \varphi_\alpha)^2 + (\partial_\tau \varphi_\alpha)^2 \right] \delta_{\alpha\nu} - \right.$$

$$\left. \frac{1}{2K} \int_0^{K/t} d\tau' \left[u^2 \cos p\Big(\varphi_\alpha(x,\tau) - \varphi_\nu(x,\tau') \Big) + \sigma \partial_x \varphi_\alpha(x,\tau) \partial_x \varphi_\nu(x,\tau') \right] \right\} , \tag{B3.4}$$

with $\sigma = 2u^2 (\rho_0 \Lambda / \rho_1 Q)^2$.

Note, that we introduced dimensionless spatial and imaginary time variables,

$$\Lambda x \to x ,$$

$$\Lambda v \tau \to \tau ,$$

which will be used throughout chapter B - beginning here. Furthermore all lengths (e.g. correlation lengths, λ_T, L_{FL}, l_{imp}, and L), wave vectors (e.g. k, k_F, and Q) and Matsubara frequencies are dimensionless accordingly, from now on. Additionally we rescale the elastic constant

$$\Lambda c \to c \,,$$

for convenience to avoid the appearance of Λ.

Figure B.2: Momentum "shell" in the space of (discrete) Matsubara frequencies (ω_n) and momenta (k). Only modes of the phase φ in the stripe $1/b \leq |k| \leq 1$ with $b = 1 + 0^+$ are integrate in one RG step.
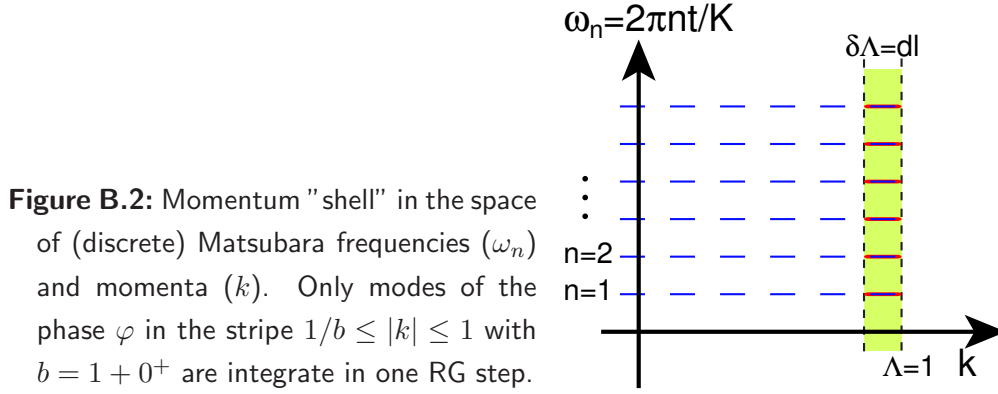
Integrating over the high momentum modes of $\varphi(x,\tau)$ in a momentum shell of infinitesimal width $1/b \leq |k| \leq 1$ with the rescaling parameter $b = 1 + 0^+$, but arbitrary frequencies (see Fig. B.2) and rescaling $x \to x' = x/b$, $\tau \to \tau' = \tau/b$, we obtain the following renormalization group flow equations (up to one loop):

$$\frac{dt}{dl} = t \,, \tag{B3.5a}$$

$$\frac{dK}{dl} = -\frac{1}{2}p^4 u^2 K B_0\left(p^2 K, \frac{K}{2t}\right)\coth\frac{K}{2t}, \tag{B3.5b}$$

$$\frac{du^2}{dl} = \left[3 - \frac{p^2 K}{2}\coth\frac{K}{2t}\right]u^2 \,, \tag{B3.5c}$$

$$\frac{d\sigma}{dl} = \sigma \,, \tag{B3.5d}$$

where $dl = \ln b$. For some more details on the RG calculation we relegate to appendix E1.1 where we have written the RG-flow also for dimensions $|d - 1| \ll 1$. The complete calculations can be found in [Gla03]. Note, that the renormalization group equation for terms in the replica Hamiltonian which follow from higher order harmonics in the charge density look similar to those presented in (B3.5c) with p replaced by np, $n > 1$, integer. Therefore these terms are negligible close to the quantum phase transition considered below. One should keep in mind though, that in the region where $K \ll 1$ at zero temperature, also

those higher harmonics become relevant. But since this is also the parameter range where we leave the weak pinning regime, the RG breaks down anyways.

For legibility we have introduced the following functions:

$$B_i(\nu, y) = \int\limits_0^y d\tau \int\limits_0^\infty dx \, \frac{g_i(\tau, x)}{\Upsilon(\tau, x)} \frac{\cosh(y - \tau)}{\cosh y}, \tag{B3.6}$$

$$\Upsilon(\tau, x) = \left[1 + \left(\frac{y}{\pi}\right)^2 \left(\cosh\frac{\pi x}{y} - \cos\frac{\pi\tau}{y} \right) \right]^{\nu/4}, \tag{B3.7}$$

with

$$g_0(\tau, x) = \delta(x)\tau^2. $$

Note, that $B_0(p^2 K, \frac{K}{2t}) \to 0$ for $K \to 0$ (see Fig. E.1 in appendix E1.1).
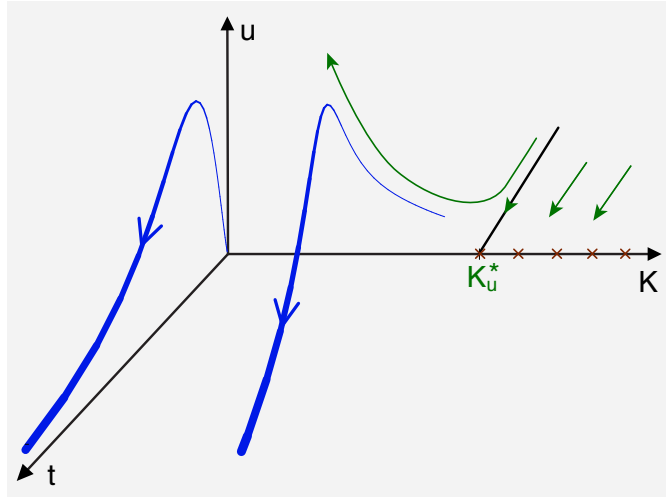
Figure B.3: Typical flow diagram for $w = \varpi = 0$ in the three dimensional parameter space of K, u and t, proportional to the strength of quantum, disorder and thermal fluctuations, respectively.

The strength of the thermal fluctuations t is only rescaled, since there is no non-trivial renormalization of t (i.e., of the elastic constant c) because of a statistical tilt symmetry [SVBO88]. Note, that (B3.4) is written in rescaled dimensionless parameters and the different renormalization of the kinetic and elastic term is reflected in the different renormalization of v and c, i.e., K and t, respectively.

From the flow equation for u^2 (B3.5c) one directly sees that, depending on the sign of the prefactor, the behavior changes from increase for small t and K to decrease for high K or t.

There is no first order RG correction to σ and the change of σ with length scale is simply given by rescaling, see (B3.5d). The two-loop contribution to σ is much more involved than the one-loop contributions for the other flow equations and gives no qualitatively different result for the flow of σ. As seen from (B3.5d), the forward scattering amplitude always increases as $\sigma_0 e^l$ on larger length scales and is therefore not well controlled in the RG sense. But, since the flow of σ does not feed back into the other flow equations it has only minor relevance for our considerations. And indeed, we can get rid of the forward scattering term $f/\pi U(x)\frac{\partial \varphi}{\partial x}$ by introducing the field $\hat{\varphi}_b(x)$ by [SVBO88]

$$\hat{\varphi}(x) = \hat{\varphi}_b(x) - \varphi_f(x) , \quad \varphi_f(x) = \int_0^x dy c(y) , \tag{B3.8}$$

where $c(x) \equiv \frac{U(x)f}{\pi c \Lambda}$, with $\overline{c(x)} = 0$ and $\overline{c(x)c(x')} = \frac{\pi}{2}\sigma\delta(x - x')$. This can easily be verified by inserting this decomposition of $\hat{\varphi}(x)$ into the initial Hamiltonian (B2.4) written in dimensionless units, and using (B2.5) and the definition of σ for deriving the averages of $c(x)$. Note, that x is dimensionless. The typical flow described by the flow equations (B3.5a) to (B3.5c) is shown in Fig. B.3, obtained by a numerical solution.

symbol here	Giamarchi and Schulz	Haldane
$\varphi, \hat{j}$	$\sqrt{2}\phi, \sqrt{2}/\pi\partial_\tau\phi$	$\theta - \pi\rho_0 x, \pi^{-1}\dot{\theta}$
$\hat{P}$	$\hbar\Pi/\sqrt{2}$	$-\frac{\hbar}{\pi}\nabla\varphi$
K	$2K_\rho$	$\sqrt{v_j/v_N}$
v	u_ρ	$\sqrt{v_j v_N}$
c	$\frac{\hbar u_\rho}{2\pi K_\rho}$	$\hbar v_N/\pi$
p	1	2

Table BI: Notation guide. Symbols used in this chapter compared to the notation in Ref. [GS88] by Giamarchi and Schulz (charge operators) and Ref. [Hal81] by Haldane.

3.2 Zero temperature - a review

The special case $t = 0$ was previously considered, e.g., in [GS88, GS87] (for a better comparison see the *notation guide* listed in table BI).

The flow equations for K and u at zero temperature read:

$$\frac{dK}{dl} = -\frac{1}{2}p^4 u^2 K B_0(p^2 K, \infty) , \tag{B3.9a}$$

$$\frac{du^2}{dl} = \left[3 - \frac{p^2 K}{2}\right]u^2 , \tag{B3.9b}$$

with

$$B_0(\nu, \infty) = \int_0^\infty d\tau\, \tau^2 e^{-\tau} \left[1 + \tau^2/2\right]^{-\nu/4}.$$

(B3.10)

The corresponding flow equation for K obtained in [GS88] deviates slightly from (B3.9a), which can be traced back to the different RG procedures. In [GS88] the authors performed the RG at strictly zero temperature and used a symmetric, circular shape of the "momentum–shell", i.e., treated the model as, effectively, isotropic in the 1+1-dimensional space-time.

This procedure may be a good approximation at zero temperature, but if one considerers finite temperatures this does not hold anymore, since the extension in τ-direction is now finite. As a result, there is a region $\pi/L < |k| < \pi/\lambda_T$ where fluctuations are mainly one-dimensional and purely thermal. This region was disregarded in previous treatments. As we will see, fluctuations from this region have an important influence on the overall phase diagram.

The critical behavior is, however, the same: there is a Kosterlitz-Thouless (KT) transition at the phase boundary K_u between a disorder dominated, pinned and a free, unpinned phase which terminates in the fixed point $K_u^* = 6/p^2$. One can derive an implicit equation for K_u by combining (B3.9a) and (B3.9b) to a differential equation

$$\frac{du^2}{dK} = \frac{1}{p^2 \eta K}(K - K_u^*),$$

(B3.11)

which has the solution

$$u^2(K) - u_0^2 = \frac{K_u^*}{p^2 \eta}\left(\frac{K - K_0}{K_u^*} - \ln \frac{K}{K_0}\right),$$

(B3.12)

where u_0 and K_0 denote the bare values of the disorder and quantum fluctuation, respectively, and $\eta \equiv B_0(p^2 K_u^*, \infty)$. Then, K_u is implicitly given by

$$u^2(K_u) = \frac{K_u^*}{p^2 \eta}\left(\frac{K_u - K_u^*}{K_u^*} - \ln \frac{K_u}{K_u^*}\right),$$

(B3.13)

where the initial condition $u^2(K_0 = K_u^*) = u_0^2 = 0$ is used. The KT-flow equations at K_u^* can be recovered by defining

$$2\gamma \equiv \frac{p^2 K}{2} - 3,$$

$$2\chi^2 \equiv \frac{3}{2}p^4 \eta u^2$$

with $|\gamma| \ll 1$. This yields

$$\frac{d\gamma}{dl} = -\chi^2,$$

(B3.14a)

$$\frac{d\chi^2}{dl} = -2\gamma\chi^2,$$

(B3.14b)

which are exactly the flow equations obtained by Kosterlitz and Thouless [KT73].
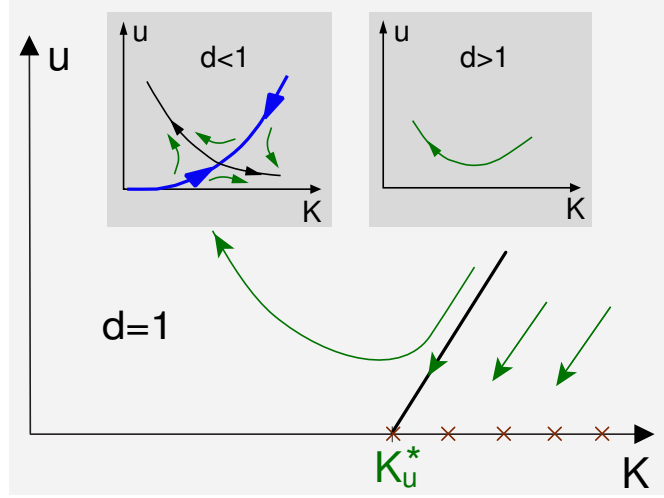
Figure B.4: Schematic zero temperature phase diagram in $d = 1$ and close to $d = 1$ dimensions (see text). u and K denote the strength of the disorder and quantum fluctuations, respectively.

Under the assumption, that a small deviation from the dimension $d = 1$ changes only the naive scaling dimensions of the fields, our results can be extended also to $d = 1 + \epsilon$ dimensions (For details see appendix E1.1). The zero temperature phase diagram is modified and illustrated in Fig. B.4. For $\epsilon < 0$ the fixed point at $(K = K_u^*, u = 0)$ is shifted to positive u-values (see left inset of Fig. B.4), whereas for $\epsilon > 0$, K and u always flow to the strong pinning fixed point (at $K = 0$ and $u \to \infty$; right inset), i.e., quantum fluctuations are too weak to renormalize the random potential to zero. The zero temperature transition disappears therefore for $d > 1$, since the fixed point lies in the unphysical $u < 0$ region of the K-u parameter space. This can easily be verified by using the rescaling of K given in eq. (E1.12c) of appendix E1.1 which results in the flow equation (E1.16). In general this discussion applies to the localization transition as well as to the Mott transition (see discussion of the the lattice potential in section 6). Note, that the flow for $d \neq 1$ is qualitatively different from that discussed in Ref. [Her98], because the model for superfluids in this paper [eq. (7) therein] is dual to our model. Since this mapping can only be done in strictly one dimension, one has to go back to the initial Hamiltonian for superfluids [Hal81] to obtain the rescaling in $d = 1 + \epsilon$.

If one includes the effect of *Coulomb interaction* in $d = 1$ dimension, phase fluctuations of the free phase field increase only as (T=0)

$$\left\langle (\varphi(x,0) - \varphi(0,0))^2 \right\rangle \sim K \ln^{1/2} |x|. \tag{B3.15}$$

As a result, phase fluctuations are too weak to suppress the disorder even for large values of K and the system is always in the pinned phase. The phase diagram is therefore similar to that in $d > 1$ dimensions.

In the pinned phase the parameters K and u flow into the classical, strong disorder region: $K \rightarrow 0, u \rightarrow \infty$.

Integration of the flow equations gives for small initial disorder and $K \ll K_u^*$ an effective correlation or localization length

$$\xi_u \approx L_{FL}^{(1-K/K_u^*)^{-1}} , \tag{B3.16}$$

at which u becomes of the order unity. This can be extracted from (B3.9b), neglecting the flow of K.

A better approximation of ξ_u, which takes also the flow of K into account, can be obtained by replacing u^2 in the flow equation for K (B3.9a) by the expression given in (B3.12). We still use the approximation, that K deviates not much from the bare value K_0 which is the case, as long as $u_0^2 l \ll 1$. Then, the solution for $K(l)$ is given by

$$K(l) \approx K_0 \left(1 - \frac{p^4}{2} u_0^2 \eta l \right) , \tag{B3.17}$$

which yields a solution of (B3.9b):

$$\ln \frac{u^2(l)}{u_0^2} \approx \left(3 - \frac{p^2}{2} K_0 \right) l + \frac{p^6}{8} \eta K_0 u_0^2 l^2 . \tag{B3.18}$$

With $u^2(\ln(\xi_u)) \approx 1$, the correlation length ξ_u is defined by

$$0 = \ln u_0^2 + \underbrace{\left(3 - \frac{p^2}{2} K_0 \right)}_{\equiv a} \ln(\xi_u) + \underbrace{\frac{p^6}{8} \eta K_0 u_0^2}_{\equiv b} (\ln(\xi_u))^2 , \tag{B3.19}$$

which yields

$$
\begin{aligned}
\ln(\xi_u) &= \frac{\sqrt{a^2 - 4b \ln u_0^2} - a}{2b} \\
&\approx -\frac{\ln u_0^2}{3 - \frac{p^2 K_0}{2}} - \frac{p^6}{8} \eta K_0 u_0^2 \frac{(\ln u_0^2)^2}{\left(3 - \frac{p^2 K_0}{2} \right)^3} ,
\end{aligned} \tag{B3.20}
$$

where the first term of the right-hand side gives the result (B3.16).

Close to the transition line, ξ_u shows KT behavior. For $K \geq K_u$, ξ_u diverges and $C(x, \tau) \sim K(l = \ln |z|) \ln |z|$ where $|z| = \sqrt{x^2 + \tau^2}$ (cf. section 4).

3.3 Strong pinning limit: Exact ground state

For large values of u our flow equations break down. Qualitatively the flow is towards large u and small K. We can, however, find the *asymptotic* behavior in this phase by solving the initial model in the *strong pinning limit exactly*. To find this solution we will assume strong pinning centers and weak thermal fluctuations:

$$U_{imp} \to \infty \quad \text{and} \quad c/(p^2 l_{imp}) \gg T. \tag{B3.21}$$

To treat this case, we go back to the initial Hamiltonian (B2.4) (with $W = \widetilde{W} \equiv 0$ and the kinetic term also vanishes because of $K \to 0$). For strong disorder it is convenient to integrate out the phase field $\varphi(x)$ at all points which are not affected by the impurities. Then the effective Hamiltonian takes the form [Fei80]

$$\mathcal{H}_{eff} = \sum_{i=1}^{N} \left\{ \frac{c}{2} \frac{(\varphi_{i+1} - \varphi_i)^2}{x_{i+1} - x_i} + U_i \rho(x_i) \right\} \, , \quad \varphi_i \equiv \varphi(x_i). \tag{B3.22}$$

Under condition (B3.21), φ_i only takes values obeying

$$p(\varphi_i + Qx_i) = 2\pi n_i + \pi \quad \text{with} \quad n_i \in \mathbb{Z} \quad \text{integer} \tag{B3.23}$$

which minimizes the backward scattering term. Defining h_i and ϵ_i by

$$n_{i+1} - n_i \equiv h_i + \left[\frac{pQl_{imp}}{2\pi} \right], \quad x_{i+1} - x_i \equiv l_{imp} + \epsilon_i \tag{B3.24}$$

with $0 \le x_1 \le x_2 \le \ldots \le x_{N+1} \le L$, the effective Hamiltonian can be rewritten as

$$\mathcal{H}_{eff} = \frac{c}{2p^2} \sum_i \frac{(2\pi)^2 \left(h_i - \frac{pQ\epsilon_i}{2\pi} - \gamma \right)^2}{l_{imp} + \epsilon_i} \, . \tag{B3.25}$$

Here $[x]$ denotes the closest integer to x (*Gaussian brackets*):

$$[x] = m \quad \text{for} \quad x \in \left] m - \frac{1}{2}, m + \frac{1}{2} \right] \, , m \in \mathbb{Z} \tag{B3.26}$$

and

$$\gamma \equiv \frac{pQl_{imp}}{2\pi} - \left[\frac{pQl_{imp}}{2\pi} \right], \tag{B3.27}$$

such that $|\gamma| \le \frac{1}{2}$.

Because thermal fluctuations are small compared to the elastic energy, see (B3.21), $(h_i - \frac{pQ\epsilon_i}{2\pi} - \gamma)$ takes on its minimal value, which is given by

$$h_i^0 = \left[\frac{pQ\epsilon_i}{2\pi} + \gamma \right]. \tag{B3.28}$$

This defines the exact ground state of the classical model: If we use (B3.24) one finds for the optimal value of the n_i's

$$n_{i+1}^0 = n_i^0 + \left[\frac{pQ}{2\pi}(\epsilon_i + l_{imp})\right] ,$$

which leads, using (B3.23), to the exact classical ground state

$$\varphi_i^0 = \frac{1}{p}\left(2\pi\left\{n_1^0 + \sum_{j<i}\left[\frac{pQ}{2\pi}(\epsilon_j + l_{imp})\right]\right\} + \pi\right) - Qx_i, \qquad (B3.29)$$

where n_1^0 has an arbitrary integer value (see Fig. B.5).
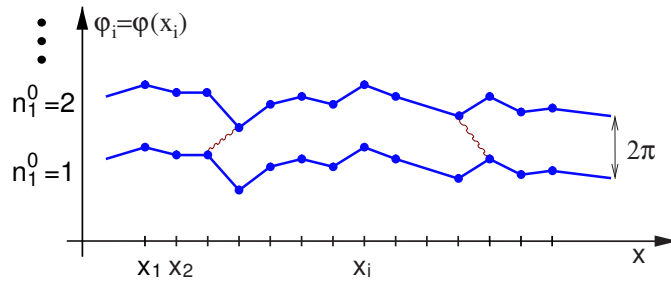
Figure B.5: Ground states in the strong pinning regime characterized by the integer number n_1^0. The wavy lines show an excitation from one ground state forming an instanton configuration which could be a mechanism for quantum tunnelling transport at low temperatures [NGD03, MNR04].

3.4 Finite temperature and crossover diagram

At *finite temperatures* thermal fluctuations wipe out the random potential, which leads to the pinning of the CDW at $t = 0$ and $K < K_u$. Thus, there is no phase transition anymore and the system is always in its delocalized phase, even if the disorder may still play a significant role on intermediate length scales.

In the special case $K \to 0$ the flow equation (B3.5c) reduces to $\frac{du^2}{dl} = \left[3 - p^2 t\right]u^2$ with solution

$$u^2(l) = u_0^2 e^{3l - p^2 t_0(e^l - 1)} . \qquad (B3.30)$$

If we write $t = t_0 e^l$, we may express l by t and hence, we may write u^2 as t-dependent function:

$$u^2(t) = u_0^2(t/t_0)^3 e^{-p^2(t-t_0)} , \qquad (B3.31)$$

which is plotted in Fig. B.3 in the t-u plane.

One sees that the flow of the disorder has a maximum at $t = 3/p^2$ or $l = \ln(3/(p^2 t_0))$, if $t_0 < 3/p^2$. For finite K, the RG flow of u in the region $K < K_u$ first increases and then decreases. The region of increase in the K-t plane is implicitly defined by $\mathcal{M}_u \equiv \left\{(K,t)|K_u^* \geq K \coth \frac{K}{2t} \geq 0\right\}$, i.e., the positions of the maxima of $u^2[K,t]$ are located on the boundary of $\mathcal{M}_u$ defined by $K_u^* = K \coth \frac{K}{2t}$.

The correlation length ξ can be found approximately by integrating the flow equations until the maximum of $u(l)$ and $t(l)/(1 + K(l))$ is of the order one (see discussion in section 4). This can be done in full generality only numerically (see Fig. B.6).
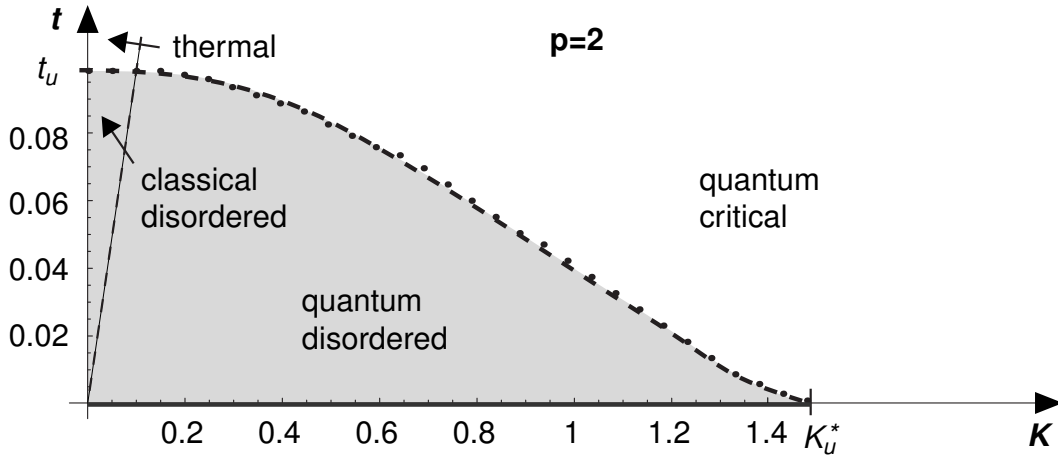
Figure B.6: The low temperature crossover diagram of a one-dimensional CDW. t and K are proportional to the temperature and the strength of quantum fluctuations, respectively. The amount of disorder corresponds to a reduced temperature $t_u \approx 0.1$. In the classical and quantum disordered region, respectively, essentially the $t = 0$ behavior is seen. The straight dashed line separating them corresponds to $\lambda_T \approx 1$, i.e., $K \approx t$, where λ_T is the de Broglie wave length. In the quantum critical region, the correlation length is given by λ_T. Pinning (localization) occurs only for $t = 0, K < K_u^*$.

It is however possible to discuss several special cases analytically. The zero temperature correlation length can still be observed as long as this is smaller than the thermal de Broglie wave length λ_T which can be rewritten for K not too close to K_u as $t \lesssim t_K \approx K t_u^{(1-K/K_u)^{-1}}$ with $t_u \approx L_{FL}^{-1}$, where we defined t_K via $\xi_u \equiv \frac{K}{t_K}$, analogously to the definition of λ_T, and used (B3.16). We call this domain the *quantum disordered region*.

For $K \geq K_u$ the correlation length ξ is given by λ_T which is larger than given by purely thermal fluctuations. For scales smaller than λ_T, the phase correlation function still increases as $\sim \ln |z|$ with a continuously varying coefficient $K_{eff}(u_0)$, as will be discussed in detail in

the next section. In this sense one observes *quantum critical behavior* in that region, despite of the fact, that the correlation length is now finite for all values of K [CHN88, CHN89].

In the *classical disordered region* $t_K < t < t_u$ the correlation length is roughly given by L_{FL} as follows from previous studies [Fei80, VF84] or by solving $u^2(\ln(\xi)) \simeq 1$ using (B3.30) for small t_0 yielding $\xi \approx u_0^{-2/3} e^{-p^2 t_0} \approx u_0^{-2/3} = L_{FL}(\pi p^4)^{1/3}$. Note, that $t_K \approx K$ for small K.

In the remaining region $t \gtrsim t_u$, the *thermal region*, we apply the mapping onto the Burgers equation (see section 4). In this case the RG-procedure applied to this equation becomes trivial, since there is only a contribution from a single momentum shell and one finds for the correlation length $\xi^{-1} \approx \frac{\pi}{2} f(T) t[1 + 1/2[t_u/(\pi p^2 t)]^3]\Lambda$.

The phase diagram depicted in Fig. B.6 is the result of the numerical integration of our flow equations and shows indeed the various crossovers discussed before.

In the *high temperature* region $(t \gg K)$ the flow equations can be solved explicitly. For $u^2(l)$ we get the same result as given in (B3.30) and the flow equation for K reduces to

$$\frac{dK}{dl} = -\frac{p^4}{2} u^2 \frac{K^4}{(2t)^3} \,, \tag{B3.32}$$

where we used $B_0(p^2 K, \frac{K}{2t} \to 0) = (K/2t)^4$. The solution of this equation is given by

$$K(l) = \left[K_0^{-3} + \frac{3p^4 u_0^2}{16 t_0^3} e^{p^2 t_0} \mathrm{Ei}(p^2 t_0, p^2 t_0 e^l) \right]^{-1/3} \,, \tag{B3.33}$$

with the incomplete exponential integral function $\mathrm{Ei}(a, b)$ defined by

$$\mathrm{Ei}(a, b) \equiv \int_a^b dt \, e^{-t}/t \,.$$

One observes that $K(l)$ saturates very quickly at a value $K(\infty) < K_0$.

4 Correlation functions

In this section we discuss the density-density and the phase correlation functions in more detail and summarize all correlation lengths in the various regimes – partly already used in the last two sections.

The (full) density-density correlation function is defined as

$$S(x, \tau) \equiv \langle \rho(x, \tau) \rho(0, 0) \rangle \,, \tag{B4.1}$$

where $\rho(x, \tau)$ is given in (B2.1). In the following we restrict our considerations to the *(charge) density wave order* part of S, which is the term proportional to ρ_1^2, i.e.

$$S_1(x, \tau) = \rho_1^2 \langle \cos p(\varphi(x, \tau) + Qx) \cos p\varphi(0, 0) \rangle \,, \tag{B4.2}$$

which defines the type of order of the density wave: If it decays algebraically we have quasi long–range order (QLRO), an exponential decay over a correlation length ξ corresponds to short–range order (SRO). The omitted parts of S decay faster than S_1 [GS89].

S_1 can be rewritten as

$$S_1(x,\tau) = \frac{\rho_1^2}{4}\left(e^{\imath pQx}\left\langle e^{\imath p(\varphi(x,\tau)-\varphi(0,0))}\right\rangle + e^{-\imath pQx}\left\langle e^{-\imath p(\varphi(x,\tau)-\varphi(0,0))}\right\rangle\right), \qquad \text{(B4.3)}$$

and using a gaussian approximation for the averages, which can be indeed *exact* in lowest order perturbation theory [DW03], we obtain

$$S_1(x,\tau) \simeq \rho_1^2 \cos(pQx)e^{-\frac{p^2}{2}\left\langle(\varphi(x,\tau)-\varphi(0,0))^2\right\rangle}. \qquad \text{(B4.4)}$$

From now on we focus on the *phase correlation function*

$$C(x,\tau) \equiv \left\langle(\varphi(x,\tau)-\varphi(0,0))^2\right\rangle, \qquad \text{(B4.5)}$$

and discuss it in various limits. Combining (B4.4) and (B4.5) we can extract a correlation length from the relation

$$\xi^{-1} = \lim_{x\to\infty}\frac{p^2}{2x}C(x,0). \qquad \text{(B4.6)}$$

An overview of all different correlation lengths is shown in table BII.

4.1 Disorder-free case

We start with the most simple case $u = 0$. Then, the correlation function in dimensionless units follows directly from the action $\mathcal{S}_0$ written in momentum space:

$$C_0(x,\tau) = \frac{2\pi t}{L}\sum_{k,n}\frac{1-e^{\imath(kx+\omega_n\tau)}}{\omega_n^2+k^2}, \qquad \text{(B4.7)}$$

with Matsubara frequencies $\omega_n = 2\pi n/\lambda_T$ and momenta $k = k_m = 2\pi m/L$.

The sums over n and k (i.e., m) can be performed approximately for sufficiently large x and τ and one obtains [Sac99]

$$C_0(x,\tau) \simeq \frac{K}{2}\ln\left(1+\left(\frac{\lambda_T}{2\pi}\right)^2\left[\cosh\left(\frac{2\pi x}{\lambda_T}\right)-\cos\left(\frac{2\pi\tau}{\lambda_T}\right)\right]\right). \qquad \text{(B4.8)}$$

The behavior of this function is considered in the following cases:

(i) At *zero temperature* $(\lambda_T \to \infty)$ (B4.8) reduces to

$$C_0(x,\tau) \simeq \frac{K}{2}\ln\left(\frac{1}{2}\left[x^2+\tau^2\right]+1\right), \qquad \text{(B4.9)}$$

i.e., the correlation function has a logarithmic dependency on x and τ and leads to an algebraic decay of S_1, i.e., the system shows QLRO.

(ii) At *finite temperatures* we can distinguish between length scales smaller and larger than λ_T.

In the first case $x \ll \lambda_T$ and $\tau \ll \lambda_T$ the $\cosh$ and $\cos$ term can be expanded to second order in the arguments and one gets the same logarithmic function as in the zero temperature case. In the opposite case $x \gg \lambda_T$, which is the usual case at high temperatures, the $\cosh$ term can be approximated by the exponential function and one finds a linear dependency on x:

$$C_0(x) \approx \pi t x = T x / c \quad \Longrightarrow \quad \xi = \frac{2}{p^2 \pi t} \equiv \xi_T, \tag{B4.10}$$

i.e., S_1 decays exponentially (SRO) over a characteristic length $\xi \sim t^{-1}$. The same result is obtained for the limit $K \to 0$ at a fixed, finite temperature.

Note, that with this result we have neglected the algebraic decay for small $x < \lambda_T$. Therefore a better interpolation formula for the correlation length is $\xi \approx \frac{2}{p^2}(\xi_T + \lambda_T)$, which takes the slow decay for small x into account. In terms of the length-scale dependent $t(l)$ this rewrites to

$$t(l = \ln(\xi)) = K + 1 \, , \tag{B4.11}$$

i.e., the correlation length is reached, if $t(l)/(1 + K)$ is of order one.
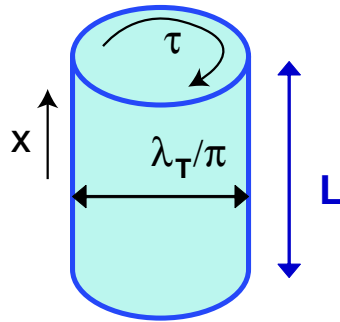
Figure B.7: Topology of the $1+1$ dimensional system at finite temperature. Due to periodic boundary conditions in imaginary time direction the system has a cylinder topology with perimeter of the thermal de Broglie wave length λ_T.

The change from QLRO on small length scales $x < \xi$ to SRO on large length scales becomes clear if one considers the cylindric topology of the system in space-time at finite temperatures: As soon as one reaches length scales of the order of the perimeter of the cylinder, which is λ_T (see Fig. B.7), starting from small scales, the system changes from two-dimensional to effectively one-dimensional behavior.

4.2 Finite disorder

If u is finite, the action of the system has a forward and a backward scattering part. With the decomposition (B3.8), the phase correlation function divides into two parts:

$$C(x, \tau) = C_b(x, \tau) + C_f(x) \qquad (B4.12)$$

and has therefore always a contribution $C_f(x) \sim |x|/\xi_f$ with $\xi_f^{-1} \sim \sigma(l = \ln|x|)$, i.e., the density wave order has always an exponentially decaying contribution and we can define

$$S_1(x, \tau) \equiv f_\rho(x) e^{-\frac{p^2}{2} C_b(x, \tau)}, \qquad (B4.13)$$

with $f_\rho(x) = \rho_1^2 \cos(pQx) e^{-\frac{p^2 \pi}{4} |x|/\xi_f}$. However, since $C_f(x)$ is not τ-dependent, it will not influence the dynamical properties of the system. Therefore all further remarks about phase correlations refer to $C_b(x, \tau)$ and consequently we will drop the subscript b in the following. Again we examine the $T = 0$ and finite temperature cases:

(i) At *zero temperature* we have to distinguish between three K-regimes: For $K > K_u$ the disorder becomes irrelevant under the RG flow and we can use the zero temperature, disorder free result for the correlation function with the pre-factor K replaced by an effective quantity $K_{eff}(l = \ln z)$ on a length scale $z = \sqrt{x^2 + \tau^2}$, defined by the flow equation for K. This effective K saturates on large scales at a fixed point value $K_{eff}(u_0)$, which may be seen in Fig. B.3. Therefore we have QLRO in this K region.

For $0 < K < K_u$ we integrate the flow of u until it reaches a value of order one, starting at small u_0, which defines the localization length ξ_u (see section 3.2), i.e., the correlation function behaves like $C(x, \tau) \sim |x|/\xi_u$, i.e., we have an additional (to C_f) exponentially decaying contribution to S_1.

The third case, $K = 0$, is discussed in the next section.

(ii) At *finite temperatures* the parameter K saturates at an effective value $K_{eff}(u_0)$ on large length scales. Therefore the correlation function for small disorder is given by (B4.8) with K replaced by $K(l = \ln z)$.

In the region $\mathcal{M}_u$ of the K-t plane (see section 3.4), u still increases and we can find an effective correlation length by comparing the length scales on which $u(l)$ or $t(l)/[1 + K(l)]$ become of order one. Then, the correlation length is the smaller length of these two.

For $K = 0$, high temperatures, but weak disorder we adopt an alternative method by mapping the (classical) one-dimensional problem onto the Burgers equation with

noise [HHF85]. With this approach one can derive an effective correlation length given by

$$\xi_B^{-1} \approx \xi_T^{-1} \left(1 + \frac{1}{2} \left[\frac{\xi_T}{2L_{FL}} \right]^3 \right) \tag{B4.14}$$

where $\xi_T \ll L_{FL}$, which changes the prefactor of the free correlation function at high temperatures (B4.10). The full calculation for this result can be found in appendix E1.3.

4.3 Strong disorder

In the last region $K = 0$ for $T \ll c/(p^2 l_{imp})$ we come back to the *strong pinning case*, discussed in section 3.3 before, and calculate the pair correlation function *exactly*. Taking into account that the h_i's are independent on different lattice sites, i.e., $\overline{h_i h_j} \propto \delta_{ij}$, the (discrete) phase correlation function is given by

$$\overline{\left\langle (\varphi_{n+1} - \varphi_1)^2 \right\rangle} = \frac{4\pi^2}{p^2} \overline{\left\langle \left(h_i - \frac{pQ\epsilon_i}{2\pi} - \gamma \right)^2 \right\rangle} \cdot n$$

$$= \frac{4\pi^2}{p^2} \overline{\left(\frac{pQ\epsilon_i}{2\pi} + \gamma - \left[\frac{pQ\epsilon_i}{2\pi} + \gamma \right] \right)^2} n \,,$$

where we used (B3.28) for the second equality. For evaluating the disorder average in this expression, one has to take into account the order statistics of the impurity distances ϵ_i. In the thermodynamic limit the probability density function for the ϵ_i's can be rewritten as

$$p(\epsilon_i) \approx \frac{l_{imp}^{-1}}{e} e^{-l_{imp}^{-1} \epsilon_i} \,, \quad -l_{imp} \leq \epsilon_i < \infty \,. \tag{B4.15}$$

A complete derivation of this expression can be found in [Gla03].

Then, the correlation function can be explicitly written as

$$\overline{\left\langle (\varphi_{n+1} - \varphi_1)^2 \right\rangle} = \frac{4\pi^2}{p^2} \int_0^\infty dx \, e^{-x} \left(\frac{x}{2\alpha} - \left[\frac{x}{2\alpha} \right] \right)^2 n \,, \tag{B4.16}$$

where we introduced the parameter $\alpha \equiv \frac{\pi}{pQl_{imp}}$ and substituted $x = l_{imp}^{-1} \epsilon_i + 1$. This integral can be evaluated exactly, which leads to the following exact expression for the pair correlation function at zero temperature, written in a continuum version:

$$C(x, \tau) = \frac{2\pi}{p\alpha} \left(1 - \frac{\alpha}{\sinh \alpha} \right) |Qx| \equiv \frac{2x}{p^2\xi}, \quad \alpha = \frac{\pi}{pQl_{imp}}. \tag{B4.17}$$

A more detailed derivation of this result is given in appendix E1.2.

Finally, we want to give an interpolating expression for $C(x, \tau)$ from $T = 0$ to high temperatures $T \gg c/(l_{imp}p^2)$ starting with the result (B4.17). In the latter case we may neglect the discreteness of h_i and hence

$$
\overline{\left\langle (\varphi_{n+1} - \varphi_1)^2 \right\rangle}
$$
$$
\approx \frac{4\pi^2}{p^2 l_{imp}} \overline{\left(-\frac{\partial}{\partial \lambda_1} \ln \left(\int dh \, e^{-\sum_i \lambda_i h^2} \right) \right)} |x|
$$
$$
= \frac{T}{c} |x| = \pi t |x| \,, \tag{B4.18}
$$

with $\lambda_i = \frac{2\pi^2 c}{Tp^2(l_{imp} + \epsilon_i)}$.

A plausible interpolation formula is then given by

$$
\overline{\left\langle (\varphi(x) - \varphi(0))^2 \right\rangle} \approx \left(2Q^2 l_{imp} \left(1 - \frac{\alpha}{\sinh(\alpha)} \right) + \frac{T}{c} \right) |x| \,, \tag{B4.19}
$$

and for $l_{imp} \gg Q^{-1}$, i.e., $\alpha \ll 1$:

$$
\overline{\left\langle (\varphi(x) - \varphi(0))^2 \right\rangle} \approx \left(\frac{\pi^2}{3p^2} l_{imp}^{-1} - \frac{7\pi^4}{180p^4} \frac{l_{imp}^{-3}}{Q^2} + \frac{T}{c} \right) |x| \,. \tag{B4.20}
$$

Hence the correlation length acquires the form

$$
\xi_{sp}^{-1} \approx p^2 Q^2 l_{imp} \left(1 - \frac{\alpha}{\sinh(\alpha)} \right) + \xi_T^{-1}. \tag{B4.21}
$$

Note, that $l_{imp}Q \geq 1$, i.e., $\alpha \leq \pi/p$ and $\xi_T \gg l_{imp}$. An approximate crossover to the weak pinning limit follows by choosing $l_{imp} \approx L_{FL}$.

length	description	eq.
ξ_B	weak pinning/high temp. length	(B4.14)
ξ_f	forward scattering length	(B4.12)
ξ_{sp}	strong pinning length	(B4.21)
ξ_T	high temp./disorder free length	(B4.10)
ξ_u	disorder localization length	(B3.16)
ξ_w	lattice pot. correlation length	sec. 6

Table BII: Overview of the dimensionless correlation lengths.

5 Application to superfluids

Next, we consider the application of the results obtained so far to a *one-dimensional Bose fluid*. Its density operator is given by eq. (B2.1) if we identify $Qf/\pi = \rho_0 = \rho_1$ ($p = 2$):

$$\rho_{SF} = \frac{f}{\pi}\partial_x\varphi + \rho_0(1 + \cos(2(\varphi + Qx))) + \ldots \tag{B5.1}$$

$\partial_x\varphi$ is conjugate to the phase θ of the Bose field operator [Hal81]. Keeping our definitions of K, t, and u; v denotes now the phase velocity of the sound waves with $v = \sqrt{\kappa/(\rho_0 m)}$ and the elastic constant is $c = \kappa/(\pi\rho_0)^2$, where κ is the compressibility per unit length (see also table BI).

With the replacements

$$K \rightarrow K^{-1}$$
$$t \rightarrow t/K^2$$
$$p = 2\,,$$

(B3.4) describes the action of the 1D-superfluid in a random potential. The correlation functions for the superfluid can be obtained correspondingly from this replacements. To avoid confusions we write down the full action in this case explicitly:

$$\frac{\mathcal{S}_{SF}}{\hbar} = \frac{K}{2\pi}\sum_{\alpha,\beta}\int_0^L dx \int_0^{K/t} d\tau \left\{ \left[(\partial_x\varphi_\alpha)^2 + (\partial_\tau\varphi_\alpha)^2\right]\delta_{\alpha\beta} - \right. \tag{B5.2}$$

$$\left. \frac{K}{2}\int_0^{K/t} d\tau' \left[u^2\cos 2\Big(\varphi_\alpha(x,\tau) - \varphi_\beta(x,\tau')\Big) + \sigma\partial_x\varphi_\alpha(x,\tau)\partial_x\varphi_\beta(x,\tau')\right]\right\}.$$

Hence the RG-equations follow from (B3.5a) to (B3.5d) with the above given replacements:

$$\frac{dt}{dl} = \left[1 + \frac{16u^2}{K^2}B_0\left(4/K, \frac{K}{2t}\right)\coth\frac{K}{2t}\right]t\,, \tag{B5.3a}$$

$$\frac{dK}{dl} = \frac{8u^2}{K}B_0\left(4/K, \frac{K}{2t}\right)\coth\frac{K}{2t}\,, \tag{B5.3b}$$

$$\frac{du^2}{dl} = \left[3 - \frac{2}{K}\coth\frac{K}{2t}\right]u^2\,, \tag{B5.3c}$$

$$\frac{d\sigma}{dl} = \sigma\,. \tag{B5.3d}$$

I.e., the transition between the superfluid and the localized phase occurs at $K_u^* = 2/3$ [GS88]. Thermal fluctuations again suppress the disorder and destroy the the superfluid localization transition in 1D.

6 Influence of a commensurate lattice potential

If the wave length λ of the CDW modulation is commensurate with the period a ($= \pi$, due to dimensionless units) of the underlying lattice such that $n\lambda = qa$ with integers n and q, the umklapp term $-2\pi(w/K)\cos(q\varphi)$ appears in the Hamiltonian [Grü94b]. Therefore we switch on the lattice potential $w \neq 0$ now. In this section we consider the case $u = 0$ and $\varpi = 0$, which leads to the sine-Gordon type model:

$$\frac{\mathcal{S}_{LP}}{\hbar} = \int\limits_0^L dx \int\limits_0^{K/t} d\tau \left[\frac{1}{2\pi K} \left\{ (\partial_x \varphi)^2 + (\partial_\tau \varphi)^2 \right\} - \frac{w}{K} \cos(q\varphi) \right]. \qquad \text{(B6.1)}$$

The model has q degenerate classical ground states given by $\varphi_m = 2\pi m/q$ with $m = 0, ..., q-1$. Performing a calculation analogous to the one above (but with $u = \varpi = 0$) the RG-flow equations read

$$\frac{dK}{dl} = \frac{\pi}{2} q^4 w^2 B_2 \left(q^2 K, \frac{K}{2t} \right) \coth \frac{K}{2t}, \qquad \text{(B6.2a)}$$

$$\frac{dt}{dl} = \left[1 + \frac{\pi}{2} q^4 w^2 B_1 \left(q^2 K, \frac{K}{2t} \right) \coth \frac{K}{2t} \right] t, \qquad \text{(B6.2b)}$$

$$\frac{dw}{dl} = \left[2 - \frac{q^2}{4} K \coth \frac{K}{2t} \right] w, \qquad \text{(B6.2c)}$$

where $B_{1,2}$ are given in (B3.6) with

$$g_1 = 2x^2 \cos x,$$
$$g_2 = (x^2 + \tau^2) \cos x.$$

Plots of the functions B_1 and B_2 can be found at the end of appendix E1.1. A plot of the numerical solution of (B6.2a) to (B6.2c) is shown in Fig. B.8.

At zero temperature (B6.2a) and (B6.2c) reduce to

$$\frac{dK}{dl} = \frac{\pi}{2} q^4 w^2 B_2 \left(q^2 K, \infty \right), \qquad \text{(B6.3a)}$$

$$\frac{dw}{dl} = \left[2 - \frac{q^2}{4} K \right] w, \qquad \text{(B6.3b)}$$
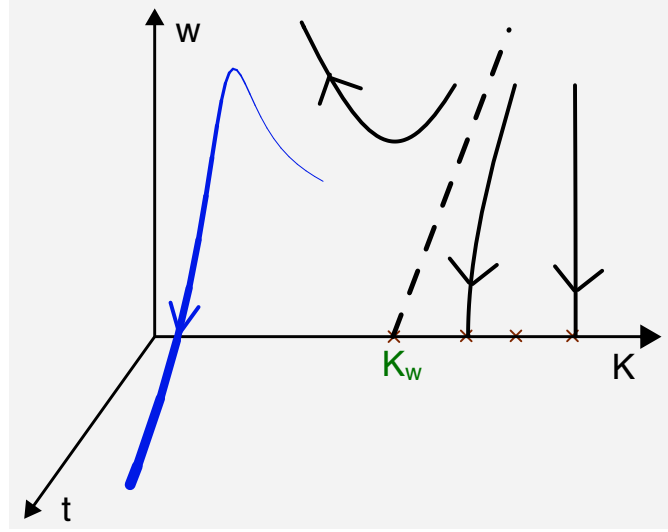
Figure B.8: Typical flow diagram for the disorder free model in the three dimensional parameter space of K, w and t. w denotes the strength of the commensurate lattice potential.

and we find, that the lattice potential becomes relevant (i.e., w grows) for $K < K_w$, where K_w is implicitly defined by

$$w^2(K_w) = \frac{K_w^{*2}}{2\pi q^2 \tilde{\eta}} \left(\frac{K_w}{K_w^*} - 1 \right)^2 , \tag{B6.4}$$

which follows from

$$\frac{dw}{dK} = -\frac{4}{q^4 \pi \tilde{\eta} w} \left(1 - \frac{K}{K_w^*} \right) , \tag{B6.5}$$

where we used (B6.3a) and (B6.3b) and the initial condition $w(K_w^* \equiv 8/q^2) = w_0 = 0$; $\tilde{\eta} = -B_2 \left(q^2 K_w^*, \infty \right)$ (≈ 0.4, for $q = 1$).

In this region the periodic potential stabilizes true long-range order of the CDW: the phase is everywhere close to one of the q classical ground states φ_m. The *depinning transition from the lattice* for $K \nearrow K_w$ is again of KT type. The correlation length ξ_w in the low-K ordered phase is defined by $w(\ln \xi_w) \approx 1$ and diverges at $K_w - 0$ [BD84, FG88, ZGvOZ97]. This can be seen by considerations analogous to the disordered case. Defining

$$\gamma = 2\frac{K}{K_w^*} - 2 ,$$
$$\chi^2 = \frac{\pi}{8} q^6 \tilde{\eta} w^2$$

(note that $\tilde{\eta} > 0$) leads for $|\gamma| \ll 1$, i.e., close to K_w^*, to the KT equations (B3.14a) and (B3.14b).

At finite temperatures we find a similar scenario as in the case where we considered the influence of the disorder: w first increases in a region in the $K{-}t$ plane which is defined by $\mathcal{M}_w \equiv \left\{ (K,t) | K_w^* \geq K \coth \frac{K}{2t} \geq 0 \right\}$, i.e., when the right-hand side of (B6.2c) is positive, but then decreases and flows into the region of large t and small w. Thus the periodic potential becomes irrelevant at finite temperatures. This can be understood as follows: at finite t the 1D quantum sine-Gordon model can be mapped on the Coulomb gas model on a torus of perimeter λ_T since periodic boundary conditions apply now in the τ-direction. Whereas the entropy of two opposite charges increases for separation $L \gg \lambda_T$ as $\ln(L\lambda_T)$, their action increases linearly with L. Thus, the charges remain bound. The one-dimensional Coulomb gas has indeed only an insulating phase [Len61].

7 Disorder and lattice potential

In this section we consider the combined influence of the disorder and the umklapp term at zero temperature. Although the RG calculation breaks down for $K < \max(K_u, K_w)$, the
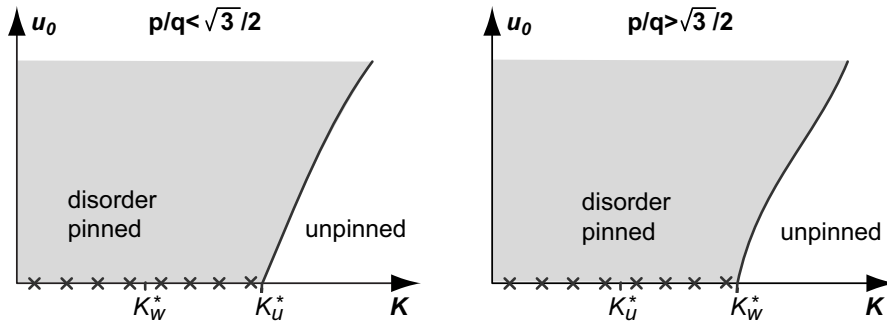
Figure B.9: Qualitative zero temperature phase diagram for a system with commensurate lattice potential and small disorder. One has to distinguish two cases: (i) $K_w^* < K_u^*$ (or $p/q < \sqrt{3}/2$) and (ii) $K_w^* < K_u^*$ (or $p/q > \sqrt{3}/2$). The phase boundaries can be estimated by Imry-Ma arguments (see text).

common influence of both the random and the commensurate potential can be estimated by combining the results obtained so far with Imry-Ma arguments [IkM75]. We distinguish the following cases:

(i) *Case:* $K > \max(K_u, K_w)$. Both disorder and the umklapp term become irrelevant and the system is asymptotically free. The order is of quasi-long-range type.

(ii) *Case:* $K_u < K < K_w$ *(i.e.* $p > \frac{\sqrt{3}}{2} q$*).* This is the region where in the absence of the umklapp term the disorder would still become irrelevant. The umklapp term favors

phase values $\varphi_m = 2\pi m/q$, $m = 0, ..., q - 1$, equally. We consider now the stability of one of these phases, say with $m = 0$, with respect to the formation of domains with $m \neq 0$ due to the disorder. Since the disorder is completely correlated in the τ-direction, it is clear that these domains - if they exist - are stripe-like with an infinite extension in this direction.

In the presence of weak disorder the free energy density of this stripe domain state is given by

$$f_{domain} = (qw^{1/2}L_x^{-1} - uL_x^{-1/2}),\qquad\qquad\text{(B7.1)}$$

where L_x denotes the extension of these domains. $qw^{1/2}$ is the surface tension of the domain wall. Minimizing f_{domain} leads to $L_x \simeq q^2 w/u^2$. To determine whether the disorder or the lattice potential dominate in the considered K region, we study the behavior of L_x on larger length scales by using the flow equations

$$L_x(l) \propto \frac{w_{eff}(l)}{u_{eff}^2(l)} \approx \frac{\xi^{-2}w(l)}{\xi^{-3}u^2(l)} = \xi \frac{w(l)}{u^2(l)},\qquad\qquad\text{(B7.2)}$$

where $\ln \xi = l$. The effective parameters follow from the unrescaled flow equations which are expressed by the renormalized and rescaled quantities as given in (B7.2). At the correlation length ξ_w, where the renormalization stops ($w \approx 1$), L_x behaves like

$$L_x(\ln \xi_w) \equiv \xi_u = \text{const} \times \frac{\xi_w}{u^2(\ln \xi_w)}\qquad\qquad\text{(B7.3)}$$

and therefore $\xi_u > \xi_w$. We conclude that even though the disorder in the absence of the periodic potential is irrelevant for $K > K_u$, the decay of u is stopped due to the suppression of the φ fluctuations which in turn are due to w, and the ordered state $\varphi = \varphi_m = 2\pi m/q$ state is destroyed on the scale ξ_u by arbitrarily weak disorder. In the space direction the system decomposes into domains of extension ξ_u. Note, that there are still long-range correlations in the τ-direction since the disorder is frozen. For these reasons we expect only two phases, a free phase for $K > K_w$ and a pinned phase for $K < K_w$ (see right diagram in Fig. B.9).

(iii) *Case:* $K_w < K < K_u$ *(i.e.* $p < \frac{\sqrt{3}}{2}q$*) or* $K < \min(K_u, K_w)$. In this case the above considerations suggest that the disorder dominates the lattice potential even more, and we again expect only two phases (see Fig. B.9).

To conclude, for $K < \max(K_u, K_w)$ disorder turns out to be always relevant with $\xi_u \approx \xi_w/u^2(\ln \xi_w)$.

8 Phase-Slips

So far the phase field was considered to be single valued. Since the order parameter (B2.2) of the CDW is complex, its phase is given however only up to multiples of 2π. Taking into account also fluctuations in its amplitude $|\Delta|$ the phase may change indeed by multiples of 2π by orbiting a zero of the amplitude. (Throughout this section we always assume $p = 1$). In two or three dimensional space phase vortices correspond to dislocations in the CDW lattice. It is well known that these dislocation play an important role in the conversion mechanism of normal electrons into those condensed in the CDW [BM91]. In strictly one-dimensional systems, such vortices may occur in space-time and correspond to quantum phase-slips. For a quantum phase-slip the contour integral (contour $\mathcal{C}$) of the phase field around the space-time vortex:

$$\oint_{\mathcal{C}} d\varphi = \oint_{\mathcal{C}} \left(\frac{\partial \varphi}{\partial x} dx + \frac{\partial \varphi}{\partial \tau} d\tau \right) = \tilde{q}\pi, \tag{B8.1}$$

is non-zero. If we rewrite $\pi^{-1} \frac{\partial \varphi}{\partial x} = \rho(x, \tau)$ and $\pi^{-1} \frac{\partial \varphi}{\partial \tau} = -\tilde{j}(x, \tau)$, we get from (B8.1)

$$\oint_{\mathcal{C}} (\rho dx - j d\tau) = -\iint dx d\tau \left(\frac{\partial \tilde{j}}{\partial x} + \frac{\partial \rho}{\partial \tau} \right) = \tilde{q}. \tag{B8.2}$$

Going over to real time $t = -\imath\tau$ and current $j(x,t) = \imath\tilde{j}(x,\tau)$ we find from (B8.2) that the continuity equation describing the flow of charges in the condensate is violated. There is an extra term $\dot{\rho}_{ext}$ which describes the creation and annihilation of electron pairs in the condensate. Thus we rewrite the continuity equation in the form

$$\dot{\rho}_{ext} + \dot{\rho}(x,t) + \partial_x j(x,t) = 0 \tag{B8.3}$$

with $\iint dx dt \, \dot{\rho}_{ext} = \tilde{q}$: at the position of a space-time vortex ($\tilde{q} = 2$), two electrons of the reservoir of normal electrons are transferred to the condensate where they form a bound pair (and vice versa).

We propose a model for these space-time vortices which is described by the last term in (B2.4) (with $\tilde{q} = 2$). Here we discuss its influence under equilibrium conditions. This operator superposes two translations of φ by $\pm\tilde{q}\pi$ left from x, i.e., it changes coherently the phase by $\pm\tilde{q}\pi$ in a macroscopic region. For vanishing disorder the model can be mapped on the sine-Gordon Hamiltonian for a field θ by using the canonical transformation $\hat{P} = -\frac{\hbar}{\pi}\partial_x\hat{\theta}$ and $-\frac{\hbar}{\pi}\partial_x\hat{\varphi} = \hat{\Pi}$ (and with K replaced by K^{-1}), which leads to the action:

$$\frac{\mathcal{S}}{\hbar} = \frac{K}{2\pi} \int\limits_0^{L\Lambda} dx \int\limits_0^{K/t} d\tau \left\{ (\partial_x\theta)^2 + (\partial_\tau\theta)^2 + \frac{2\pi\varpi}{K^2}\cos(\tilde{q}\theta) \right\} . \tag{B8.4}$$

Note, that the forward scattering term due to disorder would not influence the phase–slips if present. This can be seen as follows: The forward scattering term from (B2.4), $\int dx\, U(x)\partial_x\varphi/\pi$, is rewritten to an action

$$
\begin{aligned}
\mathcal{S}_f \;&\propto\; \int dx \int\limits_0^{\hbar\beta} d\tau\, U(x)\partial_\tau\theta(x,\tau) \\[2ex]
&= \int dx\, U(x)[\theta(x,\hbar\beta)-\theta(x,0)] - \int dx \int\limits_0^{\hbar\beta} d\tau\, [\partial_\tau U(x)]\theta(x,\tau) = 0\,, \quad \text{(B8.5)}
\end{aligned}
$$

i.e., there is no coupling of the disorder to the phase–slips. A more general argument is, to rewrite the action in the φ-field to the form $\propto \int dz(\mathbf{\nabla}_z\varphi(\mathbf{z}) - \mathbf{A}(\mathbf{z}))^2$ with $\mathbf{z} = (x,\tau)$ and calculate $Q_v = \mathrm{curl}_z\mathbf{A}(\mathbf{z})$ which is the "charge" of the frozen vortices, see Ref. [NSKL95]. If $Q_v = 0$ then there is no coupling to the forward scattering term, which is true in our case with $\mathbf{A}(\mathbf{z}) = (U(x)/\pi, 0)$.

To see the connection of the sine-Gordon model (B8.4) to space-time vortices, one rewrites the action of interacting vortices as a classical $2D$ Coulomb gas model. For illustration we show this for a single space–time vortex at (x_V, τ_V) (dimensionless units), which is introduced "by hand" in the free model ($\mathcal{H}_0$) in the following way: The vortex-free phase variable φ is replaced by a new phase $\phi = \bar{\varphi} + \varphi$, where φ is the vortex free part and $\bar{\varphi}$ is defined by

$$
\tilde{q}\pi \equiv \oint_{\mathcal{C}} d\bar{\varphi}\,, \qquad\qquad \text{(B8.6)}
$$

where $\mathcal{C}$ is a contour around the vortex in x-τ-space. The phase $\bar{\varphi}$ is then extended to a holomorphic function $\Phi \equiv \bar{\varphi} + \imath\bar{\varphi}'$ and the above equation is rewritten to

$$
\begin{aligned}
\iint dx\, d\tau\, \rho_V(x,\tau) \;&=\; \oint \left(\frac{\partial\bar{\varphi}}{\partial x}dx + \frac{\partial\bar{\varphi}}{\partial\tau}d\tau \right) \\[2ex]
&= \oint \left(\frac{\partial\bar{\varphi}'}{\partial\tau}dx - \frac{\partial\bar{\varphi}'}{\partial x}d\tau \right) \\[2ex]
&= -\iint dx\, d\tau\, (\partial_x^2\bar{\varphi}' + \partial_\tau^2\bar{\varphi}')
\end{aligned}
$$

with $\rho_V(x,\tau) = \tilde{q}\pi\delta(x - x_V)\delta(\tau - \tau_V)$. This leads to $(\partial_x^2 + \partial_\tau^2)\bar{\varphi} = -\rho_V(x,\tau)$ with solution

$$
\bar{\varphi}(z) = -\tilde{q}\pi\ln(z - z_V)\,, \qquad\qquad \text{(B8.7)}
$$

where we used again the Cauchy-Riemann differential equations and $z = \sqrt{x^2 + \tau^2}$.

I.e. we have shown that space-time vortices in $1+1$ dimensions can be described by a 2D (classical) Coulomb gas model.

Now, the Coulomb gas model can be subsequently mapped to the sine–Gordon model [JKKN77]. Note, that in order to make contact with reference [JKKN77] one has to replace in this reference $y_0 \rightarrow -\varpi/(2K)$, $K \rightarrow \tilde{q}^2/(4\pi K)$ and $\phi \rightarrow 2K/\tilde{q}\theta$ to recover (B8.4).

The initial value ϖ_0 of ϖ is proportional to the fugacity $\varpi_0 \approx e^{-S_{core}/\hbar}$ of the space-time vortices which may be not negligible close to T_c^{MF}, where the action S_{core} of the vortex core is small. To calculate the core action, one has to allow fluctuations δ of the amplitude of the complex order parameter. Therefore we write

$$\Delta_{MF}(x,t) = (|\Delta| + \delta(x,t))e^{\iota\varphi(x,t)},\qquad(B8.8)$$

and the action for δ, which follows from the *Ginzburg–Landau* free energy for the full order parameter (B8.8), is given by [Grü94b]

$$S_\delta/\hbar = \frac{1}{\hbar}\int\limits_0^L dx \int\limits_0^{\hbar\beta} d\tau \left\{ -\frac{\alpha}{2}\delta^2 + \frac{c}{2|\Delta|^2}(\partial_x\delta)^2 + \frac{c}{2v^2|\Delta|^2}(\partial_\tau\delta)^2 \right\},\qquad(B8.9)$$

with $\alpha = f(T)/(\hbar v_F)$. Note, that (B8.9) is written in dimensionfull units for a better illustration. From this action one can derive a typical length scale L_δ and time scale τ_δ of the vortex core on which $\delta \approx -|\Delta|$, i.e., the order parameter vanishes:

$$L_\delta = \sqrt{\frac{c}{\alpha|\Delta|^2}},\qquad(B8.10a)$$

$$\tau_\delta = \sqrt{\frac{c}{\alpha v^2|\Delta|^2}},\qquad(B8.10b)$$

or in rescaled dimensionless units $L_\delta = \tau_\delta = \sqrt{c/\alpha}\Lambda/|\Delta|$. The vortex core action is then approximately given by S_0 (the gaussian part of (B3.4)) evaluated for the *area* $L_\delta \cdot \tau_\delta$ in x-τ-space with a *phase change* of $\pm\tilde{q}\pi$:

$$S_{core} \approx \hbar\frac{\tilde{q}^2\pi}{K} \sim \tilde{q}^2|\alpha||\Delta|^2 L_\delta\tau_\delta.\qquad(B8.11)$$

Performing a calculation analogous to the one for the commensurate lattice potential, discussed in the previous section, (now with $u = 0$ and $w = 0$) the RG-flow equations read

$$\frac{dK}{dl} = -\frac{\pi}{2}\frac{\tilde{q}^4\varpi^2}{K^3}B_2\left(\frac{\tilde{q}^2}{K},\frac{K}{2t}\right)\coth\frac{K}{2t},\qquad(B8.12a)$$

$$\frac{dt}{dl} = \left[1 - \frac{\pi}{2}\frac{\tilde{q}^4\varpi^2}{K^4}B_1\left(\frac{\tilde{q}^2}{K},\frac{K}{2t}\right)\coth\frac{K}{2t}\right]t,\qquad(B8.12b)$$

$$\frac{d\varpi}{dl} = \left[2 - \frac{\tilde{q}^2}{4K}\coth\frac{K}{2t}\right]\varpi,\qquad(B8.12c)$$
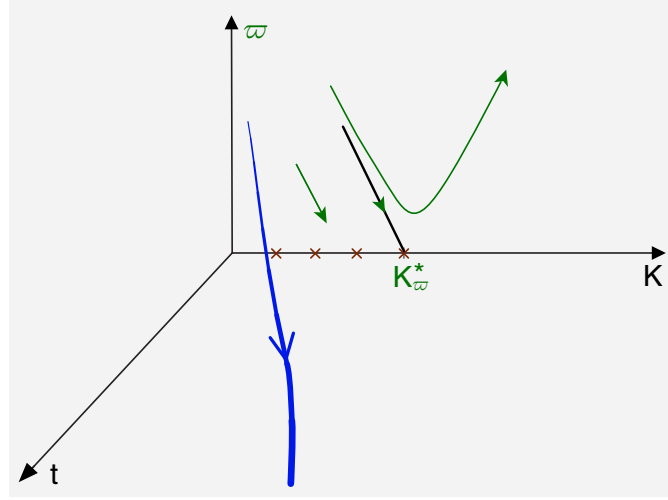
Figure B.10: Typical flow diagram for the disorder free model in the three dimensional parameter space of K, ϖ, and t.

where $B_{1,2}$ are given in (B3.6) with

$$g_1 = 2\tau^2 \cos x,$$
$$g_2 = (x^2 + \tau^2) \cos x.$$

Plots of the functions B_1 and B_2 can be found at the end of appendix 1.1. Equations (B8.12a) to (B8.12c) can again only be solved numerically and a typical solution is shown in Fig. B.10.

At zero temperature (B8.12a) and (B8.12c) reduce to

$$\frac{dK}{dl} = -\frac{\pi}{2} \frac{\tilde{q}^4 \varpi^2}{K^3} B_2\left(\frac{\tilde{q}^2}{K}, \infty\right), \tag{B8.13a}$$

$$\frac{d\varpi}{dl} = \left[2 - \frac{\tilde{q}^2}{4K}\right]\varpi, \tag{B8.13b}$$

and we find, that for $u = 0$ quantum phase-slips become relevant (i.e., ϖ grows) for $K > K_\varpi$, where K_ϖ is implicitly defined by

$$\varpi^2(K_\varpi) = \frac{K_\varpi^*}{\tilde{q}^2 \pi \tilde{\eta}} \left(\frac{K_\varpi^*}{3}(K_\varpi^{*3} - K_\varpi^3) - \frac{1}{4}(K_\varpi^{*4} - K_\varpi^4)\right), \tag{B8.14}$$

which follows from

$$\frac{d\varpi}{dK} = \frac{4K^3}{\tilde{q}^4 \pi \tilde{\eta} \varpi}\left(1 - \frac{K_\varpi^*}{K}\right), \tag{B8.15}$$

where we used (B8.13a) and (B8.13b) and the initial condition $\varpi(K_\varpi^* \equiv \tilde{q}^2/8) = 0$ ($\tilde{q} = 2$ for CDWs); $\tilde{\eta} = -B_2\left(\frac{\tilde{q}^2}{K_\varpi^*}, \infty\right)$. In this region vortices destroy the quasi-long-range order

of the CDW; $C(x, \tau) \sim |z|/\xi_\varpi$. The transition is again of KT type with a correlation length ξ_ϖ (defined by $\varpi(\ln \xi_\varpi) \approx 1$) diverging at $K \searrow K_\varpi$ [BD84, FG88, RD96, ZGvOZ97]. Again this can be seen by the same considerations as in the lattice potential case in defining $\gamma = \frac{\tilde{q}^2}{8K} - 1$ and $\chi^2 = (8/\tilde{q})^4 \pi \tilde{\eta} \varpi^2$ (note that $\tilde{\eta} > 0$) which leads for $|\gamma| \ll 1$ to the KT equations (B3.14a) and (B3.14b).

Since the flow equations are exactly the same as for for the commensurate lattice potential [(B6.2a) to (B6.2c)] if one replaces

$$K \;\; \rightarrow \;\; K^{-1}, \tag{B8.16a}$$

$$t \;\; \rightarrow \;\; t/K^2, \tag{B8.16b}$$

$$w \;\; \rightarrow \;\; \varpi/K^2, \tag{B8.16c}$$

$$q \;\; \rightarrow \;\; \tilde{q}, \tag{B8.16d}$$

one obtains qualitatively the same behavior as in that case: φ first increases in a $K-t$ region given by $\mathcal{M}_\varpi \equiv \left\{ (K,t) | 1/K_\varpi^* \geq \frac{1}{K} \coth \frac{K}{2t} \geq 0 \right\}$, i.e., when the right-hand side of (B8.12c) is positive, but then decreases and flows into the region of large t and small ϖ. Thus quantum phase-slips become irrelevant at finite temperatures, which can be understood in the same way as the lattice potential case, since we have shown that space-time vortices can be described by a Coulomb gas model [Len61].

Important to mention is, that the proposed phase-slip mechanism is only well founded for density waves, since the phase can be understood as the phase of an order parameter, and because these systems are coupled to a bath of non-condensed electrons. Therefore it is questionable if this mechanism can also be used in the Luttinger liquid theory.

The links between the Luttinger liquid model and our phase-slip picture, which can be interpreted as vortices in a XY-model, can also be found in [Gia03].

9 Disorder and phase-slips

It is now interesting to consider the combined influence of disorder and phase-slips. In doing this we write an approximate expression for the action of a single vortex in a region of linear extension L as

$$\frac{\mathcal{S}_{vortex} - \mathcal{S}_{core}}{\hbar} = \left(\frac{\tilde{q}^2}{4K} - 2 \right) \ln L - \frac{u_{eff}(L)}{K} L^{3/2}, \tag{B9.1}$$

where the first part comes from the flow equation for ϖ with $\varpi(l) \approx e^{-\mathcal{S}_{vortex}(l)/\hbar}$ and $\mathcal{S}_{vortex}(0) = \mathcal{S}_{core}$ and the second part from the averaged backward scattering term.

$u_{eff}(L)$ denotes (up to a constant) the renormalized but unrescaled disorder strength. For very low $K(< K_u, K_\varphi)$ where $u_{eff}(L) \approx u_0$ the disorder always favors vortices on the scale of the effective Fukuyama-Lee length ξ_{dis}. These vortices will be pinned in space by the disorder. On the other hand, for very large values of $K(> K_u, K_\varpi)$ phase vortices are not influenced by the disorder, since $u_{eff}(L)$ is renormalized to zero. In the remaining region we have to distinguish the cases $K_u^* \gtrless K_\varpi^*$. For $K_\varpi^* < K < K_u^*$ (i.e., $\tilde{q}p < 4\sqrt{3}$) and $u_0 = 0$ the phase correlations are lost on the scale of the KT correlation length ξ_w of the vortex unbinding transition. Not too close to this transition $\xi_\varpi \Lambda \approx e^{(\mathcal{S}_{core}/2\hbar)(1-K_\varpi^*/K)^{-1}}$ holds. Switching on the disorder, u will be renormalized by the strong phase fluctuation which leads to an exponential decay of $u_{eff}(L) \sim u_0 e^{-\mathrm{const} \times L/\xi_\varpi}$ such that disorder is irrelevant for the vortex gas as long as $\xi_\varpi \lesssim \xi_u$. We expect that the relation $\xi_\varpi \approx \xi_u$, i.e., the length scale on which both perturbations are of the same order, determines the position of the phase boundary between a pinned low K phase where vortices are favored by the disorder, and an unpinned high K phase, where vortices are induced by quantum fluctuations. This line terminates in K_ϖ^* for $u_0 \to 0$ (see Fig. B.11).
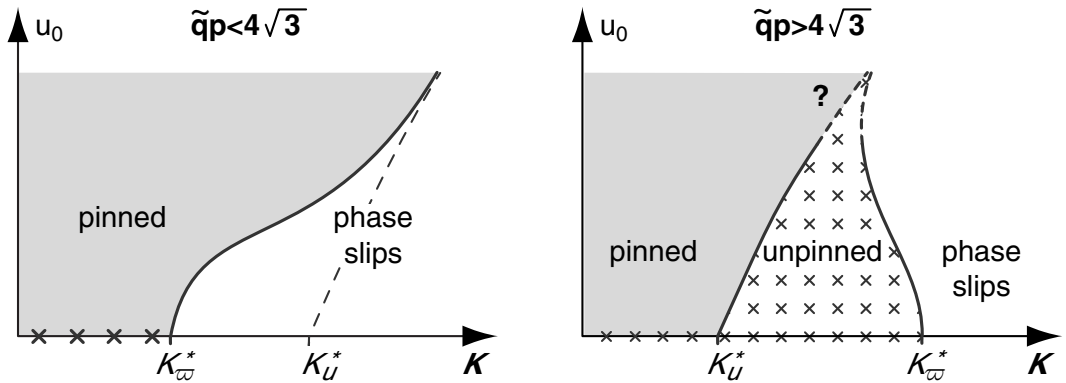
Figure B.11: $T = 0$ phase diagram for a CDW with quantum phase-slips. If $\tilde{q}p < 4\sqrt{3}$ there is a single transition between a low-K pinned and a high-K unpinned phase. In both phases the correlation length is finite. If $\tilde{q}p > 4\sqrt{3}$ these two phases are separated by a third phase in which phase-slips are suppressed and $C(x, \tau) \sim \ln|z|$. Both transitions disappear at finite t.

If $\mathcal{S}_{core}$ is large, ξ_ϖ will be large as well and $\xi_\varpi \approx \xi_u$ will be reached only for $K \approx K_u^*$. For moderate values of $\mathcal{S}_{core}$ the unpinning transition may be lowered considerably by quantum phase-slips. In the opposite case $K_u^* < K < K_\varpi^*$ (i.e., $\tilde{q}p > 4\sqrt{3}$) phase fluctuations renormalize weak disorder to zero such that vortices are still suppressed until K reaches K_ϖ, where vortex unbinding occurs. In this case two sharp phase transitions have to be expected.

10 Thermal creep and $1/f$ noise in quasi-1D charge density waves

In this section we go over to the non-equilibrium situation and study the dynamic properties of realistic charge density wave systems at low temperatures driven by a constant external field. As already mentioned in the introductory chapter, we are especially interested in the noise spectrum, which was measured experimentally.

$1/f^\gamma$ noise in CDW systems [Grü88] has been studied mainly in NbSe$_3$ and TaS$_3$ materials [Kog96]. The first experiment was done for a bulk NbSe$_3$ sample by Richard *et al.* [RMPR82] who found $\gamma \sim 0.8$. Studying transport properties of the quasi-one-dimensional CDW material TaS$_3$ at low temperatures, Zaitsev–Zotov [ZZ93] observed that slightly above the depinning threshold of the driving electric field, the exponent γ for the current noise is approximately given by $\gamma \approx 1.2$. Furthermore, the frequency range for observing this behavior gets wider as the external field increases.

It should be noted, that a phenomenological model based on fluctuations of the pinning force due to deformations of the sliding condensate was proposed to explain the broad band $1/f$ noise in CDW systems [BSRK85]. However, neither theoretical nor numerical estimation of γ has been provided so far.

Therefore the subject of this section is the computation of γ from *first principles* with the help of a one-dimensional classical model for CDWs [Gor77]. The current was obtained through numerical simulation of the overdamped equation of motion. The $1/f$ scaling is evaluated using the so-called *Wavelet Transform Modulus Maxima* (WTMM) method [ABM95]. The exponent γ was found to depend on T. At low temperatures ($T \leq 0.1$), in agreement with the experiments [ZZ93], we obtain $\gamma \approx 1.2$ in the crossover regime and if we increase T the exponent γ drops. The "exact" $1/f$-noise is observed at $T \approx 0.3$ where γ becomes 1. This interesting result is indicative of the possible occurrence of $1/f$ noise. At high temperatures γ takes on the white noise value 0.

Notably, the observed $\gamma \approx 1$ is not related to the second order depinning transition behavior at $T = 0$. Due to the asymptotic uniqueness of the sliding state [Mid92], this critical point dynamics scenario leads to the 'trivial' exponent $\gamma \approx 2$ [NF92b, Fis98]. Additionally, the observed 'flicker' noise behavior $\gamma \approx 1$ gains on its scaling range with increased distance to the critical point of the second order depinning transition.

Based on unusual current–voltage characteristics [ZZ93, ZZ94, ZZRM97a, ZZRM97b], Zaitsev-Zotov suggested that at low temperatures, quantum creep dynamics may play an important role and proposed the crossover from classical to quantum creep regime as an alternative ex-

planation for the experimental results. The strength of the quantum fluctuations in 1D CDW systems can be estimated by the dimensionless parameter K [defined in (B2.8b)] which is proportional to $\sqrt{m^*/m}$, where m^* is the effective band mass. As already mentioned before, this quantity is of the order 10^{-2} to 10^{-1} [Mak95, Grü88], indicating irrelevance (to $1/f$ noise) of quantum effects at low temperatures. Furthermore, our simulation results on the creep dynamics [GKL01] also suggest, in comparison to experiments, that quantum fluctuations do not have any visible effect with respect to the strength of the driving forces under consideration (see also discussion in [Han88, Kis88]). On the other hand, due to the small parameter K, the core action of phase-slips in the bulk is large ($S_{core} \propto 1/K$, see section 8) and hence the probability of phase-slips which is proportional to $e^{-S_{core}}$ becomes very small. It decreases even more under the renormalization group transformation discussed in the previous sections, such that we can neglect aslo phase-slips in our simulations. Therefore we will use the one-dimensional *classical model* without phase-slips (and lattice potential) to study the current noise in CDW systems.

10.1 Equation of motion

The classical Hamiltonian follows directly from the full quantum mechanical one (B2.4) in the limit $K \to 0$ or $\hbar v/c \to 0$. Including an additional term due to the external driving force E, given by

$$\mathcal{H}_E = \int\limits_0^L dx \, (Ex) \cdot (\partial_x \varphi(x)) \,, \tag{B10.1}$$

leads to

$$\mathcal{H} = \int\limits_0^L dx \left\{ \frac{c}{2} \left(\frac{\partial}{\partial x} \varphi \right)^2 - \sum_i U_i \delta(x - x_i) \times \rho_1 \cos\left(Qx + \varphi(x) \right) + Ex\partial_x\varphi(x) \right\} \,, \tag{B10.2}$$

with the elastic constant c, as defined in section 2.2. U_i and x_i denote the strength and the position of the impurity potential acting on the CDW, respectively, and E is the external electric field or driving force.

Our numerical studies are done in the weak pinning limit, i.e. again, when the Fukuyama–Lee length L_{FL} (B2.7) is large compared to the mean impurity distance l_{imp}. Therefore we will restrict ourselves in the following to the case $L_{FL} \gg l_{imp} \gg Q^{-1}$, in which the classical Hamiltonian (B10.2) can be approximated by a random field XY–model:

$$\mathcal{H} = \int dx \left\{ \frac{c}{2} \left(\frac{\partial}{\partial x} \varphi \right)^2 - V \cos\left(\varphi - \alpha(x) \right) - E\varphi(x) \right\} \,. \tag{B10.3}$$

Here $\alpha(x)$ is a random phase with zero average and $\overline{e^{i\left(\alpha(x)-\alpha(x')\right)}} = l_{imp}\delta(x - x')$, where the overbar denotes the averaging over disorder realizations. V is defined by $\overline{(U_i\rho_1)(U_j\rho_1)} \equiv V^2\delta_{ij}$ ($\overline{U_i} = 0$). The equation of motion of the (overdamped) CDW is given by a *Langevin equation*

$$\frac{\partial\varphi}{\partial t} = -\gamma\frac{\delta\mathcal{H}}{\delta\varphi} + \eta(x, t)\,, \tag{B10.4}$$

where γ is a kinetic coefficient and $\eta(x, t)$ a Gaussian thermal noise characterized by $\langle\eta\rangle = 0$ and $\langle\eta(x, t)\,\eta(x', t')\rangle = 2T\gamma\,\delta(x - x')\,\delta(t - t')$.

The length scale L_{FL} sets an energy scale $T^* = \left(c\,V^2\right)^{1/3} = c\,L_{FL}^{-1}$. We will rescale time by $L_{FL}/\gamma T^*$, temperature by T^*, and the external field E by E^*, where $E^* = T^*/L_{FL}$ is of the order of the $T = 0$ depinning threshold field E_c. In the following, E denotes the rescaled and dimensionless quantity. Using these replacements, the discrete and rescaled version of the equation of motion (B10.4) reads as follows [GKL01]

$$\frac{\Delta\varphi_i}{\Delta t} = (\varphi_{i+1} - 2\varphi_i + \varphi_{i-1}) + \sin(\varphi_i - \alpha_i) + E + \eta(i, t)\,, \quad i = 1\ldots N\,, \tag{B10.5}$$

where N is the discrete system size.

Solving this discretized equation, one can find the time dependent current $j_{cdw}(t)$ which is defined as [GKL01]

$$j_{cdw}(t) = \overline{\left\langle\frac{\partial\varphi(x, t)}{\partial t}\right\rangle_x}\,, \tag{B10.6}$$

where $\langle...\rangle_x$ denotes the average over positions.

10.2 Simulation and creep dynamics

Recently, we have studied the creep dynamics of one-dimensional classical CDWs at low temperatures [GKL01], based on model (B10.2). In the *weak pinning regime*, the creep current is

$$j_{cdw}(E) \sim T\exp(-T_0/T)\sinh\frac{\kappa E}{T}\,, \tag{B10.7}$$

where T_0 and κ are parameters [GKL01]. As one sees, the dependency of the creep velocity on the electric field is described by an analytic function, contrary to higher dimensional systems [Nat90]. The results of the simulations in that paper seem to be in agreement with the experiment by Zaitsev–Zotov [ZZ93] on the temperature dependency of the current at low T (see Fig. 2 in Ref. [ZZ93]), but the suggested field dependency of type

$$\ln\left(j_{cdw}(E)\right) \quad \sim \quad -\frac{E_0}{E} \text{ or} \tag{B10.8a}$$

$$\ln\left(j_{cdw}(E)\right) \quad \sim \quad -\frac{\tilde{E}_0^2}{E^2} \tag{B10.8b}$$

were not explored on the basis of our simulation results nor was the current noise spectrum.
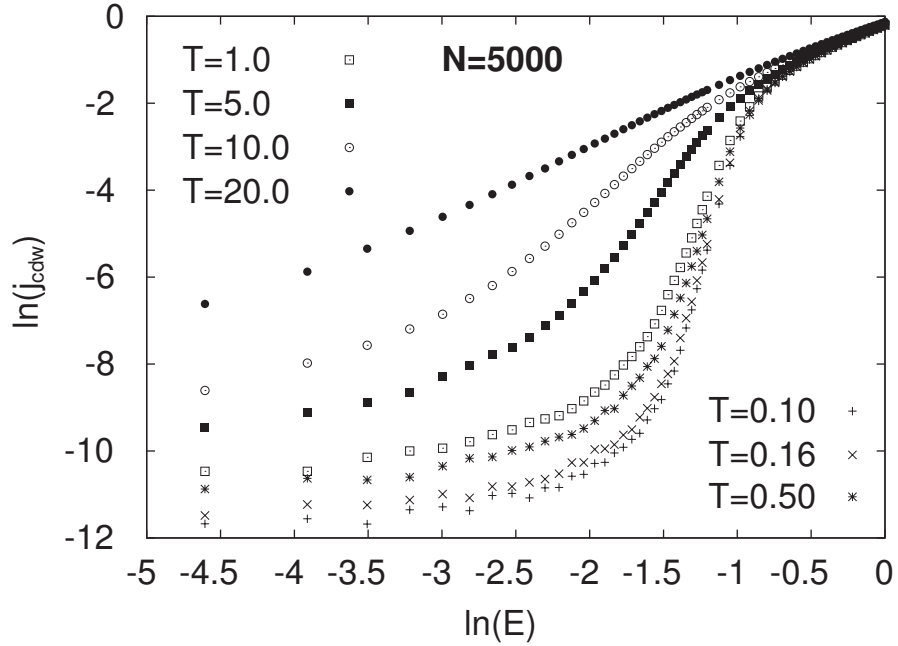
Figure B.12: Dependency of j_{cdw} on the external field E in double logarithmic representation for various values of temperature. The numerical results are averaged over $N_s = 50$ samples. For high T and high E linear behavior is recovered and for low T and E the creep regime can be found. At zero temperature one would recover the depinning transition at $\ln(E_c) \approx -1.52$ [GKL01].

Fig. B.12 gives an overview of the field dependencies of the CDW current j_{cdw} at different temperatures in a log-log plot. At high T one finds linear behavior because the system gains much thermal energy, and the pinning by impurities becomes irrelevant. As the temperature is lowered the nonlinear regime appears instead of the Ohmic one. Our result is comparable with experimental data presented in Fig. 1 of Refs. [ZZ93] and [ZZRM97b] except for very low fields and low temperatures.

Fig. B.13 (left) shows $\ln(j_{cdw})$ versus E^{-2} at low temperatures. The fit by a straight line which is valid up to $E^{-2} \sim 20$ confirms the nonlinear behavior (B10.8b) and is in fair agreement with the experiments [ZZ93, ZZRM97b]. Fig. B.13 (right) shows the same data, but plotted versus E^{-1}, partly in agreement with the experiment (see the inset in Fig. 3 of Ref. [ZZ93]) in the crossover region, where the linear dependency (B10.8a) can be fitted, but not for very low driving forces, where the creep law in the weak pinning case (B10.7) applies. Note, that in both plots the current diverges for high E, i.e., $x \to 0$, as $-\ln(x)$ (flow regime).

Figure B.13: Left: $\ln(j_{cdw})$ versus E^{-2} for low temperatures. The results are averaged over 50 samples. For very low external fields our creep formula (B10.7) can be fitted up to $E = E_c \simeq 0.22$. In the crossover regime to linear behavior, the CDW current can be fitted by the quadratic (B10.8b) behavior suggested in [ZZ93] (linear fit). Right: The same as on the left, but $\ln(j_{cdw})$ is plotted versus E^{-1}. The result agrees for medium E with data shown in the inset of Fig. 3 in Ref. [ZZ93], i.e., one can fit the linear behavior (B10.8a).
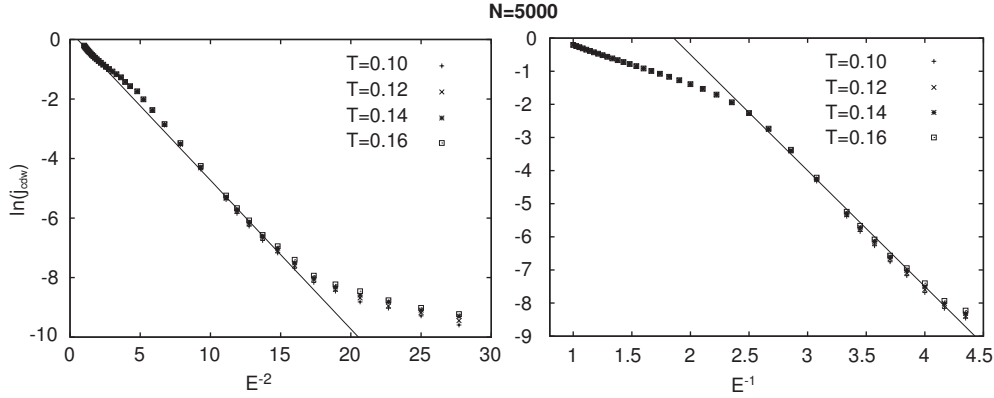
Due to this result, it is now reasonable to compare the experimentally obtained power spectrum of the CDW current in the crossover region [ZZ93] to our numerical calculated one. Following Ref. [GKL01], the equation of motion (B10.4) is integrated by a modified Runge–Kutta algorithm suitable for stochastic systems with periodic boundary conditions.

Throughout this section, we use a system size of $N = 5000$ and average the results over typically $N_s = 1000$ disorder realizations. Larger system sizes do not change the results substantially.

Fig. B.14 shows the typical time evolution of $j_{cdw}(t)$ for $E = E_c \simeq 0.22$ [GKL01] (left panel) and $E = 0.3$ (right panel) at temperature $T = 0.1$. One can see that the current exhibits strong fluctuations. The time averaged values are $\langle j_{cdw} \rangle = 0.008 \pm 0.003$ and $\langle j_{cdw} \rangle = 0.112 \pm 0.006$ for $E = E_c$ and $E = 0.3$, respectively. The spike structure is also seen, but less pronounced compared to the experimental data [ZZ93]. Nevertheless, the patterns for the two values of E look similar.

Zaitsev–Zotov studied [ZZ93] the current noise spectrum for applied electric fields with averaged driving current $\langle I \rangle \geq 220\mathrm{pA}$. Using Fig. 1 from Ref. [ZZ93] one can see that the threshold electric field in these experiments is $E_c \approx 35\mathrm{V/cm}$ and the averaged currents of $\langle I \rangle = 220\mathrm{pA}$ and $\langle I \rangle = 2.4\mathrm{nA}$ at $T = 2.4\mathrm{K}$ correspond to electric fields $E \approx 40\mathrm{V/cm}$ and $E \approx 50\mathrm{V/cm}$, respectively, i.e., the electric fields used, are greater than the threshold field. Therefore we will restrict our spectrum analysis to $E \geq E_c$.
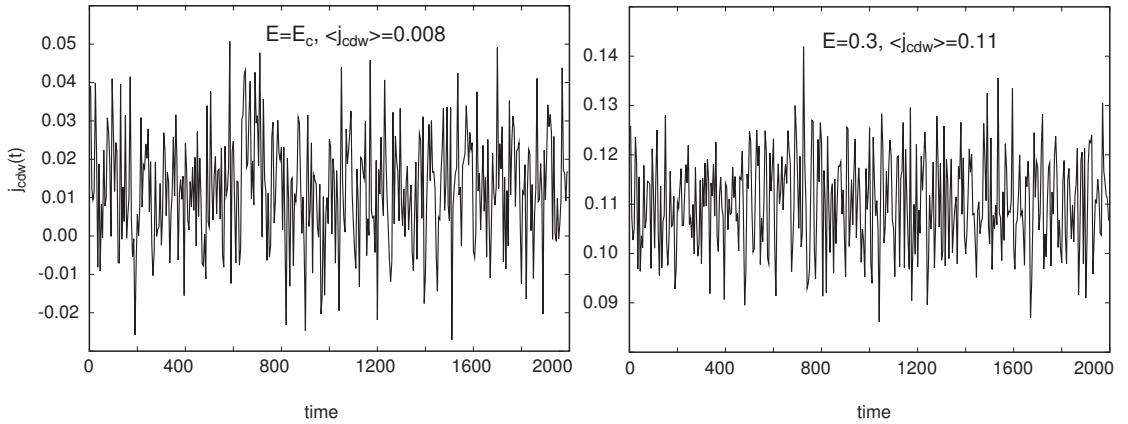
Figure B.14: Typical time dependence of the CDW current for $E = E_c \simeq 0.22$ (left panel) and $E = 0.3$ (right panel) at $T = 0.1$ for one disorder realization. The time and disorder averaged values of $j_{cdw}(t)$ are shown next to the curves ($\langle j_{cdw} \rangle$) for which we took $N = 5000$ and averaged the results over 1000 and 500 samples for $E = E_c$ and $E = 0.3$, respectively. An initial (dimensionless) time interval of length ≈ 2000 is discarded, such that the system is in an almost (see section 10.3) steady state at time 0.

10.3 Analysis of the power spectrum

Usually the exponent of the power spectrum can be calculated numerically from a time series (here the current) by a discrete Fourier transformation. This naive approach works well in the case of stationary time series, i.e., when the mean current is constant. In the case of non-stationary behavior of the CDW current, as in our simulations (see Fig. B.15), the standard Fourier transformation is not suitable for determining the exponent γ and one therefore should employ more sophisticated methods. We have chosen a wavelet transformation in particular the *Wavelet Transform Modulus Maxima* (WTMM) method [ABM95, JMA94] due to its superior properties in non-parametric scaling exponent estimation [BA02] in the presence of polynomial non-stationarities. In particular, attempts to reduce the non-stationary behavior of the current by discarding an initial time interval (as done for the calculation of $\langle j_{cdw} \rangle$, see Fig. B.14) cannot generally guarantee that the steady state is reached, since the relaxation time to a steady state can be very long (see the remark in Ref. [MF93]). The results from the Fourier transform are discussed to some extend at the end of this section.

This non-stationarity manifests itself in a low frequency non-linear bias of the CDW current and is precisely the reason why we used the wavelet transformation. The WTMM method has the ability to evaluate the scaling exponent correctly even in the presence of a polynomial
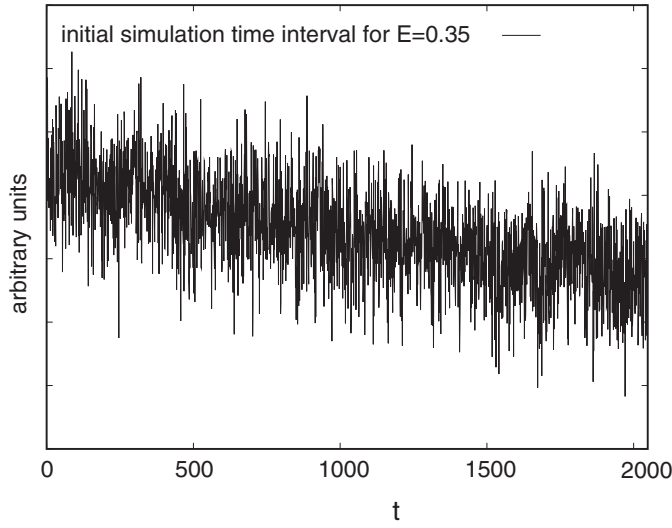
Figure B.15: In this plot the initial simulation time interval of the CDW current for $E = 0.35$ is shown. The non-stationarity manifests itself in a low frequency non-linear bias of the CDW current. This effect is precisely the reason why we used a more sophisticated method to evaluate the scaling exponent. In particular, attempts to reduce the non-stationary behavior of the current by discarding an initial time interval, as shown here, cannot guarantee that the resulting spectral exponent γ is not influenced by it.

trend of the time series, as can be seen in Fig. B.15.

The ability of the wavelet transform to provide unbiased scaling estimates of non-stationary signals is due to the property of orthogonality to polynomials up to the degree n of the base functions, of the so-called analyzing wavelets ψ with m 'vanishing moments':

$$\int_{-\infty}^{+\infty} x^n \, \psi(x) \, dx = 0 \quad \forall n, \ 0 \leq n < m \ .$$

The transform is defined as the inner product of the function $f(x)$ and the dilated and translated wavelet $\psi(x)$:

$$(Wf)(s, b) = \frac{1}{s} \int dx \, f(x) \, \psi(\frac{x - b}{s}) \ , \tag{B10.9}$$

where $s, b \in \mathbb{R}$ and $s > 0$ for the continuous version, which among other properties ensures local blindness to the polynomial bias. Indeed, the wavelet transform decomposes the signal into scale (and thus frequency) dependent components (scale and position localized wavelets), comparable to frequency localized sines and cosines based Fourier decomposition, but with additional position localization. This localization in both space and frequency, together with the wavelet's orthogonality to polynomial bias, makes it possible to access even

weak scaling behavior of singularities $h(x_0)$, otherwise masked by the stronger polynomial components:

$$f(x)_{x_0} = c_0 + c_1(x - x_0) + \cdots + c_n(x - x_0)^m + C|x - x_0|^{h(x_0)} \, ,$$

where the function f is represented through its Taylor expansion around $x = x_0$.

In the generic multifractal formulation of the WTMM formalism [ABM95], the moments q of the measure, distributed on the WTMM tree, are taken to obtain the dependency of the scaling function $\tau(q)$ on the moments q:

$$\mathcal{Z}(s, q) \sim s^{\tau(q)},$$

where $\mathcal{Z}(s, q)$ is the partition function of the q-th moment of the measure distributed over the wavelet transform maxima at the scale s considered:

$$\mathcal{Z}(s, q) = \sum_{\Omega(s)} (Wf\omega_i(s))^q \, , \tag{B10.10}$$

with $\Omega(s) = \{\omega_i(s)\}$ being the set of maxima $\omega_i(s)$ at the scale s of the continuous wavelet transform $Wf(s, t)$ of the function $f(t)$, in our case the CDW current: $f(t) = j_{cdw}(t)$. The working scale of the wavelet s is inversely proportional to the (Fourier) frequency $f \sim 1/s$ and the continuous wavelet used, is the second derivative of the Gaussian curve (*Mexican hat*).

In particular, scaling analysis with WTMM is capable of revealing the modal exponent $h(q = 0)$ for which the spectrum reaches its maximum value; this $h(q = 0)$ corresponds to the Hurst exponent H in the case of monofractal noise. This exponent is directly linked to the power spectrum exponent of the (stationary) fluctuations of the analyzed signal by $\gamma = 2H + 1$, where γ is the spectral exponent and H the Hurst exponent.

In Fig. B.16, the modal scaling exponent has been obtained by a linear fit over an appropriate scaling range from a suitably defined, weighted measure $\mathcal{M}(s)$ for the WTMM:

$$h(q = 0) = \left. \frac{d\tau(q)}{dq} \right|_{q=0} = \lim_{s \to 0} \frac{\mathcal{M}(s)}{\log(s)} \tag{B10.11}$$

with

$$\mathcal{M}(s) = \frac{\sum_{\Omega(s)} \log(Wf\omega_i(s))}{\mathcal{Z}(s, 0)} \, , \tag{B10.12}$$

for three electric field values $E = 0.25$, 0.3, and 0.35, averaged over $N_s = 1000$ disorder realizations. Consistent with the experimental findings [ZZ93], the flicker noise region becomes
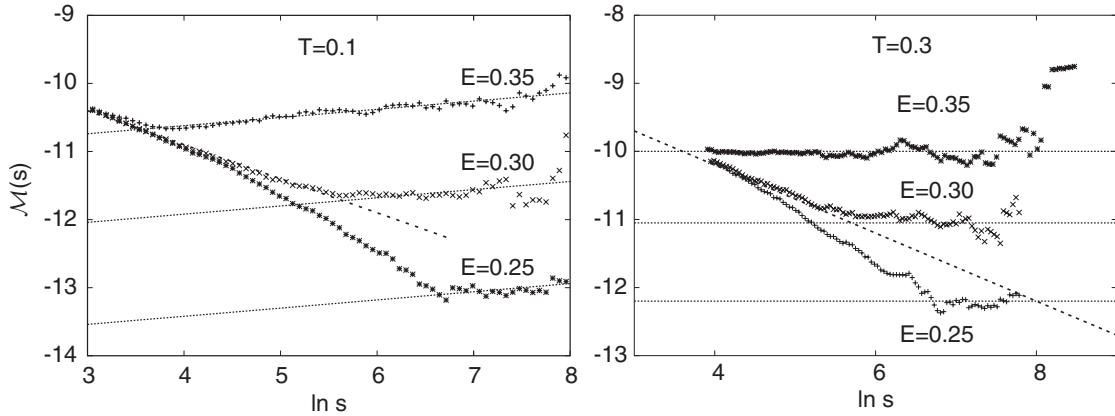
Figure B.16: Left: $\mathcal{M}(s)$ versus $\ln s$ for the CDW current $j_{cdw}(t)$ averaged over $N_s = 1000$ disorder realizations and for three values of the external electric field: $E = 0.25$, 0.3 and 0.35 which are higher than $E_c \approx 0.22$. The temperature is fixed to $T = 0.1$. The dotted straight lines denote the reference slope corresponding to $\gamma = 1.2$. The dashed line has the slope -0.5, which corresponds to the flat power spectrum of white noise $\gamma = 0$. Right: The same, but for $T = 0.3$. The dotted lines denote the reference slope $H = 0$ corresponding to $\gamma = 1.0$. Again, the dashed line corresponds to white noise.

narrower with decreasing E. More importantly, we obtain $\gamma \approx 1.2$ for low temperatures as observed in experiments [ZZ93]. An asymptotic transition to the scaling regime, character-istic to uncorrelated behavior (white noise, i.e., $\gamma = 0$) can be clearly identified for all the values of E shown (see dashed line in Fig. B.16).

Fig. B.16 (right) shows $\mathcal{M}(s)$ versus $\ln s$ for $j_{cdw}(t)$ for three values of the external electric field $E = 0.25$, 0.3 and 0.35 and $T = 0.3$. Our fitting gives $\gamma = 1$, which is important from the point of view of the exact definition of $1/f$-noise. In Fig. B.17, we provide the dependence of the exponent γ on temperature. Note the convergence towards $\gamma = 1.2$ as the temperature (and the averaged current) approaches 0. The exponent γ decays quickly with temperature and we have the uncorrelated noise value $\gamma = 0$ at high T.

Additionally, multifractal analysis can reveal possible non-linearity of $h(q)$ with respect to moments q. The WTMM tree lends itself very well to defining the partition function based multifractal analysis [ABM95].

A non-linear dependency of the scaling exponent $\tau(q)$ on the moments q is the hallmark of multifractality, while linearity corresponds to the monofractal character of the analyzed process.

Multifractal analysis has been performed over the range of moments $-3 \leq q \leq 5$. Fig.
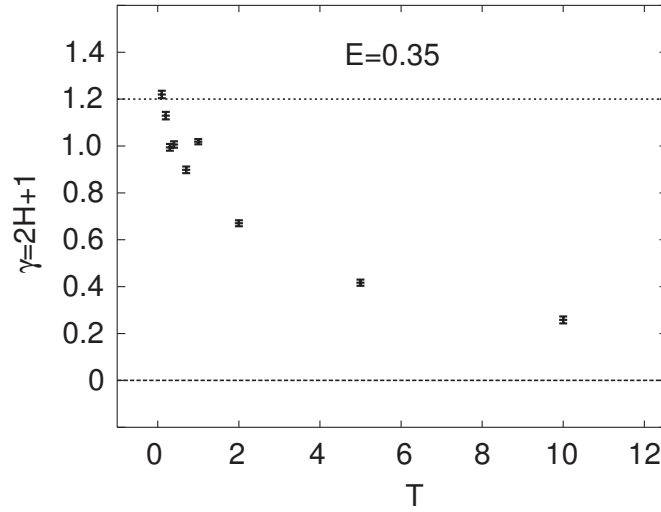
Figure B.17: The dependence of the exponent $h(q = 0)$ on temperature. Note the convergence towards $H = 0.1$, corresponding to $\gamma = 1.2$, if $T \to 0$. For high T, γ approaches the white noise value 0.
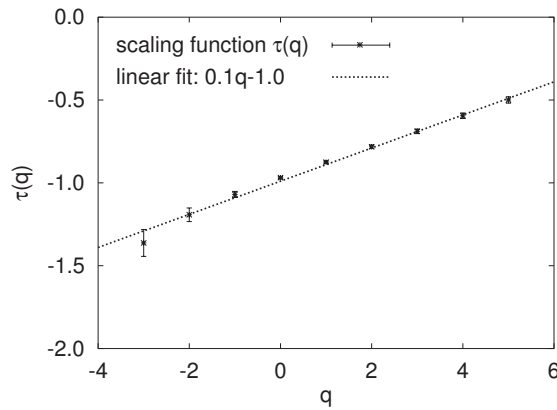
Figure B.18: $\tau(q)$ versus q for the CDW current $j_{cdw}(t)$ averaged over $N_s = 1000$ and driving force $E = 0.35$.

B.18 shows a linear relationship of $\tau(q)$ on q, discovered for the CDW current, indicating the monofractal character of the $1/f^\gamma$ CDW noise. Additionally, the exponent $\gamma = 1.2$ has been revealed through the linear dependency $\tau(q) = hq$ with $H = h = 0.1$ and $\gamma = 2H + 1$. The exponent h, which in the general, multifractal case is a function of q relates to, and can be derived from, the slope of the $\tau(q)$ spectrum: $h(q) = d\tau/dq$. The derivative $d\tau(q)/dq$ is thus constant for our CDW current and therefore $h_{cdw}(q) = h(q = 0)$ and is equal to the Hurst exponent H of the CDW current.

The primary question remaining is that of the origins of $1/f$ noise in the CDW system. In our opinion, the disorder causes the rugged energy landscape (similar to the spin glass case) leading to a wide spectrum of relaxation times. The average over such a spectrum would give

rise to the flicker noise. Our results shown in Fig. B.17 support this point of view. Namely, at low temperatures the roughness of the energy landscape becomes more important and consequently the flicker-like regime appears. Another qualitative scenario [Mil02] for the appearance of the flicker noise in our system is that the CDW may be viewed as a single particle in a quasi-periodic potential with troughs of variable depths. Such a simplified model closely resembles the "many-pendula" model of the self-organized criticality [BTW87] in which the $1/f$ noise should occur.
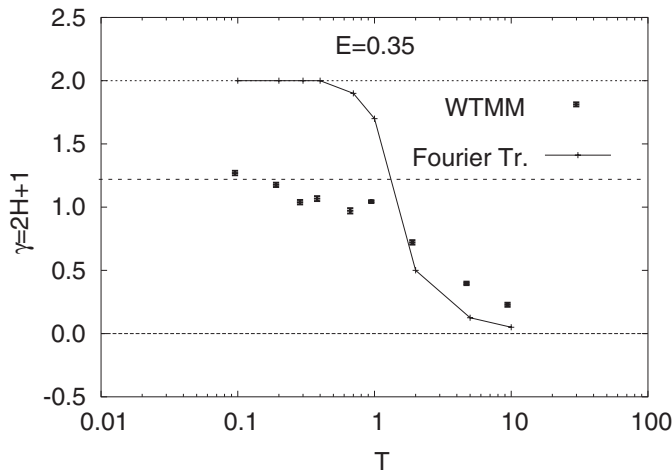
Figure B.19: The dependence of the the scaling exponent evaluated with the direct Fourier transform (line) exhibits a transition from white noise to brown noise with temperature approaching 0. The exponent evaluated using WTMM with two vanishing moments (blind to local linear trends) converges towards $H = 0.1$ corresponding to a spectral exponent $\gamma = 1.2$ (see Fig. B.17).

In Fig. B.19 (dots) the dependence of the exponent γ on temperature is shown. Note the convergence towards $\gamma = 1.2$ as the temperature (and the averaged current) approaches 0. The exponent γ decays quickly with temperature and we see the uncorrelated noise value $\gamma = 0$ at high T.

For comparison, the direct evaluation of the exponent of the power spectrum, using a fast Fourier transformation, produces an inaccurate exponent due to the non-stationarity of the CDW current; see straight line in Fig. B.19. This confirms the fact that the issue of non-stationarity of the CDW current is of critical importance to the exponent evaluation. The property of local "blindness" to polynomial trends of the wavelet transformation has the ability to evaluate the scaling exponent even in the non-stationary situation correctly.

11 Conclusion and summary

To conclude we have shown, that in one-dimensional charge and spin density waves, Luttinger liquids and suprafluids, quantum phase transitions between a disordered (or locked-in) phase and an asymptotically free phase at zero temperature are destroyed by thermal fluctuations, leaving behind a rich crossover behavior. This was demonstrated by using a *full finite temperature* renormalization group (RG) calculation. The crossover regions were characterized by the behavior of the phase pair correlation functions. For vanishing quantum fluctuations our calculation was improved by an *exact* solution in the case of strong disorder and by a mapping onto the *Burgers equation with noise* in the case of weak disorder, respectively. Both methods gave an exponential decay of density correlations.

We have also briefly discussed, that the inclusions of Coulomb interaction may destroy the unpinning (localization) transition at zero temperature.

The finite temperature calculation, used in this chapter, is also suited for treating the low frequency, low temperature behavior of dynamical properties which may depend crucially on the ratio ω/T, e.g., the frequency dependent electric conductivity. This will be postponed to a forthcoming publication.

The combined effect of disorder and the lattice potential on the zero temperature phase diagram, i.e., the competition between unpinning (Anderson) and lock-in (Mott) transition, is still controversially discussed [Sha90, GDO01] and cannot be explained by the RG-results presented here, since both perturbations become relevant for small K. However, using Imry-Ma arguments one finds, that as soon as K is below one of the two critical values (for the unpinning and lock-in transition) the disorder dominates the lattice potential and only two phases exist. This is in contrast to the proposed existence of a so-called intermediate *Mott-Glass* phase [GDO01].

Since the phase field can be interpreted as the phase of an order parameter in the case of density waves, we have discussed a possible mechanism for phase-slip processes in these systems. We find at zero temperature for high K a phase where phase-slip become relevant. However, thermal fluctuations again destroy this phase, which is clear, since the model is essentially the same as for the commensurate lattice potential. At zero temperature in the presence of disorder, quantum phase-slips in CDWs lead to additional phase transitions and shift the unpinning transition in CDWs to smaller K-values.

In the last section, we have studied the current noise in CDWs, using the classical one-dimensional Fukuyama-Lee model and a wavelet analysis of the current, obtained from the appropriate equation of motion. We have reproduced the experimental results on the current noise spectrum of a quasi one-dimensional TaS_3 sample. Our simulations support the exis-

tence of $1/f$-noise in this system. To the best of our knowledge, this is the first evidence of $1/f$ scaling obtained from first principle based simulation in a physical (i.e., CDW) system.

C AC dynamics and surface pinning in driven random elastic systems

1 Introduction

In this second main chapter of the thesis we study the *non-adiabatic* dynamics of interfaces or domain walls in a random environment. In particular we are interested in the case of a periodic driving force and the influence of surface potentials in the case of driven charge density waves.

Our first aim is to develop a description of pinning phenomena in an ac-field with finite frequency in the weak pinning limit, which is done in sections 2 and 3. As a main result we find that the zero temperature depinning transition is smeared and shows a pronounced velocity hysteresis. The latter has to be distinguished from the hysteresis of the magnetization which persists also in the adiabatic case [LNP99, NPV01a]. The transition disappears completely above a threshold frequency ω_P, related to the strength of disorder. For smaller frequencies a trace of the critical depinning can still be observed in the frequency dependency of the velocity which shows a power law behavior. We also briefly discuss the influence of thermal fluctuations. If the amplitude of the oscillating driving force is smaller than the zero temperature and frequency depinning threshold h_P, also the influence of avalanche motion of the interface has to be taken into account, if the frequency is sufficiently low (section 4).

In section 5 we compare the results of our model to experimental measurements on granular superferromagnetic materials. We calculate the complex susceptibilities numerically, especially for finite systems, based on the equation of motion for an interface and discuss the properties of the resulting *Cole-Cole* representation in contrast to the measured one. We find that the experimental system can be well described by our model.

It was a tacit assumption of these investigations that the motion of the elastic system is not hindered by effects from surfaces or internal grain boundaries. Surface barriers are however known to be relevant in most physical systems mentioned in chapter A. In superconductors they prevent the penetration of new flux lines into the probe [FZR+98]. In CDWs normal electrons have to be converted into those condensed in the CDW by a phase–slip mechanism

which is essentially a nucleation process [BKR$^+$00, RMAE92]. The motion of domain walls may be hindered by a variation of the width of the sample, such that positions of minimal width are preferred etc. Experimental [MT86b] and numerical [MT86a] studies of CDWs with contact effects revealed hysteretic behavior of the polarization.

Therefore the second aim is to consider the effect of a strong surface pinning potential in addition to the weak bulk random pinning, discussed in section 6. It turns out that, starting from a flat interface, at $T = 0$ and increasing the driving force h to $h > h_P$ the mean curvature $\mathcal{C}$ of the averaged (parabolic) displacement profile behaves as $\mathcal{C}(h) \propto (h - h_P)$. In more general situations $\mathcal{C}(h,t)$ exhibits a pronounced hysteretic behavior. At non–zero temperatures $\mathcal{C}(h,t)$ increases with time and asymptotically reaches its behavior of the pure system $\mathcal{C}(h) \propto h$. We further determine the reduction of the curvature in the case that the surface is depinned due to a sufficiently large driving force or due to thermally activated processes at the surface. The latter also mimic phase-slip processes in CDWs.

2 Model and zero frequency critical depinning

We focus on a simple realization of the problem, the motion of a D–dimensional interface profile $z(\mathbf{x}, t)$ obeying the following equation of motion[1] [Fei83]

$$\frac{1}{\gamma} \frac{\partial z}{\partial t} = \Gamma \boldsymbol{\nabla}^2 z + h_0 \cos \omega_0 t + g(\mathbf{x}, z) \,. \tag{C2.1}$$

γ and Γ denote the mobility and the stiffness constant of the interface, respectively, and $h(t) = h_0 \sin \omega_0 t$ is the ac driving force. This equation of motion follows, as discussed in section 10 of chapter B, from $\frac{1}{\gamma} \frac{\partial z}{\partial t} = -\frac{\delta \mathcal{H}}{\delta z}$ with the Hamiltonian

$$\mathcal{H} = \int d^D x \left\{ \frac{\Gamma}{2} (\nabla z)^2 - h \cdot \varphi + V(\mathbf{x}, z) \right\} \,, \tag{C2.2}$$

where $V(\mathbf{x}, z)$ denotes the random potential given by

$$V(\mathbf{x}, z) = -\int\limits_0^z d\tilde{z}\, g(\mathbf{x}, \tilde{z}) \,. \tag{C2.3}$$

The random force $g(\mathbf{x}, z)$ is assumed to be Gaussian distributed around zero ($\langle g \rangle_d = 0$) and $\langle g(\mathbf{x}, z) g(\mathbf{x}', z') \rangle_d = \delta^D(\mathbf{x} - \mathbf{x}') \Delta_0(z - z')$, where $\langle \dots \rangle_d$ denotes the random average. We further assume $\Delta_0(z) = \Delta_0(-z)$ to be a monotonically decreasing function of z for $z > 0$

---

[1]We neglected an inertia term $\rho \frac{\partial^2 z}{\partial t^2}$ which is justified as long as $\gamma \omega_0 \rho \ll 1$. A velocity hysteresis due to inertial effects has been considered by J.M. Schwarz and D.S. Fisher [SF01].

which decays to zero over a finite distance l. Under these conditions the relation between applied force $h(t)$ and the average velocity $\langle \dot{z} \rangle = v$ in the steady state shows the inversion symmetry $h \to -h$, $v \to -v$ (cf. Fig. C.1). We therefore restrict ourselves to the region $h > 0$ in the further discussion.

In [NSTL92, NF93, LNST97] eq. (C2.1) was considered in the adiabatic limit $\omega_0 \to 0$. In this case the interface undergoes a second order depinning transition at $h = h_P$, where the velocity v vanishes as a power law $v \sim (h_0 - h_P)^\beta$ for $h_0 \searrow h_P$, $\beta \le 1$ (see Fig. C.1). At $h = h_p$ the interface is self–similar with a roughness exponent ζ, $0 \le \zeta < 1$, and the dynamics is superdiffusive with a dynamical exponent z, $1 \le z \le 2$. The critical exponents were calculated up to order $\epsilon = 4 - D$ in [NSTL92, NF93] and recently to order ϵ^2 in [CDW01]. They are related by the scaling laws $\beta = \nu(z - \zeta)$ and $\nu = 1/(2 - \zeta)$ [NSTL92], where ν denotes the correlation length exponent: $\xi_0 \sim (h_0 - h_P)^{-\nu}$. For $h_0 \nearrow h_P$ the divergence of ξ_0 is related to the increasing size of avalanches.

3 AC dynamics above the depinning threshold

In the case of an ac-drive the behavior of the system is governed by the two dimensionless quantities h_0/h_P and ω_0/ω_P, where $\omega_P = \gamma h_P / l$. In this section we mainly focus on the case $0 < \omega_0 \ll \omega_P$ and $h_0 > h_P$ since this is the region where universality is expected to hold. As illustrated by the numerical solution of eq. (C2.1) for $D = 1$ at finite frequencies ω_0, the sharp depinning transition is replaced by a velocity hysteresis, which has clockwise rotation: the velocity reaches zero at $h(t) = \pm h_c$ for decreasing and increasing field, respectively (see Fig. C.1). For $h_0 \gg h_P$ a second weak hysteresis is found in the region $h > h_c \approx h_P$ which has anticlockwise rotation[2].

3.1 Mean field solution

Before solving the full problem, it is instructive to consider the mean field version of the equation of motion [Fis86]

$$\frac{1}{\tilde{\gamma}} \frac{\partial z}{\partial t} = \tilde{\Gamma}\left[z_0(t) - z(t)\right] + h(t) + \tilde{g}(z) \tag{C3.1}$$

with $z_0(t) = \langle z(t) \rangle_d$, $\langle \tilde{g}(z) \rangle_d = 0$, and $\langle \tilde{g}(z)\, \tilde{g}(z') \rangle_d = \tilde{\Delta}(z - z')$, i.e., compared to the full equation of motion (C2.1), the laplacian of the interface profile is replaced by $z_0(t) - z(t)$. For weak pinning potentials, perturbation theory can be applied. In lowest non–trivial order

---

[2]A similar hysteresis loop has seen experimentally in type-II superconductors, see, e.g., [MWA$^+$98]
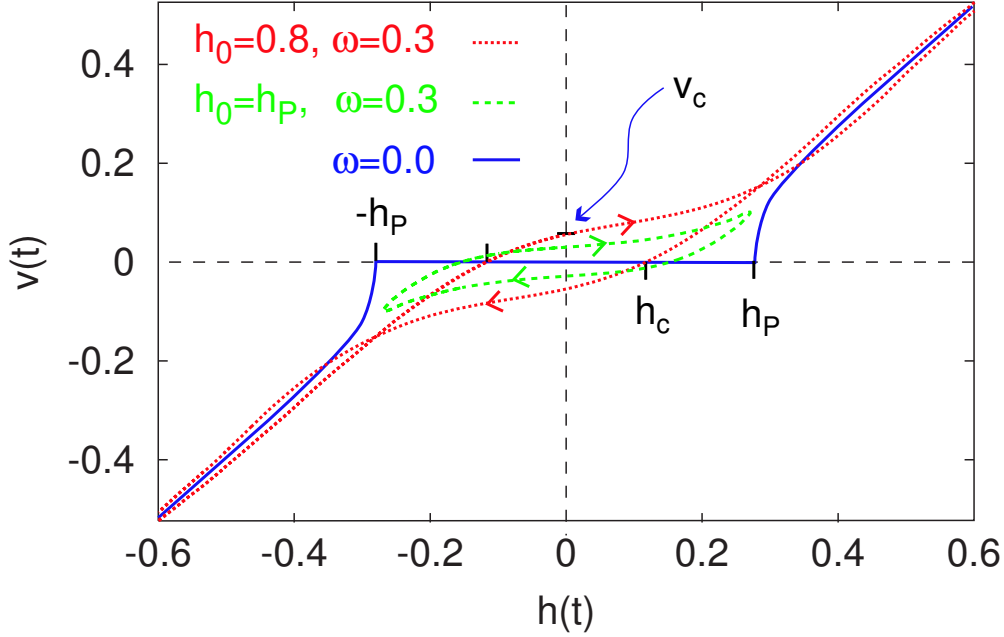
Figure C.1: Numerical solution of eq. (C2.1) for a 1D interface in the dc (solid line) and ac case (dotted line) for $\omega = \omega_0/\omega_P = 0.3$ and $h_0 > h_P \approx 0.27$. x is discretized in $N = 1000$ sites and g is random in $[-0.5, 0.5]$. The solution is averaged over typically 100 disorder (g) configurations. The arrows show the direction of the hysteresis: for $|h(t)| < h_p$ it is clockwise and for $|h(t)| > h_p$ anticlockwise. The dashed line shows the hysteresis in the case $h_0 \approx h_P$.

in g one obtains for the mean velocity (a short derivation of this expression can be found in appendix E2.1)

$$\frac{\dot{z}_0(t)}{\tilde{\gamma}} = h(t) + \int_0^\infty dt' \tilde{\gamma} e^{-\tilde{\Gamma}\tilde{\gamma}t'} \tilde{\Delta}'\left(\int_{t-t'}^t \dot{z}_0(t'')dt''\right). \tag{C3.2}$$

In the case of a dc-drive $h(t) \equiv h_0$ one finds the depinning threshold $\tilde{h}_{p,\pm}$ for $h_0 \lessgtr 0$, respectively, from the condition $\tilde{\Gamma}\tilde{h}_{p,\pm} \equiv -\lim_{\varepsilon \to 0} \tilde{\Delta}'(\pm\varepsilon)$. Thus, the force correlator has to have a cusp singularity to produce a finite threshold. A reasonable ansatz for $\tilde{\Delta}(z)$ is $\tilde{\Delta}(z) = \tilde{\Gamma}\tilde{h}_P l e^{-|z|/l}$, but the results do not depend very much on the details of the function $\tilde{\Delta}(z)$.

To treat the case of an ac-drive it is convenient to go over to dimensionless quantities $\tau = \tilde{\Gamma}\tilde{\gamma}t$, $x(\tau) = \tilde{\Gamma}z(t)/\tilde{h}_P$, and $x(\tau, \tau') \equiv x(\tau) - x(\tau - \tau')$, from which we get

$$\dot{x}(\tau) = H \sin \Omega\tau - \int_0^\infty d\tau' e^{-\tau' - |x(\tau,\tau')|/\lambda} \operatorname{sgn} x(\tau, \tau'). \tag{C3.3}$$
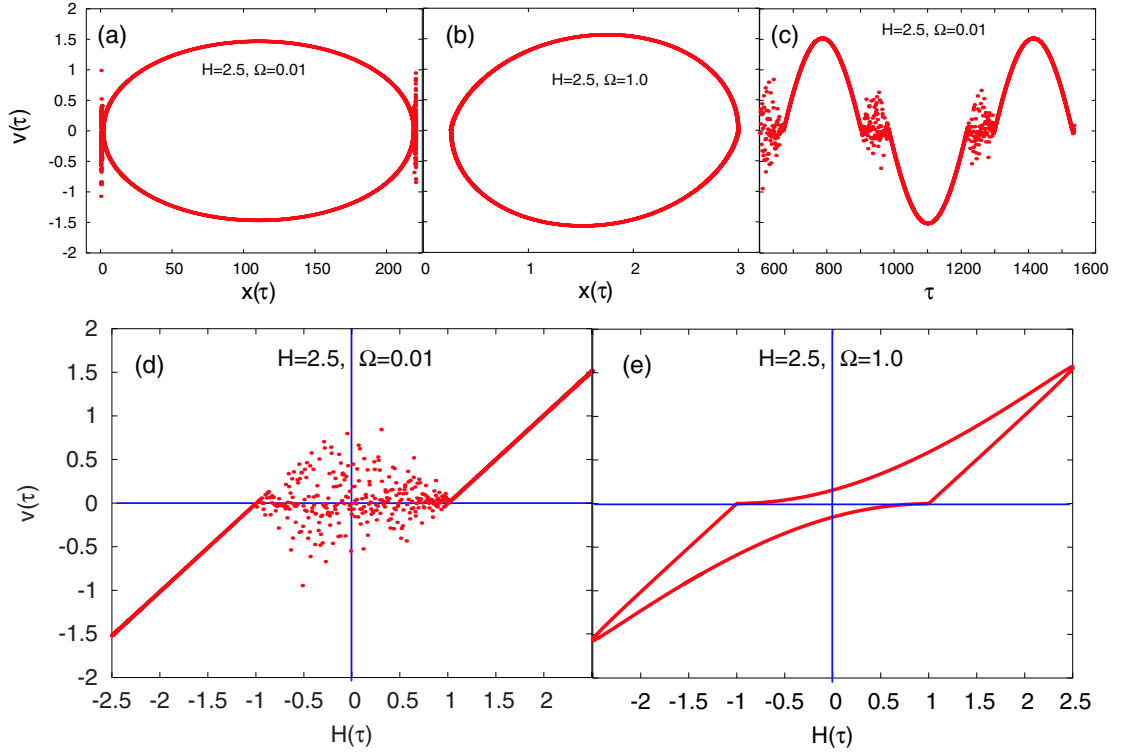
Figure C.2: These plots show the numerical integration of the mean-field solution (C3.3). (a) and (b) are phase space trajectories for $H = 2.5$ and a low (a) or a high (b) frequency with $\lambda = 1$. Graphs (a) and (c) show erratic behavior in the region $|H(\tau)| \lesssim 1$, i.e., where the approximation for (C3.2) breaks down. The resulting velocity hysteresis curves are shown in (d) and (e). Due to the erratic behavior no hysteretic behavior can be observed at low frequencies.

with the dimensionless parameters $H = h_0/\tilde{h}_P$, $\lambda = l\tilde{\Gamma}/\tilde{h}_P$, and $\Omega = \omega_0/(\tilde{\gamma}\tilde{\Gamma})$. As shown in Fig. C.2, eq. (C3.2) has erratic solutions in the region of small velocities if $\Omega \ll 1$ and $\lambda \geq 1$. The erratic behavior disappears for high frequencies $\Omega \gg 1$ and can be traced back to the sgn term in $\tilde{\Delta}'(z)$, which leads to rapidly changing force contributions in the small velocity region. This approach also fails to reproduce the features of the velocity hysteresis (see plots (d) and (e) in Fig. C.2). Therefore we have to employ more sophisticated methods to explain the hysteretic behavior of the velocity.

3.2 Scaling considerations

First we consider the relevant length scales of the problem, beginning with the case $\omega_0 = 0$. Comparison of the curvature and the random force term on the right-hand side of (C2.1) shows, that weak random forces accumulate only on the Larkin scale $L_P \approx \left[(l\Gamma)^2 / \Delta_0(0) \right]^{1/(4-D)}$ to a value comparable to the curvature force. On scales $L < L_P$ the curvature force density $\Gamma l L^{-2}$ is larger than the pinning force density, the interface is essentially flat and hence there is no pinning. For $L > L_P$ pinning force densities exceed the curvature forces, the interface becomes rough and adapts to the spatial distribution of pinning forces. The largest pinning force density then results from $L \approx L_P$ from which one estimates the depinning threshold $h_P \approx l\Gamma L_P^{-2}$. For $L \gg L_P$ perturbation theory breaks down. The renormalization group calculation performed in [NSTL92, NF93, LNST97, EK94, CDW01] results in a scale dependent mobility and renormalized pinning forces.

A finite (external) frequency ω_0 of the driving force acts as an infrared cutoff for the propagation of perturbations, resulting from the local action of pinning centers on the interface. As follows from (C2.1) [with $\gamma \rightarrow \gamma \left(L/L_P \right)^{2-z}$ for $L > L_P$ [NSTL92], i.e., $\left(L_P/L \right)^{2-z} / \gamma \omega_0 = \Gamma L^{-2}$] these perturbations can propagate up to a length scale [3]

$$ L = L_\omega \equiv L_P \left(\frac{\gamma \Gamma}{\omega_0 L_P^2} \right)^{1/z} = L_P \left(\frac{\omega_P}{\omega_0} \right)^{1/z} . \tag{C3.4} $$

(i) In the case $L_\omega < L_P$, i.e., $\omega_0 > \omega_P = \gamma \Gamma L_P^{-2} = \gamma h_P/l$, z has to be replaced by 2 which means that γ remains unchanged. During one cycle of the ac drive, perturbations resulting from local pinning centers affect the interface configuration only up to scale L_ω, such that the resulting curvature force is always larger than the pinning force – there is no pinning anymore and the velocity hysteresis disappears. Random pinning forces result merely in a slow down of the interface velocity but in no true pinning.

(ii) In the opposite case $L_\omega > L_P$, i.e., $\omega_0 < \omega_P$, the pinning forces can compensate the curvature forces at length scales larger than L_P. As a result of the adaption of the interface to the disorder, pinning forces are renormalized. This renormalization is truncated at L_ω.

In the following we will argue, that, contrary to the adiabatic limit $\omega_0 \rightarrow 0$, there is no depinning transition if $\omega_0 > 0$. Indeed, a necessary condition for the existence of a sharp transition in the adiabatic case was the requirement, that the fluctuations of the depinning threshold in a correlated volume $\delta h_P \approx h_P (L_P/\xi_0)^{(D+\zeta)/2}$ are smaller

---

[3]The consideration of higher harmonics in the interface motion results in the existence of additional length scales $L_{n\omega}$ which are however of the same scale as L_ω.

than $(h - h_P)$, i.e., $(D + \zeta)\nu \geq 2$ [NSTL92]. For $\omega_0 > 0$ the correlated volume has a maximal size L_ω and hence the fluctuations δh_P are given by

$$\frac{\delta h_P}{h_P} \approx \left(\frac{L_P}{L_\omega}\right)^{(D+\zeta)/2} = \left(\frac{\omega_0}{\omega_P}\right)^{(D+\zeta)/(2z)}. \tag{C3.5}$$
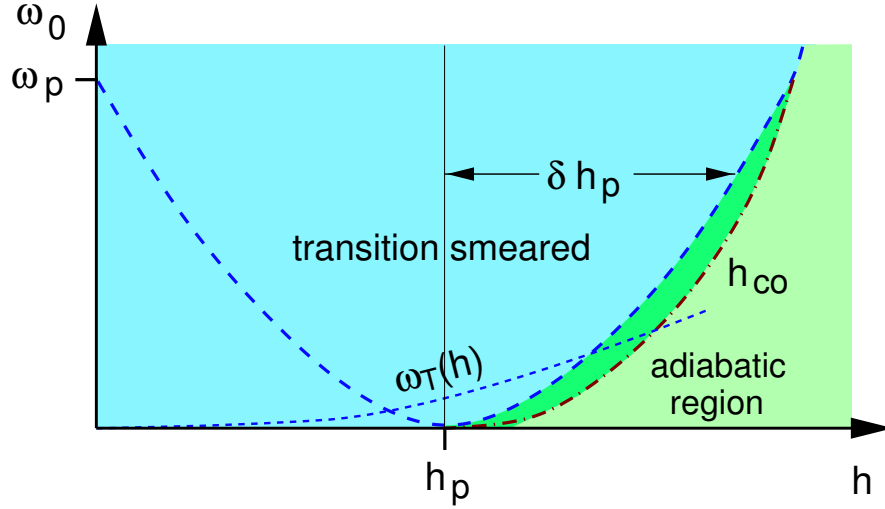
Figure C.3: Schematic frequency-field diagram for the depinning in an ac external field (with $h_0 > h_P$): For $0 < \omega_0 \ll \omega_P$ the depinning transition is smeared, but traces of the $\omega_0 = 0$ transition are seen in the frequency dependency of the velocity at $h = h_P$. This feature disappears for $\omega_0 \gg \omega_P$.

Thus, different parts of the interface see different depinning thresholds — the depinning transition is *smeared*. δh_P has to be considered as a lower bound for this smearing. A full understanding of the velocity hysteresis requires the consideration of the coupling between the different L_ω–segments of the interface, which we will do further below. When approaching the depinning transition from sufficiently large fields, $h_0 \gg h_P$ ($\omega_0 \ll \omega_P$), one first observes the critical behavior of the adiabatic case as long as $\xi_0 \ll L_\omega$. The equality $\xi_0 \approx L_\omega$ defines a field h_{co} signaling a cross-over to an *inner* critical region where singularities are truncated by L_ω. Note that $h_{co} - h_P = h_P(\omega_0/\omega_P)^{1/(\nu z)} \geq \delta h_P$ (cf. Fig. C.3). It is then obvious to make the following scaling Ansatz for the mean interface velocity ($h_0 > h_P$, $v_P = \omega_P l$)

$$v(h(t)) \approx v_P \left(\frac{\omega_0}{\omega_P}\right)^{\frac{\beta}{\nu z}} \phi_\pm \left[\left(\frac{h}{h_P} - 1\right)\left(\frac{\omega_P}{\omega_0}\right)^{\frac{1}{\nu z}}\right]. \tag{C3.6}$$

Here the subscript $\pm$ refers to the cases of $\dot{h} \gtrless 0$, respectively, and $\phi_\pm[x \to \infty] \sim x^\beta$ (for $h - h_P \gg h_P$ the classical exponent $\beta = 1$ applies). For $|x| \ll 1$, $\phi_\pm$ approaches a constant $c_\pm$. The function ϕ_- changes sign at a critical value $h_c(\omega_0) \approx h_P(1 - c_-(\omega_0/\omega_P)^{1/(\nu z)})$.
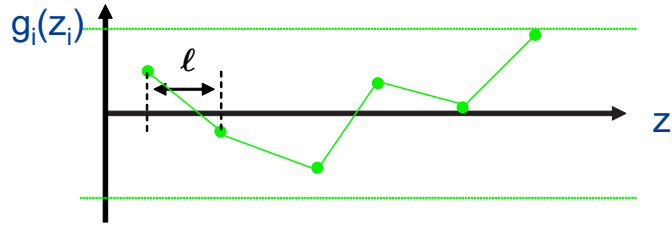
Figure C.4: Numerical realization of the disorder for a fixed position x_i. The values of g are chosen randomly in an interval $[-0.5, 0.5]$ at discrete z positions with distance $l = 0.1$. Between these discrete z-positions, g is interpolated linearly, resulting in a gaussian disorder correlator with variance l, shown in Fig. C.5.
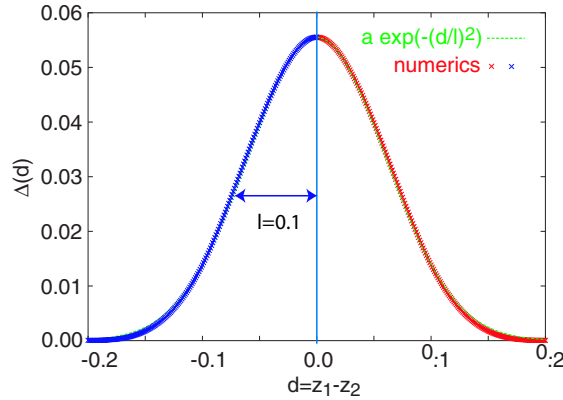
Figure C.5: Numerical calculated disorder (g)-correlator for $g \in [-0.5, 0.5]$ and $l = 0.1$.

To check the validity of (C3.6) we integrate (C2.1) numerically. For this, the $\mathbf{x}$–coordinate is discretized with a lattice constant α and the simulation time is measured in units of a time τ_0 (the dimensionless lattice Laplacian for $D = 1$ is given by $\mathbf{\nabla}^2 \varphi_i = \varphi_{i+1} + \varphi_{i-1} - 2\varphi_i$ and accordingly in higher dimensions, with lattice sites $i = 0, \ldots, L$). α and τ_0 are chosen such that $\frac{\tau_0 \gamma \Gamma}{\alpha^2} = 1$ and the dimensionless stochastic forces $\tau_0 \gamma g(\mathbf{x}, \varphi) \in [-1/2, 1/2]$ (see Figs. C.4 and C.5). The dimensionless driving force is $\tau_0 \gamma h$.

The numerical solution in $D = 1$, 2 and 3 is in good agreement with the scaling Ansatz (C3.6) as shown in Fig. C.6.

3.3 Renormalized perturbation theory

To consider the coupling between different L_ω-segments, we treat model (C2.1) in perturbation theory. After going over to a co–moving frame, one obtains in lowest non–trivial order
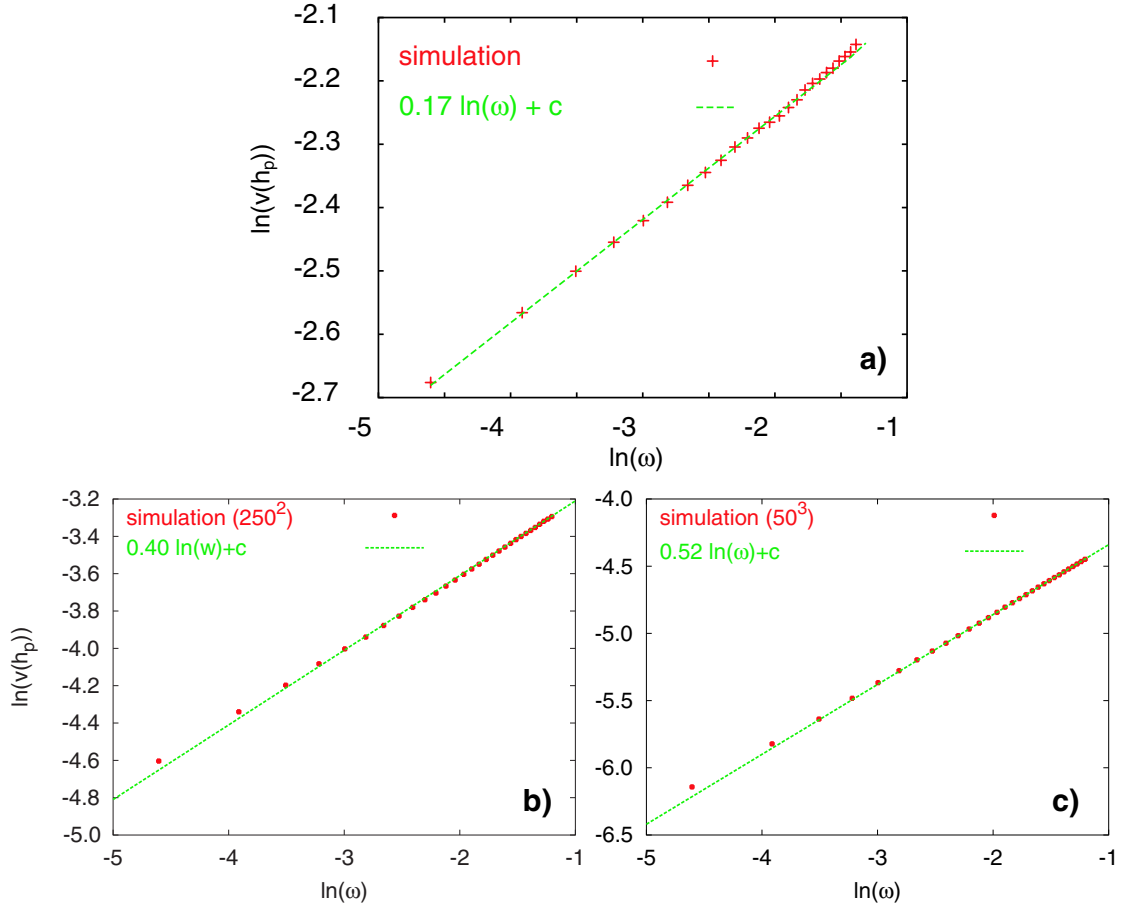
Figure C.6: Numerical results for $v(h_P)$, using eq. (C2.1), as a function of $\omega = \omega_0/\omega_P$. a) $D = 1$: The dashed line shows the prediction of eq. (C3.6) with $\beta/\nu z = 0.17$, in good agreement with the value 0.19 found in [CDW01]. b) $D = 2$: The numerically found exponent is 0.40 and from 2nd order ($\epsilon = 4 - D$)-RG: 0.46 c) $D = 3$: $\beta/\nu z = 0.52$ (num.) and 0.79 from theory.

in g the following equation for the velocity $v = \dot{z}_0(t)$, with $z_0(t) \equiv \langle z(\mathbf{x}, t) \rangle_x$ [Fei83]:

$$
\begin{aligned}
\frac{1}{\gamma} v(t) &= h(t) + \int_0^\infty dt' \int_{\mathbf{p}} \left\langle \tilde{g}'_{\mathbf{p}}\big(z_0(t)\big) \tilde{g}_{-\mathbf{p}}\big(z_0(t - t')\big) \right\rangle_d \gamma e^{-\Gamma \gamma \mathbf{p}^2 t'} \\
&\equiv h(t) + r_0(t).
\end{aligned}
\tag{C3.7}
$$

Here $\int_{\mathbf{p}} = \int \frac{d^D \mathbf{p}}{(2\pi)^D}$ and $\tilde{g}_{\mathbf{p}}(z) = \int d^D x \, e^{i\mathbf{p}\mathbf{x}} g(\mathbf{x}, z)$. Replacing the pair correlator of the random forces by $\Delta_0(z_0(t, t'))$ where $z_0(t, t') = \int_{t-t'}^t dt'' \, v(t'')$ we get

$$
r_0(t) \sim \int_0^\infty dt' (1 + \omega_P t')^{-D/2} \Delta'_0\big(z(t, t')\big),
\tag{C3.8}
$$

which results in corrections to the driving force and to the mobility which are in general non–local in time. If we assume that $\Delta_0(z)$ is an analytic function of its argument, it is easy to show that for $\omega_0 \gg \omega_P$, $r_0(t)$ is of the order $(\omega_P/\omega_0)^2$ and hence small (see appendix E2.2). In this parameter region the pinning potential merely slows down the motion of the wall in agreement with the result of our scaling considerations. In the opposite case, $\omega_0 \ll \omega_P$, perturbation theory breaks down. To treat this frequency region, it is instructive to consider first the case of a *dc-drive*, $h(t) \equiv h_0$, where the velocity is constant and hence $z(t, t') = vt'$. The t'–integral in (C3.8) leads to a correction of the mobility which diverges as $(l/v)^{(4-D)/2}$ for $v \to 0$ and $D < 4$. This divergence can be removed by a renormalization group treatment developed in [NSTL92, NF93, LNST97] (summarized in appendix E2.3). As a result of the elimination of the Fourier components $z_{\mathbf{p}'}$ with $|\mathbf{p}| < |\mathbf{p}'| < L_P^{-1}$ from eq. (C2.1), γ and $\Delta_0(z)$ are replaced there by the renormalized quantities

$$\gamma(p) \simeq \gamma(pL_P)^{-2+z} \, , \tag{C3.9a}$$

$$\Delta_p(z) \approx K_D^{-1}(\Gamma l/L_P^\zeta)^2 p^{4-D-2\zeta} \Delta^* \left(z(pL_P)^\zeta/l \right) \, . \tag{C3.9b}$$

$\Delta^*(x)$ exhibits a cusp-like singularity at $x = 0$ which develops on scales larger than L_P. In particular, $\Delta^*(x) \approx 1 - \sqrt{\epsilon - 2\zeta}|x| + (\epsilon - \zeta)x^2/6 + \mathcal{O}(|x|^3)$ for $|x| \ll 1$ [NSTL92, NF93, LNST97] and $\Delta^* e^{-\Delta^*} = e^{-1-x^2/6}$ for $x \gg 1$ [Fis86]. The renormalized disorder correlator is shown in Fig. E.5 in appendix E2.3.

In this way one generates a *renormalized* equation of motion which serves as starting point for a *convergent* perturbative expansion. The replacements (C3.9a), (C3.9b) are valid for momenta $\xi^{-1} < p < L_P^{-1}$ where ξ denotes the correlation length ξ_0 of the zero frequency depinning transition. In the spirit of the renormalization group treatment, fluctuations on scales larger than ξ can be neglected since they are uncorrelated. To get the lowest order corrections in the convergent expansion, one has to replace the bare quantities by the renormalized ones in eq. (C3.7). This leads in the limit $v \to 0$ to $r_0 = h_P \Delta^{*\prime}(0^+)/(2-\zeta) \equiv -\tilde{h}_P$ which is the RG result for the threshold value $\tilde{h}_P$. Replacing γ by $\gamma(\xi^{-1})$ on the left-hand side of eq. (C3.7), one obtains the correct result for the critical behavior of the velocity:

$$v \approx \gamma(\xi/L_P)^{2-z}(h - \tilde{h}_P) \approx v_P \left[(h - \tilde{h}_P)/\tilde{h}_P \right]^\beta \, .$$

In the case of an *ac-drive* the velocity $v(t)$ is periodic with $2\pi/\omega_0$. In each cycle of $h(t)$ the velocity goes through a region of small values, in which perturbation theory gives a contribution to γ^{-1} proportional to $\left(l/v(t) \right)^{\frac{4-D}{2}}$ as long as the period is large compared to $l/v(t)$. The cutoff t_c of the t'–integration is given by the approximate relation $t_c^{-1} \approx \omega_0 + v(t)/l$. These contributions are still large at $\omega_0, v(t) \to 0$. This breakdown of perturbation theory can be overcome by using the RG results discussed above on intermediate length scales

as in the dc case. Such a procedure is justified for momenta in the range $L_P^{-1} > |\mathbf{p}| \gg \xi^{-1}$, where ξ is now the minimum of ξ_0 and L_ω. At these scales the interface is still at criticality. Since ξ_0 depends via $h(t)$ on time and eq. (C3.7) includes retardation effects, a time dependent cutoff complicates the problem. Therefore we will restrict our consideration to the inner critical region where $\xi \approx L_\omega$; i.e., $|h_P - h| < h_P(\omega_0/\omega_P)^{1/\nu z}$. The renormalized effective equation of motion follows from (C3.7) with the replacements (C3.9a) and (C3.9b)[4]:

$$\frac{v(t)}{\gamma(L_\omega^{-1})} = h(t) + h_P \omega_P \int_0^\infty dt' \int_{\tilde{L}_\omega^{-1}}^1 d\tilde{p}\, \tilde{p}^{1+z-\zeta} e^{-\omega_P \tilde{p}^z t'} \Delta^{*\prime} \left(\int_{t-t'}^t dt'' v(t'') \tilde{p}^\zeta / l \right) , \quad \text{(C3.10)}$$

with $\tilde{L}_\omega = (\omega_P/\omega_0)^{1/z}$ and $\tilde{p} = pL_P$. Using this form of the equation of motion, we can explain the hysteresis appearing for $|h| < h_P$ (cf. Fig. C.1) more detailed. First we consider $\dot{h} < 0$: At h_c the sign of the velocity changes although the driving force is still positive. This can be understood as follows: until time $t = t_c$, with $h(t_c) = h_c$, the velocity was positive during half a period, hence the argument of the $\Delta^{*\prime}$ function is positive. Therefore the second term of the right-hand side of eq. (C3.10) is negative and cancels the positive driving force. Furthermore it is clear from this statement that h_c decreases with increasing amplitude h_0, which can also be seen in Fig. C.1.
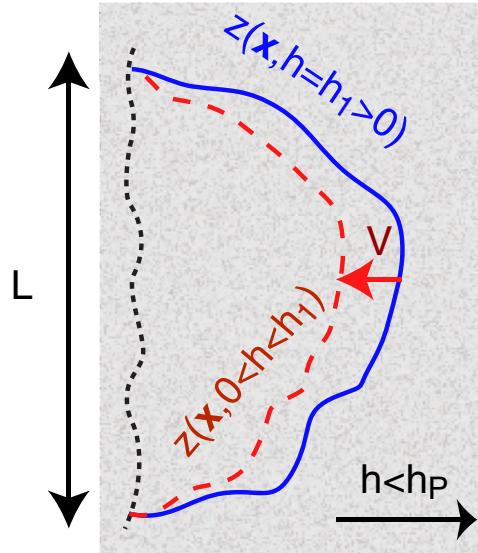
Figure C.7: Illustration of the process at h_c: A piece of the interface stopped to move in the (positive) h-direction at a driving force h_1 (solid line). Since we consider the case $\dot{h} < 0$ the elastic forces can flatten out the interface at a later time (dashed line) resulting in a negative (local) velocity.

---

[4]We neglect here contributions from momenta larger then L_P^{-1} which are expected to have a small effect if $\omega_0 \ll \omega_P$.

Physically the fact that the velocity becomes negative below h_P, even though the driving force is still positive (if $\dot{h} < 0$), can be seen in the following way: Since we are below h_P, some pieces of the interface are already pinned, while others can still move, because the local depinning field can be lower than the global one and we are considering the non-adiabatic regime. At h_c the following mechanism becomes dominant: Consider a piece of size L of the interface which has certain protrusion in z-direction which stopped to grow at a certain field value $h(t_1) = h_1 < h_P$ (see solid line in Fig. C.7). Since $\dot{h} < 0$, the field is smaller at a later time and the elastic forces then can shrink the protrusion, because they favor a flat interface, which results in a local negative velocity and therefore below h_c to a global negative velocity of the interface (see also illustration in Fig. C.7).

To solve eq. (C3.10) analytically, we consider a parameter region where the argument of $\Delta^{*\prime}(x)$ is small compared to unity; i.e., $\Delta^{*\prime}(x) \approx \Delta^{*\prime}(0^+) \operatorname{sgn}(\int_{t-t'}^{t} dt'' v(t''))$. One can show a posteriori that this condition is satisfied if $h_0 = \mathcal{O}(h_P)$. With this approximation the momentum integral in (C3.10) can be calculated, and we get (for details see appendix E2.4):

$$\frac{v(t)}{\gamma \tilde{L}_\omega^{2-z}} \approx h(t) - \frac{\tilde{h}_P}{\nu z} \left[S(t, \omega_P) - \tilde{L}_\omega^{-\frac{1}{\nu}} S(t, \omega_0) \right]. \tag{C3.11}$$

Here $S(t, \omega) \equiv \int_0^\infty d\tau \, \tau^{-\delta} \tilde{\Gamma}_\delta(\tau) \operatorname{sgn} z_0(t, \tau/\omega)$, $\delta = 1/(\nu z) + 1$, and $\tilde{\Gamma}_\delta(\tau) \equiv \Gamma_\delta(0) - \Gamma_\delta(\tau)$, where $\Gamma_\delta(\tau) = \int_\tau^\infty dt \, t^{\delta-1} e^{-t}$. $z_0(t, \tau/\omega)$ changes its sign at $t = t_0 + n\pi/\omega_0$, $n \in \mathbb{Z}$. The dominating part to $S(t, \omega)$ comes from $\tau < \mathcal{O}(1)$. To solve this integral equation for $h \geq 0$ and $\omega_0 \ll \omega_P$, we note, that the sign of $z_0(t, \tau/\omega_P)$ is always positive for $\tau < 1$ and hence $S(t, \omega_P) \approx \nu z$. For $t \lesssim t_c$ also $z_0(t, \tau/\omega_0) > 0$ for the dominating small τ region of the τ-integration in $S(t, \omega_0)$. This leads to $\phi_-(x) \approx c_- + x$, $c_- \approx S(t_c, \omega_0)/\nu z$. By decreasing t, $S(t, \omega_0)$ is diminished since regions with negative $z_0(t, \tau/\omega_0)$ contribute increasingly, which in turn explains the second weak hysteresis observed in Fig. C.1 [MWA$^+$98]. Next we consider the region $t \gtrsim t_c$, i.e., $h < h_c$, $v < 0$. By increasing t, $S(t, \omega_0)$ is reduced with respect to $S(t_c, \omega_0)$ which leads to a positive curvature of $v(h)$ for $\dot{h} < 0$. Although that region is beyond the scope of our RG calculation, since retardation effects require to consider the avalanche motion in the region $h < h_c$, it is then tempting to conclude $|v(h = 0, \dot{h} < 0)| = \mathcal{O}(\omega_0/\omega_P)^{\beta/\nu z}$. For large negative values of h, $v(h)$ has to reach again the result of the adiabatic limit. Together with the inversion symmetry this explains the inner hysteresis.

To show that this result holds in higher dimensions we have solved the equation of motion also for $D = 2$ (with discrete interface size 1000^2) and $D = 3$ (size 100^3) numerically. The resulting velocity hysteresis for $h_0 > h_P$ are plotted in Fig. C.8. One sees that the double hysteresis persists in higher dimensions and that the influence of the disorder becomes smaller
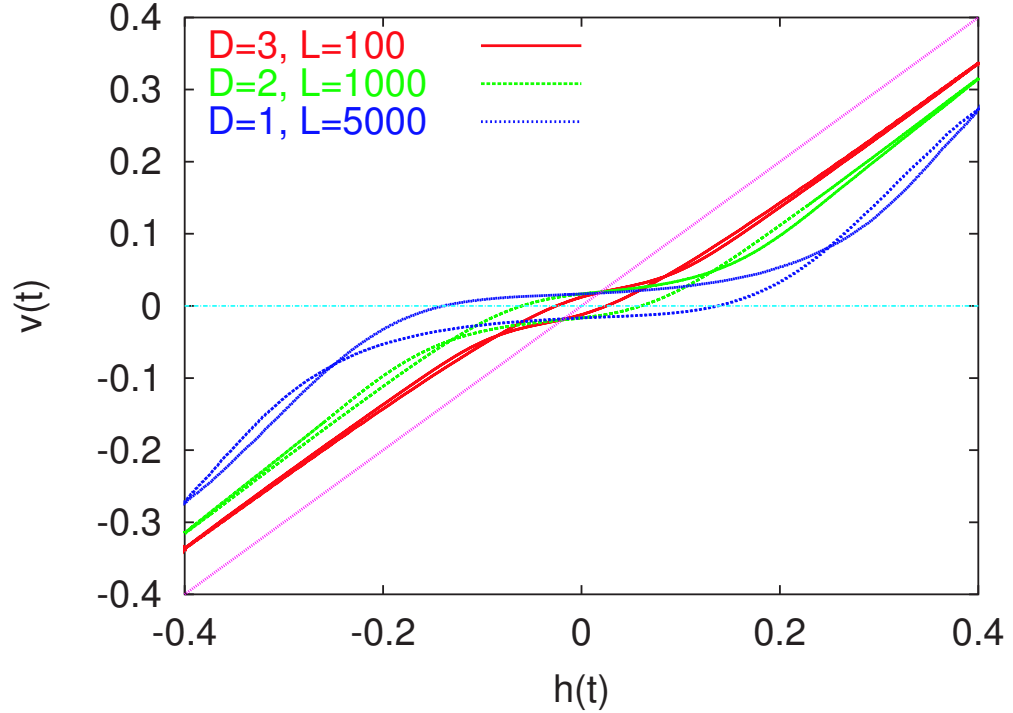
Figure C.8: Velocity hysteresis curves for $D = 1, 2, 3$. The equation of motion (C2.1) was solved numerically for interface sizes 5000, 1000^2 and 100^3, respectively.

(e.g., h_P decreases).

3.4 Thermal fluctuations

Next we briefly consider the influence of thermal fluctuations on the force - velocity relation, restricting ourselves to the low temperature region $T \ll T_P = \Gamma l^2 L_P^D$, T_P is a typical pinning energy. *(i)* In the adiabatic limit and for $|h_0 - h_P| \ll h_P$, the velocity obeys the scaling relation $v(h, T) = (h - h_P)^\beta \psi \left[(h - h_P)^\theta / T \right]$ where θ is a new exponent which depends on the shape of the potential at the scale L_P [Mid92]. For $\omega_0 > 0$ one can extend the scaling relation (C3.6) to a second scaling field $\frac{h - h_P}{h_P} \left(\frac{T_P}{T} \right)^{1/\theta}$ and one finds in particular for $h \approx h_P$

$$v(h_P, T) \approx v_P \left(\frac{\omega_0}{\omega_P} \right)^{\frac{\beta}{\nu z}} \tilde{\phi}_\pm \left[\left(\frac{T}{T_P} \right)^{\frac{1}{\theta}} \left(\frac{\omega_P}{\omega_0} \right)^{\frac{1}{\nu z}} \right], \qquad (C3.12)$$

with $\tilde{\phi}_\pm [x \to \infty] \sim x^\beta$ and $\tilde{\phi}_\pm [x \to 0] \sim \tilde{c}_\pm$. The thermal smearing of the zero frequency depinning transition is still seen at finite ω_0, as long as $\omega_0 < \omega_T(h_P) \approx \omega_P \left(\frac{T}{T_P} \right)^{\nu z / \theta}$. On

the other hand for small fields, $h \ll h_P$, the domain wall shows creep behavior

$$v(h, T) \approx v_P e^{-\frac{T_P}{T} \left(\frac{h_P}{h}\right)^\mu} \;,\;\; \mu = \frac{2\tilde{\zeta} + D - 2}{2 - \tilde{\zeta}} \;,$$

where $\tilde{\zeta}$ denoted the equilibrium roughness exponent [IV87]. *(ii)* It was shown in [NPV01a], that the creep law is valid also at finite frequencies as long as

$$\omega_0 \ll \omega_T(h) \approx \omega_P e^{-\frac{T_P}{T} \left(\frac{h_P}{h}\right)^\mu} \;,\;\; h \ll h_P \,.$$

For $\omega_0 > \omega_T(h)$ and $h_0 \ll h_P$ thermal effects are inessential. Thus, in the region $\omega_0 \ll \omega_T(h)$ (Fig. C.3) the force - velocity relation is that of the adiabatic case at finite temperature.

4 Dynamics below the threshold

Up to now we focused on the case $h_0 > h_P$. In this section we briefly discuss the non-adiabatic motion of the system in the case, when the amplitude of the driving force is smaller than the zero temperature depinning threshold.

In Fig. C.9 the numerical solution of the equation of motion (C2.1) is shown in form of the velocity hysteresis for $D = 1$. Note, that all hysteresis loops are cycled through in clockwise direction. In plot (a) the frequency is well below the pinning frequency ω_P ($\omega_0/\omega_P = 0.01$). If the amplitude is not too low one sees a pronounced "bump" in the velocity hysteresis curve when the driving force reaches its maximum or minimum value for increasing or decreasing field, respectively, which is related to the appearance of avalanches in the system [see also (d) in Fig. C.9]. This effect becomes weaker if the amplitude is lowered at fixed frequency or disappears completely for very high frequencies [see (b) and (c) in Fig. C.9]. For high frequencies one also sees that the hysteresis loop gets a phase-shift of $\pi/2$ compared to the low frequency loop and becomes narrower with increasing frequency and finally goes over to $v(t) = \gamma h(t)$ for $\omega_0 \to \infty$.

In order to understand this process physically, we can start with the case of a dc-drive in the non-adiabatic regime.

4.1 Constant driving force

First, we consider the case $\omega_0 = 0$ and $T = 0$. In the adiabatic case, this is the pinned region and therefore simply $v \equiv 0$.
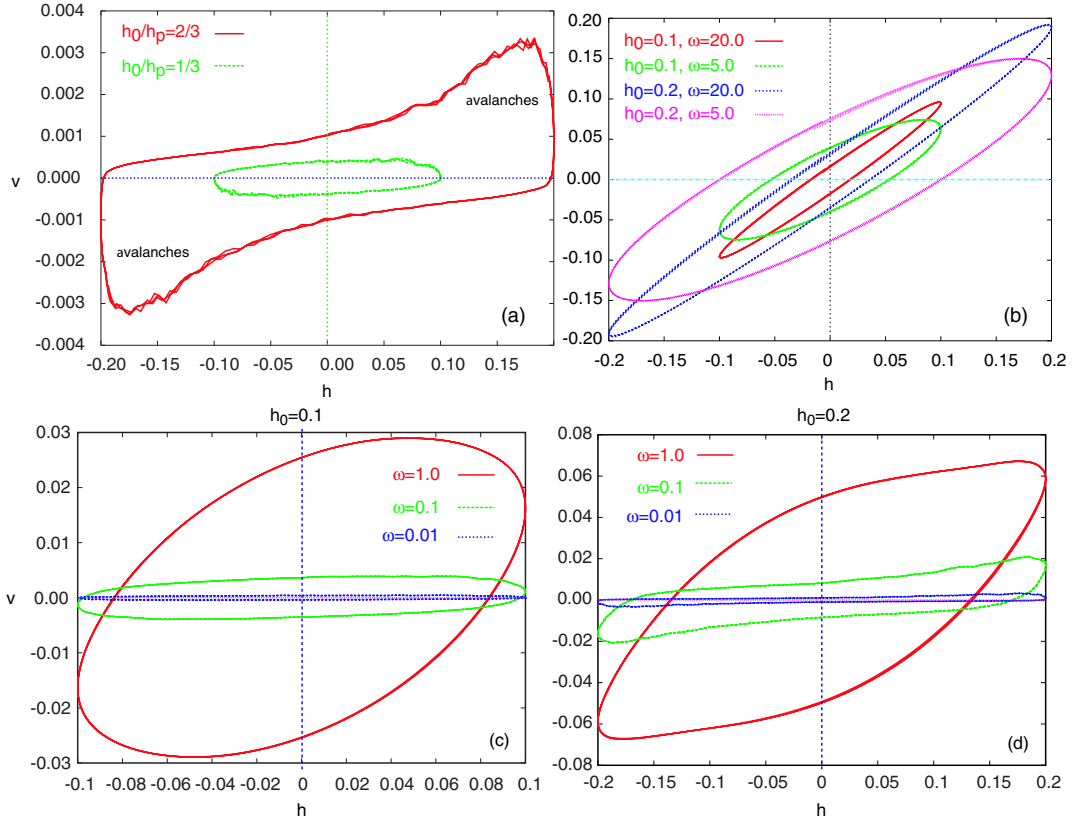
Figure C.9: Velocity hysteresis loops below threshold for $D = 1$. Hysteresis loops for very low (a) ($\omega = 0.01$) and high frequencies (b) ($\omega = 5.0$ and $\omega = 20.0$). For each frequency the amplitude was chosen such that $h_0/h_P \approx 2/3$ and $h_0/h_P \approx 1/3$. (c) For $h_0 = 0.1$ and (d) for $h_0 = 0.2$, both at frequencies $\omega = 0.01, 0.1, 1.0$.

Here, we start with an arbitrary equilibrium configuration of the interface without an applied driving force. At time $t = 0$ a constant driving force $h_0 < h_P$ is switched on and the interface moves to a new (pinned) equilibrium position by avalanche processes.

The numerically found time dependence of the averaged velocity for a one-dimensional interface is shown in Fig. C.10.

Empirically, the decay of the mean interface velocity can be fitted by

$$v(t) \approx h_0 e^{-\sqrt{t/t_0(h_p - h_0)}},$$

if h_0 is not too close to h_P. This form is reasonable in the sense, that it decays with time and the typical decay time increases if one comes closer to the depinning field. In the simulation of the one-dimensional interface the parameters are: $h_P \approx 0.27$ and $t_0 \approx 0.1$.

For a complete theoretical explanation, one has to know the statistics for the avalanches,
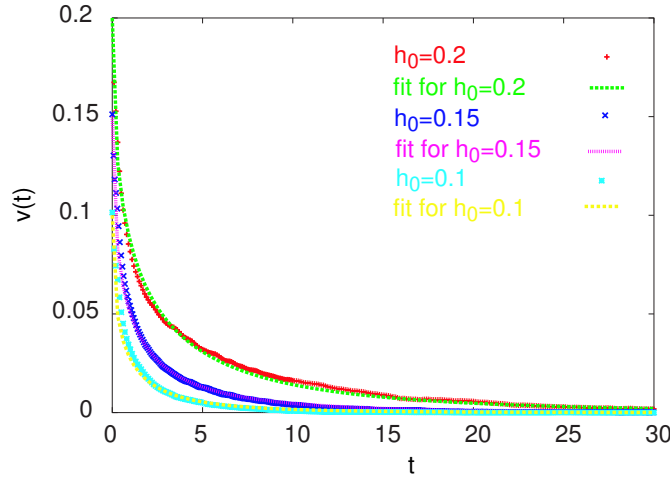
Figure C.10: Time dependence of the interface velocity for different dc-driving forces if one starts at time 0 with an arbitrary equilibrium interface configuration for $h = 0$. The fitted behavior is $v(t) \approx h_0 e^{-\sqrt{t/t_0(h_P - h_0)}}$ with $h_P \approx 0.27$ and $t_0 \approx 0.1$.

i.e., the probability to create an avalanche of a certain size at a given time, which also takes into account the history of the system. This task is still open and a forthcoming project.

4.2 (Linear) increasing driving force

Now we go over to the case of an increasing driving force. From the full numerical solution in the steady state, shown in Fig. C.9, we see, that the contribution of avalanches also increases with increasing driving force if $h > 0$. Again, we start with an equilibrium interface configuration without driving force, but now increase the driving force from 0 at times $t \leq 0$ to h_0 at a certain time $t_0 > 0$. In Fig. C.11 the resulting velocities for $h(t) = h_0 \sin(\pi/2 \cdot t/t_0)$ and $h(t) = h_0 t/t_0$ for a one-dimensional interface are shown (with $h_0 = 0.15$ and $t_0 = 50$).

One sees, that the velocity increases in the case of a linear increasing field until we stop the increase at time $t = t_0$, on the other hand we find that in the case of a sinusoidal increasing field, the velocity already decays even before the maximal value h_0 is reached [Fig. C.11 (left)], which can be seen even better in a plot v vs. h [Fig. C.11 (right)]. Qualitatively this behavior fits very well with the avalanche region of the steady state velocity hysteresis [Fig. C.9 (a)], if one neglects the initial virgin curve, observed in Fig. C.11.
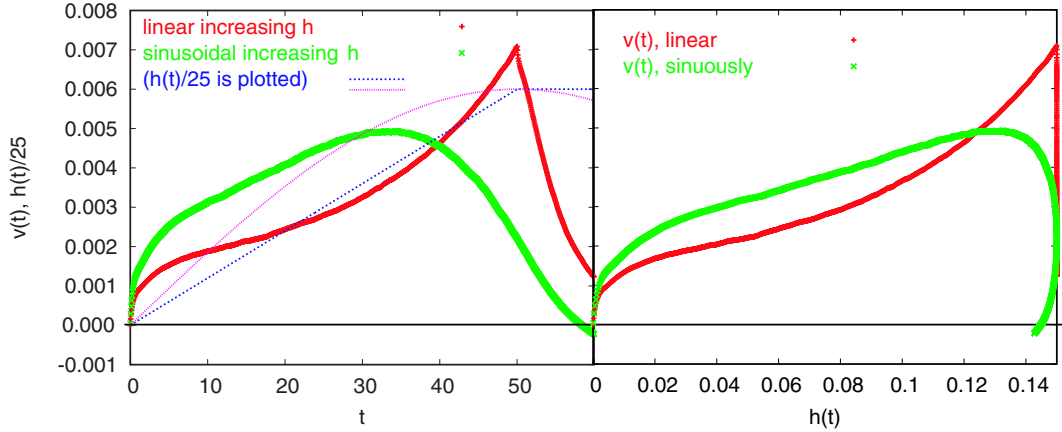
Figure C.11: Left: Time dependence of the interface velocity for linear and sinusoidal increasing driving force. Right: $v(t)$ vs. $h(t)$. In both cases $h_0 = 0.15$ and $t_0 = 50$. The velocities are averaged over 10000 disorder realizations.

4.3 AC driving

After the observations of the previous two section, we can now try to get a complete physical picture of the non-adiabatic effects below the depinning threshold.

In the ac-case, we can identify different regions in the $h_0 - \omega_0$ space below h_P, shown in Fig. C.12, which extents the picture for $h_0 > h_P$ shown in Fig. C.3.

The different regions can be characterized as follows:

(i) *asymptotically free motion for $\omega_0/\omega_P \gg 1$*: For very high frequencies the motion of the interface is essentially free in a local minimum of the pinning potential. The frequency is so high, that the time for propagation in one direction is too small to "climb up" the energy barriers. For $\omega_0 \to \infty$ the velocity is given by $v(t) = \gamma h(t)$. See also discussion in section 3.2.

(ii) *frequency creep motion without avalanches for $\omega_a(h_0) < \omega_0 < \omega_P$*: The time t_a which is needed to perform a typical avalanche sets another frequency scale $\omega_a(h)$ and can be estimated as

$$t_a \omega_P \approx (L_a/L_P)^z \approx (h_p/h)^{z/(2-\zeta)} \,, \tag{C4.1}$$

where $L_a \approx L_p(h_p/h)^{1/(2-\zeta)}$ is the typical avalanche size [NPV01a]. This means that for $t_a > 1/\omega_0$ avalanches cannot develop and therefore do not contribute to the motion of the interface. The crossover to the avalanche region is given by the frequency $\omega_a(h) \approx \omega_P(h/h_p)^{\nu z}$.
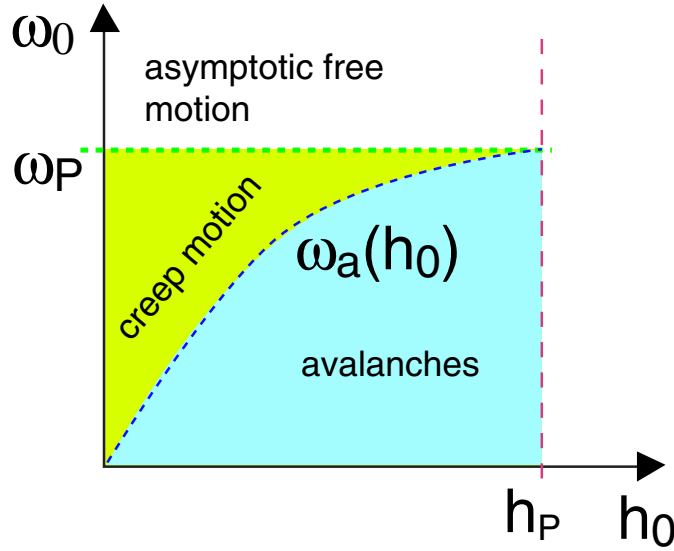
Figure C.12: Regions in h_0 - ω_0 space. Above ω_P the motion of the interface is essentially free, since it only moves in one minimum of the pinning potential. Below ω_P one finds a region where disorder is relevant, but the frequency is too high to allow for avalanches (*frequency creep motion*). Below a frequency $\omega_a(h_0)$ one can identify a region where the motion is dominated by avalanches.

Therefore the motion for $\omega_a < \omega_0 < \omega_P$ can be seen as motion in an energy minimum of the pinning potential, where the interface can "follow" the driving force (*mechanical motion*). This means that the velocity becomes zero as soon as the driving force becomes maximal, resulting in an elliptical velocity hysteresis. We can assume that the velocity semi-axis of this ellipse scales as $v(h = 0) \sim \gamma h_0 (\omega_0/\omega_P)^\kappa$. In Fig. C.13 the maximum velocity (which is given by $v_{\text{max}} \approx v(h = 0)$ in the region under consideration) is plotted versus the amplitude [left, cf. also scaling ansatz in (C3.6)] and frequency (right) showing, that κ is approximately 1.

Using this information, a reasonable interpolation formula to the asymptotically free regime is given by

$$\overline{v}(t) \approx \gamma h_0 \left(\frac{\omega_0/\omega_P}{\omega_0/\omega_P + 1} \right)^\kappa \sin \left(\omega_0 t + \frac{\pi}{2} \frac{1}{(\omega_0/\omega_P)^\alpha + 1} \right) , \qquad \text{(C4.2)}$$

where $\kappa \approx 1$.

A plot of this function is shown in Fig. C.14 and can be compared to the simulation result for $D = 1$ plotted in Fig. C.9 (b) and (c).
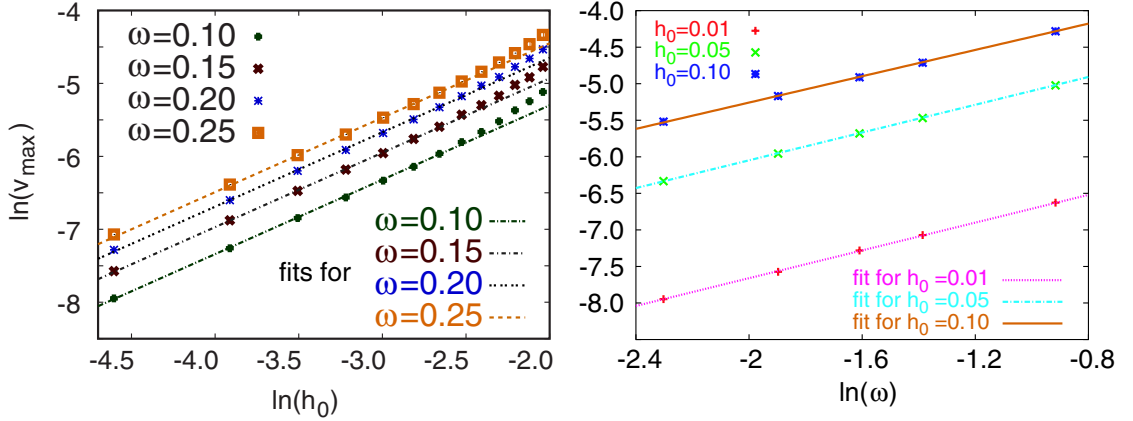
Figure C.13: Left: h_0-dependency of the maximum velocity for low h_0 and various ω. The marks show the data from the simulation yielding a linear fit with slope 1. Right: ω-dependency of the maximum velocity for various h_0. The simulation data can also be fitted linearly with slope $\kappa = 0.95$. Both plots are in the frequency creep region, although one already sees the effects of avalanches for 'high' h_0 and low frequencies in the left plot.

$\overline{v}(t)$ has the following properties:

(a) For $\omega_0 \to \infty$ the prefactor of the sine-function becomes just γh_0 and the phase-shift in the argument becomes zero, i.e., $\overline{v}(t) \approx \gamma h(t)$

(b) For $\omega_0 \to 0$ the prefactor becomes $\gamma h_0 (\omega / \omega_2)^\kappa$ and the phaseshift $\pi/2$, which describes the elliptical velocity hysteresis and gives the scaling for the *velocity semi-axis*.

(c) Is zero for $\omega_0 = 0$, since this is the pinning regime.

The velocity for $h(t) = 0$ is then given by

$$\overline{v}[h(t) = 0] \approx \gamma h_0 \left(\frac{\omega_0 / \omega_P}{\omega_0 / \omega_P + 1} \right)^\kappa \sin \left(\frac{\pi}{2} \frac{1}{(\omega_0 / \omega_P)^\alpha + 1} \right) \tag{C4.3}$$

Simulation results and fits to this expression are shown in Fig. C.15, yielding $\kappa \approx 0.94$ and $\alpha \approx 1.15$, and therefore confirming (C4.3) very well.

(iii) *non-adiabatic avalanche motion for $\omega < \omega_a$:* We consider the case $h > 0$: If h increases, one can expect the same behavior of the velocity as described in section 4.2 (except the virgin curve, which has to be replaced by an interpolation to the elliptical part for $h < 0$). After the driving force reached its maximum, the motion
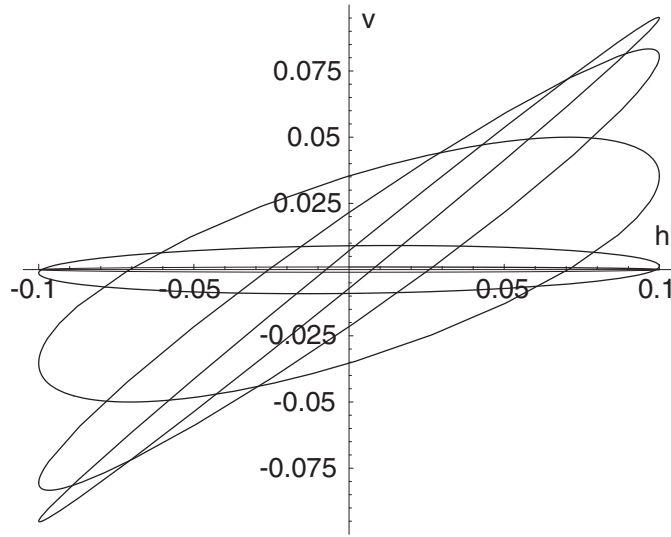
Figure C.14: Plot of eq. (C4.2) for $h_0 = 0.1$ and various frequencies ($\kappa = \alpha = 1$).
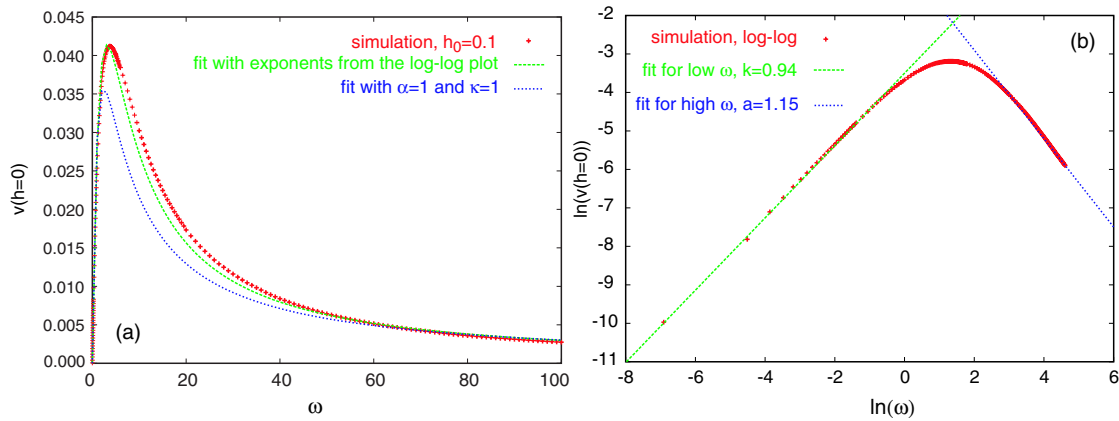
Figure C.15: Scaling of $v(h(t) = 0)$ with frequency ($h_0 = 0.1$) from the frequency creep to the asymptotically free regime. Left: $v(h = 0)$ vs. ω and fit with $\kappa = \alpha = 1$ and with values for κ and α obtained from the log-log fit. Right: log-log plot with linear fits for low (slope $\kappa \approx 0.94$) and high (slope $-\alpha \approx -1.15$) frequencies.

for $\dot{h} < 0$ of the interface can be described by the mechanical motion observed in the case $\omega_a < \omega_0 < \omega_P$, i.e., only the elliptical part of the velocity hysteresis is developed. Together with the inversion symmetry this qualitative picture is in good agreement with the simulation results, shown in Fig. C.9 (a).

We now have a qualitative physical picture of the effects below the depinning threshold.

However, for a complete theoretical description one needs an understanding of the statistics of non-adiabatic avalanches, as already mentioned.

5 Susceptibilities of finite systems: A numerical study for granular superferromagnetic CoFe/Al$_2$O$_3$

In this section we present numerical studies of the complex ac magnetic susceptibilities, motivated by recent experiments on the superferromagnetic (SFM) system [Co$_{80}$Fe$_{20}$(1.4 nm)/ Al$_2$O$_3$(3 nm)]$_{10}$ [KPB$^+$01, CSK$^+$02] being a realization of a densely packed ensemble of ferromagnetically (FM) interacting nanoparticles (see Fig. C.16).
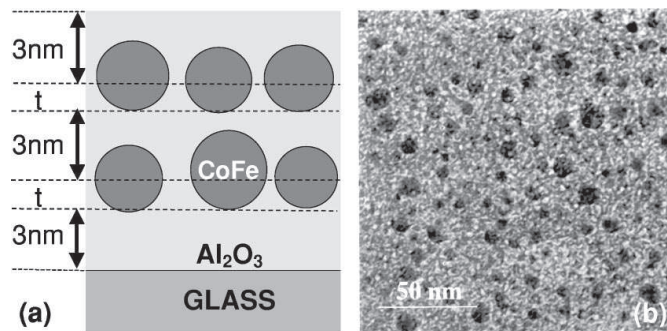
Figure C.16: Picture taken from Ref. [KPB$^+$01]: (a) Schematic cross section of a discontinuous metal-insulator multilayer system (DMIM) consisting of substrate, Al_2O_3 layers of thickness 3 nm and $CoFe$ layers of thickness t forming quasispherical nanoparticles, and (b) transmission top view electron micrograph of a $CoFe(t = 1.3\text{nm})/Al_2O_3(3\text{nm})$ bilayer, where dark circles indicate $CoFe$ nanoparticles embedded into gray-scaled Al_2O_3.

While individual single-domain FM nanoparticles exhibit superparamagnetic (SPM) behavior [Née49, Bro63, DFT97, GP00], very different kinds of phenomena can be observed in interacting ensembles, depending on the type and strength of interactions. Dipolar interactions become relevant up to a temperature of approx. 100K, since the magnetic moment is of the order $5000\mu_B$, while the particle distances are of the order 1–10nm. The complex ac susceptibility, $\chi' - \imath\chi''$, reveals that the dynamical magnetic behavior can be explained within the concept of domain wall motion in an impure ferromagnet [CSK$^+$02, PCS$^+$04a]. That means, the granular system behaves like a thin FM film, only with the difference, that the atomic moments are to be replaced by 'super-moments' of the individual particles. This arises from the *Cole-Cole plot*, χ'' versus χ' [CC41]. Hence we will focus on the Cole-Cole representation and compare it to that found experimentally.

5.1 Complex ac susceptibilities and Cole-Cole representation

Magnetic systems exhibiting relaxational phenomena can be characterized by the complex ac susceptibility. The time dependent complex ac susceptibility is defined as

$$M(t) = \tilde{\chi}(t)H(t)\,, \tag{C5.1}$$

with the *complex* external ac-field $H(t) = -\imath h_0 e^{\imath \omega_0 t}$, $[h(t) = \Re(H(t))]$, and the complex magnetization $M(t)$. In this section we study the time independent term of the Fourier series for $\tilde{\chi}(t)$

$$\tilde{\chi}_n = \frac{1}{\mathcal{T}} \int\limits_0^{\mathcal{T}} dt\, \tilde{\chi}(t) e^{\imath \Omega_n t}\,, \tag{C5.2}$$

with $\Omega_n = 2\pi n/\mathcal{T}$ and $\mathcal{T} = 2\pi/\omega_0 = 1/f$, namely:

$$\chi \equiv \chi' - \imath \chi'' = \tilde{\chi}_0 = \frac{1}{\mathcal{T}} \int\limits_0^{\mathcal{T}} dt\, \tilde{\chi}(t)\,. \tag{C5.3}$$

This defines the real and imaginary part of χ, χ' and χ'', respectively, as follows

$$\chi'(\omega_0) = \frac{1}{h_0 \mathcal{T}} \int\limits_0^{\mathcal{T}} dt\, M(t) \sin(\omega_0 t) \tag{C5.4a}$$

$$\chi''(\omega_0) = -\frac{1}{h_0 \mathcal{T}} \int\limits_0^{\mathcal{T}} dt\, M(t) \cos(\omega_0 t)\,. \tag{C5.4b}$$

Or equivalently - if we define $\tilde{\chi}(t) = \frac{dM(t)}{dH(t)} = \dot{M}(t) \left(\frac{dH}{dt}\right)^{-1}$:

$$\chi'(\omega_0) = \frac{1}{2\pi h_0} \int\limits_0^{\mathcal{T}} dt\, \dot{M}(t) \cos(\omega_0 t) \tag{C5.5a}$$

$$\chi''(\omega_0) = \frac{1}{2\pi h_0} \int\limits_0^{\mathcal{T}} dt\, \dot{M}(t) \sin(\omega_0 t)\,, \tag{C5.5b}$$

where $\dot{M}(t) \propto v(t)$, the (mean) domain wall velocity, which is a function of the external field h and temperature T.

One way of presenting the data for the complex susceptibility is the Cole-Cole or Argand representation. The imaginary part is plotted against the real part of the susceptibility,

χ'' versus χ' [CC41, Jon83]. It can serve as a fingerprint to distinguish different magnetic systems by their dynamic response. E.g., a monodisperse, i.e., all particle have the same volume V, non-interacting ensemble of SPM particles has exactly one relaxation time, $\tau = \tau_0 \exp(KV/k_B T)$ [Née49, Bro63], where K is an anisotropy constant, and will display a semicircle with the center on the χ'-axis. This can easily be derived from an analytic expression for the ac susceptibility for a monodisperse SPM ensemble with a random distribution of the anisotropy axis directions [ADJ$^+$97]: The authors of this paper derive the following expression for the real and imaginary part of the susceptibility

$$\chi'(\omega_0) = \mu_0 \frac{M_s^2}{3K}\left[1 + \frac{KV}{k_B T}\frac{1}{1+(\omega_0\tau)^2}\right],$$

$$\chi''(\omega_0) = \mu_0 \frac{M_s^2}{3}\frac{V}{k_B T}\frac{\omega_0\tau}{1+(\omega_0\tau)^2},$$

where M_s is the saturation of maximum magnetization.

Defining $\alpha \equiv \mu_0 M_s^2/3K$ and $\sigma \equiv KV/k_B T$ and eliminating ω_0 one gets

$$\chi'' = \sqrt{\left(\frac{\alpha\sigma}{2}\right)^2 - \left(\chi' - \frac{\alpha(2+\sigma)}{2}\right)^2}, \tag{C5.6}$$

which describes a circle with the radius $r = \alpha\sigma/2$ and center at $(\alpha(2+\sigma)/2; 0)$ in the Cole-Cole plane.

In the case of a particle size distribution and hence a distribution of relaxation times the Cole-Cole semicircle is expected to be shifted downward [Jon83]. Extremely high poly-dispersivity is found in spin glass systems, where the distribution of relaxation times is expected to become infinitely broad [Myd93]. Fig. C.17 shows an experimentally obtained Cole-Cole plot for the system $[\text{Co}_{80}\text{Fe}_{20}(0.9\text{ nm})/\text{ Al}_2\text{O}_3(3\text{ nm})]_{10}$ at different temperatures, $T = 50$, 55 and 60 K [PSB$^+$03], which gives a hint to the multi-dispersivity of the sample.

5.2 Numerical methods

We study the complex ac-susceptibility in two different approaches: an adiabatic approach, based on the velocity of interfaces for dc-driving and a non-adiabatic, approach based on the full equation of motion (C2.1), which both will be explained in detail in the following sections.
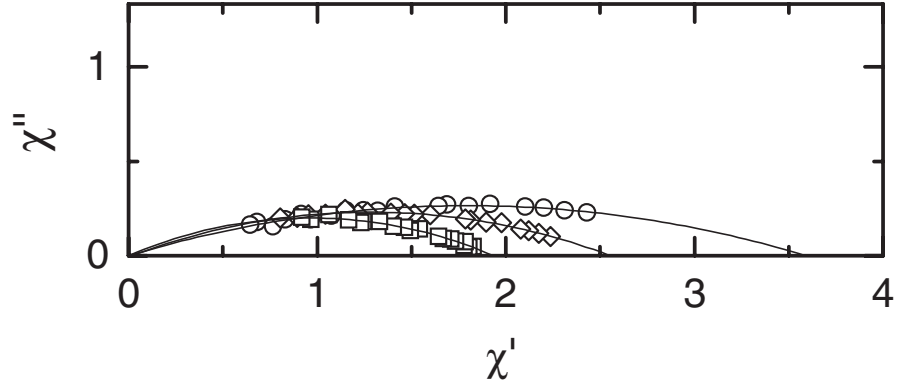
Figure C.17:   Experimentally obtained Cole-Cole plot for the system [CoFe(0.9 nm)/Al$_2$O$_3$(3 nm)]$_{10}$ at three different temperatures, $T = 50$, 55 and 60 K (Ref. [PSB$^+$03]).

5.2.1 Adiabatic approach

For the first approach, we use the expression for the mean domain-wall velocity in the adiabatic dc-driving regime, given in Ref. [NPV01b], which interpolates between the creep regime and sliding motion,

$$v(h_0, T) = \begin{cases} \gamma h_0 F(x,y) & \text{for } h_0 \neq 0, \\ 0 & \text{for } h_0 = 0, \end{cases} \tag{C5.7}$$

where $x = h_0/h_p$, $y = T_p/T$, with the driving force h_0, depinning field h_P (at $T = 0$) and a typical pinning energy T_P, γ the mobility coefficient, and

$$F(x,y) = \frac{\Theta(1-x)}{1 + (yx^{-\mu})^{\beta/\theta}} \exp\left[yx^{-\mu}(1-x)^\theta\right] \tag{C5.8}$$

$$+\Theta(x-1)\left[\frac{1}{1 + (yx^{-\mu})^{\beta/\theta}} + \left(1 - \frac{1}{x}\right)^\beta\right].$$

Here $\Theta(x)$ is the step function and μ, β, and θ the relevant critical exponents [NPV01b]. The dynamics of the domain wall is determined by the equation of motion

$$\dot{z} = v(h(t)), \tag{C5.9}$$

where z is the mean displacement from a flat starting configuration of the interface with $0 \leq z \leq L_z$ and L_z being the length of the sample in z-direction. Compared to the experiment this would be a in-plane direction of the sample. Hence the magnetization is

$$M(t) = M_s \left(\frac{2z(t)}{L_z} - 1 \right) \in [-M_s, M_s], \qquad (C5.10)$$

where M_s is the maximal magnetization of the system.

5.2.2 Non-adiabatic approach

Since equation (C5.7) was obtained for an adiabatically changing field, it can only be used as an approximation, if the frequency is sufficiently small, $\omega_0 \ll \omega_T(H)$ (see section 3.2, Fig. C.3). One should also note, that the above approach does not hold at $T = 0$ and $h_0 < h_P$, since the velocity v, and therefore χ would be zero below h_P. But we found, that for $\omega_0 > 0$ the depinning transition is smeared out and hence $v \neq 0$.

In order to include the non-adiabatic effects (e.g., the hysteresis of the velocity), one has to start with the underlying equation of motion (C2.1), sometimes also referred to as *Edwards-Wilkinson equation* [EW82]. Here we study the experimentally relevant case $D = 2$.

Note, that eq. (C2.1) is written for zero temperature. For finite temperatures an additional thermal noise term $\eta(\mathbf{x}, t)$ has to be added to the right-hand side of (C2.1). On the other hand, the relaxation times for the domain-wall creep at low temperatures are very long ($\gg \omega_0^{-1}$) and we consider only finite (not exponentially low) frequencies, such that we can concentrate on the zero temperature equation of motion, since we have shown that thermal effects are not essential if the frequencies are not too low (section 3.4).

In this section we will focus on the numerical solution of this equation for finite ($L_z < \infty$) systems. In this case, the interface will hit the boundary of the system for low enough frequencies, such that the magnetization will saturate ($-M_s \leq M \leq M_s$). Therefore we introduce the critical frequency ω_c or f_c, which depends on L_z (defined by $L_\omega \approx L_z$, i.e., $\omega_c \approx \omega_P(L_P/L_z)^z$), above which the system behaves like an infinite system, i.e., the interface does not reach the system boundary since $L_\omega < L_z$, and below which the magnetization saturates ($L_z > L_\omega$).

For the numerical integration of (C2.1) we use the same discretization and disorder realization as introduced in section 3.2. In the next section we compare the results from both approaches to the experimental measurements. Note, that we use "real" frequencies f, instead of angular frequencies ω_0 in the following.

5.3 Comparison to the experiment

Fig. C.18 shows an example of a magnetization hysteresis loops from simulations within approach 5.2.1 at $T/T_p = 1.5$ and $h_0/h_p = 1.5$, at different frequencies $f = 0.001$ (a), 0.01
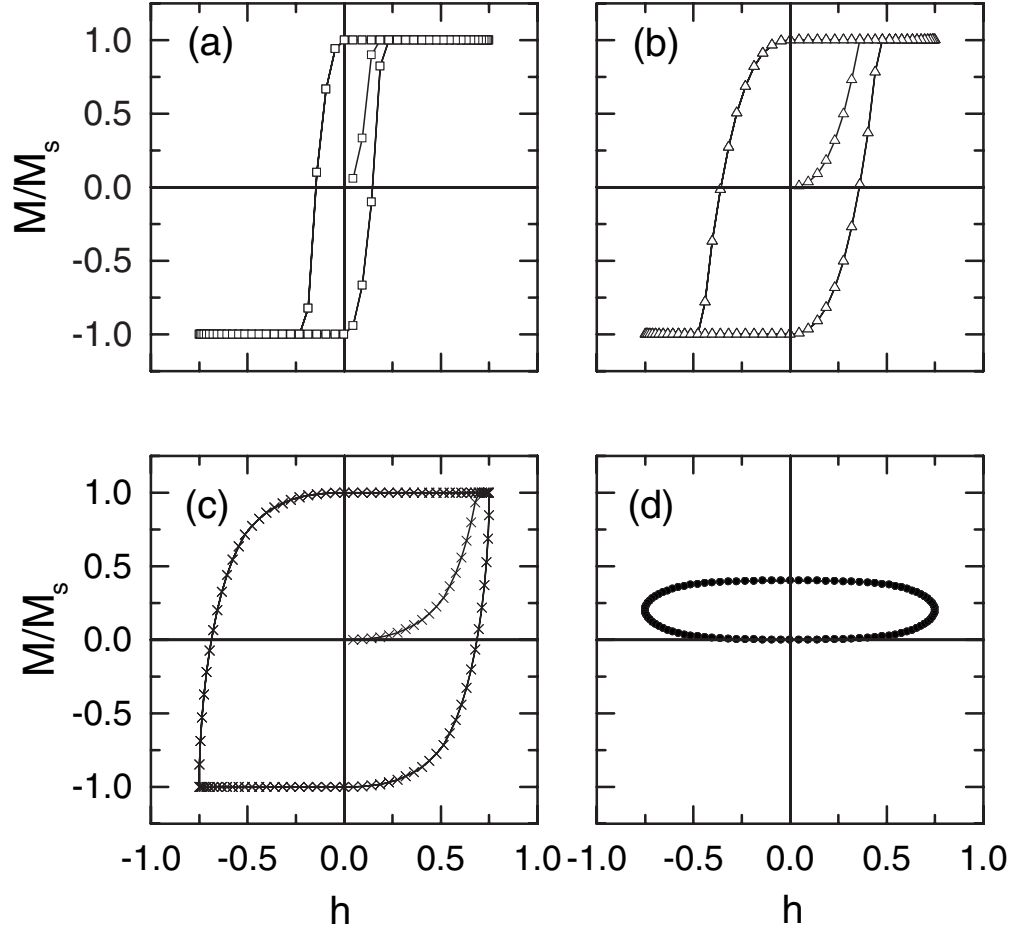
Figure C.18: M/M_s vs. h curves from simulations of a domain-wall in the adiabatic regime with $T/T_p = 1.5$, $h_0/h_P = 1.5$, $\gamma = 1.0$, $\mu = 0.24$, $\theta = 0.83$, and $\beta = 0.66$ at different frequencies $f = 0.001$ (a), 0.01 (b), 0.1 (c), and 1.0 (d).

(b), 0.1 (c), and 1.0 (d) (in dimensionless units, see 3.2). The values for the parameters and critical exponents are taken from the literature, i.e., $\gamma = 1.0$, $\mu = 0.24$ [LFC+97], $\theta = 0.83$ [NSV90b] and $\beta = 0.66$ [RHL+99][5]. With increasing frequency the hysteresis loop broadens until it becomes elliptically shaped above $f = 0.1$, loosing also its inflection symmetry. Similar results are found in experiments [CSK+02, RFMLDB02].

The ac-susceptibility of such hysteresis cycles can be calculated from equations (C5.4a) and (C5.4b). In Fig. C.19 the obtained data is shown for a specific set of values, $T/T_p = 0.5$ and $h_0/h_p = 0.8$. In (a) one finds the real and imaginary part of the ac susceptibility, χ' and

---

[5]Note, that the selection of values does not have a significant influence on the behavior under consideration here, especially the qualitative picture does not change.
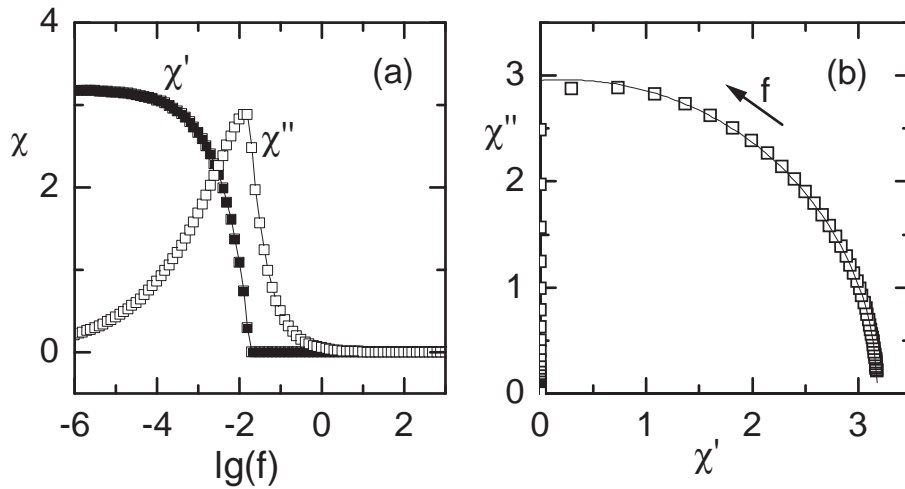
Figure C.19: (a) ac susceptibility, χ' and χ'' vs. ac frequency, f, at $T/T_p = 0.5$, $h_0/h_p = 0.8$ for $\gamma = 1.0$, $\mu = 0.24$, $\theta = 0.83$, and $\beta = 0.66$. (b) Same data, but plotted in the Cole-Cole representation, χ'' vs. χ'. The solid line represents a least square-fit of the low-frequency data to a circle. The arrow shows in the direction of increasing frequencies.

χ'', as function of the ac frequency. The real part shows an order-parameter like behavior with non-zero value below $f_c \simeq 0.02$, and vanishing value above f_c and the imaginary part has a peak around f_c.

In the Cole-Cole plot this transition appears as a sharp change of the slope and curvature. At low frequencies, $f < f_c$ one observes a quarter-circle with center on the χ' axis [Fig. C.19 (b)]. This corresponds well to the experimental result [CSK$^+$02, PCS$^+$04a] shown in Fig. C.20 and suggests the existence of *one* effective relaxation time in the system. However, for $f > f_c$ only a vertical line can be observed. This result differs from that found in experiment, where the high-frequency part is characterized by a convex shape and finite positive slope. This discrepancy is related to the breakdown of this simple adiabatic approach in the high frequency regime.

By comparison of the susceptibility data to the corresponding hysteresis loops, one finds, that $f = f_c$ marks the transition between loops saturating at high fields (low-f) and those, which do not saturate (high-f). In the second case, the domain wall is always in motion throughout the entire field cycle. The real part is then zero, whereas the imaginary part has a $1/f$ dependence [Fig. C.19 (a)], which was also suggested in Ref. [CSK$^+$02]. Note, that for *any* velocity function $v = v(H)$ with $v(H) = -v(-H)$ and without velocity hysteresis it follows, that $\chi' = 0$ and $\chi'' \propto 1/f$. This can easily be seen from Eqs. (C5.5a), (C5.5b),
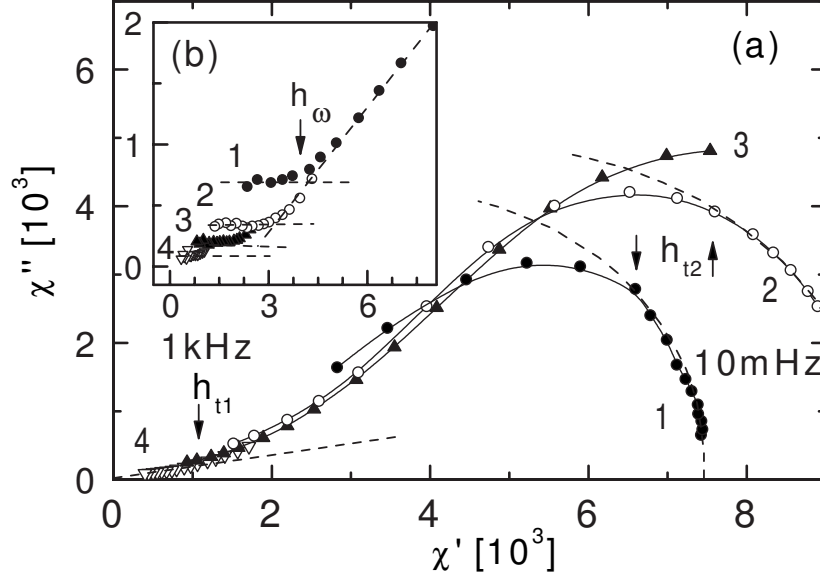
Figure C.20: Experimental Cole-Cole plot taken from Ref. [CSK$^+$02] showing χ'' vs. χ' obtained on the SFM granular system [CoFe(1.4nm)/Al$_2$O$_3$(2nm)]$_{10}$.

and $\dot{M} \propto v$. It means, that no linear part can be found in the Cole-Cole plot by considering only the adiabatic motion of one domain wall.

To improve the model, one has to employ a more realistic description of the domain wall by using the above introduced approach 5.2.2, which we are going to discuss now.

In Fig. C.21 the results for the magnetization hysteresis of a domain wall from eq. C2.1 for $h_0 = 0.5$ are shown ($h_p \approx 0.27$). The plots (a) to (c) show hysteresis loops for different frequencies in the case, when the domain wall never touches the sample boundary. At low frequencies one finds a symmetric loop with respect to the M axis (a) similar to the result shown above in Fig. C.18(d). This symmetry is lost upon increasing the frequency [(b) and (c)] and the loop becomes tilted. This tilting is responsible for a non-vanishing real part of the ac susceptibility and cannot be observed in the adiabatic approach 5.2.1. The tilting corresponds to the appearance of the velocity hysteresis. That means, there exists no functional relationship between the velocity and the field anymore, as it is the case in the adiabatic regime.

The resulting susceptibilities are plotted in Fig. C.22. In (a) and (b) the real and imaginary part vs. $\lg(f)$ and the corresponding Cole-Cole plot, respectively, are shown for an infinite
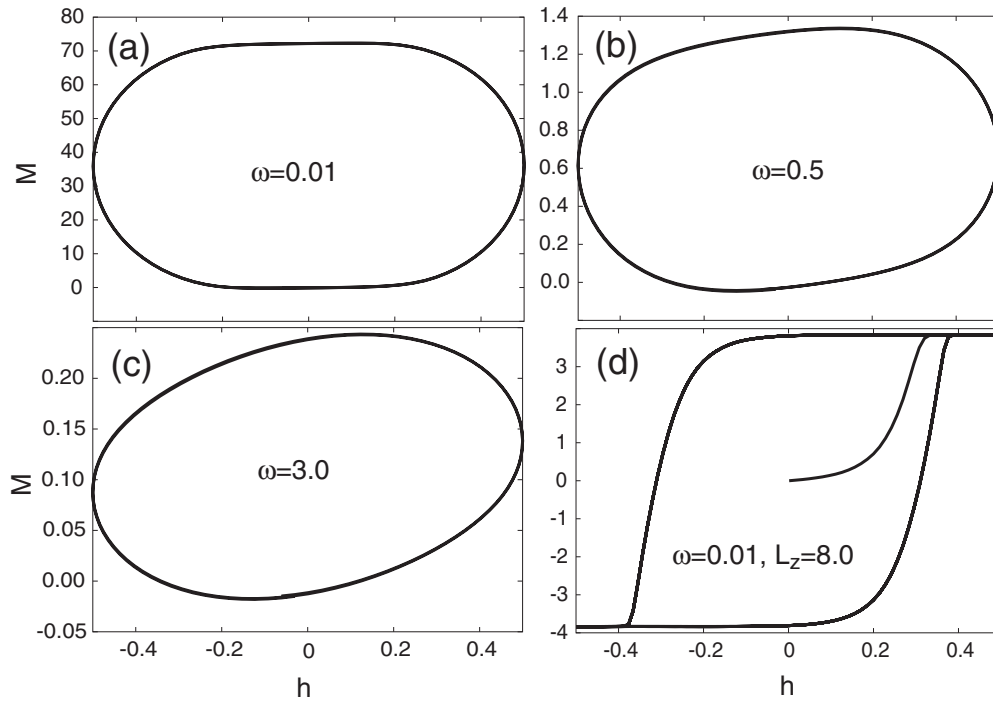
Figure C.21: M vs. h curves from simulations of the equation of motion (C2.1) with $h_0 = 0.5$ and different frequencies, $\omega = 0.01$ (a), 0.5 (b), and 3.0 (c), where the domain wall does not touch the boundaries. (d) shows the magnetization curve for $\omega = 0.01$ with the domain wall touching the boundary, including the virgin curve.

system ($L_z \to \infty$), when the domain wall never touches the boundary. In (c) and (d) the same plots are shown for a finite system ($L_z = 8.0$). While the low-frequency parts resemble those from approach 5.2.1, the high-frequency part shows a completely different behavior. For $\chi' \to 0$ we find in the Cole-Cole plot (inset in Fig. C.22 (d)) a convex shaped curve similar as in the experiment (Fig. C.20). One can expect that χ goes to 0 with $\omega_0 \to \infty$, since the velocity hysteresis disappears for $\omega_0 \to \infty$. Obviously the more realistic second model is capable to describe the behavior found experimentally. However, two drawbacks still exist. First, the Cole-Cole plot from the simulation shows a rather steep and narrow increasing part compared to the experiment. Second, we cannot retrieve the saturating part for maximum frequencies, where the imaginary part becomes constant, which was suggested in [CSK$^+$02] (see Fig. C.20, inset).

There are several ways to improve the model for a better description of the experimental situation, e.g.:

- We have simulated only one domain wall. More realistic would be a multi-domain
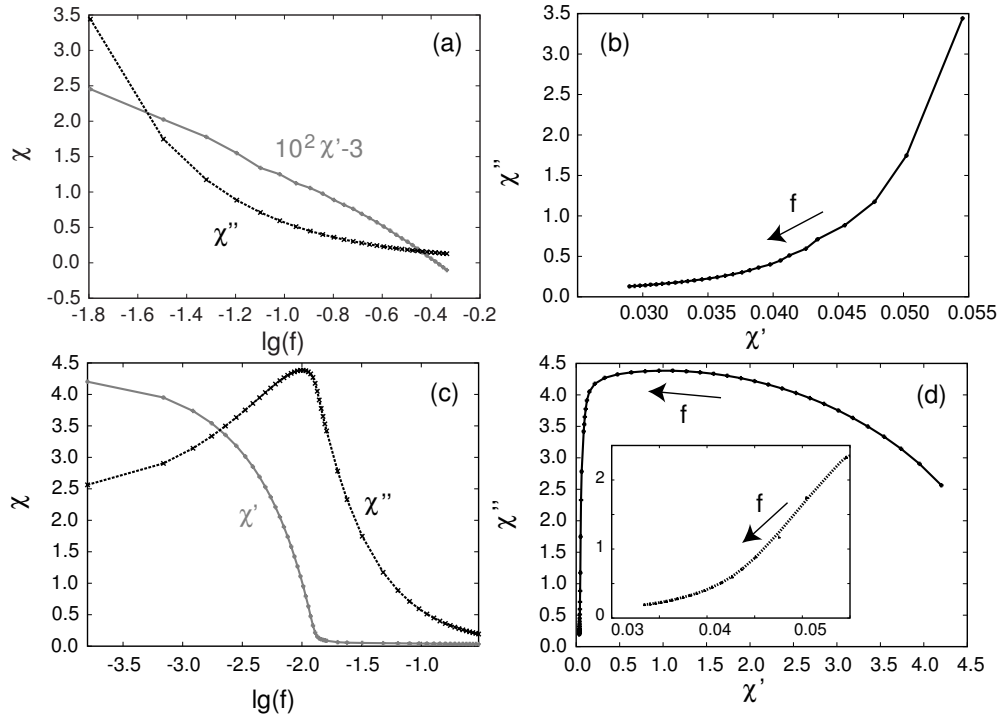
Figure C.22: Real and Imaginary part of the ac susceptibility vs. frequency, calculated with the equation of motion (C2.1) for only high frequencies (a) and a wide frequency spectrum (c). All simulations were performed with $h_0 = 0.5$. Plots (b) and (d) are the Cole-Cole plots corresponding to the data shown in (a) and (c), respectively. The inset in (d) shows the high frequency behavior in more detail. Again the arrows show in direction of increasing frequencies.

model with many (isolated) domains of different sizes. In this case each domain would have another f_c, such that the rather sharp drop of χ' at f_c for one domain would be smeared out, leading to a more realistic scenario of the Cole-Cole plot for high frequencies.

- Additional to this multi-domain model, one could take interactions of the domain walls into account. Unfortunately this requires mayor modifications of the equation of motion (C2.1), e.g., inclusion of "overhangs", which cannot be described in terms of the displacement field z.

- Inclusion of thermal noise in the equation of motion (C2.1) might decrease χ'' at low frequencies faster, leading to an expansion of the convex high-f region compared to the low-f region.

It would be interesting to study the effect of those modifications, which we will postpone to a future work.

6 Displacement profile of charge density waves and domain walls at critical depinning

In this section we consider the effect of strong surface potentials on the motion of an interface in a random medium. As already mentioned, we are especially interested in the case of charge density waves, since these surface potentials are important for the conversion process of normal electrons to the condensed CDW ones.

6.1 Model for surface potentials

Therefore we switch back to the CDW notation and replace the displacement function z by the CDW phase field φ (which is D dimensional in this section). The model is however the same as presented in eq. (C2.2), but in order to include the surface potential the (random) potential (C2.3) has to be modified to

$$
V(\mathbf{x}, \varphi) = - \int\limits_0^\varphi d\varphi' g(\mathbf{x}, \varphi')[1 - \rho(\mathbf{x})] + \frac{\Gamma}{a^2} V_s(\varphi)\rho(\mathbf{x}) \,, \tag{C6.1}
$$

which includes the random force g in the bulk and a surface contribution V_s. The factor $(1 - \rho(\mathbf{x}))$ is essentially 1 in the bulk and drops to zero in the vicinity ($a \ll L$) of $x_1 = 0$ and $x_1 = L$ (see illustration in Fig. C.23), e.g.,

$$
\rho(\mathbf{x}) = e^{-x_1/a} + e^{(x_1-L)/a} \,, \tag{C6.2}
$$

where the surface potential $V_s(\varphi)$ is assumed to act, which favors the values of $\varphi(0, \mathbf{x}_\perp)$ and $\varphi(L, \mathbf{x}_\perp)$ at $2\pi\mathbb{Z}$.

Again, the random force $g(\mathbf{x}, \varphi)$ is assumed to be Gaussian distributed with $\langle g \rangle_d = 0$ and $\langle g(\mathbf{x}, \varphi)g(\mathbf{x}', \varphi') \rangle_d = \delta^{(D)}(\mathbf{x} - \mathbf{x}')\Delta_0(\varphi - \varphi')$. As already discussed, $\Delta_0(\varphi) = \Delta_0(-\varphi)$ is an analytical monotonically decreasing function of φ for domain walls, which decays to zero over a finite distance l. For CDWs $g \propto \sin(\varphi - \alpha(\mathbf{x}))$ with a random phase $\alpha(\mathbf{x}) \in [0, 2\pi[$ and therefore $\Delta_0(\varphi)$ is periodic with $\Delta_0(\varphi) = \Delta_0(\varphi + 2\pi\mathbb{Z})$ (cf. appendix E2.3).

The details of the interaction between the elastic system and the surface depend on the specific system under consideration. Here, we will restrict ourselves to a periodic surface potential which has applications in type-II superconductors and may also serve as a first step for the treatment of conversion phenomena in CDWs.

The equation of motion is also the same as (C2.1) with appropriate boundary conditions for $\varphi(0, \mathbf{x}_\perp)$ and $\varphi(L, \mathbf{x}_\perp)$. Thermal fluctuations are included as in the equation of motion (B10.4). Important to note is, that we study the equation of motion in the adiabatic situation
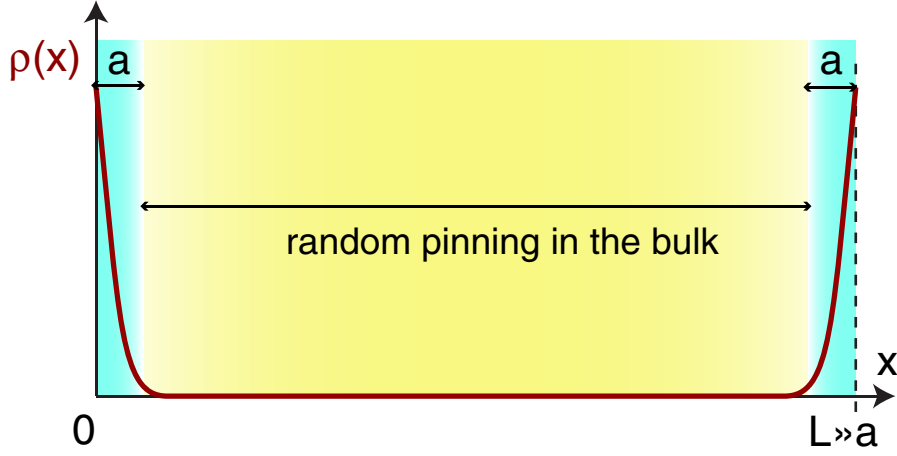
Figure C.23: Illustration of the potential, including a surface portion which acts in the vicinity $a \ll L$ of the surface and the random pinning forces in the bulk.

with driving force $h = h_0$ in contrast to the non-adiabatic ac-motion studied in the previous sections.

In the well known case $V_s \equiv 0$ [NSTL92, NF92a, NF93, EK94, CDW01, DWC02], i.e., when the system undergoes the depinning transition at a critical value h_P of the external driving force at zero temperature, the average displacement profile is macroscopically flat. At non–zero temperatures the depinning transition is smeared out and goes over into a creep motion for $h_0 \ll h_P$ [IV87].

Here we will consider the opposite case where a *strong* surface potential V_s, obeying $\max\{V'_s\} \gg h_P a^2/\Gamma$, slows down or completely prevents the motion of the elastic object. We study the history-dependent curvature $\mathcal{C}(h,t)$ of the parabolic displacement profile. The steady state solution for the average phase is given by

$$\varphi_0 \equiv \langle \varphi \rangle = vt + \frac{\mathcal{C}_s(h)}{2}(L - x_1)x_1 \,. \tag{C6.3}$$

where $\mathcal{C}_s(h) = \mathcal{C}_s(h, t \to \infty)$ is the saturation value of the curvature.

6.2 Infinite surface barriers

We begin with the case $V_s \to \infty$, where the depinning transition is suppressed. To determine $\mathcal{C}(h,t)$ we first apply perturbation theory. Using the decomposition $\varphi(\mathbf{x}) = \varphi_0(\mathbf{x}) + \varphi_1(\mathbf{x})$ with $\langle \varphi_1(\mathbf{x}) \rangle_d = 0$ in the equation of motion and expanding $g(\mathbf{x}, \varphi_0 + \varphi_1)$ to linear order in φ_1, we get after averaging over the disorder

$$\frac{1}{\gamma}\dot{\varphi}_0 = -\Gamma\mathcal{C}(t) + h + \langle g_\varphi(\mathbf{x}, \varphi_0(\mathbf{x}, t))\varphi_1(\mathbf{x}, t) \rangle_d \,, \tag{C6.4}$$

where $g_\varphi(\mathbf{x}, \varphi) \equiv \frac{\partial}{\partial \varphi} g(\mathbf{x}, \varphi)$. Calculating φ_1 also to first order of g we get from (C6.3) and (C6.4) $\mathcal{C}_s = \mathcal{C}_0 = h/\Gamma$ since $\Delta'_0(0) = 0$, i.e., there seems to be no influence of the disorder. Here, the situation is completely analogous to that at the conventional depinning transition [NSTL92]. However, as we know from critical depinning, this is the situation below the Larkin scale L_P.

Next we discuss renormalized perturbation theory starting from a situation where $\mathcal{C}_s = 0$. As long as $h \leq h_P$, the elastic object is pinned and boundary pinning does not matter, hence $\mathcal{C}(h, t) = 0$. At $h = h_P$ the elastic object is in the same critical state as at the depinning transition. Therefore we can use the results of the renormalization group calculation from section 3.3 in this case. As a result γ and $\Delta_0(z)$ are replaced there by the renormalized, momentum p dependent quantities $\gamma(p)$ and $\Delta_p(z)$, respectively, given in (C3.9a) and (C3.9b). Note, that for CDWs the dynamical exponent ζ is zero [NF93, NF92a]. The most important feature of $\Delta_p(\varphi)$ is, that $\Delta^*(\varphi)$ has a cusp–like singularity at the origin. The renormalized equation for $\mathcal{C}(h, t \to \infty)$ is given by

$$\Gamma\mathcal{C}(h,t) = h + h_{P,0}\omega_P \int\limits_0^\infty dt' \int\limits_0^1 d\tilde{p} \times \tag{C6.5}$$

$$\times \tilde{p}^{1+z-\zeta} e^{-\omega_P \tilde{p}^z t'} \Delta^{*\prime} \left([-\mathcal{C}(t) + \mathcal{C}(t-t')]\frac{x_1}{2}(x_1 - L)\right),$$

where $\tilde{\mathbf{p}} = \mathbf{p}L_P$, $\omega_P = \gamma h_{P,0}/l$, and the approximate depinning force $h_{P,0} = l\Gamma L_P^{-2}$. After having increased h adiabatically to a fixed value slightly larger than h_P, $\mathcal{C}(h,t)$ saturates for $t \to \infty$ and hence the difference $\mathcal{C}(t) - \mathcal{C}(t-t')$ vanishes. As a result the argument of $\Delta^{*\prime}$ also vanishes and the right-hand side of (C6.5) becomes independent of x_1. Since $\mathcal{C}(t) > \mathcal{C}(t-t')$ the argument of $\Delta^{*\prime}$ approaches zero from positive values. Thus we get for the saturation value $\mathcal{C}_s(h)$

$$\mathcal{C}_s(h) = \frac{h - h_P}{\Gamma} = \frac{l}{L_P^2}\frac{h - h_P}{h_{P,0}}, \qquad h_P = \frac{h_{P,0}}{2 - \zeta}\Delta^{*\prime}(0^+). \tag{C6.6}$$

One can understand this result in the following way: Using the decomposition $\varphi = \varphi_0 + \varphi_1$ in the asymptotic region, where $\mathcal{C}(t)$ saturates, the equation of motion can be written as

$$\frac{1}{\gamma}\dot{\varphi}_1 = \Gamma\mathbf{\nabla}^2\varphi_1 + h - \Gamma\mathcal{C} + g_1(\mathbf{x}, \varphi_1), \tag{C6.7}$$

where $g_1(\mathbf{x}, \varphi_1) = g(\mathbf{x}, \varphi_0(\mathbf{x}) + \varphi_1(\mathbf{x}))$. $g_1(\mathbf{x}, \varphi)$ and $g(\mathbf{x}, \varphi)$ have the same statistical properties. According to (C6.7) the force acting on the field φ_1 is now reduced by the curvature force $-\Gamma\mathcal{C}$. Therefore, the depinning of the φ_1-field seems to occur at $h \nearrow \tilde{h}_P = h_P + \Gamma\mathcal{C}_s$. However, since the boundary conditions fix $\varphi_1(0) = \varphi_1(L) = 0$ and hence

$\langle \dot{\varphi}_1 \rangle = 0$ for all values of h, the system *is always at its depinning transition*, which implies (C6.6). Starting from some $h < h_P$ and $\mathcal{C}_s = 0$, $\mathcal{C}_s$ will stay at this value until h reaches h_P. For $h > h_P$, $\mathcal{C}_s$ obeys (C6.6). The same argument can be used for negative forces $h < 0$. Then we find for $h < -h_P$: $\Gamma \mathcal{C}_s(h) = h + h_P = -(|h| - h_P)$ since $\Delta^{*\prime}(0^-) = -\Delta^{*\prime}(0^+)$.

A *scaling argument* supports the validity of eq. (C6.6) to all orders in g: Close to the $V_s = 0$ depinning transition the correlation length ξ diverges as $\xi \approx L_P \left((h - h_P)/h_P \right)^{-\nu}$. For $L' < \xi$ the *roughness* – the mean square displacement of a piece of linear size L' of the elastic object – scales as $w^2(L') \approx l^2 \left(L'/L_P \right)^{2\zeta}$ [NSTL92, NF93, NF92a, EK94, CDW01, DWC02]. If we choose the system size $L \approx \xi$ we expect that the roughness scales as the height of the parabolic $\varphi-$profile on the same scale, $w(\xi) \approx \mathcal{C}\xi^2$, which is indeed fulfilled if we use the scaling law $\nu = 1/(2 - \zeta)$

$$\mathcal{C} = \frac{w(\xi)}{\xi^2} = \frac{l}{L_P^2} \left(\frac{h - h_P}{h_P} \right)^{\nu(2-\zeta)} \approx \frac{h - h_P}{\Gamma} . \tag{C6.8}$$

6.3 Hysteresis

Next we consider the case, that we increase h adiabatically from $h \lesssim h_P$ to a value h_{max}, where $\mathcal{C}(h, t)$ reaches $\mathcal{C}_{\mathsf{max}}$, and then *decrease* h again. In this case $\mathcal{C}(h, t) < \mathcal{C}(h, t - t')$ and hence the argument of $\Delta^{*\prime}$ becomes negative. Instead of (C6.6) we get from (C6.5)

$$\Gamma \mathcal{C}_{\mathsf{max}} \equiv h_{\mathsf{max}} - h_P = h + h_P . \tag{C6.9}$$

The effective force acting on the elastic object is now given by $h - \Gamma \mathcal{C}_{\mathsf{max}}$. While further decreasing h, there is no change of $\mathcal{C}(h, t)$ until the effective force reaches the threshold $-h_P = h - \Gamma \mathcal{C}_{\mathsf{max}} = h - (h_{\mathsf{max}} - h_P)$. According to the last relation, this happens at $h = \tilde{h}_{\mathsf{max}} = h_{\mathsf{max}} - 2h_P$. Analogous arguments can be used for reversing the fields from $\dot{h} < 0$ to $\dot{h} > 0$. Thus $\mathcal{C}_s$ undergoes a *hysteresis* which consists of the two parallel segments given by $\mathcal{C}_s \Gamma = (h \mp h_P)$ and two horizontal segments determined by $\mathcal{C}_{\mathsf{max}} = (h_{\mathsf{max}} - h_P)/\Gamma$ and $\mathcal{C}_{\mathsf{min}} = (h_{\mathsf{min}} + h_P)/\Gamma$, respectively. Indeed, similar hysteresis effects of the strain have been observed in CDWs [MT86b, LOCT01]. Note, that in [MT86b] the polarization is measured, which is proportional to $\mathcal{C}_s$.

These findings are fully supported by numerical simulations, as shown in Fig. C.24 which were done using the same discretization and dimensionless parameters as described in section 3.2.
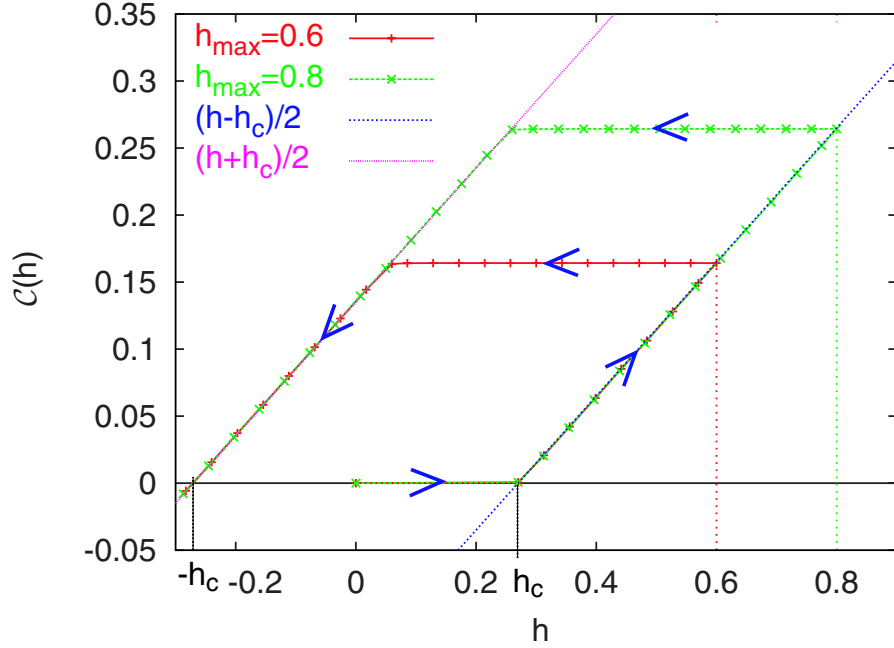
Figure C.24: Hysteresis of $\mathcal{C}(h)$ at $T = 0$ for an one-dimensional interface. The driving force is first increased to $h_{\max} = 0.6$ or $h_{\max} = 0.8$, respectively, and then decreased to $-h_P \approx -0.27$. The arrows show the direction of the hysteresis. The numerical simulation was done for an interface with length $L = 1000$ and averaged over 300 disorder configurations.

6.4 Curvature at finite temperature

Next we want to consider the problem of finite temperatures. Changing h only adiabatically we may use equilibrium statistical mechanics. It is convenient to go over to the field $\tilde{\varphi}(\mathbf{x}) = \varphi(\mathbf{x}) + \frac{h}{2\Gamma}x_1(x_1 - L)$. The Hamiltonian rewritten in $\tilde{\varphi}$ has the same statistical properties as the initial one (C2.2), since $V_R(\mathbf{x}, \varphi) = -\int^\varphi d\varphi' g(\mathbf{x}, \varphi')$ is a *random* function of both arguments. This can most easily seen by using the replica method [You99]. The disorder averaged free enthalpy follows from the *replica Hamiltonian*

$$\mathcal{H}_n = \frac{\Gamma}{2} \sum_{a,b=1}^{n} \int_{\mathbf{x}} \left\{ (\boldsymbol{\nabla}\tilde{\varphi}_a)^2 \delta_{a,b} - \frac{\Gamma}{T} R(\tilde{\varphi}_a - \tilde{\varphi}_b) \right\} , \tag{C6.10}$$

with $\langle V_R(\mathbf{x}, \varphi)V_R(\mathbf{x}', \varphi')\rangle_d = \delta^{(D)}(\mathbf{x} - \mathbf{x}')R(\varphi - \varphi')$. Apparently, the replica Hamiltonian is the same as that following from (C2.2). It is worth to mention that this is true only if the random potential $V_R(\mathbf{x}, \varphi)$ is strictly uncorrelated in $\mathbf{x}$-direction. The application of surface barriers implies therefore $\mathcal{C} = h/\Gamma$ and $\left\langle \langle (\tilde{\varphi}(\mathbf{x}) - \tilde{\varphi}(\mathbf{x}'))^2 \rangle_d \right\rangle^{1/2} \simeq l \, (L/L_P)^{\tilde{\zeta}}$ where

$\tilde{\zeta}$ denotes the equilibrium roughness exponent corresponding to Hamiltonian (C6.10). Thus the displacement profile is the same as in the pure case. For non–adiabatic changes of h, traces of the $T = 0$ hysteresis are expected to be seen at non–zero temperatures (cf. Fig. C.25).
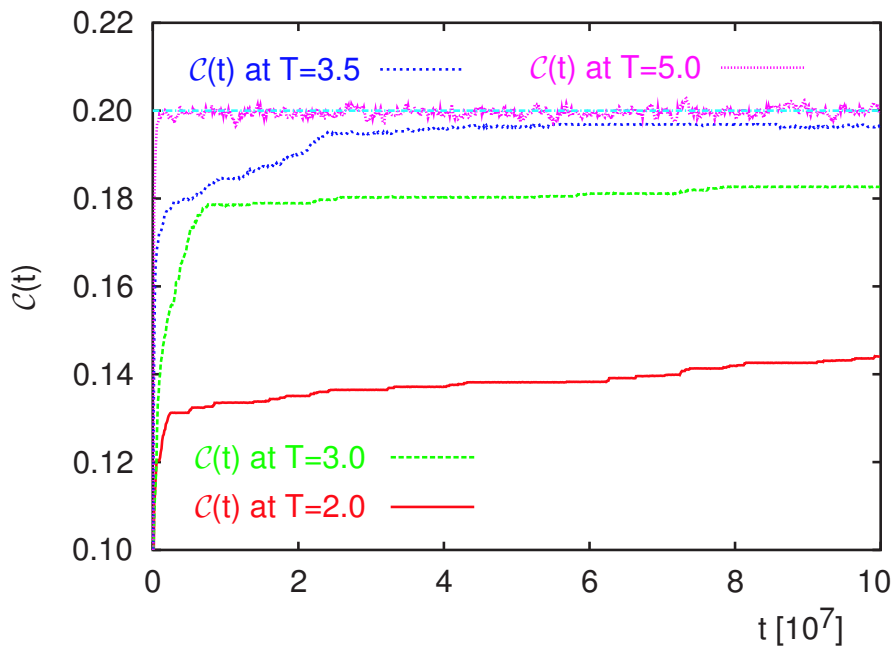
Figure C.25: Simulation–time resolved coefficient $\mathcal{C}(t)$ for a driving force of $h = 0.2$ at various temperatures. The simulation was done for a system of discrete length $L = 1000$ and for one disorder configuration of CDW–type for each temperature (see text).

The numerical solution of the equation of motion with thermal noise at finite temperatures and $V_s = \infty$ is in agreement with these analytical considerations. Fig. C.25 shows the coefficient $\mathcal{C}(t)$ as it approaches its saturation value $\mathcal{C}_s = h/\Gamma$ with time. Strictly speaking, we are not in a steady state, until $\mathcal{C}(t)$ has reached its saturation value and hence the phase profile deviates slightly from the parabolic shape. In Fig. C.25, $\mathcal{C}(t)$ is calculated from the parabolic least square fit to the profile. Note, that for *low* temperatures ($T < 5.0$ in the simulation, where T is the dimensionless variance of the thermal noise) this approach is very slow, noticeable by the occurring steps, triggered by avalanches, even at large times. For high T ($T = 5.0$), one sees that $\mathcal{C}(t)$ fluctuates around the saturation value due to thermal noise. Therefore the $T = 0$ hysteresis of $\mathcal{C}$ vanishes at finite temperatures.

6.5 Critical Depinning

So far the surface potential was assumed to fix the value of φ at the surfaces $x_1 = 0$ and $x_1 = L$. We will now assume that the surface potential is reduced, such that a macroscopic motion of the elastic object is possible. To determine the mutual interaction between the bulk and the surface we have to consider the effective equation of motion of the surface. Denoting $\varphi(0, \mathbf{x}_\perp) = \varphi_s(\mathbf{x}_\perp)$ the effective equation of motion of the surface field can be written as (a is assumed to be of the order of the lattice spacing)

$$\frac{1}{\gamma}\dot{\varphi}_s = \Gamma\mathcal{C}\frac{L}{2a} + \Gamma\boldsymbol{\nabla}_\perp^2\varphi_s + h - \frac{\Gamma}{a^2}V_s'(\varphi_s). \tag{C6.11}$$

An analogous equation can be written for $\varphi(L, \mathbf{x}_\perp)$. In (C6.11) we have replaced the force resulting from the displacement in the bulk by the corresponding average force. In the steady state $\boldsymbol{\nabla}_\perp^2\varphi_s = 0$ and eq. (C6.11) has a depinning threshold $h_{s,c} \gg h_P$ determined by

$$\Gamma\mathcal{C}(h_{P,s})\frac{L}{2a} + h_{P,s} - \frac{\Gamma}{a^2}\max\left\{V_s'(\varphi)\right\} = 0. \tag{C6.12}$$

For $h > h_{P,s} \gg h_P$ the macroscopic velocity is given by the steady state solution $v = \dot{\varphi}_s$ which follows from integrating (C6.11) with $\boldsymbol{\nabla}_\perp^2\varphi_s = 0$. The corresponding solution

$$v(t) = v_p\Phi\left(\frac{\Gamma\mathcal{C}(t)\frac{La}{2} + ha^2}{\Gamma V_{s,max}'}, t\right) \tag{C6.13}$$

depends of course on the specific form of the surface potential, $v_p = \gamma h_{P,0}$. Eq.(C6.13) has to be combined with the effective equation for the bulk ($h > h_P$) [NSTL92]

$$\left(\frac{v(t)}{v_p}\right)^{1/\beta} = \frac{h - h_P}{h_{P,0}} - \mathcal{C}(t)\frac{L_P^2}{l}, \tag{C6.14}$$

which follows from (C3.9a) and (C6.6). Note, that we used the condition $a \ll L_P$ such that the surface potential does not change the bulk depinning threshold. Eqs. (C6.13) and (C6.14) determine both the velocity and the curvature $\mathcal{C}$ as a function of the driving force. If we increase h from $h = 0$ with $\mathcal{C} = 0$, $\mathcal{C}$ remains zero until we reach h_P. For $h_P < h < h_{P,s}$, $\mathcal{C}$ obeys (C6.6). At $h_{P,s}$ the elastic object is depinned and with increasing velocity the curvature is reduced compared to a non-moving object which is subject to the same force, as follows from (C6.14). If the surface potential is periodic, also $v(t)$ will be periodic and the bulk depinning transition is slightly smeared out (as seen in section 3. We will assume that this effect is weak. In principal it can be avoided by adding some randomness to the surface potential.
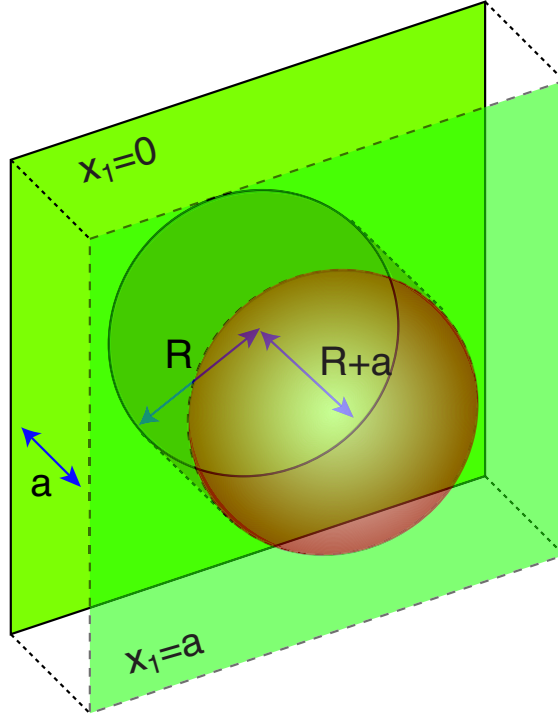
Figure C.26: Illustration of a nucleation droplet at the surface. The droplet consist of a cylindrical piece (the cylinder axis is perpendicular to the $x_1 = 0$ plane) in the surface layer of height a and radius R and an attached semi-sphere with the same radius.

6.6 Nucleation and Creep

At finite but low temperatures the surface field may exhibit a creep motion even if $h \ll h_{P,s}$. Creep proceeds via the formation of droplets at the surfaces $x_1 = 0$ and $x_1 = L$, where φ is changed by 2π with respect to the bulk value of φ. The droplet consists of a cylindrical piece (the cylinder axis is perpendicular to the plane defined by $x_1 = 0$) in the surface layer of height a and radius R and an attached semi-sphere with the same radius (shown in Fig. C.26). The width of the droplet wall, confining the cylinder, is of the order $a' = a/\sqrt{V_s''}$.

Keeping only the leading order terms we get for the energy of the droplet

$$E_{\mathsf{dp}}(R) = 2\Gamma R^{D-2} \left\{ \sqrt{V_s''} + \ln \frac{R}{a'} - \pi\mathcal{C}RL - fR^2/\Gamma \right\} .$$

The critical droplet size $R_c \ll L$ follows by minimizing $E_{\mathsf{dp}}(R)$ with respect to R as $R_c \approx \sqrt{V_s''}/(\mathcal{C}L)$ or $R_c = (\mathcal{C}L)^{-1}$ in $D = 3$ or $D = 2$, respectively. In deriving E_{dp}, we have neglected the contribution from the disorder, which is correct as long as $R_c < L_P$, i.e.,

$L \gg L_P$. The nucleation rate of droplets and hence the creep velocity is given by

$$\frac{v_{D=3}}{v_p} = A \exp\left(-B \frac{V_s'' \Gamma}{\mathcal{C} L T}\right), \; \frac{v_{D=2}}{v_p} = A' \left(\frac{\mathcal{C} L a'}{\sqrt{V_s''}}\right)^{B'\Gamma/T}, \tag{C6.15}$$

which replaces (C6.13) in the case $h \ll h_{P,s}$ and $T > 0$ (cf. [RMAE92]). The present treatment is too crude to give the coefficients A, A', B, and B'. Again, (C6.15) has to be considered together with (C6.14) to determine $\mathcal{C}$ and v. In CDWs, where φ can be multi-valued, nucleation processes also occur deep in the bulk [RMAE92]. The droplet energy then does not contain a term $\sim h$, leaving the relations (C6.15) essentially unchanged.

7 Conclusion and summary

To conclude, we have shown in the first part of this chapter, that the sharp depinning transition of an interface driven by a dc-field is smeared, showing a pronounced velocity hysteresis, if the external drive is oscillating. The size of the hysteresis is described by the power laws in equations (C3.5) and (C3.6), which are supported by an approximate renormalization group analysis and numerical simulations. With help of the renormalized perturbation theory we could also explain the double hysteresis shape of the velocity in the case, when the amplitude of the ac-field is larger than the zero temperature, adiabatic depinning field (cf. eq. C3.11). Thermal fluctuations lead to an additional smearing (due to thermal creep motion) of the depinning transition if the external frequency is sufficiently low.

For amplitudes below the depinning field, also avalanche motion of the interface has to be taken into account, leading to a pronounced 'bump' in the velocity hysteresis which can be explained by the increasing size (and number) of avalanches triggered with increasing external field. In the frequency region, where avalanches do not play a role, we find an interpolation function for the velocity, which explains the numerically found results.

To compare our model to experimental measurement, we studied two numerical approaches based on a "linear" interface depinning model. We compared the experimental and numerical obtained complex susceptibilities in order to get a better understanding of the magnetic behavior found in the superferromagnetic granular multilayer system $[Co_{80}Fe_{20}(1.4nm)/ Al_2O_3(3nm)]_{10}$.

In the first approach, we used the mean velocity of a domain wall in the adiabatic limit to calculate the susceptibility. With this one can explain the monodisperse dynamic response evident by a partial semicircle centered around the χ' axis in the Cole-Cole representation. However, it fails to describe the increasing convex part for higher frequencies. This behavior

can be found by taking the full equation of motion into account, where an elastic interface is driven in general *non-adiabatically* in a random medium. This model for an impure ferromagnet is capable to describe the main features of the experimental results. We find that the appearance of a velocity hysteresis is a crucial element in the dynamical response of the superferromagnet. In addition the results confirm, that the above mentioned granular system is neither a superparamagnetic nor a superspin glass system.

Finally, we have studied the influence of strong surface potentials to the adiabatic motion of the interface in the last part of this chapter. Especially, we have analyzed the curvature of the parabolic displacement profile. We have shown that surface pinning of impure elastic systems lead to an onset of curvature $\mathcal{C}$ only above a threshold value h_P of the random force. In general, $\mathcal{C}$ exhibits a pronounced rhombic hysteresis if the external field is changed adiabatically at zero temperature which disappears completely at finite temperatures. Since this is only true in the adiabatic case and the temporal evolution of the curvature to the value of the clean system can be exponentially slow for low temperatures, hysteretic behavior could still be observed at finite temperatures in experiments. We have also shown that the curvature can be reduced above the surface depinning transition or at finite temperatures, when nucleation processes at the surface allow for creep motion.

D Addendum: Thermal transport in two-dimensional Bose-Einstein condensates

In this chapter we present some results for the thermal transport in low dimensional Bose gases at temperatures below the critical temperature: $T \ll T_c$. The results are only peripheral related to the two previous main chapters of the thesis, since we studied interacting, but *clean* Bose systems. Due to the interaction, the non-condensated bosons can scatter at each other. For this process we calculate the scattering rate using *Fermi's* golden rule which is used to derive transport properties for different types of interaction. We also obtain the *weak localization correction* to the thermal conductivity, related to the inter boson scattering, similar to the case of electrons scattered in a disordered system. In the conclusions it is discussed, how the obtained results can be applied to elastic systems, especially to a vortex line model.

1 Introduction

Interaction Bose gases are subject of intensive theoretical and experimental research, especially since the first experimental realization of Bose-Einstein condensates (BECs) in 1995 (for a short review see, e.g., Ref. [Ket99]).

In this chapter we concentrate on the two-dimensional (2D) case (see also [FGI93]). As it is well known, an ideal Bose gas can only form a BEC at finite temperatures for $d > 2$. However, including interactions in the 2D system, a transition to a superfluid state occurs [FH88].

The two-dimensional geometry can be realized, e.g., with a highly anisotropic external trapping potential. The theory of trapped BECs is extensively discussed, e.g., in [DGPS99, PHS00, ZNG99, Gra98, Das02]. Another possibility is to create films of various Bose gases, e.g., by absorbing Helium on a surface substrate [SYF93, CTYC98, BCT99] or Hydrogen on liquid ^{4}He [SVY$^+$98].

Here we consider the effect of interactions between *non-condensated* bosons (the so-called

over-condensate) below the superfluid or BEC transition temperature T_c for two cases: (i) for short-range (hard sphere) and (ii) long-range (Coulomb) interaction. As we will see, the (Bogoliubov) energy spectrum of these quasi-particles changes its behavior from an almost free, quadratic dispersion at high energies to a linear, acoustic *phonon* behavior in the case of short-range interaction or a gapped *plasmon* dispersion for Coulomb interaction. The crossover occurs at energies of the order of the chemical potential μ.

In analogy to disordered electron systems, where electrons scatter at impurities and quantum interference leads to weak localization correction in the metallic (not localized) regime, the different bosonic excitations give rise to scattering of free quasi-particles at phonons or plasmons. Note, that the boson system is *clean*, i.e., the scattering mechanism is different from that in the electronic case. The influence of additional disorder in the Bose system is briefly discussed at the end of this chapter.

We calculate the related scattering rate, which is used to obtain an expression for the thermal conductivity of the system. The almost free quasi-particles with $\mu \ll \varepsilon_k \approx T \ll T_c$ are scattered quasi-elastically at the low energy excitations (acoustical phonons or plasmons). In order to have quasi-elastic scattering, the inelastic scattering or energy relaxation time τ_ε has to be larger than the quasi-particle scattering time τ_0. We show that the latter depends on temperature as $T^{-1/2}$ and τ_ε scales as $T^{1/2}$, i.e., the ratio $\tau_\varepsilon / \tau_0$ is much larger than 1 in the temperature region under consideration. It should be mentioned that the chemical potential corresponds to the Debye energy in an electronic system and the BEC temperature to the Fermi energy.

Since the transport or momentum relaxation time in the Bose gas is also of order of the energy relaxation time and therefore larger than the scattering time, we can furthermore calculate quantum or *weak-localization correction* to the thermal conductivity, which are due to interference effects and show a logarithmic temperature dependence, in analogy with a metallic system [AAK82, ABG$^+$02, AGG85].

The case of long-range interactions could have a direct application in vortex systems, since a d dimensional time dependent boson system can be mapped to a $d+1$ dimensional vortex system [Nel88] and therefore, the results for the Bose system can be applied to vortex arrays.

The study of the short-range interaction is more of academic, than of practical relevance, since the interval of possible quasi-particle energies is, even for very weak interactions, too small to result in an observable effect.

2 Model

The model for interacting bosons in a clean two dimensional system is given by

$$
\begin{aligned}
\hat{\mathcal{H}} &= \int_V d^2r\, \hat{\Psi}^\dagger(\mathbf{r}) \Big[-\frac{\hbar^2}{2m}\nabla^2 - \mu + \frac{1}{2}\int_V d^2r'\, \hat{\Psi}^\dagger(\mathbf{r}')U(\mathbf{r}-\mathbf{r}')\hat{\Psi}(\mathbf{r}') \Big] \hat{\Psi}(\mathbf{r}) \quad \text{(D2.1)} \\
&\equiv \mathcal{H}_0 + \mathcal{H}_{int}\,,
\end{aligned}
$$

where $U(\mathbf{r})$ is the interaction potential and μ the chemical potential.

We discuss two different realizations of the interaction U. First, short-range interaction with $U^{sr}(\mathbf{r}) = U_0\delta^2(\mathbf{r})$ which is a good model for uncharged bosons and second long-range Coulomb interaction for charged particles. For the second model we have to take screening effects into account, such that the interaction can be written as $U^{lr}(\mathbf{r}) = U_0/a^2 K_0(|\mathbf{r}|/a)$, where K_0 is the modified Bessel function of second kind or MacDonald function. K_0 diverges logarithmically for small arguments and vanishes exponentially for large arguments, which reflects the screening. Since we are interested in the mapping of the two-dimensional Bose system to a 3D vortex system, the long-range interaction is most interesting and relevant.

An important feature of K_0 is the fact that the Fourier components U_k^{lr} are finite for $k = 0$[1] and vanish as k^{-2} for $k \to \infty$. Therefore the chemical potential for a weakly interacting Bose gas, given by

$$
\mu \approx nU_{k=0}\,, \tag{D2.2}
$$

is finite for both interaction realizations. Here n is the condensate density.

The full wave function $\hat{\Psi}$ can be decomposed into two parts: $\hat{\Psi} = \hat{\xi}_0 + \hat{\psi}$, where $\hat{\xi}_0$ describes the condensate and $\hat{\psi}$ the bosons which are not in the condensate, the *over-condensate*. Since $T \ll T_c$, almost all bosons are in the condensate and we can treat the condensate wave function as a $\mathbb{C}$-number $\xi_0 \simeq \sqrt{n}$. The remaining model for the over-condensate can be diagonalized to $\hat{\mathcal{H}} = \hat{\mathcal{H}}_0 + \sum_k \varepsilon_k \hat{b}_k^\dagger \hat{b}_k$ using the *Bogoliubov* transformation (see, e.g., [Fet72])

$$
\hat{\psi}(r) = \frac{1}{\sqrt{V}}\sum_k \hat{b}_k u_k e^{i\mathbf{r}\cdot\mathbf{k}} - \hat{b}_k^\dagger v_k^* e^{-i\mathbf{r}\cdot\mathbf{k}}\,, \tag{D2.3}
$$

where u_k and v_k are coefficient functions and $\hat{b}_k^\dagger$, $\hat{b}_k$ are boson creation and annihilation operators, respectively, with $\left[\hat{b}_q, \hat{b}_k^\dagger\right] = \delta_{q,k}$ and $\left[\hat{b}_q^{(\dagger)}, \hat{b}_k^{(\dagger)}\right] = 0$. To obtain the functions u_k and v_k one has to solve the Bogoliubov-de Gennes equations which can – for our model – be simplified to

$$
\begin{pmatrix} u_k \\ v_k \end{pmatrix} = [f_1(k) \pm f_2(k)] \begin{pmatrix} v_k \\ u_k \end{pmatrix}\,, \tag{D2.4}
$$

---

[1] $\int_0^\infty dx\, K_0(x) = \pi/2$

with

$$f_1(k) \equiv (U_{k=0}/U_k + 1) + \frac{1}{nU_k}(\varepsilon_{0,k} - \mu) \,,$$

$$f_2(k) \equiv \frac{\varepsilon_k}{nU_k} \,, \quad \varepsilon_{0,k} = \frac{\hbar^2 k^2}{2m} \,,$$

where U_k are the Fourier components of $U(\mathbf{r})$. For a detailed derivation, see appendix E3.1. The solution for the eigen-energies ε_k follows from $f_1^2(k) - f_2^2(k) = 1$, and u_k and v_k are given by

$$\begin{pmatrix} u_k \\ v_k \end{pmatrix} = \left(\frac{f_1(k)}{f_2(k)} \pm 1 \right)^{1/2} \,.$$

The solutions for the Bogoliubov energy spectra for the two interaction cases are given by

$$(\varepsilon_k^{sr})^2 = \varepsilon_{0,k}(\varepsilon_{0,k} + 2\mu) \text{ and}$$

$$(\varepsilon_k^{lr})^2 = \varepsilon_{0,k}^2 + \hbar^2 U_0 n/(ma^2) \,.$$

For the short-range interaction the spectrum behaves as $\varepsilon_k^{sr} \approx \varepsilon_{0,k}$ for $|\mathbf{k}| \gg q_D = mv/\hbar$ [the analogue to the Debye wave vector], i.e., we have almost free quasi-particles, and $\varepsilon_k^{sr} \approx \hbar|\mathbf{k}|v$ for $|\mathbf{k}| \ll q_D$ with velocity $v = \sqrt{\mu/m}$, i.e., shows an acoustic phonon dispersion. In case of the long-range interaction we also find the free spectrum for high energies of order T and ε_k^{lr} shows the *constant* gapped behavior of plasmons for small wave vectors.

The solutions for the coefficient functions u_k and v_k are

$$\begin{pmatrix} u_k \\ v_k \end{pmatrix} = \left(\frac{\varepsilon_{0,k} + \mu}{\varepsilon_k} \pm 1 \right)^{1/2} \,. \tag{D2.5}$$

Since we have an almost free spectrum for both interactions for energies $\varepsilon_k \approx T \gg \mu$, we see immediately that in this regime: $u_k \approx \sqrt{2}$ and $v_k \approx 0$.

3 Scattering rates and thermal conductivity

Using this model and the results from the Bogoliubov transformation, we can now calculate the scattering rate between the over-condensate particles. In general, the lifetime of a given excitation (k) is determined by two processes:

(i) decay-coalescence (Beliaev): $\mathbf{k} \leftrightarrow \mathbf{k}' + \mathbf{q}$ and

(ii) absorption-emission (Szepfalusy-Kondor [SK74]): $\mathbf{k} + \mathbf{q} \leftrightarrow \mathbf{k}'$.

We are especially interested in these processes when k is a high-energy quasi-particle with almost free spectrum $\varepsilon_{0,k}$, which is the case for $\varepsilon_k \approx T \gg \mu$, and q is a low-energy

(acoustic) phonon with linear spectrum in the case of a δ-interaction or a plasmon spectrum for long-range Coulomb interaction. Thus, we are considering small angle scattering, where the change of the momentum of the quasi-particles is small and the typical energy transfer $\Delta\varepsilon_k \equiv \varepsilon_k - \varepsilon_{k-q}$ is for both types of interaction $\Delta\varepsilon_k \approx \frac{\hbar^2 q^2}{2m}$.

The scattering rate for quasi particles, resulting from these two processes can be calculated using *Fermi's Golden Rule*

$$\frac{1}{\tau_0(\mathbf{k})} = \frac{1}{2}\sum_{\mathbf{q}} \left[W_{k\leftrightarrow(k-q,q)} + W_{k+q\leftrightarrow(k,q)} \right] , \tag{D3.1}$$

with the scattering probability

$$W_{k\leftrightarrow(k-q,q)} = \frac{2\pi}{\hbar}\delta\left(\varepsilon_k - \varepsilon_{k-q} - \varepsilon_q\right) \times \tag{D3.2}$$
$$\left|\langle n_k, n_{k-q}+1, n_q+1|\mathcal{H}_{int}|n_k+1\rangle\right|^2 .$$

The states in the matrix elements are Fock states (all unchanged occupation numbers are omitted) with

$$\langle n_k\rangle = \frac{1}{e^{\varepsilon_k/T}-1} \longrightarrow \begin{cases} T/\varepsilon_k & , \ \varepsilon_k \ll T \\ 1 & , \ \varepsilon_k \gg T \end{cases} . \tag{D3.3}$$

In order to give a contribution to this scattering rate, we have to take third-order terms in $\hat{\psi}$ of the interaction part into account:

$$\mathcal{H}_{int} = \frac{\sqrt{n}}{2}\int d^2r\,d^dr'\,U(|\mathbf{r}-\mathbf{r}'|) \times \tag{D3.4}$$
$$\left(\hat{\psi}^\dagger(\mathbf{r}')\hat{\psi}(\mathbf{r}')\hat{\psi}(\mathbf{r}) + \hat{\psi}^\dagger(\mathbf{r})\hat{\psi}(\mathbf{r}')\hat{\psi}(\mathbf{r})\right) + H.c.$$

Inserting the transformation (D2.3) into (D3.4) and using the standard definition of the creation and annihilation operators $\hat{b}_k^\dagger$ and $\hat{b}_k$, respectively, and the orthogonality of the Fock states, results in the following expression for the matrix elements for $U^{sr}(\mathbf{r})$

$$\langle n_k, n_{k-q}+1, n_q+1|\,H_{int}\,|n_k+1\rangle$$
$$= U_0\sqrt{n/V}2u_{k-q}u_k(u_q-v_q)\times$$
$$\sqrt{n_q+1}\sqrt{n_k+1}\sqrt{n_{k-q}+1} \tag{D3.5}$$

where V is the volume. The second matrix element in (D3.1) for the absorption-emission process is calculated analogously.

Using $u_k \approx \sqrt{2}$ for the high energy quasi-particles and (D3.3), the scattering rate (D3.1) gives

$$\frac{1}{\tau_0\left(\mathbf{k}\right)} \approx 16\frac{U_0^2 n m^2 T}{\hbar^5 q_D|\mathbf{k}|} \propto \sqrt{T} . \tag{D3.6}$$

As already mentioned in the introduction there exists a drawback with the short-range inter-action: According to Fisher *et al.* [FH88] the critical temperature in 2D (the transition is of Kosterlitz-Thouless type) behaves as $T_c \sim n/m \ln[\ln(na^2)]$ or more precisely (see [KPS01] and references therein)

$$T_c^{2D} \sim \frac{\hbar^2 n}{m} \ln \frac{\nu}{g},$$

where $g = \frac{U_0 m/\hbar^2}{1 + U_0 m/\hbar^2 \ln \frac{1}{na^2}}$ and ν is a number ($\nu \approx 380$ according to Ref. [KPS01]). On the other hand the chemical potential behalves as $\mu \sim n/m \log(na^2)$. Thus the temperature interval, where the scattering is effective, $\mu < T < T_c$, can exist for weak interactions, but is not wide enough to be observable. Since for the practically interesting case of vortices, which is discussed in the following, the interaction is of long-range type, the T-interval is reasonably wide.

In the case of a Coulomb potential $U^{lr}(\mathbf{r})$ the matrix elements are more involved, but if we use again the approximation $u_k \approx \sqrt{2}$ for quasi-particles and the fact, that the Fourier components of the interaction potential vanish as $\sim k^{-2}$ for large wave vectors, those simplify to

$$\langle n_k, n_{k-q} + 1, n_q + 1| H_{int} |n_k + 1\rangle$$
$$= 2U_q \sqrt{n/V} \sqrt{n_q}(u_q - v_q). \tag{D3.7}$$

Together with the matrix elements, this leads to the scattering rate

$$\frac{1}{\tau_0(\mathbf{k})} \approx 8 \frac{U_0^2 n m^2 T}{\pi |\mathbf{k}| \hbar^5} \int_0^\infty \left(\frac{U_q}{U_0}\right)^2 \frac{q^2 dq}{q^4 + q_0^4} \propto \sqrt{T}, \tag{D3.8}$$

where $q_0^4 \equiv 4U_0 mn(a\hbar)^{-2}$. For a detailed derivation of the scattering rates in both interaction case, see appendix E3.2.

Now we use those results to calculate the thermal conductivity of the system, which can be written as (using the Boltzmann equation)

$$\kappa = \frac{1}{d} \int d\varepsilon \varepsilon v^2(\varepsilon) \tau_0(\varepsilon) \rho(\varepsilon) \frac{\partial n(\varepsilon, T)}{\partial T}, \tag{D3.9}$$

where d is the spatial dimensionality, $v(\varepsilon)$ the particle velocity, and $\rho(\varepsilon)$ the density of states (DOS). The distribution function $n(\varepsilon, T)$ (for $T < T_c$) follows the usual Bose statistics (D3.3).

Using the square-root temperature dependence of the scattering time, $\partial n(\varepsilon, T)/\partial T = \varepsilon(4T^2 \sinh^2(\varepsilon/2T))^{-1}$, $v^2(T) \sim T/m$, and that in 2D the DOS is independent of ε [i.e.,

$\rho \sim m/\hbar^2$], and neglecting numerical prefactors one obtains [2]

$$\kappa \sim T^2 \tau_0(T) \propto T^{5/2} \,. \tag{D3.10}$$

To obtain the quantum corrections of the thermal conductivity (D3.9), which can be calculated analogous to the weak localization correction [LR85, BK94] of the electric conductivity, we need to calculate the transport or momentum relaxation time for small angle scattering, defined by

$$\frac{1}{\tau_{tr}(k)} = \frac{1}{2} \sum_{\mathbf{q}} \frac{q^2}{k^2} \left[W_{k \leftrightarrow (k-q,q)} + W_{k+q \to k} \right] \sim \frac{1}{T} \sqrt{T} = T^{-1/2} \,,$$

which gives for the correction

$$\begin{aligned} \frac{\Delta \kappa}{\kappa} &\sim - \int_{\tau_0}^{\tau_{tr}} dt \, v \frac{1}{(Dt)^{d/2}} \\ &\sim v \ln(\tau_{tr}/\tau_0)/D \,, \quad d = 2 \,, \end{aligned} \tag{D3.11}$$

where D is the particle diffusion coefficient.

Here we have implicitly used, that the weak localization correction, which is valid for the electric conductivity, can be applied to the thermal conductivity. The thermal conductivity can be related to the electric one via the Wiedemann-Franz law ($\kappa/\sigma = LT$, where L is the Lorenz number), which is valid if we are in the quasi-elastic scattering regime. To ensure that we are in this regime, the energy relaxation (or inelastic scattering) time τ_ε has to be estimated, which is defined by

$$\frac{1}{\tau_\varepsilon(k)} = \frac{1}{2} \sum_{\mathbf{q}} \left[W_{k \leftrightarrow (k-q,q)} \frac{\Delta \varepsilon_k}{T} + W_{k+q \to k} \frac{\Delta \varepsilon_{k+q}}{T} \right] \,,$$

where W are the scattering probabilities given in (D3.2) and $\Delta \varepsilon_k$ is the energy difference of the quasi particle energies. Since $\Delta \varepsilon_k \approx \frac{\hbar^2 q^2}{2m}$, it follows directly: $\tau_\varepsilon(T) \sim \sqrt{T}$ where (D3.8) is used. For particle energies $\mu \ll T \ll T_c$ this inelastic scattering is much larger than the bare scattering time $\tau_0(T)$.

4 Conclusion and possible application

We have studied clean, but interacting two-dimensional Bose systems. For different types of interactions, we have calculated the scattering rates for over-condensate particles using Fermis golden rule. This rather simple approach was not used before to obtain this rate.

---

[2] $\int_0^\infty x^n / \sinh^2(x/a) dx = n! 2^{1-n} \zeta(n) a^{n+1}$ for $n \in \mathbb{N}^{\geqslant 2}$

Using this method, we could derive the thermal conductivity and the related *weak localization correction*.

Since a d-dimensional (time dependent) boson system can be mapped to a $d+1$ dimensional (classical) vortex system, see, e.g., Ref. [Nel88], the results for the Bose system can also be applied to vortex arrays.

A possible application is given by the relation between the electric conductivity and the tilt modulus of vortex systems, described by Balents *et al.* in [BS95]. In our case the electric and thermal conductivity are related via the Wiedemann-Franz law, since we are in the quasi-elastic scattering regime. The weak localization correction to the thermal conductivity lead therefore also to a correction of the electric conductivity and finally of the vortex tilt modulus. But this needs a careful analysis of the prerequisite for application of the electric conductivity to the tilt response.

The influence of disorder in boson systems gives, among other effects, rise to corrections of the transition temperature [LV02], the problem of boson localization [NV93], and the superfluid-insulator transition. The presence of disorder leads in addition, to scattering at impurities with an associated scattering time. One can expect two situation

(i) $\mu \ll \hbar/\tau_u \ll T_c$, where τ_u is the scattering rate due to disorder. In this case the localization effects become relevant before the interaction with phonons becomes important. Therefore corrections to transport coefficients due to over-condensate scattering cannot be observed.

(ii) $\hbar/\tau_u \ll \mu \ll T_c$. In this case, localization effects do not become important before the interaction kicks in and we can still use the results for the clean system.

But since this is beyond the scope of this chapter, a more detailed investigation could be a future project.

E Appendix

1 Appendix to chapter B

1.1 Renormalization of the disorder

We present a short overview of the used finite temperature anisotropic renormalization group method in the case of the replicated disorder term. Starting point is the action (B3.4).

The phase field $\varphi(x,\tau) = \frac{t}{KL\Lambda} \sum_{\omega_n} \sum_{|k| \leq 1} e^{i(\omega_n \tau + kx)} \varphi_{k,\omega_n}$ with the Matsubara frequencies $\omega_n = 2\pi n t/K$ and $k = 2\pi m/(L\Lambda)$ (note that rescaled coordinates are used) is split in a slow ($|k| < b^{-1}$) and a fast mode part ($b^{-1} \leq |k| \leq 1$), where $b = e^{-dl}$ is a rescaling parameter of order 1. Notice, that the $\varphi_{\lessgtr}$ still have all Matsubara Fourier components.

In order to find the RG-corrections of the other parameters in the model, we follow *Wilson* [WK73] and expand $\left\langle\left\langle e^{-\mathcal{S}_u^{(n)}/\hbar} - 1\right\rangle\right\rangle_{0,>}$ in small $(u/K)^2$, with

$$\frac{\mathcal{S}_u^{(n)}}{\hbar} = -\frac{u^2}{4\pi K^2} \sum_{\alpha,\beta} \iint d\tau d\tau' \int dx\, R[\varphi_\alpha(x,\tau) - \varphi_\beta(x,\tau')] \qquad \text{(E1.1)}$$

where $R[f] \equiv \cos(pf)$. $\langle\langle \ldots \rangle\rangle_{0,>}$ denotes the cumulative or connected average over the fast modes in the "momentum stripes" with the free gaussian model. The correction in first order is given by

$$\frac{\mathcal{S}_{u,1}^{(n)}}{\hbar} = \left\langle\left\langle \frac{\mathcal{S}_u^{(n)}}{\hbar} \right\rangle\right\rangle_{0,>}. \qquad \text{(E1.2)}$$

For calculating the cumulative average of the functional R, R is expanded in small $\Delta\varphi_> \equiv \varphi_{\alpha,>}(x,\tau) - \varphi_{\beta,>}(x,\tau')$, e.g.

$$\begin{aligned}
\langle\langle R[\Delta\varphi] \rangle\rangle_{0,>} &= -p^2 \big(R[\Delta\varphi_<] \left\langle \varphi_{\alpha,>}^2 \right\rangle_{0,>} \\
&\quad - R[\Delta\varphi_<] \left\langle \varphi_{\alpha,>}(x,\tau)\varphi_{\beta,>}(x,\tau') \right\rangle_{0,>} \big) + \mathcal{O}(\Delta\varphi_>^4). \qquad \text{(E1.3)}
\end{aligned}$$

The first term in (E1.3) gives a correction to the disorder parameter u and the second term a correction to K. The free thermal average over the fast modes can be evaluated with the

free propagator $(k^2 + \omega_n^2)^{-1}$ and using the formula

$$\sum_{n=-\infty}^{\infty} \frac{\cos(nx)}{n^2 + a^2} = \frac{\pi}{|a|} \frac{\cosh((\pi - x)a)}{\sinh(\pi|a|)} \ , \ 0 \le x \le 2\pi$$

to treat the *sum* over the Matsubara frequencies yielding

$$\langle \varphi_{\alpha,>}(x,\tau)\varphi_{\beta,>}(x,\tau') \rangle_{0,>} = \frac{K}{2} \frac{\cosh(K/2t - |\Delta\tau|)}{\sinh(K/2t)} \delta_{\alpha,\beta} \ln b \,, \tag{E1.4}$$

with $\Delta\tau \equiv \tau - \tau'$.

In order to find a good gaussian approximation for R, we perform a variational calculation for a sine–Gordon model:

$$\mathcal{H}_{SG} = \mathcal{H}_0 + \mathcal{H}_1 \equiv \mathcal{H}_0 - \mu \int d^d r \, \cos(\varphi(\mathbf{r})) \,, \tag{E1.5}$$

where $\mathcal{H}_0$ is the gaussian part. We approximate $\mathcal{H}_1$ by

$$\tilde{\mathcal{H}}_1 = \int d^d r \, \frac{\kappa(\mathbf{r})}{2} \varphi^2(\mathbf{r}) \,, \tag{E1.6}$$

and define $\tilde{\mathcal{H}} \equiv \mathcal{H}_0 + \tilde{\mathcal{H}}_1$. To find the optimal function $\kappa(\mathbf{r})$, the *variational free energy* [1] $\mathcal{F}_{var}$, with

$$\mathcal{F}_{SG} \le \mathcal{F}_{var} \equiv \tilde{\mathcal{F}} + \left\langle \mathcal{H}_{SG} - \tilde{\mathcal{H}} \right\rangle_{\tilde{\mathcal{H}}} \tag{E1.7}$$

is minimized with respect to κ:

$$\begin{aligned}
0 = \frac{\delta \mathcal{F}_{var}}{\delta \kappa(\tilde{\mathbf{r}})} &= \beta \left\langle \mathcal{H}_{SG} - \tilde{\mathcal{H}} \right\rangle_{\tilde{\mathcal{H}}} \left\langle \frac{\varphi^2(\tilde{\mathbf{r}})}{2} \right\rangle_{\tilde{\mathcal{H}}} - \beta \left\langle (\mathcal{H}_{SG} - \tilde{\mathcal{H}}) \frac{\varphi^2(\tilde{\mathbf{r}})}{2} \right\rangle_{\tilde{\mathcal{H}}} \\
&= \frac{\beta}{2} \int d^d r \, \langle \kappa(\mathbf{r}) - \mu \cos(\varphi(\mathbf{r})) \rangle_{\tilde{\mathcal{H}}} \langle\langle \varphi^2(\mathbf{r})\varphi^2(\tilde{\mathbf{r}}) \rangle\rangle_{\tilde{\mathcal{H}}} \,.
\end{aligned} \tag{E1.8}$$

For the last equality we took into account that the averages are gaussian such that we could apply the *Wick theorem*. From (E1.8) we finally get

$$\kappa(\mathbf{r}) = \mu \langle \cos(\varphi(\mathbf{r})) \rangle_{\tilde{\mathcal{H}}} = \mu \exp\left(-\frac{1}{2} \langle \varphi^2(\mathbf{r}) \rangle_{\tilde{\mathcal{H}}} \right) \,. \tag{E1.9}$$

For small disorder (E1.9) yields for $R[\Delta\varphi_<]$ the approximate expression

$$R[\Delta\varphi_<] \simeq -\frac{p^2}{2} (\Delta\varphi_<)^2 e^{-\frac{p^2}{2} \langle (\Delta\varphi_<)^2 \rangle_{0,<}} \,. \tag{E1.10}$$

---

[1] The inequality for the variational free energy follows directly from $1 - \frac{1}{x} \le \ln(x) \le x - 1$ for $x > 0$, if one considers the expression $K(\hat{\rho}_{SG}, \hat{\rho}) \equiv Tr\hat{\rho}(\ln(\hat{\rho}) - \ln(\hat{\rho}_{SG})$, where $\hat{\rho}$ denotes the *density matrix* of the system.

The same result can be obtained in terms of an operator product expansion [KdO80] of $R[f]$. In order to get a RG correction to K a gradient expansion of $(\Delta\varphi_<)^2$ in (E1.10) in small $\Delta\tau$ is performed, which is justified by the exponential decay of the correlation function (E1.4) on the integration interval such that higher orders in $\Delta\tau$ do not contribute to the RG correction: $(\Delta\varphi_<)^2 \approx (\partial_T\varphi_<(x,T)\Delta\tau)^2$ with $T = (\tau + \tau')/2$.

The pair correlation function in the argument of the exponential function in (E1.10) can be approximated by the expression already shown in (B4.8), i.e.,

$$\langle(\varphi(x,\tau) - \varphi(0,0))^2\rangle_0 \simeq \frac{K}{2}\ln\left(1 + \left(\frac{K}{2\pi t}\right)^2\left[\cosh\left(\frac{2\pi tx}{K}\right) - \cos\left(\frac{2\pi t\tau}{K}\right)\right]\right).$$
(E1.11)

After integration of the fast modes of φ, one rescales the system to maintain the fluctuation strength and the spatial density of the degrees of freedom ($l = \ln b$):

$$x \quad \rightarrow \quad x' = xb^{-1},$$
$$\tau \quad \rightarrow \quad \tau' = \tau b^{-z}, \quad T \rightarrow T' = Tb^z,$$
$$\varphi \quad \rightarrow \quad \varphi' = \varphi b^{-\zeta},$$

which leads to rescaled parameters. For our model these are given by (here in d dimensions)

$$c' = cb^{d+z-2+2\zeta}, \tag{E1.12a}$$
$$v' = vb^{z-1}, \tag{E1.12b}$$
$$K' = Kb^{1-d-2\zeta}, \tag{E1.12c}$$
$$t' = tb^{2-d-2\zeta}, \tag{E1.12d}$$
$$u' = ub^{2-d/2}, \tag{E1.12e}$$
$$\sigma' = \sigma b^{2-d}, \tag{E1.12f}$$
$$w' = wb^{2d}. \tag{E1.12g}$$

Due to the invariance of the system under a phase shift of $2n\pi$, ζ is zero for symmetry reasons.

The RG contribution to the flow equation for u^2 follows from the first term of (E1.3) and (E1.4) with $\Delta\tau = 0$:

$$u'^2 = u^2\left(1 - \frac{p^2K}{2}\coth\frac{K}{2t}\ln b\right). \tag{E1.13}$$

Together with (E1.12e) ($d = 1$) one gets

$$\frac{u'^2 - u^2}{dl} = \left(3 - \frac{p^2K}{2}\coth\frac{K}{2t}\right)u^2. \tag{E1.14}$$

The RG correction to K follows from the second term of (E1.3) with (E1.4) and (E1.10):

$$K' = K \left(1 - \frac{p^4}{2} u^2 \coth \frac{K}{2t} \int\limits_0^{K/(2t)} d\tau \, \tau^2 \frac{\cosh\left(\frac{K}{2t} - \tau\right)}{\cosh \frac{K}{2t}} \times \right.$$
$$\left. e^{-\frac{p^2}{2} \left\langle (\varphi(0,\tau) - \varphi(0,0))^2 \right\rangle_0 \ln b} \right), \qquad (E1.15)$$

and the flow equation (for $d = 1 + \epsilon$) follows from (E1.12c):

$$\frac{K' - K}{dl} = \left[-\epsilon - \frac{p^4}{2} u^2 \coth \frac{K}{2t} B_0 \left(p^2 K, \frac{K}{2t} \right) \right] K \qquad (E1.16)$$

with B_0 given in (B3.6), for which we used (E1.11).
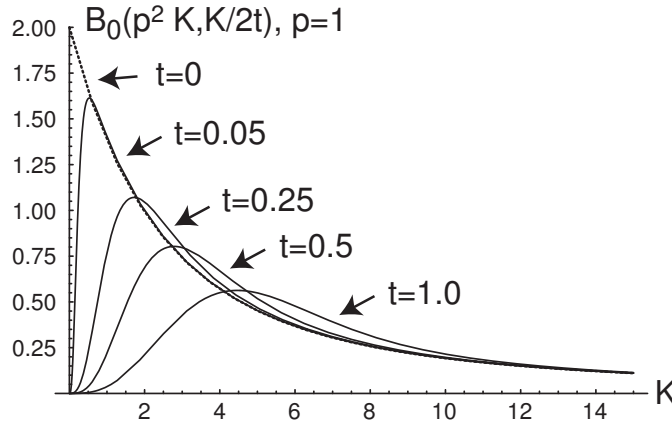
Figure E.1: Function $B_0(p^2 K, \frac{K}{2t})$ plotted with respect to K for different temperatures.

The function B_0 which appears in this flow equation is plotted in Fig. E.1.

For completeness we also plot the functions B_1 and B_2 in the relevant K-region for the lattice unpinning transition [see eqs. (B6.2a) and (B6.2b) or (B8.12a) and (B8.12b)]. Note, that for evaluating these functions at zero temperature, one has to execute the integrals at finite temperature first and then take the limit $t \to 0$.

1.2 Strong pinning

To calculate the phase correlation function in the strong pinning limit, it is necessary to study the order statistics of the impurity distances $\epsilon_i = (x_i - x_{i-1}) - l_{imp}$. Following David [Dav70], we obtain for the probability density function (pdf) of the ϵ_i's in the case
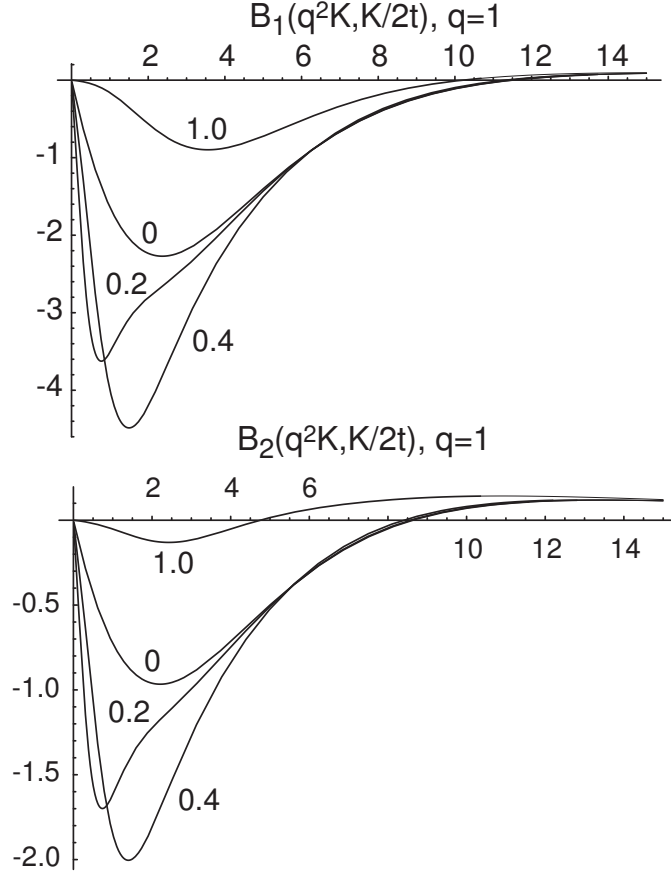
Figure E.2: Function $B_1(q^2K, \frac{K}{2t})$ and $B_2(q^2K, \frac{K}{2t})$ plotted with respect to K for different temperatures, written next to the graphs, and $q = 1$.

of uniformly distributed impurity positions $0 \le x_i \le L$: $p(\epsilon_i) = l_{imp}^{-1}(1 - \frac{1}{L}(\epsilon_i + l_{imp}))^{N-1}$ with $-l_{imp} \le \epsilon_i \le L - l_{imp}$. In the thermodynamic limit the pdf can be rewritten as

$$p(\epsilon_i) \approx \frac{l_{imp}^{-1}}{e} e^{-l_{imp}^{-1}\epsilon_i}, \quad -l_{imp} \le \epsilon_i < \infty. \tag{E1.17}$$

With this, one can calculate the n-th moment $\overline{\epsilon_i^n}$ (for $n > 1$, $\overline{\epsilon_i} = 0$) as follows:

$$\overline{\epsilon_i^n} = \int_{-l_{imp}}^{\infty} \frac{l_{imp}^{-1}}{e} e^{-l_{imp}^{-1}\epsilon_i} \epsilon_i^n \, d\epsilon_i$$

$$= \frac{l_{imp}^{-1}}{e}(-1)^n \left.\frac{\partial^n}{\partial \lambda^n}\right|_{\lambda = l_{imp}^{-1}} \frac{e^{\lambda l_{imp}}}{\lambda}. \tag{E1.18}$$

Using $\left.\frac{\partial^n}{\partial x^n}\right|_{x=1} \frac{e^{x-1}}{x} = (-1)^n n! \left(\sum_{k=1}^{n} \frac{(-1)^k}{k!} + 1\right)$ yields: $\overline{\epsilon_i^n} = \frac{n!}{c^n} \sum_{k=2}^{n} \frac{(-1)^k}{k!}$ and for the correlator $\overline{\epsilon_i \epsilon_j} = l_{imp}^2 \delta_{ij}$.

With this results we can derive the pair correlation function (B4.17). Therefore we calculate the discrete version $\overline{\left\langle (\varphi_n - \varphi_1)^2 \right\rangle}$ in the limit $T \to 0$. With the definitions given below eq. (B3.22), we can rewrite:

$$(\varphi_n - \varphi_1)^2 = \frac{4\pi^2}{p^2} \left(\sum_{i=1}^{n-1} \left(h_i - \frac{pQ\epsilon_i}{2\pi} - \gamma \right) \right)^2 . \tag{E1.19}$$

Using $\overline{\epsilon_i} = \overline{h_i} = 0$ and $\overline{h_i h_j} \propto \delta_{ij}$ leads to

$$\overline{\left\langle (\varphi_{n+1} - \varphi_1)^2 \right\rangle} = \frac{4\pi^2}{p^2} \underbrace{\overline{\left\langle \left(h_i - \frac{pQ\epsilon_i}{2\pi} - \gamma \right)^2 \right\rangle}}_{\equiv \tilde{C}} \cdot n . \tag{E1.20}$$

Because only the value $\left[\frac{pQ\epsilon_i}{2\pi} + \gamma \right]$ for h_i is taken into account for evaluation of the thermal average, we get

$$\begin{aligned}
\tilde{C} &= \overline{\left(\frac{pQ\epsilon_i}{2\pi} + \gamma - \left[\frac{pQ\epsilon_i}{2\pi} + \gamma \right] \right)^2} \\
&= \int_{-l_{imp}}^{\infty} d\epsilon_i \frac{l_{imp}^{-1}}{e} e^{-l_{imp}^{-1}\epsilon_i} \left(\frac{pQ\epsilon_i}{2\pi} + \gamma - \left[\frac{pQ\epsilon_i}{2\pi} + \gamma \right] \right)^2 .
\end{aligned}$$

If we substitute $x = l_{imp}^{-1}\epsilon_i + 1$ and take into account that $[x + n] = [x] + n$ for $n \in \mathbb{Z}$, we get

$$\tilde{C} = \int_0^{\infty} dx \, e^{-x} \left(\frac{x}{2\alpha} - \left[\frac{x}{2\alpha} \right] \right)^2 \tag{E1.21}$$

with the parameter $\alpha = \frac{\pi}{pQl_{imp}}$. Now the quadratic term in the integral is expanded, which leads to the following three (converging) integrals

$$\begin{aligned}
I_1 &\equiv \frac{1}{4\alpha^2} \int_0^{\infty} dx \, e^{-x} x^2 = \frac{1}{2\alpha^2} , \\
I_2 &\equiv -\frac{1}{\alpha} \int_0^{\infty} dx \, e^{-x} x \left[\frac{x}{2\alpha} \right] \\
&= -\frac{1}{\alpha} \sum_{k=1}^{\infty} \int_{(2k-1)\alpha}^{(2k+1)\alpha} dx \, e^{-x} x \left[\frac{x}{2\alpha} \right] \tag{E1.22} \\
I_3 &\equiv \int_0^{\infty} dx \, e^{-x} \left[\frac{x}{2\alpha} \right]^2 , \\
&= \sum_{k=1}^{\infty} \int_{(2k-1)\alpha}^{(2k+1)\alpha} dx \, e^{-x} \left[\frac{x}{2\alpha} \right]^2 ,
\end{aligned}$$

with $\tilde{C} = I_1 + I_2 + I_3$. For $(2k-1)\alpha \le x \le (2k+1)\alpha$, $k \in \mathbb{Z}$, $\left[\frac{x}{2\alpha}\right] = k$, such that the *Gaussian brackets* in the finite integrals in I_2 and I_3 can be replaced by k or k^2, respectively:

$$
\begin{aligned}
I_2 &= -\frac{1}{\alpha} \sum_{k=1}^{\infty} k \int_{(2k-1)\alpha}^{(2k+1)\alpha} dx\, e^{-x} x\,, \\
I_3 &= \sum_{k=1}^{\infty} k^2 \int_{(2k-1)\alpha}^{(2k+1)\alpha} dx\, e^{-x}\,.
\end{aligned}
\tag{E1.23}
$$

The values of these two simple integrals are

$$
\begin{aligned}
\int_{(2k-1)\alpha}^{(2k+1)\alpha} dx\, e^{-x} x &= 2e^{-2k\alpha}\left((1+2k\alpha)\sinh(\alpha) - \alpha\cosh(\alpha)\right), \\
\int_{(2k-1)\alpha}^{(2k+1)\alpha} dx\, e^{-x} &= 2e^{-2k\alpha}\sinh(\alpha)\,.
\end{aligned}
$$

The remaining sums in I_2 and I_3 are only derivatives of the geometric series which can be easily evaluated.

The result is

$$
\begin{aligned}
\tilde{C} &= \frac{1}{2\alpha}\left(\frac{1}{\alpha} - \frac{1}{\sinh(\alpha)}\right) \\
&= \frac{1}{12} - \frac{7}{720}\alpha^2 + \frac{31}{30240}\alpha^4 + \mathcal{O}(\alpha^6)\,,
\end{aligned}
\tag{E1.24}
$$

where the expansion is useful only if α is small, i.e., $Ql_{imp} \gg 1$. If we would have neglected the order statistics of the impurity distances we would get only the leading constant: $\tilde{C} = 1/12$.

(E1.24) yields the presented expression for the pair correlation function (B4.17).

1.3 Correlation length in the classical region at finite temperature

In the weak pinning limit, $1 \ll l_{imp}Q \ll c/(U_{imp}\rho_1)$ or $L_{FL} \gg l_{imp}$, the classical Hamiltonian can be rewritten to a *random-field XY-model*

$$
\mathcal{H}_{class}(L) = \int_0^L dx \left\{ \frac{c}{2}\left(\partial_x\varphi(x) - \tilde{\sigma}\right)^2 + \frac{U_{imp}\rho_1}{l_{imp}}\cos[p(\varphi(x) - \alpha(x))] \right\}, \tag{E1.25}
$$

where $\alpha(x)$ is a random phase with zero average and

$$\overline{e^{\imath p\big(\alpha(x)-\alpha(x')\big)}} = l_{imp}\delta(x-x').\tag{E1.26}$$

In the following we consider only the backward scattering term of the correlation function C_b and therefore neglect the forward scattering term $\tilde{\sigma} = U_{imp}f/(c\pi l_{imp})$.

The goal is now to find an effective temperature, which replaces T in the correlation function for the free case (B4.18). We start with a *Burgers*-like equation, which one gets after a *Cole-Hopf transformation* from the transfer matrix equation, for the *restricted* free energy $\mathcal{F}(x,\varphi) = -T\ln\mathcal{Z}(x,\varphi)$ with the partition function

$$\mathcal{Z}(x,\varphi) \equiv \int\limits_{\varphi(0)}^{\varphi(x)=\varphi} \mathcal{D}\varphi\, e^{-H(x)/T}\,.$$

The equation reads

$$\frac{\partial\mathcal{F}}{\partial x} = \frac{T}{2c}\frac{\partial^2\mathcal{F}}{\partial\varphi^2} - \frac{1}{2c}\left(\frac{\partial\mathcal{F}}{\partial\varphi}\right)^2 + \underbrace{\frac{U_{imp}\rho_1}{l_{imp}}\cos[p(\varphi(x)-\alpha(x))]}_{U(x,\varphi)}\,.\tag{E1.27}$$

Using the Fourier transform $\mathcal{F}(x,\varphi) = \int\frac{dk\,d\omega}{(2\pi)^2}e^{\imath(\omega\varphi-kx)}\mathcal{F}(k,\omega)$ (analogous for $U(x,\varphi)$), (E1.27) is rewritten as

$$-\imath k\mathcal{F}(k,\omega) = -\frac{T\omega^2}{2c}\mathcal{F}(k,\omega) + U(k,\omega) +\tag{E1.28}$$

$$\frac{1}{2c}\int\frac{dk'\,d\omega'}{(2\pi)^2}\omega'(\omega-\omega')\mathcal{F}(k-k',\omega-\omega')\mathcal{F}(k',\omega')\quad,$$

with

$$U(k,\omega) = \frac{\pi U_{imp}\rho_1}{l_{imp}}\left\{h_+(k)\delta(\omega-p) + h_-(k)\delta(\omega+p)\right\},\tag{E1.29}$$

$$h_\pm(k) \equiv \int dx\, e^{\imath[kx\mp p\alpha(x)]}\,.$$

Introduction the dimensionless quantities

$$g_0(k,\omega) = \frac{1}{\pi t\omega^2/2 - \imath k/\Lambda}\,,\tag{E1.30}$$

$$\epsilon = \frac{U_{imp}\rho_1}{l_{imp}\Lambda^2 c}\,,\tag{E1.31}$$

$$u(k,\omega) = (\epsilon\Lambda c)^{-1}U(k,\omega)\,,\tag{E1.32}$$

and setting $\mathcal{F}(k,\omega) \equiv c\epsilon g(k,\omega)u(k,\omega)$ we obtain the following, self-consistent equation for the Green's function $g(k,\omega)$:

$$g(k,\omega)u(k,\omega) = g_0(k,\omega)u(k,\omega) + \frac{\epsilon}{2}g_0(k,\omega)\int \frac{dk'\,d\omega'}{\Lambda(2\pi)^2}\omega'(\omega-\omega')\times$$
$$\times g(k-k',\omega-\omega')g(k',\omega')u(k-k',\omega-\omega')u(k',\omega') \quad \text{(E1.33)}$$

For $\epsilon < 1$, i.e., for weak disorder, this equation is iterated to first non–vanishing order in ϵ (*one-loop* approximation) and averaged over disorder. The disorder average $\overline{u(k,\omega)u(k',\omega')}$ can be calculated using (E1.29) and (E1.26), which gives

$$\overline{u(k,\omega)u(k',\omega')} = \Lambda^2\pi^2\Big\{\overline{h_+(k)h_-(k')}\delta(\omega-p)\delta(\omega'+p) +$$
$$+\overline{h_-(k)h_+(k')}\delta(\omega+p)\delta(\omega'-p)\Big\}$$
$$= 2\Lambda^2 l_{imp}\pi^3\delta(k+k')\delta(\omega+\omega')\{\delta(\omega+p)+\delta(\omega-p)\}$$
$$\equiv 2\delta(k+k')\delta(\omega+\omega')D(\omega,k)\,. \quad \text{(E1.34)}$$

Therefore, we get for g in order ϵ^2

$$g(k,\omega) = g_0(k,\omega) + \epsilon^2 g_0^2(k,\omega)\int \frac{dk'\,d\omega'}{\Lambda^2(2\pi)^4}(\omega-\omega')\omega'\omega(-\omega')\times$$
$$\times g_0(k',\omega')g_0(k-k',\omega-\omega')g_0(-k',-\omega')D(k',\omega')\,. \quad \text{(E1.35)}$$
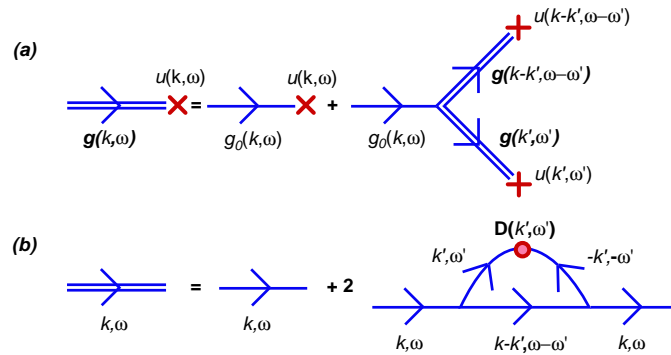
Figure E.3: Diagrams for (a) eq. (E1.33) and (b) eq. (E1.35).

The diagrams visualizing eqs. (E1.33) and (E1.35) are depicted in figure E.3.

For $k = 0$ (E1.35) reduces to

$$g(0,\omega) = g_0(0,\omega)\left[1 + \epsilon^2\frac{p^2 l_{imp}}{8\pi t\omega}\int dk'\frac{1}{(k'/\Lambda)^2 + (\pi p^2 t/2)^2} \times\right.$$

$$\left.\times\left\{\frac{p-\omega}{\pi t(\omega-p)^2/2 - \imath k'/\Lambda} - \frac{p+\omega}{\pi t(\omega+p)^2/2 - \imath k'/\Lambda}\right\}\right]. \quad \text{(E1.36)}$$

Because we calculate the correlation length in the thermal regime (see figure B.6) with $t \gtrsim t_u$ the k'-integral in (E1.36) gives the biggest contribution to g at small ω. In this case the k'-integral can be easily calculated which leads to

$$g(0,\omega \ll 1) \approx g_0(0,\omega)\left(1 - \epsilon^2\frac{\Lambda l_{imp}}{2\pi^3 p^2 t^3}\right) \quad \text{(E1.37)}$$

or for the effective Temperature T_{eff}

$$\frac{1}{T_{eff}} \approx \frac{1}{T}\left(1 - \epsilon^2\frac{\Lambda l_{imp}}{2\pi^3 p^2 t^3}\right) = \frac{1}{T}\left(1 - \frac{1}{2}\left(\frac{t_u}{\pi p^2 t}\right)^3\right), \quad \text{(E1.38)}$$

which yields for the correlation length

$$\xi^{-1} \approx \frac{\pi}{2}f(T)t\left[1 + \frac{1}{2}\left(\frac{t_u}{\pi p^2 t}\right)^3\right]\Lambda, \quad \text{(E1.39)}$$

as written in the text. For high temperatures $t \gg t_u$ we recover the linear t dependency of the free case.

A related calculation for directed polymers and interface growth can be found in [MHKZ89]. Note, that in this paper x plays the role of φ and t the role of x in the above calculation.

1.4 Symbol reference

Table EI: List of used quantities in chapter B

symbol	quantity	eq. ref.
a	lattice constant	
$b = e^{-l}$	rescaling parameter of order 1	
B_i	functions used in flow equations	(B3.6)
c	elastic constant	(B2.4a)
$C(x,\tau), C_f, C_b$	phase correlation functions	(B4.5), (B4.12)

Table EI: (continued...)

symbol	quantity	eq. ref.
d	spatial dimension	
$f(T)$	condensate density	(B2.4)
$\mathcal{F}$	free energy	(B3.1)
g	dimensionless electron-phonon coupling constant	(B2.4)
g_i	functions used in B_i	(B3.6)
g_q	electron-phonon coupling constants	(B2.2)
h_i	integers (cf. strong pinning)	(B3.24)
$\hat{\mathcal{H}}$, $\hat{\mathcal{H}}_0$	Hamiltonian (complete and free)	(B2.4)
k, k_n	wave vectors	
k_F	Fermi wave vector	
K, $K(l)$, K_0	dimensionless parameter for quantum fluctuations	(B2.8b)
K_u, K_u^*	K-values defining the separatrix/fixed point of the disorder unpinning transition	(B3.13)
K_w, K_w^*	K-values defining the separatrix/fixed point of the lattice unpinning transition	(B6.4)
L	system length	(B2.4)
L_{FL}	Fukuyama-Lee or Larkin length	(B2.7)
l_{imp}	mean impurity distance	(B2.5)
$\mathcal{L}_0$	free (gaussian) part of the Lagrangian	(B3.2))
n_i	integers (cf. strong pinning)	(B3.23)
N_{imp}	number of impurities	(B2.4b)
p	commensurability used in the density	(B2.1)
$p(\epsilon_i)$	probability density function of ϵ_i	(B4.15)
$\hat{P}$	momentum operator, conjugate to $\hat{\varphi}$	(B2.4)
Q	density wave vector	(B2.1)
q	commensurability used in the lattice potential	(B2.4c)
$\mathcal{S}$, $\mathcal{S}_0$	action (full and gaussian part)	(B3.4)
$\mathcal{S}^{(n)}$	replicated action	(B3.2)
$\mathcal{S}_{SF}$, $\mathcal{S}_{LP}$	action for superfluids and lattice potential	(B5.2)
S, S_1	density correlation functions	(B4.1), (B4.2)

Table EI: (continued...)

symbol	quantity	eq. ref.
T	temperature	
T_c^{MF}	mean-field condensation temperature	
t, $t(l)$, t_0	parameter for thermal fluctuations	(B2.8a)
$t_u = 1/(\Lambda L_{FL})$	crossover temperature from classical disordered to thermal regime	
t_K	temperature separating the thermal and disordered regime	
$U(x)$	disorder potential	(B2.4b)
U_i	impurity potential	(B2.4b)
U_{imp}	mean impurity potential	(B2.5)
u, $u(l)$, u_0	dimensionless parameter for disorder fluctuations	(B2.8c)
v_F	Fermi velocity	
v	phason velocity	(B2.4)
$V_c(x)$	Coulomb potential	(B2.10)
W	lattice potential strength	(B2.4c)
$\widetilde{W}$	phase-slip probability	(B2.4d)
w, $w(l)$, w_0	dimensionless parameter for lattice potential strength	(B2.8d)
x_i	impurity positions	(B2.4b)
z	dimensionless distance in τ-x-space	
α	parameter used in the strong pinning limit	(B4.17)
β	inverse temperature	
γ	parameter for KT flow equations	(B3.14a)
Δ	order parameter	(B2.2)
ϵ_i	deviation from mean impurity distance	(B3.24)
ζ	transverse width of the quasi one-dimensional system	
η, $\tilde{\eta}$	$= B_0(p^2 K_u^*, \infty)$, $= -B_2(q^2/K_w^*, \infty)$, respectively	
λ	density wave length	
λ_T	de Broglie wave length	(B2.9)
Λ	momentum cutoff	

Table EI: (continued...)

symbol	quantity	eq. ref.
ξ, ξ_u, ξ_w, etc.	correlation lengths	table BII
ϖ, ϖ_0, $\varpi(l)$	dimensionless parameter for phase-slip probability	(B2.8e)
$\rho(x)$, $\rho_{SF}(x)$	charge/spin or superfluid density	(B2.1), (B5.1)
ρ_0	mean density	(B2.1)
ρ_1	density amplitude for harmonic part of $\rho(x)$	(B2.1)
σ	forward scattering amplitude	(B3.4)
τ	imaginary time coordinate	
φ	phase variable	(B2.2)
χ	parameter for KT flow equations	(B3.14b)
Υ	auxiliary function	(B3.7)
ω_n	Matsubara frequencies	

2 Appendix to chapter C

2.1 Mean-field equation of motion

In this appendix we briefly present the derivation of the solution of the mean-field equation of motion.

The mean-field equation is obtained from the initial equation of motion (C2.1) by taking the limit of infinite-range elastic interaction, i.e., all $z(\mathbf{x}, t)$ (for all $\mathbf{x}$) couple to all other $z(\mathbf{x}', t)$ with the same strength, which is of order $1/N$ for a proper normalization (N is the number of discrete segments in $\mathbf{x}$-direction). This is equivalent to the limit $D \to \infty$.

The elastic forces can then be expressed in a form, that all $z(\mathbf{x}', t)$ are uniformly coupled to the mean interface position $z_0(t) = \langle\langle z(\mathbf{x}, t)\rangle_x\rangle_d$ instead of the *nearest neighbor coupling* in (C2.1). Therefore the redundant spatial dependence of z and g can be dropped and one obtains

$$\frac{1}{\tilde{\gamma}}\frac{\partial z}{\partial t} = \tilde{\Gamma}\left[z_0(t) - z(t)\right] + h(t) + \tilde{g}(z)\,. \tag{E2.1}$$

The interface displacement z can be decomposed to $z(t) = z_0(t) + \mathfrak{z}(t)$ with $\langle\mathfrak{z}(t)\rangle_d = 0$ and the equation of motion for $z_0(t)$ follows directly from (E2.1) after averaging over the disorder:

$$\frac{1}{\tilde{\gamma}}\dot{z}_0(t) = h(t) + \langle\tilde{g}(z_0(t) + \mathfrak{z}(t))\rangle_d\,. \tag{E2.2}$$

Subtracting this from (E2.1) gives

$$\left(\frac{1}{\tilde{\gamma}}\frac{\partial \mathfrak{z}(t)}{\partial t} + \tilde{\Gamma}\mathfrak{z}(t)\right) = \tilde{g}(z_0(t) + \mathfrak{z}(t)) - \langle \tilde{g}(z_0(t) + \mathfrak{z}(t))\rangle_d . \tag{E2.3}$$

The Greens function for this partial differential equation is given by

$$G_0(t - t_0) = \tilde{\gamma}\Theta(t - t_0)e^{-\tilde{\Gamma}\tilde{\gamma}(t-t_0)} \qquad \text{with} \tag{E2.4}$$

$$\left(\frac{1}{\tilde{\gamma}}\frac{\partial}{\partial t} + \tilde{\Gamma}\right)G_0(t - t_0) = \delta(t - t_0) .$$

Using this, the formal solution for $\mathfrak{z}(t)$ can be written as

$$\mathfrak{z}(t) = \int\limits_{-\infty}^{\infty} dt' \left[h(t') + \tilde{g}(z_0(t') + \mathfrak{z}(t')) - \frac{1}{\tilde{\gamma}}\dot{z}(t')\right]G_0(t - t') . \tag{E2.5}$$

Expanding $\tilde{g}(z_0 + \mathfrak{z})$ in (small) $\mathfrak{z}$, iterating (E2.5) once and averaging over disorder one obtains

$$\frac{1}{\tilde{\gamma}}\dot{z}_0(t) = h(t) + \int\limits_{-\infty}^{\infty} dt' \, G(t - t') \left\langle \tilde{g}'(z_0(t))\tilde{g}(z_0(t'))\right\rangle_d . \tag{E2.6}$$

Using the disorder correlator and the expression for G_0, given in (E2.4), (E2.6) can be rewritten to

$$\frac{1}{\tilde{\gamma}}\dot{z}_0(t) = h(t) + \int\limits_{-\infty}^{t} dt' \, \Delta'(z_0(t) - z_0(t'))\tilde{\gamma}e^{-\tilde{\Gamma}\tilde{\gamma}(t-t')} , \tag{E2.7}$$

which can be transformed to (C3.2) by the shift $t - t' \to t'$.

2.2 Perturbation theory

For the solution of the initial equation of motion (C2.1) in perturbation theory, we go over to a co-moving frame via $z(\mathbf{x}, t) = z_0(t) + \mathfrak{z}(\mathbf{x}, t)$ with $z_0(t) = \langle z(\mathbf{x}, t)\rangle_x$ and $\langle \mathfrak{z}\rangle = 0$ and define $v(t) \equiv \dot{z}_0(t)$.

With this, the equation of motion can be rewritten as

$$\mathfrak{z}(\mathbf{x}, t) = \int d^D x' \int dt' \, \mathcal{G}_0(\mathbf{x} - \mathbf{x}', t - t') \left\{h(t') - \frac{v(t')}{\gamma} + g(\mathbf{x}', z_0(t') + \mathfrak{z}(\mathbf{x}', t'))\right\} \tag{E2.8}$$

with the *Greens function* $\mathcal{G}_0(\mathbf{x}, t)$, defined by

$$\left(\frac{1}{\gamma}\frac{\partial}{\partial t} - \Gamma\boldsymbol{\nabla}^2\right)\mathcal{G}_0(\mathbf{x} - \mathbf{x}_0, t - t_0) = \delta(\mathbf{x} - \mathbf{x}_0, t - t_0) . \tag{E2.9}$$

Expanding $g(\mathbf{x}', z_0(t') + \mathfrak{z}(\mathbf{x}', t')$ in small $\mathfrak{z}$ and iterating (E2.8) leads in lowest, non vanishing order to

$$
\begin{aligned}
v(t) &\doteq \gamma h(t) + \gamma \left\langle \partial_{z_0} g(\mathbf{x}, z_0(t)) \left(\int d^D x' \int dt'\, \mathcal{G}_0(\mathbf{x} - \mathbf{x}', t - t') g(\mathbf{x}', z_0(t')) \right) \right\rangle \\
&= \gamma h(t) + \int_{-\infty}^{\infty} dt'\, \mathcal{G}_0(\mathbf{0}, t - t') \partial_{z_0} \Delta(z_0(t) - z_0(t')),
\end{aligned}
\tag{E2.10}
$$

with

$$
\mathcal{G}_0(\mathbf{0}, t) = \Theta(t) \int_{\Omega} \frac{d^D p}{(2\pi)^D} e^{-\Gamma \gamma \mathbf{p}^2 t} \gamma,
\tag{E2.11}
$$

where $\Omega = \left\{ \mathbf{p}; |\mathbf{p}| < \Lambda \approx L_P^{-1} \right\}$.

If one assumes, that Δ does not depend one $\mathbf{p}$, (E2.10) can be evaluated to

$$
\frac{v(t)}{\gamma} = h(t) + \frac{\gamma K_D}{2} \int dt'\, \Delta'(z_0(t, t'))(\Gamma \gamma t')^{-D/2} \tilde{\Gamma}_{D/2}(L_P^{-2} \Gamma \gamma t')
\tag{E2.12}
$$

with $z_0(t, t') \equiv z_0(t) - z_0(t - t')$, $K_D = 2^{1-D} \pi^{-D/2} \Gamma(D/2)$, and $\tilde{\Gamma}_x(y) \equiv \Gamma(x) - \Gamma_x(y)$, where $\Gamma_x(y)$, $\Gamma(x) = \Gamma_x(0)$ are the incomplete and complete Gamma function, respectively. With the approximation $(1 + x)^{-\alpha} \approx \alpha x^{-\alpha} \tilde{\Gamma}_\alpha(x)$, the velocity is given by

$$
\begin{aligned}
\frac{v(t)}{\gamma} &\approx h(t) + h_P^2 \gamma \frac{D}{4} \int_0^{\infty} dt'\, (1 + \omega_P t')^{-D/2} \frac{\Delta^{*\prime}(z_0(t, t')/l)}{l} \\
&\equiv h(t) + r_0(t),
\end{aligned}
\tag{E2.13}
$$

where we introduced Δ^* by $\Delta(z) = K_D^{-1}(\Gamma l)^2 L_P^{D-4} \Delta^*(z/l)$ (cf. eq. (C3.7) and (C3.8)). Next we want to analyze $r_0(t)$ for $\Delta^*(x) = e^{-x^2}$ and for the free solution $v_0(t) = \gamma h(t)$, i.e.,

$$
r_0(t) = -\frac{h_P^2 \gamma D}{2l^2} \int_0^{\infty} dt'\, (1 + \omega_P t')^{-D/2} z_0(t, t') e^{-(z_0(t, t')/l)^2}.
\tag{E2.14}
$$

Since perturbation theory works (best) for $h(t) > h_P$, we calculate $r_0(t)$ at $t = t_1 \equiv \frac{\pi}{2\omega_0}$, i.e., for $h(t) = h_0$. Therefore it is $z_0(t_1, t') = \frac{\gamma h_0}{\omega_0} \sin(\omega_0 t')$ and after substituting $\tau = \omega_0 t'$ we get

$$
r_0(t_1) = -\left(\frac{\omega_P}{\omega_0} \right)^2 h_0 \frac{D}{2} \int_0^{\infty} d\tau \left(1 + \frac{\omega_P}{\omega_0} \tau \right)^{-D/2} \sin(\tau) e^{\frac{\omega_P}{\omega_0} \frac{h_0}{h_P}^2 \sin^2(\tau)},
\tag{E2.15}
$$

where the sine function ensures the convergence of the integral. For $\omega_0 \gg \omega_P$ the exponential function can be neglected one has to estimate the value of an integral of form

$$
I_a(b) \equiv \int_0^{\infty} dx\, (1 + bx)^{-a} \sin(x).
\tag{E2.16}
$$

It it easy to show that $|I_a(b)| \leq 2$ for all $a, b > 0$:

$$
\begin{aligned}
I_a(b) &= \sum_{n=0}^{\infty} \underbrace{\int_{n\pi}^{(n+1)\pi} dx\, (1+bx)^{-a} \sin(x)}_{\gtrless 0 \text{ for even/odd } n} \\
&\leq \sum_{n=0}^{\infty} \left(\int_{2n\pi}^{(2n+1)\pi} dx\, \frac{\sin(x)}{(1+b2n\pi)^a} - \int_{(2n+1)\pi}^{2(n+1)\pi} dx\, \frac{\sin(x)}{(1+b2(n+1)\pi)^a} \right) \\
&= 2 \sum_{n=0}^{\infty} \left((1+2\pi n b)^{-a} - (1+2\pi(n+1)b)^{-a} \right) \\
&= 2(1+2\pi 0 b)^{-a} = 2 \,.
\end{aligned}
$$

In fact it is even $|I_a(b)| \leq 1$, but the important result is that this integral is of order 1. Therefore we have shown that r_0 is of order $\left(\frac{\omega_P}{\omega_0} \right)^2$.

2.3 Review of the RG for the disorder correlator

In this appendix we give a short overview and the main ideas of the renormalization of the disorder correlator $\Delta(z)$ since it is a main ingredient of the calculations on chapter C. This "review" is based on Refs. [LNST97, NSTL92].

The disorder correlator is defined by the random force $g(\mathbf{x}, z)$ with $\langle g \rangle_d = 0$ by

$$\langle g(\mathbf{x}, z) g(\mathbf{0}, 0) \rangle_d = \Delta_\parallel(\mathbf{x}) \Delta(z) \,. \tag{E2.17}$$

The precise form of the correlation $\Delta_\parallel(\mathbf{x})$ which extends over a length $l_\parallel$ in the x-direction is not of crucial importance. Throughout the thesis we used $l_\parallel \to 0$, i.e., $\Delta_\parallel(\mathbf{x}) = \delta^D(\mathbf{x})$.

However, the form of the symmetric function $\Delta(z)$ is very important. Therefore we should distinguish between different situation for the random force g:

- *random-field disorder*: g could be a gaussian distributed force and the random force correlator $\Delta(z)$ is a monotonically decreasing function of z and decays exponentially over a length l.

- *random-bond disorder*: In this case g can be written as gradient of a random potential V_R, i.e., $g \simeq -\partial_z V_R(\mathbf{x}, z)$, which is correlated over a length l, i.e., $\Delta(z) = -R''(z)$, where $R(z)$ is the random potential correlator.

- *charge density waves*: g can be written as a periodic function: $g(\mathbf{x}, z) = g_0 \cos(z - \alpha(\mathbf{x}))$, with a random phase $\alpha(\mathbf{x})$. Therefore $\Delta(z)$ is also periodic with zero mean value.
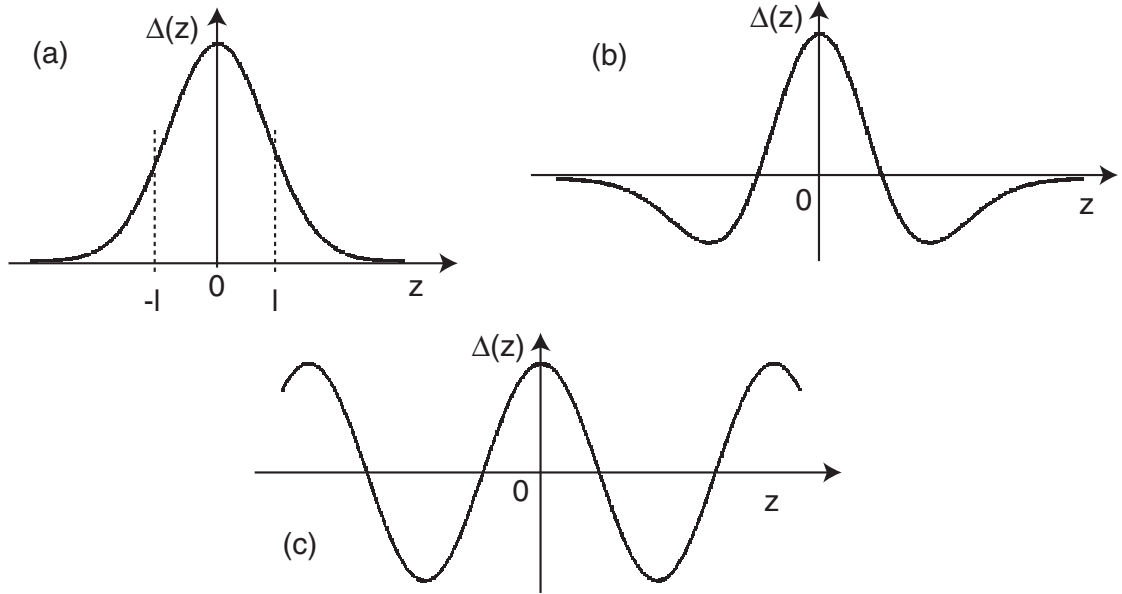
Figure E.4: Random force correlator $\Delta(z)$ for (a) random-field disorder, (b) random-bond disorder, and (c) charge density waves

Illustrations of these three cases are shown in Fig. E.4.

As we have seen in the main introduction chapter, the critical dimension for the disorder is 4, above which curvature forces always win over the pinning forces. Below 4 dimensions, the curvature forces cannot balance the random forces on scales larger than the Larkin length L_P, where the interface becomes rough.

So far we have used the perturbation theory in order to solve the equation of motion (C2.1), but we have seen, that the perturbative corrections to the interface velocity diverge as $v^{-\frac{4-D}{2}}$ near the depinning transition at zero temperature when $v \to 0$.

To overcome this divergency, one has to perform a functional RG procedure in $D = 4 - \epsilon$ for the disorder correlator. Therefore we can represent $\Delta(z)$ as

$$\Delta(z) \equiv \sum_{n=0}^{\infty} \frac{(-1)^n}{(2n)!} z^{2n} Q_{2n} \,, \tag{E2.18}$$

since $\Delta(z)$ is analytical function at $z = 0$. $Q_{2n} \equiv \int_k k^{2n} \Delta_k$ are called the moments of $\Delta(z)$, and Δ_k are the Fourier components of $\Delta(z)$. By differentiating (E2.18) one obtains formally

the flow equation

$$\frac{\partial \Delta(z)}{\partial \ln b} = \sum_{n=0}^{\infty} \frac{(-z^2)^n}{(2n)!} b \frac{\partial Q_{2n}}{\partial b} , \qquad (E2.19)$$

with the rescaling parameter b. A perturbative expansion of an appropriately chosen parameter (see eq. (42) in [LNST97]) gives the following renormalization prescription of the moments Q_{2n} in one-loop order:

$$b \frac{\partial Q_{2n}}{\partial \ln b} = \frac{K_D}{\Gamma^2} b^\epsilon \sum_{j=1}^{n} \binom{2n+1}{2j} Q_{2j} Q_{2(n-j+1)} , \qquad (E2.20)$$

with $K_D^{-1} = 2^{D-1} \pi^{D/2} \Gamma(D/2)$.

In order to get a functional RG equation, one has to express the right-hand side of (E2.19) in term of $\Delta(z)$, using (E2.20), which results finally in

$$\frac{d\Delta(z)}{d \ln b} = -\frac{K_D}{\Gamma^2} b^\epsilon \frac{d^2}{dz^2} \left[\frac{1}{2} \Delta^2(z) - \Delta(z)\Delta(0) \right] . \qquad (E2.21)$$

Using this terminology, the flow equation for γ in first order in ϵ can be written as [NSTL92]

$$\frac{d \ln \gamma}{d \ln b} = -\frac{K_D}{\Gamma^2} Q_2 b^\epsilon . \qquad (E2.22)$$

Note, that there is no renormalization of Γ in this order.
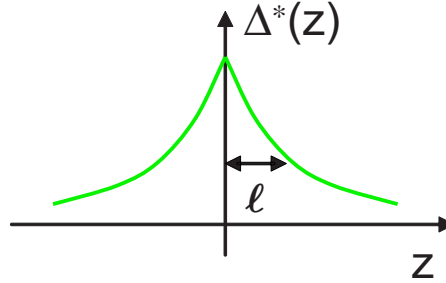
Figure E.5: Renormalized disorder correlator showing a cusp-like shape.

The fixed point form of $\Delta(z)$ is discussed in the main text, which can be obtained from (E2.21) with the ansatz

$$\Delta(y) = \text{const.} \times L^{2\zeta-\epsilon} \hat{\Delta}(yL^{-\zeta}) \qquad (E2.23)$$

and $\Delta^*(y) = \lim_{L \to \infty} \hat{\Delta}(y)$. The constant is chosen such that $\Delta^*(0) = 1$. The resulting equation for $\Delta^*(y)$ is given by

$$(\epsilon - 2\zeta)\Delta^*(y) + \zeta y \Delta^{*\prime}(y) - \left(\Delta^{*\prime}(y) \right)^2 - \Delta^{*\prime\prime}(y) \left(\Delta^*(y) - 1 \right) = 0 . \qquad (E2.24)$$

The fixed point solution in the case of random-field disorder in shown in Fig. E.5.

2.4 Renormalized perturbation theory

Now we combine the results from the perturbation theory shown in appendix 2.2 and the results from the functional RG presented in 2.3 to overcome the breakdown of perturbation theory.

Therefore one has to consider the momentum dependency of γ and Δ given in (C3.9a) and (C3.9b), respectively, and as a result the Greens function from the perturbation theory is modified to

$$\mathcal{G}_0(\mathbf{0},t) = \Theta(t) \int_\Omega \frac{d^D p}{(2\pi)^D} \, e^{-\Gamma\gamma(|\mathbf{p}|)\mathbf{p}^2 t} \gamma(|\mathbf{p}|)\,, \tag{E2.25}$$

with $\Omega = \left\{ \mathbf{p}; \xi^{-1} < |\mathbf{p}| < \Lambda \approx L_P^{-1} \right\}$, where $\xi = \min(\xi_0, L_\omega)$.

Using this replacements in (E2.10) one gets the expression given in (C3.10) as follows

$$
\begin{aligned}
\frac{v(t)}{\gamma(L_\omega^{-1})} &= h(t) + \int_{-\infty}^{\infty} dt' \, \mathcal{G}_0(\mathbf{0},t)(\Delta_p') \\
&= h(t) + K_D^{-1} \left(\frac{\Gamma l}{L_P^\zeta} \right)^2 \int_0^\infty dt' \int_\Omega \frac{d^D p}{(2\pi)^D} e^{-\Gamma\gamma(|\mathbf{p}|)\mathbf{p}^2 t} \gamma(|\mathbf{p}|) p^{4-D-2\zeta} \times \\
&\qquad \times \frac{\partial}{\partial z(t,t')} \Delta^*(z(t,t')(pL_p)^\zeta/l) \\
&= h(t) + \underbrace{\frac{\gamma\Gamma^2 l}{L_P^4}}_{=h_P \omega_P} \int_0^\infty dt' \int_{\tilde{L}_\omega^{-1}}^1 d\tilde{p} \, \tilde{p}^{1+z+\zeta} e^{-\omega_P \tilde{p}^z t'} \Delta^*(z(t,t')\tilde{p}^\zeta/l)\,.
\end{aligned}
$$

If $\Delta^{*\prime}(x)$ depends only on the sign of x, the dependency on $\tilde{p}$ of $\Delta^{*\prime}$ in (C3.10) can be neglected and with

$$\int_{\tilde{L}_\omega^{-1}}^1 d\tilde{p} \, \tilde{p}^{1+z-\zeta} e^{-\omega_P \tilde{p}^z t'} = \frac{1}{z}(t'\omega_P)^{-\delta} \left(\Gamma_\delta(t'\omega_P \tilde{L}_\omega^{-z}) - \Gamma_\delta(t'\omega_P) \right) \tag{E2.26}$$

and $\delta = \frac{2+z-\zeta}{z} = 1 + \frac{1}{\nu z}$ one obtains

$$
\begin{aligned}
\frac{v(t)}{\gamma(L_\omega - 1)} &= h(t) + \frac{h_P \omega_P}{z} \int dt' \, (\omega_P t')^{-\delta} \left(\tilde{\Gamma}_\delta(t'\omega_P) - \tilde{\Gamma}_\delta(t'\omega_0) \right) \Delta^{*\prime}(0^+) \operatorname{sgn}(z(t,t')/l) \\
&= h(t) - \frac{\tilde{h}_P}{\nu z} \int_0^\infty d\tau \left[S(\tau, \omega_P) - \tilde{L}_\omega^{-1/\nu} S(\tau, \omega_0) \right]\,, \tag{E2.27}
\end{aligned}
$$

with $S(\tau, \omega) \equiv \tau^{-\delta} \tilde{\Gamma}_\delta(\tau) \operatorname{sgn}(z(t, \tau/\omega))$.

2.5 Symbol reference

Table EII: List of symbols used in chapter C

symbol	quantity
a	length scale for the surface potential
$\mathcal{C}, \mathcal{C}_s$	curvature and its saturation value ($t \to \infty$)
D	dimension of the interface
f	frequency ($\omega_0/(2\pi)$)
$g(\mathbf{x}, z)$	random force
$\mathcal{H}$	Hamiltonian
$\mathcal{H}_n$	replica Hamiltonian
$h(t)$	driving force
h_0	amplitude of the driving force
$h_P, \tilde{h}_P$	(real) depinning threshold ($\approx h_{P,0} = \Gamma l L_P^{-2}$) and its RG value
$h_{P,s}$	surface depinning threshold
h_c	force at which the velocity becomes 0 in the non-adiabatic velocity hysteresis loop
h_{c0}	field at which $L_\omega \approx \xi_0$
K_D	$= 2^{1-D}\pi^{-D/2}/\Gamma(D/2)$
L	system size
L_ω	perturbation propagation length scale
L_P	Larkin length
l	variance of the disorder correlator
M	magnetization
M_s	maximal magnetization
r_0	perturbative correction to v
R_c	critical droplet size
$R(\varphi)$	random potential correlator
$S(t, \omega)$	$= \int_0^\infty d\tau\, \tau^{-\delta} \tilde{\Gamma}_\delta(\tau)\, \mathrm{sgn}\, z_0(t, \tau/\omega)$, auxiliary function
t_c	$\approx (\omega_0 + v(t)/l)^{-1}$, time cutoff
$\mathcal{T}$	time for one ac cycle

Table EII: (continued...)

symbol	quantity
T	temperature
T_P	$=$, typical temperature
v	$= \langle \dot{z}(\mathbf{x}, t) \rangle_x$, (mean) velocity
v_P	$= \omega_P l$
$V(\mathbf{x}, z)$	potential (random V_R & surface V_s)
$z(\mathbf{x}, t)$, $z_0(t)$	interface profile and its mean value
z	dynamical critical exponent
α	numerical length unit
$\alpha(x)$	random phase
β	critical exponent for the velocity at depinning
$\Delta(z)$, $\Delta_0(z)$	random force correlators
Δ^*	fixed point disorder correlator
ϵ	$= 4 - D$
ζ, $\tilde{\zeta}$	roughness exponent
η	thermal noise
θ	scaling exponent
γ	mobility constant
Γ	stiffness constant
Γ_δ	incomplete Γ-function
μ	$= \frac{2\zeta + D - 2}{2 - \zeta}$, exponent in dc interface velocity
μ_0	magnetic permeability of vacuum $4\pi \times 10^{-7}$Wb/(A m)
ν	critical exponent for the correlation length
ξ, ξ_0	correlation length
$\rho(x)$	function defining the area where the surface potential acts
τ_0	numerical time unit
$\phi_\pm$	scaling function
φ	(CDW) phase profile
φ_s	phase field at the surface
ω_0	external (angular) frequency of the driving force
χ, χ', χ''	complex susceptibility and its real and imaginary part

symbol	quantity
ω_P	typical "pinning" frequency

3 Appendix to chapter D

3.1 Bogoliubov transformation

In this appendix we derive the Bogoliubov-de Gennes equations for an interacting Bose system and solve it in the case when there is no external potential. The full Hamiltonian of the interacting Bose system (condensate and over-condensate), including an external trapping potential is given by

$$\hat{\mathcal{H}} = \int_V d^d r\, \Psi^\dagger(\mathbf{r}) \left[-\frac{\hbar^2}{2m}\nabla^2 + V_{ex}(\mathbf{r}) - \mu + \frac{1}{2}\int_V d^d r'\, \Psi^\dagger(\mathbf{r}')U(|\mathbf{r}-\mathbf{r}'|/a)\Psi(\mathbf{r}') \right] \Psi(\mathbf{r}) \tag{E3.1}$$

with

$$V_{ex}(\mathbf{r}) = \frac{m}{2}\sum_{i=1}^{d}\omega_i^2 r_i^2\,. \tag{E3.2}$$

Using the decomposition $\Psi = \xi_0 + \psi$ of the complete wave function (ξ_0 is the condensate wave function, ψ of the over-condensate) and using the Bogoliubov transformation

$$\psi(r) = \sum_k \hat{b}_k u_k(r) - \hat{b}_k^\dagger v_k^*(r)\,, \tag{E3.3a}$$

$$\psi^\dagger(r) = \sum_k \hat{b}_k^\dagger u_k^*(r) - \hat{b}_k v_k(r)\,, \tag{E3.3b}$$

the Hamiltonian can be rewritten as

$$\hat{\mathcal{H}} = \hat{\mathcal{H}}_0 + \sum_k \varepsilon_k \hat{b}_k^\dagger \hat{b}_k\,. \tag{E3.4}$$

To obtain the functions $u_k(\mathbf{r})$ and $v_k(\mathbf{r})$ one has to solve the Bogoliubov-de Gennes equation

$$\int_V d^d r' \, U(|\mathbf{r} - \mathbf{r}'|/a) \Big[|\xi_0(\mathbf{r}', t)|^2 u_k(\mathbf{r}, t) + \xi_0^*(\mathbf{r}', t)\xi_0(\mathbf{r}, t)u_k(\mathbf{r}', t)$$

$$-\xi_0(\mathbf{r}', t)\xi_0(\mathbf{r}, t)v_k(\mathbf{r}', t) \Big] = \imath\hbar\partial_t u_k(\mathbf{r}, t) - \left[-\frac{\hbar^2\nabla^2}{2m} - \mu + V_{ex} \right] u_k(\mathbf{r}, t) \quad \text{(E3.5a)}$$

$$\int_V d^d r' \, U(|\mathbf{r} - \mathbf{r}'|/a) \Big[|\xi_0(\mathbf{r}', t)|^2 v_k(\mathbf{r}, t) + \xi_0(\mathbf{r}', t)\xi_0^*(\mathbf{r}, t)v_k(\mathbf{r}', t)$$

$$-\xi_0^*(\mathbf{r}', t)\xi_0^*(\mathbf{r}, t)u_k(\mathbf{r}', t) \Big] = -\imath\hbar\partial_t v_k(\mathbf{r}, t) - \left[-\frac{\hbar^2\nabla^2}{2m} - \mu + V_{ex} \right] v_k(\mathbf{r}, t) \, \text{(E3.5b)}$$

with the normalization condition

$$\int_V d^d r \, (u_k(\mathbf{r})u_{k'}^*(\mathbf{r}) - v_k(\mathbf{r})v_{k'}^*(\mathbf{r})) = \delta_{k,k'} \, . \tag{E3.6}$$

With $\xi_0 \approx \sqrt{n}$ and the ansatz $\begin{pmatrix} u_k(\mathbf{r}, t) \\ v_k(\mathbf{r}, t) \end{pmatrix} = e^{-\imath\varepsilon_k t/\hbar} \begin{pmatrix} u_k(\mathbf{r}) \\ v_k(\mathbf{r}) \end{pmatrix}$ these equations can be simplified to

$$n\int_V d^d r' \, U(|\mathbf{r} - \mathbf{r}'|/a) \begin{pmatrix} u_k(\mathbf{r}) + u_k(\mathbf{r}') - v_k(\mathbf{r}') \\ v_k(\mathbf{r}) + v_k(\mathbf{r}') - u_k(\mathbf{r}') \end{pmatrix}$$

$$= \left(\frac{\hbar^2\nabla^2}{2m} + \mu - V_{ex} \pm \varepsilon_k \right) \begin{pmatrix} u_k(\mathbf{r}) \\ v_k(\mathbf{r}) \end{pmatrix} . \tag{E3.7}$$

For vanishing external potential $V_{ex} = 0$ one can go over to Fourier representation:

$$U(\mathbf{r} - \mathbf{r}') = \frac{1}{\sqrt{V}} \int d^d q \, e^{\imath\mathbf{q}(\mathbf{r} - \mathbf{r}')} U_q \, , \quad \begin{pmatrix} u_k(\mathbf{r}) \\ v_k(\mathbf{r}) \end{pmatrix} = \frac{e^{\imath\mathbf{k}\mathbf{r}}}{\sqrt{V}} \begin{pmatrix} u_k \\ v_k \end{pmatrix} \tag{E3.8}$$

and one obtains:

$$n\int d^d q \, U_q \begin{pmatrix} u_k\delta^d(\mathbf{q}) + (u_k - v_k)\delta^d(\mathbf{k} - \mathbf{q}) \\ v_k\delta^d(\mathbf{q}) + (v_k - u_k)\delta^d(\mathbf{k} - \mathbf{q}) \end{pmatrix} = \left(-\frac{\hbar^2 k^2}{2m} + \mu \pm \varepsilon_k \right) \begin{pmatrix} u_k \\ v_k \end{pmatrix} \tag{E3.9}$$

and finally

$$nU_{k=0} \begin{pmatrix} u_k \\ v_k \end{pmatrix} + nU_k \begin{pmatrix} u_k - v_k \\ v_k - u_k \end{pmatrix} = \left(-\frac{\hbar^2 k^2}{2m} + \mu \pm \varepsilon_k \right) \begin{pmatrix} u_k \\ v_k \end{pmatrix}$$

$$\Rightarrow \begin{pmatrix} u_k \\ v_k \end{pmatrix} = [f_1(k) \pm f_2(k)] \begin{pmatrix} v_k \\ u_k \end{pmatrix} \tag{E3.10}$$

with

$$f_1(k) \quad = \quad (U_{k=0}/U_k + 1) + \frac{1}{nU_k}(\varepsilon_{0,k} - \mu)\,, \tag{E3.11}$$

$$f_2(k) \quad = \quad \frac{\varepsilon_k}{nU_k}\,, \tag{E3.12}$$

$$\varepsilon_{0,k} \quad = \quad \frac{\hbar^2 k^2}{2m}\,. \tag{E3.13}$$

Note, that for $V_{ex}(\mathbf{r}) \neq 0$ this procedure fails.

From the last equation one finds immediately

$$f_1^2(k) - f_2^2(k) = 1 \tag{E3.14}$$

which gives an equation for the Bogoliubov energies ε_k. The solution for u_k and v_k is given by

$$\begin{pmatrix} u_k \\ v_k \end{pmatrix} = \left(\frac{f_1(k)}{f_2(k)} \pm 1 \right)^{1/2}\,. \tag{E3.15}$$

Since the quantity $w_k \equiv (u_k - v_k)^2$ is important to calculate the scattering rates, it can be written in terms of f_1, f_2 as

$$w_k = \frac{2}{f_2(k)}(f_1(k) - 1)\,. \tag{E3.16}$$

So far no assumptions about the interaction potential are made. The cases of a short-range (delta) and for a long-range (Coulomb) potential are treated next.

3.1.1 Short-range potential

In the most simple case of a short-range potential given by

$$U(\mathbf{r}) = U_0 \delta(\mathbf{r})\,, \tag{E3.17}$$

i.e., $U_k = U_0$, one obtains

$$f_1(k) \quad = \quad 2 + \frac{1}{nU_0}(\varepsilon_{0,k} - \mu)\,, \tag{E3.18}$$

$$f_2(k) \quad = \quad \frac{\varepsilon_k}{nU_0}\,, \tag{E3.19}$$

and with $\mu \approx U_0 n_{0,max}$ ($n_{0,max}$ is the maximum condensate density $\approx |\xi_0|^2$ for $T \ll T_c$) the solutions for ε_k, u_k and v_k are given by

$$\varepsilon_k^2 \quad = \quad \varepsilon_{0,k}(\varepsilon_{0,k} + 2\mu)\,, \tag{E3.20}$$

$$\begin{pmatrix} u_k \\ v_k \end{pmatrix} \quad = \quad \left(\frac{\varepsilon_{0,k} + \mu}{\varepsilon_k} \pm 1 \right)^{1/2}\,. \tag{E3.21}$$

And for w_k one finds easily: $w_k = 2\varepsilon_{0,k}/\varepsilon_k$.

3.1.2 Coulomb potential

Next we consider a Coulomb potential in two dimensions, given by

$$U(\mathbf{r}) = U_0/a^2 \ln(|\mathbf{r}|/a) \tag{E3.22}$$

or in Fourier representation: $U_k = -U_0/k^2$. a is a scattering length $\sim U_0 m/\hbar^2$. To avoid the divergency at $k = 0$, one has to take screening effects into account, i.e., a better potential is $U(\mathbf{r}) = U_0/a^2 K_0(|\mathbf{r}|/a)$, where K_0 is the modified Bessel function of second kind.

In lowest-order the potential has the form [FGI93]

$$U_k = -U_0 \frac{k^2}{k^4 + 8\pi U_0 nm/a^2} . \tag{E3.23}$$

However, if we just use $\mu \approx nU_{k=0}$ and $U_k = -U_0/k^2$ for large k, we obtain the following solutions

$$\varepsilon_k^2 = \varepsilon_{0,k}^2 + \frac{\hbar^2 U_0 n}{ma^2}, \tag{E3.24a}$$

$$f_1(k) = 1 + \varepsilon_{0,k}/(nU_k), \tag{E3.24b}$$

$$f_2(k) = \varepsilon_{0,k}/(nU_k), \tag{E3.24c}$$

$$w_k = 2\varepsilon_{0,k}/\varepsilon_k . \tag{E3.24d}$$

3.2 Scattering rates for short-range interaction

Scattering of Bogoliubov quasi-particles occurs in third order in the over-condensate operators. Using again the decomposition of Ψ into condensate and over-condensate part

$$\Psi = \xi_0 + \psi, \ (\xi_0 = \xi_0^\dagger = \sqrt{n})$$

and expand the interaction Hamiltonian up to third order in ψ :

$$
\begin{aligned}
\hat{\mathcal{H}}_{int} &= \frac{1}{2}U_0 \int dr \left(\Psi^\dagger\right)^2 \Psi^2 = \frac{1}{2}U_0 \int dr \left(\xi_0 + \psi^\dagger\right)^2 (\xi_0 + \psi)^2 \\
&= \frac{1}{2}U_0 \int dr \left(\xi_0^2 + 2\xi_0\psi^\dagger + \psi^{\dagger 2}\right)\left(\xi_0^2 + 2\xi_0\psi + \psi^2\right) \\
&= U_0\sqrt{n} \int dr \left(\psi^\dagger\psi^2 + \left(\psi^\dagger\right)^2 \psi\right) = U_0\sqrt{n} \int dr\psi^\dagger\psi^2 + \mathsf{H.c.}
\end{aligned}
$$

where only 3rd order terms were taken into account in the last equality.

In general, the lifetime of a given excitation (k) is determined by two processes: decay-coalescence

$$k \leftrightarrow k' + q \tag{E3.25}$$

and absorption-emission

$$k + q \leftrightarrow k'. \tag{E3.26}$$

Later on, we will be interested in process (E3.25) in when k is a high-energy quasi-particle with almost free spectrum and q is a low-energy phonon (q) with linear spectrum.

Due to this two processes the scattering rate can be calculated using *Fermi's golden rule*:

$$
\begin{aligned}
\frac{1}{\tau_0(\mathbf{k})} &= \frac{2\pi}{\hbar} \sum_{\mathbf{q}} \frac{1}{2} \Big[|\langle n_k, n_{k-q}+1, n_q+1|H_{int}|n_k+1\rangle|^2 \, \delta\left(\varepsilon_k - \varepsilon_{k-q} - \varepsilon_q\right) \\
&\quad + |\langle n_{k+q}, n_k+1, n_q+1|H_{int}|n_{k+q}+1\rangle|^2 \, \delta\left(\varepsilon_k + \varepsilon_q - \varepsilon_{k+q}\right) \Big]. \tag{E3.27}
\end{aligned}
$$

(all unchanged occupation numbers are omitted in the states).

The matrix elements are calculated using the Bogoliubov transformation

$$\psi(r) = \sum_k \hat{b}_k u_k(r) - \hat{b}_k^\dagger v_k^*(r),$$

where

$$\begin{pmatrix} u_k \\ v_k \end{pmatrix} = \left(\frac{\hbar^2 k^2/2m + \mu}{\sqrt{\hbar^2 k^2/2m\,(\hbar^2 k^2/2m + 2\mu)}} \pm 1 \right)^{1/2}.$$

Notice, that u_k, v_k are real (see last section 3.1).

And the Bogoliubov spectrum is given by

$$\varepsilon_k^2 = \frac{\hbar^2 \mathbf{k}^2}{2m} \left(\frac{\hbar^2 \mathbf{k}^2}{2m} + 2\mu \right).$$

For $2\mu \gg \frac{\hbar^2 \mathbf{k}^2}{2m}$ (phonons):

$$\varepsilon_q = \hbar|\mathbf{q}|v\,,$$

with the velocity $v = \sqrt{\mu/m}$. We can define a "*Debye wave vector*" by

$$q_D \equiv \frac{mv}{\hbar}\,.$$

We also need the Bose factors

$$\langle n_k \rangle = \frac{1}{e^{\varepsilon_k/T} - 1} \rightarrow \begin{cases} T/\varepsilon_k & ,\ \varepsilon_k \ll T \\ 1 & ,\ \varepsilon_k \gg T \end{cases}.$$

And the Bose operators and states are defined by the standard relations:

$$\left[\hat{b}_q, \hat{b}_k^\dagger\right] = \delta_{q,k}\,,$$

$$\left[\hat{b}_q^{(\dagger)}, \hat{b}_k^{(\dagger)}\right] = 0\,,$$

$$\hat{b}_k^\dagger\left|\ldots, n_k, \ldots\right\rangle = \sqrt{n_k + 1}\left|\ldots, n_k + 1, \ldots\right\rangle\,,$$

$$\hat{b}_k\left|\ldots, n_k > 0, \ldots\right\rangle = \sqrt{n_k}\left|\ldots, n_k - 1, \ldots\right\rangle\,,$$

$$\left\langle\ldots, 0, n_k, 0, \ldots\right|\left.\ldots, 0, n_k', 0, \ldots\right\rangle = \delta_{n_k, n_k'}\,.$$

For (test-) particles $\left(2\mu \ll \varepsilon_k = \frac{\hbar^2 \mathbf{k}^2}{2m} \approx T \ll T_c\right)$ one can use the following approximations:

$$v_k \approx 0\quad,\quad u_k \approx \sqrt{2}\,.$$

Substituting Bogoliubov transforms into $\hat{\mathcal{H}}_{int}$, we get $(U_0 = w)$

$$
\begin{aligned}
\hat{\mathcal{H}}_{int} &= \frac{U_0\sqrt{n}}{V^{3/2}}\int_V dr \sum_{k,k',k''}\left(\hat{b}_k^\dagger u_k^* e^{-ikr} - \hat{b}_k v_k e^{ikr}\right) \\
&\quad \left(\hat{b}_{k'} u_{k'} e^{ik'r} - \hat{b}_{k'}^\dagger v_{k'}^* e^{-ik'r}\right)\left(\hat{b}_{k''} u_{k''} e^{ik''r} - \hat{b}_{k''}^\dagger v_{k''}^* e^{-ik''r}\right) + \text{H.c.}\ (\text{E3.28}) \\
&= U_0\sqrt{n/V}\sum_{k,q}\underbrace{\left(\hat{b}_k^\dagger \hat{b}_q \hat{b}_{k-q}\right)}_{1} u_k u_q u_{k-q} - \underbrace{\left(\hat{b}_k^\dagger \hat{b}_q \hat{b}_{q-k}^\dagger\right)}_{2} u_k u_q v_{q-k}
\end{aligned}
$$

$$-\underbrace{\left(\hat{b}_k^\dagger \hat{b}_q^\dagger \hat{b}_{k+q}\right)}_{3} u_k v_q u_{k+q} + \underbrace{\left(\hat{b}_k^\dagger \hat{b}_q^\dagger \hat{b}_{-k-q}^\dagger\right)}_{4} u_k v_q v_{-k-q}$$

$$-\underbrace{\left(\hat{b}_k \hat{b}_q \hat{b}_{-k-q}\right)}_{5} v_k u_q u_{-k-q} + \underbrace{\left(\hat{b}_k \hat{b}_q \hat{b}_{k+q}^\dagger\right)}_{6} v_k u_q v_{k+q}$$

$$+\underbrace{\left(\hat{b}_k \hat{b}_q^\dagger \hat{b}_{q-k}\right)}_{7} v_k v_q u_{q-k} - \underbrace{\left(\hat{b}_k \hat{b}_q^\dagger \hat{b}_{k-q}^\dagger\right)}_{8} v_k v_q v_{k-q}$$

$$+\underbrace{\left(\hat{b}_k^\dagger \hat{b}_q^\dagger \hat{b}_{k+q}\right)}_{9} u_k u_q u_{k+q} - \underbrace{\left(\hat{b}_k^\dagger \hat{b}_q^\dagger \hat{b}_{-k-q}^\dagger\right)}_{10} u_k u_q v_{-k-q}$$

$$-\underbrace{\left(\hat{b}_k^\dagger \hat{b}_q \hat{b}_{k-q}\right)}_{11} u_k v_q u_{k-q} + \underbrace{\left(\hat{b}_k^\dagger \hat{b}_q \hat{b}_{q-k}^\dagger\right)}_{12} u_k v_q v_{q-k}$$

$$-\underbrace{\left(\hat{b}_k \hat{b}_q^\dagger \hat{b}_{q-k}\right)}_{13} v_k u_q u_{q-k} + \underbrace{\left(\hat{b}_k \hat{b}_q^\dagger \hat{b}_{k-q}^\dagger\right)}_{14} v_k u_q v_{k-q}$$

$$+\underbrace{\left(\hat{b}_k \hat{b}_q \hat{b}_{-k-q}\right)}_{15} v_k v_q u_{-k-q} - \underbrace{\left(\hat{b}_k \hat{b}_q \hat{b}_{k+q}^\dagger\right)}_{16} v_k v_q v_{k+q}\qquad(\text{E3.29})$$

where $\int_V e^{ikr} = V\delta_{k,0}$ is used.

Now we can calculate the matrix element $\langle n_k, n_{k-q} + 1, n_q + 1| H_{int} |n_k + 1\rangle$ and use the convention that k is a particle momentum henceforth.

For this matrix element the only relevant terms of the interaction Hamiltonian are: 2, 3, 8, 9, 12, 14 (which contain two creation and one annihilation operator).

In order to produce the 'bra' state from the 'ket' state, the annihilation and one creation operator in these terms have to be particle operators, therefore — since $v_k = 0$ — only the terms 2, 3, and 9 "survive" due to prefactors.

- Term 2 gives a contribution, if $\tilde{\mathbf{q}} - \tilde{\mathbf{k}} = \mathbf{q}$ and $\tilde{\mathbf{q}} = \mathbf{k}$:

$$-u_{k-q}u_k v_q \sqrt{n_q + 1}\sqrt{n_k + 1}\sqrt{n_{k-q} + 1}$$

- Term 3 gives a contribution, if $\tilde{\mathbf{q}} = \mathbf{q}$ and $\tilde{\mathbf{k}} + \tilde{\mathbf{q}} = \mathbf{k}$:

$$-u_{k-q}v_q u_k \sqrt{n_q + 1}\sqrt{n_k + 1}\sqrt{n_{k-q} + 1}$$

- Term 9 gives a contribution, if $\tilde{\mathbf{k}} + \tilde{\mathbf{q}} = \mathbf{k}$ and $\tilde{\mathbf{k}} = \mathbf{k}$ or $\mathbf{q} = \tilde{\mathbf{k}}$:

$$2u_{k-q}u_q u_k \sqrt{n_q + 1}\sqrt{n_k + 1}\sqrt{n_{k-q} + 1}$$

(the momenta with tilde denote the momenta in the Hamiltonian.)

Therefore the matrix element is given by

$$\langle n_k, n_{k-q} + 1, n_q + 1| H_{int} |n_k + 1\rangle$$
$$= U_0\sqrt{n/V}\, 2u_{k-\tilde{q}}u_k(u_q - v_q)\sqrt{n_q + 1}\sqrt{n_k + 1}\sqrt{n_{k-q} + 1}. \qquad \text{(E3.30)}$$

For one test-particle with $k \gg q$ and $T \gg \varepsilon_q$ this reduces to

$$4U_0\sqrt{n/V}(u_q - v_q)\sqrt{n_q}. \qquad \text{(E3.31)}$$

It follows simply (since the result is real):

$$|\langle n_k, n_{k-q} + 1, n_q + 1| H_{int} |n_k + 1\rangle|^2 \approx 16U_0^2 \frac{n}{V}(u_q - v_q)^2 n_q.$$

The other matrix element follows from the above one, by substituting $\mathbf{k} \to \mathbf{k} + \mathbf{q}$, i.e., it gives the same result for the probability in the golden rule.

Using these results, the scattering rate is given by

$$\frac{1}{\tau_0\,(\mathbf{k})} \approx 16\pi U_0^2 \frac{n}{\hbar V} \sum_{\mathbf{q}} w_q n_q \left[\delta(\varepsilon_k - \varepsilon_{k-q} - \varepsilon_q) + \delta(\varepsilon_k + \varepsilon_q - \varepsilon_{k+q})\right]$$

$$\approx 16\pi U_0^2 n \frac{T}{\hbar} \frac{1}{(2\pi)^d} \int d^d q\, w_q/\varepsilon_q \left[\delta(\varepsilon_k - \varepsilon_{k-q} - \varepsilon_q) + \delta(\varepsilon_k + \varepsilon_q - \varepsilon_{k+q})\right] \quad \text{(E3.32)}$$

with

$$w_q \equiv (u_q - v_q)^2 = \sqrt{2/m}\hbar|\mathbf{q}| \left(\frac{\hbar^2 \mathbf{q}^2}{2m} + 2\mu\right)^{-1/2}.$$

In the last step the factor n_q is replaced by T/ε_q.

This can be simplified to

$$\frac{1}{\tau_0\,(\mathbf{k})} \approx \frac{64\pi}{(2\pi)^d} \frac{U_0^2 nmT}{\hbar^3} \int d^d q\, \left(\mathbf{q}^2 + (2q_D)^2\right)^{-1} \left[\delta(\varepsilon_k - \varepsilon_{k-q} - \varepsilon_q) + \delta(\varepsilon_k + \varepsilon_q - \varepsilon_{k+q})\right].$$

In two dimensions this can be written in polar coordinates as

$$\frac{1}{\tau_0\,(\mathbf{k})} \approx \frac{16}{\pi} \frac{U_0^2 nmT}{\hbar^3} \int dq\, q \left(q^2 + (2q_D)^2\right)^{-1} \times$$

$$\int d\phi \left[\delta(\varepsilon_k - \varepsilon_{k-q} - \varepsilon_q) + \delta(\varepsilon_k + \varepsilon_q - \varepsilon_{k+q})\right].$$

- The first delta function (assumption $\mathbf{k} - \mathbf{q}$ is a "particle" wave vector) demands that

$$\varepsilon_k - \varepsilon_{k-q} - \varepsilon_q = \frac{\hbar^2}{m}|\mathbf{k}|q\cos\phi - \varepsilon_q - \frac{\hbar^2 q^2}{2m}$$

is zero, which results in the condition for the angle ϕ: $\cos\phi = \frac{1}{2|\mathbf{k}|}\left(q + \sqrt{q^2 + (2q_D)^2}\right)$. Since the right-hand side of this inequality is greater than zero it has two solutions if it is smaller than 1. In this case the ϕ-integral gives:

$$\frac{2m}{\hbar^2|\mathbf{k}|q} \sqrt{1 - \left[\frac{1}{2|\mathbf{k}|}\left(q + \sqrt{q^2 + (2q_D)^2}\right)\right]^2}.$$

Since $q_D \ll |\mathbf{k}|$ the complete square-root factor can be neglected for the q-integration, which can then be extended to ∞.

- The second delta function (assumption $\mathbf{k} - \mathbf{q}$ is a "particle" wave vector) demands that

$$\varepsilon_k + \varepsilon_q - \varepsilon_{k+q} = \varepsilon_q - \frac{\hbar^2 q^2}{2m} - \frac{\hbar^2}{m}|\mathbf{k}|q\cos\phi$$

is zero which gives: $\cos\phi = \frac{1}{2|\mathbf{k}|}\left(\sqrt{q^2 + (2q_D)^2} - q\right) \leq q_D/|\mathbf{k}| \ll 1$, which has always two solutions and the ϕ-integral gives:

$$\frac{2m}{\hbar^2|\mathbf{k}|q} \sqrt{1 - \left[\frac{1}{2|\mathbf{k}|}\left(\sqrt{q^2 + (2q_D)^2} - q\right)\right]^2}.$$

The second term under the square-root is always small and can be neglected in the q-integral. Finally, one gets

$$\frac{1}{\tau_0\left(\mathbf{k}\right)} \approx \frac{16}{\pi}\frac{U_0^2 nmT}{\hbar^3}\int\limits_0^\infty dq\,\frac{4m}{\hbar^2|\mathbf{k}|}\left(q^2+(2q_D)^2\right)^{-1} = 16\frac{U_0^2 nm^2 T}{\hbar^5 q_D|\mathbf{k}|}\propto\sqrt{T}\,.$$

3.3 Scattering for Coulomb interaction

The interaction Hamiltonian in third order of ψ is given by

$$\hat{\mathcal{H}}_{\text{int}} = \frac{\sqrt{n}}{2}\int d^2r\,d^d r'\,U(|\mathbf{r}-\mathbf{r}'|) \tag{E3.33}$$

$$\left(\psi^\dagger(\mathbf{r}')\psi(\mathbf{r}')\psi(\mathbf{r})+\psi^\dagger(\mathbf{r})\psi(\mathbf{r}')\psi(\mathbf{r})+\psi^\dagger(\mathbf{r})\psi^\dagger(\mathbf{r}')\psi(\mathbf{r}')+\psi^\dagger(\mathbf{r})\psi^\dagger(\mathbf{r}')\psi(\mathbf{r})\right)$$

and in Fourier representation:

$$\hat{\mathcal{H}}_{\text{int}} = \frac{\sqrt{n}}{2V^2}\int d^2r\,d^d r'\,d^d q\sum_{k,k',k''} e^{\imath\mathbf{q}(\mathbf{r}-\mathbf{r}')}U_q\times \tag{E3.34}$$

$$\Big[(b_k^\dagger e^{-\imath\mathbf{k}\mathbf{r}'}u_k-b_k e^{\imath\mathbf{k}\mathbf{r}'}v_k)(b_{k'}e^{\imath\mathbf{k}'\mathbf{r}'}u_{k'}-b_{k'}^\dagger e^{-\imath\mathbf{k}'\mathbf{r}'}v_{k'})(b_{k''}e^{\imath\mathbf{k}''\mathbf{r}}u_{k''}-b_{k''}^\dagger e^{-\imath\mathbf{k}''\mathbf{r}}v_{k''})+$$

$$(b_k^\dagger e^{-\imath\mathbf{k}\mathbf{r}}u_k-b_k e^{\imath\mathbf{k}\mathbf{r}}v_k)(b_{k'}e^{\imath\mathbf{k}'\mathbf{r}'}u_{k'}-b_{k'}^\dagger e^{-\imath\mathbf{k}'\mathbf{r}'}v_{k'})(b_{k''}e^{\imath\mathbf{k}''\mathbf{r}}u_{k''}-b_{k''}^\dagger e^{-\imath\mathbf{k}''\mathbf{r}}v_{k''})+$$

$$(b_k^\dagger e^{-\imath\mathbf{k}\mathbf{r}}u_k-b_k e^{\imath\mathbf{k}\mathbf{r}}v_k)(b_{k'}^\dagger e^{-\imath\mathbf{k}'\mathbf{r}'}u_{k'}-b_{k'}e^{\imath\mathbf{k}'\mathbf{r}'}v_{k'})(b_{k''}e^{\imath\mathbf{k}''\mathbf{r}'}u_{k''}-b_{k''}^\dagger e^{-\imath\mathbf{k}''\mathbf{r}'}v_{k''})+$$

$$(b_k^\dagger e^{-\imath\mathbf{k}\mathbf{r}}u_k-b_k e^{\imath\mathbf{k}\mathbf{r}}v_k)(b_{k'}^\dagger e^{-\imath\mathbf{k}'\mathbf{r}'}u_{k'}-b_{k'}e^{\imath\mathbf{k}'\mathbf{r}'}v_{k'})(b_{k''}e^{\imath\mathbf{k}''\mathbf{r}}u_{k''}-b_{k''}^\dagger e^{-\imath\mathbf{k}''\mathbf{r}}v_{k''})\Big],$$

i.e., integrating over r and r' gives two δ-functions and hence an additional Fourier factor U_k — compared to the short-range case — appears in the momentum summation

Again, only terms of the form 2, 3, and 9 (as written for the short-range case) give contributions to the matrix elements:

- Term 2 type terms give:

$$-(U_{\tilde{k}-\tilde{q}}+U_{\tilde{q}})/2\,u_{\tilde{k}-\tilde{q}}u_{\tilde{k}}v_{\tilde{q}}\sqrt{n_{\tilde{q}}+1}\sqrt{n_{\tilde{k}}+1}\sqrt{n_{\tilde{k}-\tilde{q}}+1}$$

- Term 3 type terms give:

$$-(U_{\tilde{k}+\tilde{q}}+U_{\tilde{q}})/2\,u_{\tilde{k}-\tilde{q}}v_{\tilde{q}}u_{\tilde{k}}\sqrt{n_{\tilde{q}}+1}\sqrt{n_{\tilde{k}}+1}\sqrt{n_{\tilde{k}-\tilde{q}}+1}$$

- Term 9 type terms give:

$$(U_{\tilde{k}}+U_{\tilde{q}})u_{\tilde{k}-\tilde{q}}u_{\tilde{q}}u_{\tilde{k}}\sqrt{n_{\tilde{q}}+1}\sqrt{n_{\tilde{k}}+1}\sqrt{n_{\tilde{k}-\tilde{q}}+1}$$

Again, $u_k \approx \sqrt{2}$ can be used for quasi particles and the occupation numbers for particle can be set to 1. Since the Fourier components decay as k^{-2} for $k \to \infty$ the U_k's with particle waves vectors can be neglected, hence

$$\left\langle n_{\tilde{k}}, n_{\tilde{k}-\tilde{q}} + 1, n_{\tilde{q}} + 1 \right| H_{int} \left| n_{\tilde{k}} + 1 \right\rangle$$

$$\approx 2 U_{\tilde{q}} \sqrt{n/V} (u_{\tilde{q}} - v_{\tilde{q}}) \sqrt{n_{\tilde{q}}} \,. \tag{E3.35}$$

The scattering rate is then calculated analogous to the δ-interaction case, using the same approximations for the angle integration, and one obtains

$$\frac{1}{\tau_0(\mathbf{k})} \approx 8 \frac{U_0^2 n m^2 T}{\pi |\mathbf{k}| \hbar^5} \int_0^\infty \left(\frac{U_q}{U_0}\right)^2 \frac{q^2 dq}{q^4 + q_0^4} \propto \sqrt{T} \,, \tag{E3.36}$$

with $q_0^4 \equiv 4 U_0 m n (a\hbar)^{-2}$.

3.4 Influence of a trapping potential

Here, we briefly consider the influence of a trapping potential on the equations for u_k and v_k. These can be rewritten as (for a δ-potential and $\mu \approx U_0 |\xi_0|^2$):

$$(\hat{D} + \mu) u_k(\mathbf{r}) - \mu v_k(\mathbf{r}) = \varepsilon_k u_k(\mathbf{r}) \,, \tag{E3.37}$$

$$(\hat{D} + \mu) v_k(\mathbf{r}) - \mu u_k(\mathbf{r}) = -\varepsilon_k v_k(\mathbf{r}) \,. \tag{E3.38}$$

Introducing $f_k(\mathbf{r}) \equiv u_k(\mathbf{r}) + v_k(\mathbf{r})$ and $g_k(\mathbf{r}) \equiv u_k(\mathbf{r}) - v_k(\mathbf{r})$ one gets

$$\hat{D} f_k(\mathbf{r}) = \varepsilon_k g_k(\mathbf{r}) \,, \tag{E3.39}$$

$$(\hat{D} + 2\mu) g_k(\mathbf{r}) = \varepsilon_k f_k(\mathbf{r}) \,, \tag{E3.40}$$

with the differential operator

$$\hat{D} \equiv -\frac{\hbar^2}{2m} \nabla^2 + V_{ex}(\mathbf{r}) = \sum_i \hat{D}_i \,, \quad \hat{D}_i = -\frac{\hbar^2 \partial_{x_i}^2}{2m} + \frac{m}{2} \omega_i^2 x_i^2 \,. \tag{E3.41}$$

A solution in the Thomas-Fermi regime $\mu \gg \hbar \omega_i$ is given in [ÖST$^+$97]. In order to see the crossover to lower dimensions, one (for quasi-2D condensates) or two (for quasi-1D, cigar shape condensates) trap frequencies have to go to ∞ such that the Thomas-Fermi result is not applicable. The full solution − unfortunately very non-trivial − in the limit $\omega_1 \to \infty$ and $\omega_2 = \omega_3 = 0$ (should) reduce to the 2D result of the previous section.

3.5 Symbol reference

Table EIII: List of symbols used in chapter D

symbol	definition
a	scattering length
$\hat{b}_k$, $\hat{b}_k^\dagger$	boson annihilation and creation operators
g	$= \frac{U_0 m/\hbar^2}{1+U_0 m/\hbar^2 \ln(na^2)^{-1}}$
$\hat{\mathcal{H}}$	Hamiltonian
$\hat{\mathcal{H}}_{\text{int}}$	interaction part of the Hamiltonian
K_0	modified Bessel function of second kind
n	boson concentration
n_k	occupation numbers
m	boson mass
q_D	"Debye wave vector"
q_0	$= (4U_0 nm(a\hbar)^{-2})^{1/4}$
T	temperature
T_c	BEC transition temperature
$U(r)$, U_k	interaction potential and Fourier components
U_0	interaction strength
u_k, v_k	Bogoliubov functions
$v = \sqrt{\mu/m}$	phonon velocity
V	volume
$V_{ex}(r)$	trapping potential
ϵ_k	Bogoliubov spectrum
κ	thermal conductivity
μ	chemical potential
ν	$= 380$
ρ, ρ_0	DOS, for free particles
$\tau_0(k)$	scatting time of over condensate particles
$\tau_\epsilon(k)$	energy relaxation time of over condensate particles
$\tau_{\text{tr}}(k)$	transport time of over condensate particles
Ψ	complete wave function
ψ	over-condensate wave function

Bibliography

[AA85]   B.L. Altshuler and A.G. Aronov. *Electron-Electron Interaction in Disordered Conductors*, volume 10 of *Modern Problems in Condensed Matter Science*, page 1. North-Holland, Amsterdam, 1985.

[AAK82]   B.L. Altshuler, A.G. Aronov, and D.E. Khmelnitsky. *J. Phys.: Condens. Matter*, 15:7367, 1982.

[ABG+02]   V. V. Afonin, J. Bergli, Y. M. Galperin, V. L. Gurevich, and V. I. Kozub. *Phys. Rev. B*, 66:165326, 2002.

[ABM95]   A. Arneodo, E. Bacry, and J.F. Muzy. *Physica A*, 213:232, 1995.

[ADJ+97]   J.-O. Andersson, C. Djurberg, T. Jonsson, P. Svedlindh, and P. Nordblad. *Phys. Rev. B*, 56:13983, 1997.

[AGG85]   V.V. Afonin, Y.M. Glaperin, and V.L. Gurevich. *Sov. Phys. JETP*, 61:1130, 1985.

[BA02]   A. Arneodo B. Audit, J.F. Muzy. *IEEE Trans. Information Theory*, 48:2938, 2002.

[BCT99]   Massimo Boninsegni, Milton W. Cole, and Flavio Toigo. *Phys. Rev. Lett.*, 83:2002, 1999.

[BD84]   R. M. Bradley and S. Doniach. *Phys. Rev. B*, 30:1138, 1984.

[BDP+93]   J.D. Brock, D.A. DiCarlo, W.J. Prdulka, N. Sutton, E. Sweetland, and R.E. Thorne. *J. Phys. IV France*, 3:115, 1993.

[BFG+94]   G. Blatter, M. V. Feigel'man, V. B. Geshkenbein, A. I. Larkin, and V. M. Vinokur. *Rev. Mod. Phys.*, 66:1125, 1994.

[BK94]   D. Belitz and T. R. Kirkpatrick. *Rev. Mod. Phys.*, 66:261, 1994.

[BKR+00]   S. Brazovskii, N. Kirova, H. Requardt, F. Ya. Nad, P. Monceau, R. Currat, J. E. Lorenzo, G. Grübel, and Ch. Vettier. *Phys. Rev. B*, 61:10640, 2000.

[BM91]   S. Brazovskii and S. Matveenko. *J. Phys. I (France)*, 1:269, 1991.

[BM99]   S. Brazovski and P. Monceau, editors. *Proceedings of the Internationa Workshop on Electronic Crystals ECRYS 99*, volume 9 of *Journal de Physique IV Proceedings*. Societe Francaise de Physique, 1999.

[BN04]   Serguei Brazovskii and Thomas Nattermann. *Adv. Phys.*, 53:177, 2004.

[Bro63]   W. F. Brown, Jr. *Phys. Rev.*, 130:1677, 1963.

[BS95]   Leon Balents and Steven H. Simon. *Phys. Rev. B*, 51:15610, 1995.

[BSRK85]   S. Bhattacharya, J. P. Stokes, Mark O. Robbins, and R. A. Klemm. *Phys. Rev. Lett.*, 54:2453, 1985.

[BTW87]   Per Bak, Chao Tang, and Kurt Wiesenfeld. *Phys. Rev. Lett.*, 59:381, 1987.

[CC41]   K. S. Cole and R. H. Cole. *J. Chem. Phys.*, 9:341, 1941.

[CDW01]   Pascal Chauve, Pierre Le Doussal, and Kay Jrg Wiese. *Phys. Rev. Lett.*, 86:1785, 2001.

[CHN88]   Sudip Chakravarty, Bertrand I. Halperin, and David R. Nelson. *Phys. Rev. Lett.*, 60:1057, 1988.

[CHN89]   Sudip Chakravarty, Bertrand I. Halperin, and David R. Nelson. *Phys. Rev. B*, 39:2344, 1989.

[CO82]   John L. Cardy and S. Ostlund. *Phys. Rev. B*, 25:6899, 1982.

[CSK$^+$02]   X. Chen, O. Sichelschmidt, W. Kleemann, O. Petracic, Ch. Binek, J. B. Sousa, S . Cardoso, and P. P. Freitas. *Phys. Rev. Lett.*, 89:137203, 2002.

[CTYC98]   Gabor A. Csathy, Daryl Tulimieri, Jongsoo Yoon, and Moses H. W. Chan. *Phys. Rev. Lett.*, 80:4482, 1998.

[Das02]   Kunal K. Das. *Phys. Rev. A*, 66:053612, 2002.

[Dav70]   H. A. David. *Order Statistics*. John Wiley & Sons, Inc., 1970.

[DFT97]   J. L. Dormann, D. Fiorani, and E.J. Tronc. *Adv. Chem. Phys.*, 98:283, 1997.

[DGPS99]   Franco Dalfovo, Stefano Giorgini, Lev P. Pitaevskii, and Sandro Stringari. *Rev. Mod. Phys.*, 71:463, 1999.

[DW03]   Pierre Le Doussal and Kay Jörg Wiese. *Phys. Rev. E*, 68:046118, 2003.

[DWC02]   Pierre Le Doussal, Kay Jörg Wiese, and Pascal Chauve. *Phys. Rev. B*, 66:174201, 2002.

[EG86]   U. Eckern and A. Geier. *Z. Phys. B*, 65:15, 1986.

[EK94]   Deniz Ertas and Mehran Kardar. *Phys. Rev. E*, 49:R2532, 1994.

[EW82]   S. F. Edwards and D.R. Wilkinson. *Proc. R. Soc. London Ser. A*, 381:17, 1982.

[Fei80]   M. Feigelman. *Sov. Phys. JETP*, 52:555, 1980.

[Fei83]   M.V. Feigel'man. *Sov. Phys. JETP*, 58:1076, 1983.

[Fet72]   A.L. Fetter. *Ann. Phys.*, 70:67, 1972.

[FG88]   Matthew P. A. Fisher and G. Grinstein. *Phys. Rev. Lett.*, 60:208, 1988.

[FGI93]   M. V. Feigelman, V. B. Geshkenbein, and L. B. Ioffe. *Phys. Rev. B*, 48:16641, 1993.

[FH88]   Daniel S. Fisher and P. C. Hohenberg. *Phys. Rev. B*, 37:4936, 1988.

[Fis83]   Daniel S. Fisher. *Phys. Rev. Lett.*, 50:1486, 1983.

[Fis86]   Daniel S. Fisher. *Phys. Rev. Lett.*, 56:1964, 1986.

[Fis98]   D.S. Fisher. *Phys. Rep.*, 301:113, 1998.

[FL78]   H. Fukuyama and P. A. Lee. *Phys. Rev. B*, 17:535, 1978.

[Fuk84]   H. Fukuyama. *Lect. Notes Phys.*, 217:487, 1984.

[FZR$^+$98] Dan T. Fuchs, Eli Zeldov, Michael Rappaport, Tsuyoshi Tamegai, Shuuichi Ooi, and Hadas Shtrikman. *Nature*, 391:373, 1998.

[GDO01]   T. Giamarchi, P. Le Doussal, and E. Orignac. *Phys. Rev. B*, 64:245119, 2001.

[Gia03]   Thierry Giamarchi. *Quantum Physics in One Dimension*, volume 121 of *The International Series of Monigraphs on Physics*. Oxford Press, Oxford, 2003.

[GKL01]   A. Glatz, S. Kumar, and M.S. Li. *Phys. Rev. B*, 64:184301, 2001.

[Gla03]   Andreas Glatz. *cond-mat*, 0:0302133, 2003.

[GN02a]   A. Glatz and T. Nattermann. *Phys. Rev. Lett.*, 88:256401, 2002.

[GN02b]   A. Glatz and T. Nattermann. *J. Phys. IV France*, 12:125, 2002.

[GN04a]   Andreas Glatz and Thomas Nattermann. *Phys. Rev. B*, 69:115118, 2004.

[GN04b]   Andreas Glatz and Thomas Nattermann. *Phys. Rev. Lett.*, 92:257205, 2004.

[GNP02]   A. Glatz, T. Nattermann, and V. Pokrovsky. *J. Phys. IV France*, 12:275, 2002.

[GNP03]   A. Glatz, T. Nattermann, and V. Pokrovsky. *Phys. Rev. Lett.*, 90:047201, 2003.

[Gor77]   L.P. Gorkov. *JETP Lett.*, 25:358, 1977.

[GP00]   J. L. García-Palacios. *Adv. Chem. Phys.*, 112:1, 2000.

[Gra98]   Robert Graham. *Phys. Rev. Lett.*, 81:5262, 1998.

[Grü88]   G. Grüner. *Rev. Mod. Phys.*, 60:1129, 1988.

[Grü94a]   G. Grüner. *Rev. Mod. Phys.*, 66:1, 1994.

[Grü94b]   George Grüner. *Density Waves in Solids*, volume 89 of *Frontiers in Physics*. Addison-Wesley, 1994.

[GS87]   T. Giamarchi and H.J. Schultz. *Europhys. Lett.*, 3:1287, 1987.

[GS88]   T. Giamarchi and H. J. Schulz. *Phys. Rev. B*, 37:325, 1988.

[GS89]   T. Giamarchi and H. J. Schulz. *Phys. Rev. B*, 39:4620, 1989.

[Hal81]   F. D. M. Haldane. *Phys. Rev. Lett.*, 47:1840, 1981.

[Han88]   P.H. Handel. *J. Phys.: Condens. Matter*, 21:2435, 1988.

[Her98]   Igor F. Herbut. *Phys. Rev. B*, 58:971, 1998.

[HHF85]   David A. Huse, Christopher L. Henley, and Daniel S. Fisher. *Phys. Rev. Lett.*, 55:2924, 1985.

[Hoo76]   F.N. Hooge. *Physica B*, 83:14, 1976.

[IkM75]   Yoseph Imry and Shang keng Ma. *Phys. Rev. Lett.*, 35:1399, 1975.

[IV87]   L.B. Ioffe and V.M. Vinokur. *J. Phys.: Condens. Matter*, 20:6149, 1987.

[JKKN77]   Jorge V. Jose, Leo P. Kadanoff, Scott Kirkpatrick, and David R. Nelson. *Phys. Rev. B*, 16:1217, 1977.

[JMA94]   E. Bacry J.F. Muzy and A. Arneodo. *Int. J. of Bifurcation and Chaos*, 4:245, 1994.

[Jon83]   A. K. Jonscher. *Dielectric Relaxation in Solids*. Chelsea Dielectrics Press, London, 1983.

[Kar98]   Mehran Kardar. *Phys. Rep.*, 301:85, 1998.

[KdO80]   H.J.F. Knops and L.W.J. den Ouden. *Physica A*, 103:597, 1980.

[Ket99]   W. Ketterle. *Phys. Today*, 52:30, 1999.

[Kis88]   L.B. Kiss. *Rev. Solid State Science*, 2:569, 1988.

[Kog96]   Sh. Kogan. *Electronic noise and fluctuations in solids*. Cambridge University Press, 1996.

[Kor89]   S.E. Korshunov. *Sov. Phys. JETP*, 68:609, 1989.

[KPB⁺01]   W. Kleemann, O. Petracic, Ch. Binek, G. N. Kakazei, Yu. G. Pogorelov, J. B. Sousa, S. Cardoso, and P. P. Freitas. *Phys. Rev. B*, 63:134423, 2001.

[KPS01]   V. A. Kashurnikov, N. V. Prokof'ev, and B. V. Svistunov. *Phys. Rev. Lett.*, 87:120402, 2001.

[KT73]   J.M. Kosterlitz and D.J. Thouless. *J. Phys.: Condens. Matter*, 6:1181, 1973.

[Len61]   A. Lenard. *J. Math. Phys.*, 2:682, 1961.

[LF78]   P. A. Lee and H. Fukuyama. *Phys. Rev. B*, 17:542, 1978.

[LFC⁺97]   S. Lemerle, J. Ferré, C. Chappert, V. Mathet, T. Giamarchi, and P. Le Doussal. *Phys. Rev. Lett.*, 80:849, 1997.

[LFC⁺98]   S. Lemerle, J. Ferre, C. Chappert, V. Mathet, T. Giamarchi, and P. Le Doussal. *Phys. Rev. Lett.*, 80:849, 1998.

[LNP99]   Igor F. Lyuksyutov, Thomas Nattermann, and Valery Pokrovsky. *Phys. Rev. B*, 59:4260, 1999.

[LNST97]   H. Leschhorn, T. Nattermann, S. Stepanow, and L.-H. Tang. *Ann. Phys. (Leipzip)*, 6:1, 1997.

[LOCT01]   S. G. Lemay, K. O'Neill, C. Cicak, and R. E. Thorne. *Phys. Rev. B*, 63:081102, 2001.

[LR85]   Patrick A. Lee and T. V. Ramakrishnan. *Rev. Mod. Phys.*, 57:287, 1985.

[LV02]   A. V. Lopatin and V. M. Vinokur. *Phys. Rev. Lett.*, 88:235503, 2002.

[Mak95]   K. Maki. *Phys. Lett. A*, 202:313, 1995.

[MF93]   A. Alan Middleton and Daniel S. Fisher. *Phys. Rev. B*, 47:3530, 1993.

[MG95]   H. Maurey and T. Giamarchi. *Phys. Rev. B*, 51:10833, 1995.

[MHKZ89]   Ernesto Medina, Terence Hwa, Mehran Kardar, and Yi-Cheng Zhang. *Phys. Rev. A*, 39:3053, 1989.

[Mid92]   A. Alan Middleton. *Phys. Rev. Lett.*, 68:670, 1992.

[Mil02]   Edoardo Milotti. *physics*, 0:0204033, 2002.

[MNR04]   Sergey V. Malinin, Thomas Nattermann, and Bernd Rosenow. *cond-mat*, 0:0403651, 2004.

[MT86a]   H. Matsukawa and H. Takayama. *Physica B*, 143:80, 1986.

[MT86b]   L. Mihaly and G. X. Tessema. *Phys. Rev. B*, 33:5858, 1986.

[MWA$^+$98] V. Metlushko, U. Welp, I. Aranson, S. Scheidl, V. M. Vinokur, G. W. Crabtree, K. Rogacki, and B. Dabrowski. *cond-mat*, 0:9804121, 1998.

[Myd93]   J.A. Mydosh. *Spin Glasses : An Experimental Introduction*. Taylor and Francis, London, 1993.

[Nat87]   T. Nattermann. *Europhys. Lett.*, 4:1241, 1987.

[Nat90]   Thomas Nattermann. *Phys. Rev. Lett.*, 64:2454, 1990.

[Née49]   L. Néel. *Ann. Geophys.*, 5:99, 1949.

[Nel88]   David R. Nelson. *Phys. Rev. Lett.*, 60:1973, 1988.

[NF92a]   Onuttom Narayan and Daniel S. Fisher. *Phys. Rev. Lett.*, 68:3615, 1992.

[NF92b]   Onuttom Narayan and Daniel S. Fisher. *Phys. Rev. B*, 46:11520, 1992.

[NF93]   Onuttom Narayan and Daniel S. Fisher. *Phys. Rev. B*, 48:7030, 1993.

[NGD03]   Thomas Nattermann, Thierry Giamarchi, and Pierre Le Doussal. *Phys. Rev. Lett.*, 91:056603, 2003.

[NPV01a]   T. Nattermann, V. Pokrovsky, and V. M. Vinokur. *Phys. Rev. Lett.*, 87:197005, 2001.

[NPV01b]   T. Nattermann, V. Pokrovsky, and V. M. Vinokur. *Phys. Rev. Lett*, 87:197005, 2001.

[NS00]   Thomas Nattermann and Stefan Scheidl. *Adv. Phys.*, 49:607, 2000.

[NSKL95]   T. Nattermann, S. Scheidl, S.E. Korshunov, and M.S. Li. *J. Phys. I (France)*, 5:565, 1995.

[NSTL92]   T. Nattermann, S. Stepanow, L.-H. Tang, and H. Leschhorn. *J. Phys. II (France)*, 2:1483, 1992.

[NSV90a]   T. Nattermann, Y. Shapir, and I. Vilfan. *Phys. Rev. B*, 42:8577, 1990.

[NSV90b]   T. Nattermann, Y. Shapir, and I. Vilfan. *Phys. Rev. B*, 42:8577, 1990.

[NV93]   David R. Nelson and V. M. Vinokur. *Phys. Rev. B*, 48:13060, 1993.

[ÖST$^+$97]   P. Öhberg, E. L. Surkov, I. Tittonen, S. Stenholm, M. Wilkens, and G. V. Shlyapnikov. *Phys. Rev. A*, 56:R3346, 1997.

[PCS$^+$04a] O. Petracic, X. Chen, O. Sichelschmidt, Ch. Binek, W. Kleemann, A. Glatz, T. Nattermann, S. Cardoso, and P. P. Freitas. *J. Magn. Magn. Mater.*, 2004. in press.

[PCS$^+$04b] O. Petracic, X. Chen, O. Sichelschmidt, Ch. Binek, W. Kleemann, A. Glatz, T. Nattermann, S. Cardoso, and P. P. Freitas. *J. Mag. Magn. Mat.*, 272:E1201, 2004.

[PGK04]   O. Petracic, A. Glatz, and W. Kleemann. *cond-mat*, 0:0406590, 2004.

[PHS00]   D. S. Petrov, M. Holzmann, and G. V. Shlyapnikov. *Phys. Rev. Lett.*, 84:2551, 2000.

[PSB$^+$03]   O. Petracic, S. Sahoo, Ch. Binek, W. Kleemann, J. B. Sousa, S. Cardoso, and P. P. Freitas. *Phase Transit.*, 76:367, 2003.

[RD96]   Scot R. Renn and Ji-Min Duan. *Phys. Rev. Lett.*, 76:3400, 1996.

[REDG89]   M. A. Rubio, C. A. Edwards, A. Dougherty, and J. P. Gollub. *Phys. Rev. Lett.*, 63:1685, 1989.

[RFMLDB02] I. Ruiz-Feal, T. A. Moore, L. Lopez-Diaz, and J. A. C. Bland. *Phys. Rev. B*, 65:054409, 2002.

[RHL$^+$99]   L. Roters, A. Hucht, S. Luebeck, U. Nowak, and K. D. Usadel. *Phys. Rev. E*, 60:5202, 1999.

[RKM$^+$86]   W. Reim, R. H. Koch, A. P. Malozemoff, M. B. Ketchen, and H. Maletta. *Phys. Rev. Lett.*, 57:905, 1986.

[RMAE92]   Satish Ramakrishna, Michael P. Maher, Vinay Ambegaokar, and Ulrich Eckern. *Phys. Rev. Lett.*, 68:2066, 1992.

[RMPR82]   J. Richard, P. Monceau, M. Papoular, and M. Renard. *J. Phys.: Condens. Matter*, 15:7157, 1982.

[Sac99]   Subir Sachdev. *Quantum Phase Transitions*. Cambridge University Press, 1999.

144

[Sch93]   H. J. Schulz. *Phys. Rev. Lett.*, 71:1864, 1993.

[SDM01]   J.P. Sethna, K.A. Dahmen, and C.R. Myers. *Nature*, 410:242, 2001.

[SF01]   J. M. Schwarz and Daniel S. Fisher. *Phys. Rev. Lett.*, 87:096107, 2001.

[SGL04a]   Z. R. Struzik, A. Glatz, and M. S. Li. *Europhys. Lett.*, 66:385, 2004.

[SGL04b]   Zbigniew R. Struzik, Andreas Glatz, and Mai S. Li. Search for flicker noise in one-dimensional charge density wave systems. In Dragana Popovic, Michael B. Weissman, and Zoltan A. Racz, editors, *Proceedings of SPIE: Fluctuations and Noise in Materials*, volume 5469, page 328, 2004.

[Sha90]   R. Shankar. *Int. J. Phys. B*, 4:2371, 1990.

[SK74]   P. Szepfalusy and I. Kondor. *Ann. Phys.*, 82:1, 1974.

[SVBO88]   U. Schultz, J. Villain, E. Brezinand, and H. Orland. *J. Stat. Phys.*, 51:1, 1988.

[SVY$^+$98] A. I. Safonov, S. A. Vasilyev, I. S. Yasnikov, I. I. Lukashevich, and S. Jaakkola. *Phys. Rev. Lett.*, 81:4545, 1998.

[SYF93]   Lindsay M. Steele, Charles J. Yeager, and Daniele Finotello. *Phys. Rev. Lett.*, 71:3673, 1993.

[Tho96]   R.E. Thorne. *Phys. Today*, 49:42, 1996.

[TS01]   Y. Tomio and Y. Suzumura. *J. Phys. Soc. Jap.*, 70:2884, 2001.

[VF84]   J. Villain and J.F. Fernandez. *Z. Phys. B*, 54:139, 1984.

[Voi94]   Johannes Voit. *Rep. Prog. Phys.*, 58:977, 1994.

[Vos79]   *Proceedings of the 33rd Annual Symposium on Frequency Control, Atlantic City, NJ*. Electronic Industries Association, Washington, 1979.

[WE97]   C. R. Werner and U. Eckern. *Ann. Phys. (Leipzip)*, 6:595, 1997.

[WK73]   K.G. Wilson and J. Kogut. *Phys. Rep.*, 12:75, 1973.

[You99]   P.A. Young, editor. *Spin Glasses and Random Fields*, volume 12 of *Series on Directions in Condensed Matter Physics*. World Scientific Publishing Co., Singapore, 1999.

[ZGvOZ97]   Andrei D. Zaikin, Dmitrii S. Golubev, Anne van Otterlo, and Gergely T. Zimanyi. *Phys. Rev. Lett.*, 78:1552, 1997.

[ZNG99]   E. Zaremba, T. Nikuni, and A. Griffin. *J. Low Temp. Phys.*, 116:277, 1999.

[ZZ93]   S. V. Zaitsev-Zotov. *Phys. Rev. Lett.*, 71:605, 1993.

[ZZ94]   S. V. Zaitsev-Zotov. *Phys. Rev. Lett.*, 72:587, 1994.

[ZZRM97a]   S. V. Zaitsev-Zotov, G. Remenyi, and P. Monceau. *Phys. Rev. B*, 56:6388, 1997.

[ZZRM97b]   S. V. Zaitsev-Zotov, G. Remenyi, and P. Monceau. *Phys. Rev. Lett.*, 78:1098, 1997.

Acknowledgements

mein Dank gilt:

- ⊛ vor allem dem Betreuer dieser Arbeit Prof. Thomas Nattermann,

- ⊛ und auch Valerii Vinokur, der mich während meines Aufenthalts in Argonne betreut hat,

- ⊛ Prof. Valery Pokrovsky, mit dem ich in Köln und in College Station (Texas) zusammenarbeiten durfte,

- ⊛ Prof. Dmitrii Maslov,

- ⊛ Stefan Scheidl, Bernd Rosenow, Thorsten Emig und Simon Bogner für viele Diskussionen und guten Ratschläge,

- ⊛ ebenso Igor Beloborodov, meinem Zimmernachbarn in Argonne,

- ⊛ Prof. Wolfgang Kleemann und Oleg Petracic für die Diskussionen zu Experimenten an magnetischen Systemen,

- ⊛ Mai Suan Li und Zbigniev Struzik für die gute Zusammenarbeit - auch über weite Distanzen (Chicago - Warschau - Tokyo - Köln),

- ⊛ den übrigen Kollegen in der Arbeitsgruppe und Zimmergenossen, Frank, Christoph, Philipp und Rauno,

- ⊛ und auch den Kollegen und Freunden in Argonne: Andrei, Andreas, Alex, Helmut, Vitalii, Galina, Katya und Anja,

- ⊛ und natürlich meinen Eltern, die mich während meines Studiums immer unterstützt haben.

Zusammenfassung

In der vorliegenden Arbeit werden ungeordnete elastische Systeme im quanten- und klassischen Regime, sowie deren dynamische Eigenschaften untersucht. Die Arbeit besteht aus zwei Hauptteilen:

Im ersten Teil untersuchen wir das Phasendiagramm von schwach ungeordneten Systemen bei tiefen Temperaturen. Als Methode wird dabei ein Renormierungsgruppenverfahren benutzt, welches den Einfluss von thermischen Fluktuationen voll mit berücksichtigt. Die Resultate können z.B. auf Ladungsdichtewelllen oder Luttinger Flüssigkeiten angewendet werden. In der klassischen Region des Phasendiagramms, d.h. dort, wo Quantenfluktuationen irrelevant sind, haben wir das Modell für starke Unordung exakt gelöst und den Grundzustand sowie die Korrelationsfunktion gefunden. Weiterhin haben wir für hohe Temperaturen (im klassischen Bereich) das Problem auf eine Burgers Gleichung mit Unordnung abgebildet und so die Korrelationslänge bestimmt. Im Fall $T = 0$ konnten wir den Phasenübergang zwischen einer gepinnten (oder lokalisierten) Phase bei schwachen Quantenfluktuationen und einer nicht gepinnten (delokalisierten) Phase bei starken Quantenfluktuationen reproduzierten, welcher schon von Fukuyama oder Giamarchi und Schulz untersucht worden ist.

Bei endlichen Temperaturen wird dieser Lokalisierungs-Phasenübergang unterdrückt, d.h., dass das Unordungspotential durch thermische Fluktuationen ausgewaschen wird, sobald man auf Längenskalen größer der thermischen de Broglie Wellenlänge ist. Die Residuen des Phasenübergangs werden dabei in dem Zurückbleiben eines reichhaltigen Crossover-Diagramms widergespiegelt. In diesem Crossover-Diagramm finden wir vier verschiedene Skalenbereiche: ein klassisch ungeordenten, einen quanten ungeordneten, einen quantenkritischen und einen thermischen Bereich. Die Resultate können direkt auf ungeordnete Supraflüssigkeiten angewendet werden. Anschließend wird das Renormierungsverfahren noch auf die Behandung eines kommensurablen Gitterpotentials, und im Falle von Ladungsdichtewellen auf den Einfluss von Quanten-phase-slips erweitert. Diese beiden Effekte führen zu einem neuen Szenario für den Lokalisierungsübergang bei $T = 0$.

Zusätzlich analysieren wir das Rauschspektrum des Stromes in einem klassischen Ladungsdichtewellensystem. Dazu lösen wir die überdämpfte Bewegungsgleichung numerisch. Bei tiefen Temperaturen, gerade überhalb des Depinningübergangs, zeigt das Spektrum ein $1/f$ Verhalten, was auch *Funkelrauschen* (flicker noise) genannt wird. Die Resultate stimmen gut mit experimentellen Messungen an quasi-eindimensionalen Ladungsdichtewellensystemen überein.

Im zweiten Teil untersuchen wir das Verhalten einer elastischen Interface, welche durch ein oszillierendes externes Feld getrieben wird. Die mittlere Geschwindigkeit zeigt dabei ein hysteretisches Verhalten, so dass der Depinningübergang im Fall der adiabatisch, mit konstantem Feld getriebenen

Interface, aufgeweicht wird. Die Geschwindigkeitsausdehnung dieser Hysteresekurve wird dabei durch eine neue Längenskala, welche durch die Frequenz des angelegten Feldes und - im Falle von kleinen Frequenzen - von den kritischen Exponenten des Depinningüberganges festgelegt wird. Mit Hilfe von Skalenargumenten und einer perturbativen Renormierungsgruppenanalyse leiten wir ein Potenzverhalten der Geschwindigkeit, als Funktion der Amplitude und Frequenz her, welches numerisch bestätigt wird. Thermische Fluktuationen führen zu einer zusätzlichen Aufweichung des Depinningverhaltens. Wenn die Amplitude des externen Feldes kleiner als das Depinningfeld ist, muss bei der Bewegung des Inferace auch das Auftreten von Lawinen mitberücksichtigt werden, um die Geschwindigkeitshysterese zu erklären.

Um die Gültigkeit unseres Modells im Vergleich mit Experimenten zu überprüfen, bestimmen wir die komplexe Suszeptibilität mit Hilfe eines adiabatischen und eines nicht-adiabatischen Zugangs numerisch für endliche Systeme und vergleichen sie mit Messungen an dem superferromagnetischen, granularen Vielschichtsystem $[\text{Co}_{80}\text{Fe}_{20}(1.4\text{nm})/\text{Al}_2\text{O}_3(3\text{nm})]_{10}$. Als Resultat finden wir, dass das Modell für oszillierend getriebene Domänenwände die Haupteigenschaften des Experimentes beschreibt.

Im letzten Abschnitt dieses Teils untersuchen wir noch den Einfluss von starken Oberflächenpotentialen auf die Bewegung von elastischen Systemen. Wenn das Oberflächenpotential das Depinning vollständig verhindert, zeigt die Krümmung des ausgebildeten parabolischen Profils eine ausgeprägte rhombische Hysterese, deren Breite zweimal dem Depinning Feld des Systems entspricht. Diese Hysterese verschwindet bei endlichen Temperaturen, wenn die angelegt Kraft adiabatische geändert wird. Im Falle eines Depinnings des Oberflächenpotentials durch die angelegte Kraft oder thermisches Kriechen wird die Krümming des Profils mit steigender Geschwindigkeit verringert. Die Resultate können z.B. auf getriebene magnetische Domänenwände, Flussliniengitter oder Ladungsdichtewellen angewendet werden.

Als Zusatz studieren wir niedrigdimensionale wecheselwirkenden – aber, im Gegensatz zu den vorherigen beiden Hauptteilen, saubere – Bose Systeme bei tiefen Temperaturen. Die Wechselwirkung führt im allgemeinen zu Streuprozessen zwischen den Überkondensat-Teilchen, für welche wir die Streuzeiten mit Hilfe von *Fermis* goldener Regel berechnen können. Damit kann dann die thermische Leitfähigkeit und schwache Loklisierungskorrekturen bestimmt werden. Dieses wird für kurz- und langreichweitige Wechselwirkungen getan. Da ein d-dimensionales Bose System auf ein $(d+1)$-dimensionales Vortexgitter abgebildet werden kann, können die Resultate z.B. zu einer Versteifung des Flussliniengitters führen.

Erklärung

Ich versichere, dass ich die von mir vorgelegte Dissertation selbständig angefertigt, die benutzten Quellen und Hilfsmittel vollständig angegeben und die Stellen der Arbeit - einschließlich Tabellen, Karten und Abbildungen -, die anderen Werken im Wortlaut oder dem Sinn nach entnommen sind, in jedem Einzelfall als Entlehnung kenntlich gemacht habe; dass diese Dissertation noch keiner Fakultät oder Universität zur Prüfung vorgelegen hat; dass sie - abgesehen von den unten angegebenen Teilpublikationen - noch nicht veröffentlicht worden ist sowie, dass ich eine solche Veröffentlichung vor Abschluss des Promotionsverfahrens nicht vornehmen werde. Die Bestimmungen dieser Promotionsordnung sind mir bekannt. Die von mir vorgelegte Dissertation ist von Herrn Prof. Dr. Thomas Nattermann betreut worden.

Köln, den 20. Juli 2004

Andreas Glatz

Teilpublikationen

- ▶ Andreas Glatz, Diplomarbeit, *Quasi One-Dimensional Charge-Density-Waves at Low Temperatures*, Universität zu Köln, 2001. [Gla03]

- ▶ Andreas Glatz and Thomas Nattermann, *One-dimensional disordered density waves and superfluids: The role of quantum phase slips and thermal fluctuations*, Phys. Rev. Lett. **88**, 256401 (2002). [GN02a]

- ▶ Andreas Glatz and Thomas Nattermann, *Influence of thermal fluctuations on quantum phase transitions in one-dimensional disordered systems: Charge density waves and Luttinger liquids*, Phys. Rev. B **69**, 115118 (2004). [GN04a]

- ▶ Andreas Glatz, Thomas Nattermann, and Valery L. Pokrovsky, *Domain wall depinning in random media by ac fields*, Phys. Rev. Lett. **90**, 047201 (2003). [GNP03]

▶ Andreas Glatz and Thomas Nattermann, *Displacement Profile of Charge Density Waves and Domain Walls at Critical Depinning*, Phys. Rev. Lett. **92**, 257205 (2004). [GN04b]

▶ Z. R. Struzik, A. Glatz, and M. S. Li, $1/f$ *noise in a one-dimensional charge density wave system*, Europhys. Lett. **66**, 385 (2004). [SGL04a]

▶ Zbigniew R. Struzik, Andreas Glatz and Mai S. Li, *Search for flicker noise in one-dimensional charge density wave systems*, Proceedings of SPIE: Fluctuations and Noise in Materials, Vol. **5469**, 328 (2004). [SGL04b]

▶ Andreas Glatz and Thomas Nattermann, *Quantum phase slips and thermal fluctuations in one-dimensional disordered density waves*, J. Phys. IV - Proceedings **12**, 125 (2002). [GN02b]

▶ Andreas Glatz and Thomas Nattermann, *Domain walls in random media driven by AC fields*, J. Phys. IV - Proceedings **12**, 275 (2002). [GNP02]

▶ O. Petracic, X. Chen, O. Sichelschmidt, Ch. Bineka, W. Kleemann, A. Glatz, T. Nattermann, S. Cardoso, and P.P. Freitas, *Superferromagnetic domain state dynamics in discontinuous $CoFe/Al_2O_3$ multilayers*, J. Mag. Magn. Mat. 272, E1201 (2004). [PCS$^+$04b]

▶ O. Petracic, A. Glatz, and W. Kleemann, *Complex ac susceptibility studies on a model for granular superferromagnetic $CoFe/Al_2O_3$*, submittiert zu Phys. Rev. B, cond-mat/0406590. [PGK04]